JOURNAL OF FLUID MECHANICS

VOLUME 10 PART 3

MAY 1961

PUBLISHED BY

CAMBRIDGE UNIVERSITY PRESS

BENTLEY HOUSE, 200 EUSTON ROAD, LONDON, N.W.1

AMERICAN BRANCH: 32 EAST 57TH STREET, NEW YORK 22, N.Y.

Price 30*s.* (*U.S.A.* $5.00)

The JOURNAL OF FLUID MECHANICS exists for the publication of theoretical and experimental investigations of all aspects of the mechanics of fluids, and is issued in four parts per volume.

EDITORS

DR G. K. BATCHELOR, DR T. BROOKE BENJAMIN

Department of Applied Mathematics and Theoretical Physics, University of Cambridge, Free School Lane, Cambridge, England

ASSISTANT EDITORS

DR J. R. A. PEARSON, DR O. M. PHILLIPS

ASSOCIATE EDITORS

PROF. G. F. CARRIER

Pierce Hall, Harvard University, Cambridge 38, *Massachusetts, U.S.A.*

DR W. C. GRIFFITH

Lockheed Missiles and Space Division, Palo Alto, California, U.S.A.

M. J. LIGHTHILL

Royal Aircraft Establishment, Farnborough, Hampshire, England

PROF. R. R. LONG

School of Engineering, The Johns Hopkins University, Baltimore 18, *Maryland, U.S.A.*

DR P. G. SAFFMAN

Department of Mathematics, King's College, London, W.C. 2, *England*

Authors wishing to have papers published in the JOURNAL should communicate them to any one of the persons named above, choosing one in their own country where possible.

Authors are urged to ensure that their papers are written clearly and attractively, in order that their work will be readily accessible to readers.

Manuscripts should be typed in double spacing on one side of the paper only, with references listed at the end in alphabetical order of authors. Drawings should be done on a large scale in Indian ink on tracing cloth or drawing paper, the lettering being shown clearly in pencil for reproduction by the printer; the list of captions should be typed at the end of the manuscript. Proofs of papers from overseas will usually be despatched to authors by airmail. There is no charge for publication. Authors are entitled to receive 50 offprints of a paper in the JOURNAL free of charge, and additional offprints can be purchased if ordered in advance.

SUBSCRIPTIONS

The subscription price for a volume of four parts is £5. 10*s*. net, post free, payable in advance; separate parts 30*s*. net, plus postage. Subscriptions may be sent to any bookseller, or to the Cambridge University Press, Bentley House, 200 Euston Road, London, N.W.1.

Subscribers in the United States should send their orders to the Cambridge University Press, American Branch, 32 East 57th Street, New York 22, N.Y. The subscription price per volume is $18.50, post free, payable in advance; separate parts $5.00, plus postage.

Quotations for available back volumes and parts may be obtained on application to the Cambridge University Press.

Swimming of a waving plate

By T. YAO-TSU WU

California Institute of Technology, Pasadena, California

(Received 23 September 1960)

The purpose of this paper is to study the basic principle of fish propulsion. As a simplified model, the two-dimensional potential flow over a waving plate of finite chord is treated. The solid plate, assumed to be flexible and thin, is capable of performing the motion which consists of a progressing wave of given wavelength and phase velocity along the chord, the envelope of the wave train being an arbitrary function of the distance from the leading edge. The problem is solved by applying the general theory for oscillating deformable airfoils. The thrust, power required, and the energy imparted to the wake are calculated, and the propulsive efficiency is also evaluated. As a numerical example, the waving motion with linearly varying amplitude is carried out in detail. Finally, the basic mechanism of swimming is elucidated by applying the principle of action and reaction.

1. Introduction

'How does a fish swim'? is indeed a fascinating question. Geometrically, fishes of many varieties have their bodies in a planar form of finite aspect ratio, that is, their bodies have finite length and width and are thin in the third dimension; other varieties have slender cylindrical forms. Almost without exception all fishes have a flexible body to the extent that they can perform undulating motions in swimming. Physical observations further indicate that in general the motion of the deformable body consists of a train of waves, which are not standing waves, but which progress astern. Furthermore, the wave amplitude usually grows toward the tail. Most fishes propel themselves in water at speeds corresponding to a Reynolds number, based on their length, of the order of 10^5 or higher. Presumably the inertia forces in the surrounding fluid are an important factor in producing the propulsion; the viscosity of the fluid, other than generating drag, is important in creating circulation around the swimming body, and only in this role does it affect the propulsive forces. Taylor (1951, 1952*a*, *b*) has discussed certain aspects of propulsion of swimming bodies. In the first two references Taylor treated the problem of swimming microscopic organisms in viscous fluid where viscosity plays the leading role. In the third reference he investigated the swimming of long narrow animals. It is the purpose of this paper to study the mechanism of marine propulsion for very large Reynolds number and to discuss its important features such as the effect, on the propulsive force and the swimming efficiency, of the wavelength, the phase velocity of the wave, and the spatial variation in amplitude of the wave.

In order to simplify the determination of these complicated effects, this analysis is limited to the relatively simple case of a two-dimensional waving plate of negligible thickness. The fluid is assumed to be incompressible and inviscid, but with the Kutta condition imposed at the trailing edge of the plate. The problem then becomes the general problem of airfoils in unsteady motion. In order to represent the body profile in swimming, the plate must have infinite degrees of freedom. The solution of the case for airfoils in oscillatory motion of general form has been obtained by Küssner & Schwarz (1940); this solution is used as the starting point for further analysis in this work. However, the calculation of the propulsive force on the airfoil in unsteady motion has only been investigated for a limited number of simple cases, presumably because it is of small importance in any application in aeronautics. Kármán & Burgers (1943, p. 304) calculated the propulsive force and the work expended in maintaining the motion, but only for the most simple case of a rigid plate in transverse oscillation, thus providing a qualitative theory for flapping flight. Another calculation of the propulsive force, for the particular case of a rigid wing, is given by Nekrasov (1948). Since the problem is of primary interest in connexion with the flight of birds, and especially with the swimming of fishes, the thrust, the power required for maintaining the motion and the energy imparted to the fluid are calculated here for the general case of a waving deformable plate.

For further application of the general result, consideration is given to the motion of a flexible plate which consists of a train of progressive waves, the amplitude of the wave being taken as an arbitrary function of the distance along the plate, which is assumed to possess a Taylor expansion. In this general case it is found that the time-average of the energy imparted to the fluid, $\langle E_w \rangle$, is always positive; it vanishes if, and only if, the circulation around the swimming plate remains constant. A subsidiary result indicates that the time-average of the power input, $\langle P \rangle$, can be negative (implying that energy can be extracted from the fluid), but only in case of an oscillatory motion with at least two degrees of freedom. It is also shown that when energy is taken out of the fluid, the average thrust on the body cannot be positive. As a simple example, the waving motion with linearly varying amplitude is carried out in detail, the results plotted in diagrams and their physical significance discussed.

Finally, an attempt is made to elucidate the basic mechanism of swimming by applying the principle of action and reaction. When the plate acquires a forward momentum as it swims through a fluid, the fluid is pushed in the backward direction with the net total momentum equal and opposite to that of the action. Investigation of the strength of the vortex sheet shed from the trailing edge of the plate indicates that the forward thrust is positive only when the vorticity is so oriented that the fluid in the wake is pushed backwards from the tail, and the thrust is negative otherwise. Thus the momentum of the fluid in reaction is well concentrated in the vortex wake, appearing in the form of a jet of fluid expelled from the plate.

After this paper had been submitted, the author learned of M. J. Lighthill's work on a related subject (the swimming of slender fish) presented briefly in the Forty-Eighth Wilbur Wright Memorial Lecture (Lighthill 1960*a*) and sub-

sequently in a separate paper (Lighthill 1960*b*). In these references the theory is worked out for slender fish. The problem dealt with in this paper, however, is concerned with what may be called a two-dimensional flat fish. The theory for swimming of real fishes ought perhaps to lie somewhere in between these two limiting cases. It may be speculated that this subject also has some application in the aeroelasticity of oscillating wings.

2. Formulation of the problem; the acceleration potential

Consider the two-dimensional incompressible flow of an inviscid fluid generated by the motion of a deformable solid plate of zero thickness spanning from $x = -1$ to $x = 1$ in an otherwise uniform stream of constant velocity U in the positive x-direction. The motion of the flexible plate may be prescribed in the general form by

$$y = h(x,t) \quad \text{for} \quad -1 < x < 1, \tag{1}$$

where $h(x,t)$ is an arbitrary continuous function of x for every time t, the maximum amplitude of h and $\partial h/\partial x$ being assumed very small compared with unity. The flow velocity $\mathbf{q}$ has x- and y-components given by $\mathbf{q} = (U+u, v)$ and satisfies the continuity equation

$$\operatorname{div} \mathbf{q} = u_x + v_y = 0. \tag{2}$$

(The subscript x, or y, denotes partial differentiation with respect to x, or y.) By assuming the perturbation velocity u, v to be small compared with U, the Euler equations of motion for the ideal fluid may be linearized to give

$$\left(\frac{\partial}{\partial t} + U\frac{\partial}{\partial x}\right)\mathbf{q} = -\frac{1}{\rho}\operatorname{grad} p = \operatorname{grad}\phi, \tag{3}$$

where

$$\phi(x,y,t) = (p_\infty - p)/\rho, \tag{4}$$

in which ρ is the density, p the pressure of the fluid and p_∞ the pressure at infinity. The constant term p_∞ is included in the above definition of ϕ for convenience. The function ϕ is Prandtl's acceleration potential, as $\operatorname{grad}\phi$ gives the acceleration field of the flow. Taking the divergence of (3) and making use of (2), we obtain

$$\phi_{xx} + \phi_{yy} = 0. \tag{5}$$

Hence ϕ is a harmonic function of (x,y) for every t. Consequently a conjugate harmonic function $\psi(x,y,t)$ may be defined by the Cauchy–Riemann equations

$$\phi_x = \psi_y, \quad \phi_y = -\psi_x. \tag{6}$$

It then follows that in terms of the complex variable $z = x+iy$, the complex acceleration potential

$$f(z,t) = \phi(x,y,t) + i\psi(x,y,t) \tag{7}$$

is an analytic function of z at all times. Here, $i = \sqrt{-1}$ is the imaginary unit for the space variables (x,y). In terms of $f(z,t)$ and the complex velocity

$$w(z,t) = u(x,y,t) - iv(x,y,t), \tag{8}$$

(3) may also be written

$$\frac{\partial f}{\partial z} = \frac{\partial w}{\partial t} + U\frac{\partial w}{\partial z}. \tag{9}$$

For given $f(z,t)$, w can be obtained from (9) by integration

$$w(z,t) = \frac{1}{U}\int_{-\infty}^{z} g\left(z_1, t+\frac{z_1-z}{U}\right) dz_1, \quad g(z,t) \equiv \frac{\partial f(z,t)}{\partial z}, \tag{10}$$

provided, of course, the integral exists. In the above, w is assumed to vanish at $z = -\infty$, the upstream infinity.

In unsteady flow, unlike steady flow, a vortex sheet will in general be shed from the solid plate to form a vortex wake, i.e. a surface across which the tangential velocity component is discontinuous, even in two-dimensional motions. The pressure p, however, is continuous everywhere inside the flow except across the solid plate. In particular, it is also continuous across the wake. Since ϕ is a linear function of p (see (4)), it follows that $f(z,t)$ must be a regular function of z for every t inside the flow except at the solid plate. Though the complex velocity w is also an analytic function of z, w may, however, admit discontinuities across the vortex wake, in addition to the singularities at the plate boundary. For this reason it is convenient to work with the acceleration potential; its application also results in considerable simplification in the analysis.

The boundary condition that the component of the flow velocity normal to the moving solid boundary must vanish may be linearized to give

$$v = \frac{\partial h}{\partial t} + U\frac{\partial h}{\partial x} \quad \text{on} \quad y = \pm 0 \quad (-1 < x < 1). \tag{11}$$

The corresponding condition on $f(z,t)$ can be derived from (3) and (6) as

$$-\frac{\partial \psi}{\partial x} = \frac{\partial v}{\partial t} + U\frac{\partial v}{\partial x} = \left(\frac{\partial}{\partial t} + U\frac{\partial}{\partial x}\right)^2 h(x,t) \quad \text{on} \quad y = \pm 0 \quad (-1 < x < 1). \tag{12}$$

It is seen from (11) and (12) that v and ψ are even in y, and hence from the Cauchy–Riemann equations, u and ϕ must be odd in y. Since ϕ is regular everywhere inside the flow, it follows that

$$\phi(x,0,t) = 0 \quad \text{for} \quad |x| > 1 \quad \text{and for all } t. \tag{13}$$

At the trailing edge of the plate, $z = 1$, the Kutta condition requires

$$|f(1,t)| < \infty, \quad \text{for all } t. \tag{14}$$

It should be pointed out, however, that in order to be possible to distinguish the trailing edge from the leading edge, the case of $U = 0$ should be treated as a limiting case of $U \to 0$ with the configuration $h(x,t)$ so given that the flow at $z = 1$ is in the direction of positive x. Furthermore, it is required that

$$f(z,t) \to 0 \quad \text{as} \quad |z| \to \infty; \quad w(z,t) \to 0 \quad \text{as} \quad z \to -\infty. \tag{15}$$

This completes the statement of the problem.

Of particular interest in the present work is the case in which the profile of the flexible plate has a progressive wave of arbitrary amplitude given by

$$h(x,t) = A(x)\cos(kx - \omega t + \epsilon) \quad \text{for} \quad |x| < 1, \tag{16}$$

where k is the wave-number, ω the circular frequency (which is taken to be positive throughout this work), ϵ an arbitrary phase angle and $A(x)$ the arbitrary

amplitude of the wave motion. It is convenient to introduce the imaginary unit $j = \sqrt{-1}$ for the time variable t, e.g. $\exp(j\omega t) = \cos\omega t + j\sin\omega t$. The different notation j is used here so that it will not be confused with the imaginary unit i for the space variables x, y. (Thus, though $i^2 = -1$ and $j^2 = -1$, $ij \neq -1$.) In this notation the most general form of the simple harmonic motion of the flexible plate, including (16) as a special case, can be written

$$h(x,t) = h_1(x)\, e^{j\omega t} \quad \text{for} \quad |x| < 1, \tag{17}$$

where $h_1(x)$ is an arbitrary real function of x, but may in general be complex with respect to j. Taking the real part of the above expression for the eventual physical interpretation is of course understood.

By the conformal transformation

$$z = \tfrac{1}{2}(\zeta + \zeta^{-1}), \tag{18a}$$

the original z-plane, cut along the x-axis from $x = -1$ to $x = 1$, is mapped onto the region outside the unit circle $|\zeta| = 1$. On the unit circle, $\zeta = \exp(i\theta)$, and hence

$$x = \cos\theta. \tag{18b}$$

Since the plate has zero thickness, h and $\partial h/\partial x$ must be even functions of θ. We assume that $h_1(x)$ in (17) can be expanded in a Fourier cosine series

$$h(x,t) = \left[\tfrac{1}{2}\beta_0 + \sum_{n=1}^{\infty} \beta_n \cos n\theta\right] e^{j\omega t}, \tag{19a}$$

where

$$\beta_n = \frac{2}{\pi}\int_0^{\pi} h_1(x)\cos n\theta\, d\theta \quad (n = 0, 1, 2, \ldots). \tag{19b}$$

The coefficients β_n, like $h_1(x)$, may be complex in j. From (18b),

$$\partial/\partial x = -(\csc\theta)\,\partial/\partial\theta \quad \text{for} \quad y = 0, \quad |x| < 1.$$

Hence, from (19),

$$\frac{\partial h}{\partial x} = \frac{1}{\sin\theta}\sum_{n=1}^{\infty} n\beta_n \sin n\theta\, e^{j\omega t} = \left[\frac{\gamma_0}{2} + \sum_{n=1}^{\infty} \gamma_n \cos n\theta\right] e^{j\omega t}, \tag{20a}$$

from which it is readily seen that

$$\gamma_{n-1} - \gamma_{n+1} = 2n\beta_n \quad (n = 1, 2, \ldots). \tag{20b}$$

The coefficients γ_n can be solved from the above recursion formula to yield

$$\gamma_{2n} = 2\sum_{m=n}^{\infty} (2m+1)\beta_{2m+1}, \quad \gamma_{2n+1} = 2\sum_{m=n}^{\infty} (2m+2)\beta_{2m+2} \quad (n = 0, 1, 2, \ldots). \tag{20c}$$

Substituting (19), (20) in (11), we obtain

$$v(x, \pm 0, t) = -U\left[\tfrac{1}{2}\lambda_0 + \sum_{n=1}^{\infty} \lambda_n \cos n\theta\right] e^{j\omega t} \quad \text{on} \quad x = \cos\theta, \tag{21a}$$

where

$$\lambda_n = -(\gamma_n + j\sigma\beta_n), \quad \sigma = \omega/U, \quad \text{for} \quad n = 0, 1, 2, \ldots. \tag{21b}$$

The quantity $\sigma = \omega/U$ is called the reduced frequency referred to the half-chord which has been normalized to unity. If the chord is c, σ assumes the value $\omega c/2U$.

The solution for $f(z,t)$ satisfying conditions (21) and (12)–(15) has been obtained by Küssner & Schwarz (1940); the method may be briefly outlined as follows. If the acceleration potential $f(z,t)$ is invariant under the mapping (18), i.e. $f(z,t) = f\{z(\zeta),t\}$, then the solution must assume the form

$$f(z,t) = \phi + i\psi = iU^2\left[\frac{a_0}{\zeta+1} + \sum_{n=1}^{\infty}\frac{a_n}{\zeta^n}\right]e^{j\omega t} \quad \text{for} \quad |\zeta| > 1, \tag{22a}$$

where the coefficients a_n are real with respect to i so that condition (13) is satisfied. The term with a_0 in (22a) represents the singularity at the leading edge $\zeta = -1$; the infinite series represents an analytic function which, when $\partial h/\partial x$ has no discontinuity on the plate, is regular on and outside the unit circle $|\zeta| = 1$. To determine the a_n, we note that on the plate, $\zeta = e^{i\theta}$,

$$\phi = U^2\left[\frac{a_0}{2}\tan\frac{\theta}{2} + \sum_{n=1}^{\infty} a_n \sin n\theta\right]e^{j\omega t}, \tag{22b}$$

$$\psi = U^2\left[\frac{a_0}{2} + \sum_{n=1}^{\infty} a_n \cos n\theta\right]e^{j\omega t}. \tag{22c}$$

Substituting (21) and (22c) in (12), we readily obtain

$$a_n = \lambda_n + \frac{j\sigma}{2n}(\lambda_{n-1} - \lambda_{n+1}) \quad \text{for} \quad n = 1, 2, 3, \ldots. \tag{23a}$$

The coefficient a_0 has to be determined by applying (10), the imaginary part of which becomes, in the present case of periodic motion,

$$v(x,y,t) = -\frac{1}{U}e^{-j\sigma x}\int_{-\infty}^{x} e^{j\sigma\xi}\frac{\partial\psi(\xi,y,t)}{\partial\xi}\,d\xi.$$

Choosing (x,y) to be any point on the plate (such as $x = -1+0$, $y = +0$), and applying conditions (21) and (22c), then by appropriate integration by parts and making use of (23a), we find that the infinite series cancel and the final result yields

$$a_0 = (\lambda_0 + \lambda_1)C(\sigma) - \lambda_1, \tag{23b}$$

$$C(\sigma) = \frac{K_1(j\sigma)}{K_0(j\sigma) + K_1(j\sigma)} = F(\sigma) + jG(\sigma), \tag{23c}$$

where K_0 and K_1 are the modified Bessel functions of the second kind. F and G are respectively the real and imaginary part of $C(\sigma)$, which is usually called Theodorsen's function (for its tabulated value, see Luke & Dengler 1951).

3. Hydrodynamic forces

The pressure difference across the plate, according to (4) and (22b), is

$$\begin{aligned}(\Delta p) \equiv p(x,0-,t) - p(x,0+,t) &= \rho[\phi(x,0+,t) - \phi(x,0-,t)] \\ &= \rho U^2\left[a_0\tan\tfrac{1}{2}\theta + 2\sum_{n=1}^{\infty} a_n \sin n\theta\right]e^{j\omega t},\end{aligned} \tag{24}$$

the positive sense of Δp being in the positive y-direction.

(1) ***Lift.*** The lift on the solid plate is

$$L = \int_{-1}^{1} (\Delta p)\, dx = \int_{0}^{\pi} (\Delta p) \sin\theta\, d\theta = \pi\rho U^2 (a_0 + a_1)\, e^{j\omega t}. \tag{25}$$

(2) ***Moment.*** The moment of force about the mid-chord, positive in the nose-up sense, is

$$M = -\int_{-1}^{1} (\Delta p)\, x\, dx = \tfrac{1}{2}\pi\rho U^2 (a_0 - a_2)\, e^{j\omega t}. \tag{26}$$

The real parts (with respect to j) of (25) and (26) give respectively the lift and moment on the plate due to the motion given by the real part of (19). These results are of course known in unsteady wing theory (e.g. see Robinson & Laurmann 1956).

(3) ***Thrust.*** The thrust, taken to be positive in the negative x-direction, acting on the solid plate is given by

$$T = \int_{-1}^{1} (\Delta p)_R \left(\frac{\partial h}{\partial x}\right)_R dx + T_S = T_P + T_S \tag{27}$$

in which the quantity with subscript R denotes the real part (with respect to j) of that quantity, and T_S represents the thrust due to the leading edge suction. Since the thrust contains the non-linear terms of small amplitude, in calculating the integral in (27) the real physical quantities, given by the real part of their complex representations, must be used directly. For the subsequent analysis it is convenient to separate the real and imaginary parts of the following functions. For $n = 0, 1, 2, \ldots$,

$$\left.\begin{aligned} \beta_n\, e^{j\omega t} &= B'_n + jB''_n, \quad \gamma_n\, e^{j\omega t} = \Gamma'_n + j\Gamma''_n, \\ a_n\, e^{j\omega t} &= A'_n + jA''_n, \quad \lambda_n\, e^{j\omega t} = \Lambda'_n + j\Lambda''_n. \end{aligned}\right\} \tag{28}$$

Then

$$(\Delta p)_R = \rho U^2 \left\{ A'_0 \tan\tfrac{1}{2}\theta + 2 \sum_{n=1}^{\infty} A'_n \sin n\theta \right\}, \tag{29a}$$

$$\left(\frac{\partial h}{\partial x}\right)_R = \tfrac{1}{2}\Gamma'_0 + \sum_{m=1}^{\infty} \Gamma'_m \cos m\theta. \tag{29b}$$

Substituting (29) into the integral for T_P in (27), we obtain

$$\begin{aligned} T_P = \rho U^2 \int_0^{\pi} &\left\{ A'_0 (1 - \cos\theta) + \sum_{n=1}^{\infty} A'_n [\cos(n-1)\theta - \cos(n+1)\theta] \right\} \\ &\times \left\{ \tfrac{1}{2}\Gamma'_0 + \sum_{m=1}^{\infty} \Gamma'_m \cos m\theta \right\} d\theta \end{aligned}$$

$$= \tfrac{1}{2}\pi\rho U^2 \left\{ A'_0 (\Gamma'_0 - \Gamma'_1) + \sum_{n=1}^{\infty} A'_n (\Gamma'_{n-1} - \Gamma'_{n+1}) \right\}, \tag{30a}$$

or

$$T_P = \tfrac{1}{2}\pi\rho U^2 \left\{ A'_0 (\Gamma'_0 - \Gamma'_1) + 2 \sum_{n=1}^{\infty} n A'_n B'_n \right\}. \tag{30b}$$

The last expression follows from (20*b*) and (28). T_P can still be expressed in another form by eliminating A'_n (for $n \geqslant 1$) from (30). Substituting (20*b*), (21*b*), (23) into (28), we have

$$\Gamma'_{n-1}-\Gamma'_{n+1} = 2nB'_n, \quad \Gamma''_{n-1}-\Gamma''_{n+1} = 2nB''_n, \quad \text{for} \quad n = 1, 2, \ldots; \tag{31a}$$

$$A'_n = (\sigma^2/2n)(B'_{n-1}-B'_{n+1}) + 2\sigma B''_n - \Gamma'_n, \quad \text{for} \quad n = 1, 2, \ldots; \tag{31b}$$

$$\begin{aligned} A'_0 &= (\Lambda'_0+\Lambda'_1)F(\sigma) - (\Lambda''_0+\Lambda''_1)G(\sigma) - \Lambda'_1 \\ &= (\sigma B''_0 - \Gamma'_0)F(\sigma) - (\sigma B''_1 - \Gamma'_1)[1-F(\sigma)] \\ &\qquad + [\sigma(B'_0+B'_1) + (\Gamma''_0+\Gamma''_1)]G(\sigma). \end{aligned} \tag{31c}$$

Hence $\sum_{n=1}^{\infty} A'_n(\Gamma'_{n-1}-\Gamma'_{n+1}) = \sigma^2 \sum_{n=1}^{\infty} B'_n(B'_{n-1}-B'_{n+1}) + 4\sigma \sum_{n=1}^{\infty} nB'_nB''_n$

$$- \sum_{n=1}^{\infty} \Gamma'_n(\Gamma'_{n-1}-\Gamma'_{n+1}) = \sigma^2 B'_0B'_1 - \Gamma'_0\Gamma'_1 + 4\sigma \sum_{n=1}^{\infty} nB'_nB''_n.$$

Therefore

$$T_P = \tfrac{1}{2}\pi\rho U^2\left\{A'_0(\Gamma'_0-\Gamma'_1) - \Gamma'_0\Gamma'_1 + \sigma^2 B'_0B'_1 + 4\sigma \sum_{n=1}^{\infty} nB'_nB''_n\right\}. \tag{32}$$

This expression exhibits more explicitly the dependence of T_P on the reduced frequency σ since apart from A'_0 the coefficients B_n, Γ_n are seen to depend on σ only as a linear combination of $\sin\omega t$ and $\cos\omega t$.

The leading edge suction arises from the singular pressure at the leading edge, hence for its determination the non-linear terms in the expression for the pressure in the neighbourhood of the leading edge must be taken into account. The exact expression for the pressure is given by the Bernoulli equation

$$(p-p_\infty)/\rho = -\partial\Phi/\partial t - \tfrac{1}{2}(U+w_R)(U+\overline{w}_R) + \tfrac{1}{2}U^2,$$

where $\overline{w}_R$ denotes the complex conjugate of $w_R = u_R - iv_R$ with respect to i, the subscript R indicating the real part in j, and Φ is the velocity potential such that $u_R = \partial\Phi/\partial x$, $v_R = \partial\Phi/\partial y$. Now from (10) and (22),

$$w(z,t) = U\, e^{j\omega t - j\sigma z}\int_{-\infty}^{z} e^{j\sigma z_1}\frac{d}{dz_1}\left[\frac{ia_0}{\zeta_1+1} + \sum_{n=1}^{\infty}\frac{ia_n}{\zeta_1^n}\right]dz_1, \tag{33}$$

where $z_1 = \frac{1}{2}(\zeta_1+\zeta_1^{-1})$. Hence by integration by parts, it is readily seen that the asymptotic representation of $w(z,t)$ near the leading edge is

$$w(z,t) \cong \frac{iUa_0}{\zeta+1}e^{j\omega t} + O(1) \quad \text{as} \quad \zeta \to -1.$$

The part of w which is real in j thus reads

$$w_R(z,t) \cong \frac{iUA'_0}{\zeta+1} + O(1) \cong -\frac{UA'_0}{\{2(z+1)\}^{\frac{1}{2}}} + O(1) \quad \text{as} \quad z \to -1. \tag{34a}$$

From this result it can be seen that the velocity potential Φ and $\partial\Phi/\partial t$ remain bounded near the leading edge and hence

$$p - p_\infty \cong -\tfrac{1}{2}\rho w_R\overline{w}_R\left[1 + O\left(\frac{1}{|w_R|}\right)\right] \quad \text{as} \quad z \to -1. \tag{34b}$$

Since $\partial\Phi/\partial t$ makes no contribution to p near the leading edge, the problem of the unsteady suction force hence reduces to the same problem for the steady motion in the sense that the time-dependent quantities appear only as parameters (or coefficients) in the expression for p. Let the x- and y-components of the singular force acting at the leading edge be denoted by X_S and Y_S, then by applying Blasius's formula to a small circle of radius ϵ surrounding the leading edge,

$$X_S - iY_S = \frac{i\rho}{2}\oint_\epsilon w_R^2\,dz = -\tfrac{1}{2}\pi\rho U^2 A_0'^2.$$

Therefore $Y_S = 0$, and the leading edge thrust is

$$T_S = -X_S = \tfrac{1}{2}\pi\rho U^2 A_0'^2. \tag{35}$$

From (27), (32) and (35), the total thrust is

$$T = \tfrac{1}{2}\pi\rho U^2\Big\{(A_0'+\Gamma_0')\,(A_0'-\Gamma_1') + \sigma^2 B_0' B_1' + 4\sigma\sum_{n=1}^{\infty} nB_n' B_n''\Big\}. \tag{36}$$

Two limiting cases are of particular interest.

(i) $\sigma \to 0$. For $\sigma \ll 1$, $F(\sigma)$ and $G(\sigma)$ of (23*c*) can be expanded as

$$F(\sigma) = 1 - \tfrac{1}{2}\pi\sigma + O(\sigma^2\log\sigma), \quad G(\sigma) = \sigma(\gamma + \log\tfrac{1}{2}\sigma) + O(\sigma^2\log\sigma), \tag{37}$$

where γ is Euler's constant, $\gamma = 0{\cdot}5771\ldots$. Substituting (31) and (37) in (36), we obtain

$$T = \tfrac{1}{2}\pi\rho U^2\{-(\sigma\log\tfrac{1}{2}\sigma)\,(\Gamma_0' + \Gamma_1')\,(\Gamma_0'' + \Gamma_1'') + O(\sigma)\} \quad \text{for} \quad \sigma \ll 1. \tag{38}$$

Since Γ_n' and Γ_n'' depend on σ only in the form of a linear combination of $\sin\omega t$ and $\cos\omega t$, T therefore tends to zero like $\sigma\log\sigma$ as $\sigma \to 0$. This is, of course, D'Alembert's paradox, as should be expected, that a rigid body immersed in a steady flow of an ideal fluid experiences no drag.

(ii) $\sigma \gg 1$. In this case, use of the asymptotic expansions of the Bessel functions in (23*c*) yields

$$F(\sigma) \sim \frac{1}{2}\left[1 + \frac{1}{8\sigma^2} + O(\sigma^{-4})\right], \quad G(\sigma) \sim -\frac{1}{8\sigma}\left[1 - \frac{11}{128\sigma^2} + O(\sigma^{-4})\right]. \tag{39}$$

Hence from (31*c*) and (36) we obtain

$$T \sim \tfrac{1}{2}\pi\rho U^2\{\sigma^2[B_0' B_1' + \tfrac{1}{4}(B_0'' - B_1'')^2] + O(\sigma)\} \quad \text{for} \quad \sigma \gg 1. \tag{40}$$

Thus, T behaves like σ^2 as $\sigma \to \infty$.

4. Power required; energy conservation

If the prescribed motion is to be maintained, then an external force equal and opposite to the pressure force across the plate must be applied. Over a segment of the plate of length dx, this external force is $-(\Delta p)_R\,dx$, acting in the positive y-direction. The power required to maintain the motion is equal to the time rate of work done by this external force, or

$$P = -\int_{-1}^{1} (\Delta p)_R \left(\frac{\partial h}{\partial t}\right)_R dx, \tag{41}$$

where $(\partial h/\partial t)_R$ denotes the real part of $\partial h/\partial t$ which, by (19) and (28), is

$$\left(\frac{\partial h}{\partial t}\right)_R = -\omega\left[\tfrac{1}{2}B_0'' + \sum_{m=1}^{\infty} B_m'' \cos m\theta\right].$$

Substituting this equation and (29a) into (41) and integrating, we obtain

$$P = \tfrac{1}{2}\pi\rho U^2\omega\left\{A_0'(B_0'' - B_1'') + \sum_{n=1}^{\infty} A_n'(B_{n-1}'' - B_{n+1}'')\right\}. \tag{42a}$$

Upon elimination of A_n' from the above series, by using (31b), and after some rearrangement of the terms, we finally have

$$P = \tfrac{1}{2}\pi\rho U^3\sigma\left\{A_0'(B_0'' - B_1'') + 2\sigma B_0'' B_1'' - B_0''\Gamma_1' - B_1''\Gamma_0' + 2\sum_{n=1}^{\infty} nB_n' B_n'' + \sigma^2 \sum_{n=1}^{\infty} \frac{1}{2n}(B_{n-1}' - B_{n+1}')(B_{n-1}'' - B_{n+1}'')\right\}. \tag{42b}$$

From this result it is noted that P vanishes with vanishing σ and behaves like σ^3 for large σ.

From the principle of conservation of energy, the power input P (or the energy put into the system per unit time) must be equal to the time rate of work done by the thrust, TU, plus the kinetic energy imparted to the fluid in unit time. Let the last quantity be denoted by E_W, then

$$P = TU + E_W. \tag{43}$$

Making use of (36) and (42b), we obtain

$$E_W = \tfrac{1}{2}\pi\rho U^3\left\{(\sigma B_0'' - \Gamma_0' - A_0')(\sigma B_1'' - \Gamma_1' + A_0') + \sigma^2(B_0'' B_1'' - B_0' B_1') - 2\sigma\sum_{n=1}^{\infty} nB_n' B_n'' + \sigma^3 \sum_{n=1}^{\infty} \frac{1}{2n}(B_{n-1}' - B_{n+1}')(B_{n-1}'' - B_{n+1}'')\right\}. \tag{44a}$$

From (21b) and (28),

$$\Lambda_n' = \sigma B_n'' - \Gamma_n', \quad \Lambda_n'' = -(\sigma B_n' + \Gamma_n'') \quad \text{for} \quad n = 0, 1, 2, \ldots, \tag{44b}$$

which can be used to rewrite (44a) as

$$E_W = \tfrac{1}{2}\pi\rho U^3\left\{(\Lambda_0' - A_0')(\Lambda_1' + A_0') - \sigma\sum_{n=1}^{\infty} \frac{1}{2n}(\Lambda_{n-1}' - \Lambda_{n+1}')(\Lambda_{n-1}'' - \Lambda_{n+1}'')\right\}. \tag{44c}$$

The energy lost E_W can be determined by an alternative method. By the basic principle of hydrodynamics, E_W is equal to the time rate of work done by the pressure over the body surface, that is

$$E_W = -\int_{S_B} p\mathbf{n}.\mathbf{q}\, dS,$$

where $\mathbf{n}$ is the unit vector normal to the body surface S_B, pointing away from the fluid. At the leading edge where p and $\mathbf{q}$ are singular, S_B is replaced by a small circle ϵ around the leading edge. Thus

$$E_W = \oint_{\epsilon} (-p\mathbf{n}).\mathbf{q}\, dS_\epsilon - \int_{-1+0}^{1} (\Delta p)_R v_R(x, 0, t)\, dx.$$

Using the solution (34*a*, *b*) in the first integral, we find that this integral is equal to $-T_S U$ where T_S is the leading edge suction (see (35)). The second integral is readily integrable; the final result is found to be identically (44*c*).

5. Average value of thrust and energy; efficiency of propulsion

Since we are primarily interested in the average values of the thrust and the power input over a single period $\tau = 2\pi/\omega$, we now define the time average of an arbitrary function of the time $g(t)$ by

$$\langle g(t)\rangle = \frac{1}{\tau}\int_0^\tau g(t)\,dt. \tag{45}$$

To determine the average values of the infinite series in (36), (42*b*) and (44), we write

$$\beta_n = \beta_n' + j\beta_n'' \quad (n = 0, 1, 2, \ldots), \tag{46a}$$

where β_n' and β_n'' are the real and imaginary parts of β_n. Then from (28),

$$B_n' = \beta_n' \cos\omega t - \beta_n'' \sin\omega t, \quad B_n'' = \beta_n'' \cos\omega t + \beta_n' \sin\omega t. \tag{46b}$$

Expressions similar to these may be written for Γ_n', Γ_n'', Λ_n', Λ_n''. By using the relations

$$\langle\cos^2\omega t\rangle = \langle\sin^2\omega t\rangle = \tfrac{1}{2}, \quad \langle\sin\omega t\cos\omega t\rangle = 0, \tag{47}$$

it is evident that

$$\langle B_n' B_n''\rangle = 0, \quad \langle(B_{n-1}' - B_{n+1}')(B_{n-1}'' - B_{n+1}'')\rangle = 0, \tag{48a}$$

$$\langle B_0' B_1'\rangle = \langle B_0'' B_1''\rangle = \tfrac{1}{2}(\beta_0'\beta_1' + \beta_0''\beta_1''). \tag{48b}$$

Therefore the time averages of the infinite series in (36), (42*b*) and (44) vanish and consequently

$$\langle T\rangle = \tfrac{1}{2}\pi\rho U^2\langle(A_0' + \Gamma_0')(A_0' - \Gamma_1') + \sigma^2 B_0' B_1'\rangle, \tag{49}$$

$$\langle P\rangle = \tfrac{1}{2}\pi\rho U^3\sigma\langle A_0'(B_0'' - B_1'') + 2\sigma B_0'' B_1'' - B_0''\Gamma_1' - B_1''\Gamma_0'\rangle, \tag{50}$$

$$\langle E_W\rangle = \tfrac{1}{2}\pi\rho U^3\langle(\Lambda_0' - A_0')(\Lambda_1' + A_0')\rangle. \tag{51}$$

These expressions indicate that $\langle T\rangle$, $\langle P\rangle$, $\langle E_W\rangle$ depend on the time average of quantities which contain only five coefficients: Γ_0, Γ_1, B_0, B_1 and A_0. These equations are for the moment left in the above relatively simple form; their values for a specific case will be calculated in detail in § 7.

It is of interest to point out that $\langle E_W\rangle$ in general is positive definite. To show this result we first make use of (31*c*) and write (51) as

$$\langle E_W\rangle = \tfrac{1}{2}\pi\rho U^3\langle(\Lambda_0' + \Lambda_1')^2 F(1-F) + (\Lambda_0' + \Lambda_1')(\Lambda_0'' + \Lambda_1'')(2F-1)G - (\Lambda_0'' + \Lambda_1'')^2 G^2\rangle. \tag{52}$$

We further write, as in (46),

$$\lambda_n = \lambda_n' + j\lambda_n'' \quad (n = 0, 1, 2, \ldots), \tag{53a}$$

and hence from (28)

$$\Lambda_n' = \lambda_n' \cos\omega t - \lambda_n'' \sin\omega t, \quad \Lambda_n'' = \lambda_n'' \cos\omega t + \lambda_n' \sin\omega t. \tag{53b}$$

Then from (47) it follows that

$$\langle(\Lambda_0'+\Lambda_1')^2\rangle = \langle(\Lambda_0''+\Lambda_1'')^2\rangle = \tfrac{1}{2}\{(\lambda_0'+\lambda_1')^2+(\lambda_0''+\lambda_1'')^2\},$$
$$\langle(\Lambda_0'+\Lambda_1')(\Lambda_0''+\Lambda_1'')\rangle = 0.$$

Therefore (52) becomes

$$\langle E_W\rangle = \tfrac{1}{4}\pi\rho U^3\{(\lambda_0'+\lambda_1')^2+(\lambda_0''+\lambda_1'')^2\}[F-(F^2+G^2)]. \tag{54}$$

From the known behaviour of the Theodorsen function (see (23c)), it can be shown that $F \geqslant (F^2+G^2)$ for $\sigma \geqslant 0$ and the equality holds only if $\sigma = 0$. Therefore it follows from (54) that in general $\langle E_W\rangle \geqslant 0$; it vanishes only in the special cases $\sigma = 0$ and $\lambda_0 = -\lambda_1$. The first case is the steady motion for which the result $E_W = 0$ is obvious. The second case includes the trivial limiting case of $\lambda_0 = \lambda_1 = 0$, but the general case with non-vanishing λ_0 and λ_1 is of more interest. As will be shown in the following section, the case of $\lambda_0 = -\lambda_1$, with $\lambda_0 \neq 0$, corresponds to the condition under which the circulation around the solid plate remains constant (zero) so that no trailing vortex wake will be shed from the plate, even in wavy motion.

From the above result it follows that $\langle P\rangle - \langle TU\rangle = \langle E_W\rangle$ is non-negative. Hence, when energy is taken out of the fluid ($\langle P\rangle$ negative), $\langle T\rangle$ cannot be positive. However, no definite statement, such as the above for $\langle E_W\rangle$, can be claimed separately for $\langle T\rangle$ and $\langle P\rangle$. When $\langle T\rangle \geqslant 0$, and hence $\langle P\rangle \geqslant U\langle T\rangle \geqslant 0$, we may define the average efficiency for producing useful thrust by

$$\eta = U\langle T\rangle/\langle P\rangle. \tag{55}$$

6. Circulation around the plate; vortex sheet strength

The vortex wake is assumed to lie along the x-axis downstream of the trailing edge. The strength of the vortex sheet at a point $P(x, 0)$ of the wake is denoted by $\gamma(x, t)$. The circulation $\delta\Gamma$ around a small rectangular circuit passing through the points $A(x, +0)$, $B(x+\delta x, +0)$, $C(x+\delta x, -0)$, $D(x, -0)$, in this order, is approximately

$$\delta\Gamma = \int_{ABCDA} \mathbf{q}.d\mathbf{s} = u(x, +0)\,\delta x - u(x, -0)\,\delta x,$$

which must be equal to the total vorticity within the circuit, $\gamma\delta x$. This statement may be regarded as the definition of γ. Since u is odd in y, we therefore have

$$\gamma(x, t) = 2u(x, +0, t). \tag{56}$$

Furthermore, at any point of the wake, $x > 1$,

$$\frac{\partial\gamma}{\partial t} + U\frac{\partial\gamma}{\partial x} = 2\left(\frac{\partial u}{\partial t} + U\frac{\partial u}{\partial x}\right)_{y=+0} = 2\left(\frac{\partial\phi}{\partial x}\right)_{y=+0} = 0$$

by virtue of (3) and (13). Hence for $x > 1$, γ is a function of the single variable $(x-Ut)$ only. Thus, if the value of γ at the trailing edge is known, i.e.

$$\gamma(1, t) = 2u(1, +0, t) = g(t),$$

say, then

$$\gamma(x, t) = g\left(t - \frac{x-1}{U}\right) \quad \text{for} \quad x \geqslant 1. \tag{57}$$

In a co-ordinate system fixed in the fluid at infinity, the trailing edge of the plate travels a distance $-U\,dt$ along the x axis in the interval dt. If in the same time interval the circulation around the plate changes by the amount $d\Gamma$ from the value $\Gamma(t)$, then from the trailing edge there separates a vortex of strength $-d\Gamma$, which in turn is spread out into a vortex sheet of strength γ distributed over a length $U\,dt$ immediately behind the trailing edge. Hence

$$\frac{d\Gamma}{dt} = -U\gamma(1,t) = -2Uu(1,+0,t). \tag{58}$$

The circulation $\Gamma(t)$ around the plate can then be obtained by integration. Thus, once the value of u at the trailing edge is known, the strength of the vortex wake and the circulation around the plate can be determined from (57) and (58).

To calculate u, we first substitute (22a) in (10) and integrate by parts, giving

$$\begin{aligned} w(z,t) &= \frac{1}{U} e^{-j\sigma z} \int_{-\infty}^{z} e^{j\sigma z_1} \frac{\partial f(z_1,t)}{\partial z_1}\, dz_1 \\ &= \frac{1}{U}\left\{ f(z,t) - j\sigma\, e^{-j\sigma z} \int_{-\infty}^{z} e^{j\sigma z_1} f(z_1,t)\, dz_1 \right\}. \end{aligned}$$

Now $\phi = Re\, f = 0$ on $y = 0$, $|x| > 1$; hence by separating the real and imaginary parts (in $i = \sqrt{-1}$), making use of (22), and by taking $\theta = \cos^{-1} x$ as the integration variable over the plate, we obtain

$$\begin{aligned} u(1,+0,t) &= -\frac{j\sigma}{U} e^{-j\sigma} \int_{-1}^{1} e^{j\sigma x} \phi(x,+0,t)\, dx \\ &= -j\sigma U\, e^{j(\omega t-\sigma)} \int_0^{\pi} e^{j\sigma\cos\theta} \left[\frac{a_0}{2}(1-\cos\theta) + \sum_{n=1}^{\infty} a_n \sin n\theta \sin\theta \right] d\theta. \end{aligned}$$

Substituting from (23a) into the above integral and integrating the terms with the factor $(j\sigma/2n)$ by parts, we find

$$\begin{aligned} &u(1,+0,t)\, e^{-j(\omega t-\sigma)}/(\tfrac{1}{2}j\sigma U) \\ &\quad = -\int_0^{\pi} e^{j\sigma\cos\theta} \left\{ a_0(1-\cos\theta) + 2\sum_{n=1}^{\infty} \left[\lambda_n + \frac{j\sigma}{2n}(\lambda_{n-1}-\lambda_{n+1}) \right] \sin n\theta \sin\theta \right\} d\theta \\ &\quad = -\int_0^{\pi} e^{j\sigma\cos\theta} \left\{ a_0(1-\cos\theta) + \sum_{n=1}^{\infty} \lambda_n [\cos(n-1)\theta - \cos(n+1)\theta] \right. \\ &\qquad\qquad \left. + \sum_{n=1}^{\infty} (\lambda_{n-1}-\lambda_{n+1}) \cos n\theta \right\} d\theta. \end{aligned}$$

The infinite series in the above integrand terminates after rearrangement. Now (see Watson 1944)

$$\int_0^{\pi} e^{j\sigma\cos\theta} \cos n\theta\, d\theta = \pi j^n J_n(\sigma) = \pi I_n(j\sigma),$$

where J_n is the Bessel function and I_n the modified Bessel function, both of the first kind. Hence

$$u(1,+0,t) = -\tfrac{1}{2}\pi j\sigma U\, e^{j(\omega t-\sigma)} \{(\lambda_1+a_0)\, I_0(j\sigma) + (\lambda_0-a_0)\, I_1(j\sigma)\}.$$

By using (23) and the relation (see Watson 1944, p. 80)

$$I_0(z)\,K_1(z)+I_1(z)\,K_0(z)=\frac{1}{z},$$

the above expression may be written

$$u(1,+0,t)=-\tfrac{1}{2}\pi U\,e^{j(\omega t-\sigma)}\frac{\lambda_0+\lambda_1}{K_0(j\sigma)+K_1(j\sigma)}. \tag{59}$$

If $\lambda_0+\lambda_1=0$, then it follows from (57)–(59) that the circulation around the plate remains constant for all time and hence the vortex wake disappears. Furthermore, it can be shown that $K_0(j\sigma)+K_1(j\sigma)$ has no zero for real σ (see Erdélyi & Kermack 1945). Therefore the necessary and sufficient condition for constant circulation around the flexible plate is

$$\lambda_0+\lambda_1=0, \tag{60a}$$

which may be expressed, by using (20) and (21), in terms of the β_n as

$$j\sigma(\beta_0+\beta_1)+2\sum_{n=1}^{\infty}n\beta_n=0. \tag{60b}$$

The motion for which the β_n's (see (19)) satisfy (60*b*) is the one in which no trailing vortices will be shed.

The circulation around the plate, from (58) and (59), is

$$\Gamma(t)=\pi U\,e^{j(\omega t-\sigma)}\frac{\lambda_0+\lambda_1}{j\sigma[K_0(j\sigma)+K_1(j\sigma)]}. \tag{61}$$

In the limit of steady motion, $\omega\to 0$, $\sigma\to 0$, the denominator of the above expression tends to unity, and $\lambda_n\to-\gamma_n$ (see (21*b*)), hence $\Gamma\to-\pi U(\gamma_0+\gamma_1)$. Also, as $\sigma\to 0$, $a_n\to\lambda_n$ for $n=0,1,2,\ldots$ (see (23)), and so from (25) the lift becomes

$$L=\pi\rho U^2(\lambda_0+\lambda_1)=-\pi\rho U^2(\gamma_0+\gamma_1)=\rho U\Gamma,$$

in agreement with the theorem of Joukowski.

7. The flexible plate with progressive waves

Consider in particular the motion of a flexible plate which consists of a train of progressive waves of wavelength $\lambda=2\pi/k$ and frequency $\omega/2\pi$, as given by

$$h(x,t)=\left[\sum_{m=0}^{\infty}b_m\exp(j\epsilon_m)\,x^m\right]e^{j(\omega t-kx)}\quad(-1<x<1), \tag{62a}$$

where b_m are taken to be real coefficients, ϵ_m are constant phase angles, the amplitude of the wave being taken as an arbitrary function of x as represented by the series. Without losing generality we may take $\epsilon_0=0$. The above equation may also be written

$$h(x,t)=\sum_{m=0}^{\infty}b_m\,j^m\left(\frac{\partial}{\partial k}\right)^m\exp\{j(\omega t-kx+\epsilon_m)\}\quad(-1<x<1). \tag{62b}$$

In terms of the variable θ defined by (18*b*), we may write (Watson 1944, p. 22)

$$e^{-jkx}=e^{-jk\cos\theta}=J_0(k)+2\sum_{n=1}^{\infty}(-j)^n J_n(k)\cos n\theta, \tag{63}$$

where $J_n(k)$ is the Bessel function of the first kind. Thus

$$h(x,t) = \sum_{m=0}^{\infty} b_m j^m \exp(j\epsilon_m)\left[J_0^{(m)}(k) + 2\sum_{n=1}^{\infty}(-j)^n J_n^{(m)}(k)\cos n\theta\right] e^{j\omega t}, \quad (64)$$

where $J_n^{(m)}(k)$ stands for $d^m J_n(k)/dk^m$. If the wave propagates in the negative x-direction, k assumes negative values; this can be obtained by the continuation

$$J_n(k) = (-)^n J_n(-k), \quad J_n^{(m)}(k) = (-)^{m+n} J_n^{(m)}(-k). \quad (65)$$

Comparing (64) with (19), we find that

$$\beta_n = 2\sum_{m=0}^{\infty} b_m j^{m-n}\exp(j\epsilon_m) J_n^{(m)}(k) \quad (n = 0, 1, 2, \ldots). \quad (66)$$

Substituting (66) in (20c) and using the relations (Erdélyi 1953, vol. 2, p. 99)

$$\left.\begin{aligned} kJ_{2n}(k) &= 2\sum_{\nu=n}^{\infty}(-)^{\nu-n}(2\nu+1)J_{2\nu+1}(k) \quad (n = 0, 1, 2, \ldots),\\ kJ_{2n+1}(k) &= 2\sum_{\nu=n}^{\infty}(-)^{\nu-n}(2\nu+2)J_{2\nu+2}(k) \quad (n = 0, 1, 2, \ldots),\end{aligned}\right\} \quad (67)$$

we obtain, for $n = 0, 1, 2, \ldots$,

$$\gamma_n = 2j^{-(n+1)}\sum_{m=0}^{\infty} b_m j^m \exp(j\epsilon_m)\left(\frac{d}{dk}\right)^m [kJ_n(k)]. \quad (68)$$

Substituting (66) in (28), we find, for $n = 0, 1, 2, \ldots$,

$$\left.\begin{matrix} B'_{2n} \\ -B''_{2n+1}\end{matrix}\right\} = 2(-)^n \sum_{m=0}^{\infty} D_{\mathrm{I}}(m,t)\left\{\begin{matrix} J_{2n}(k) \\ J_{2n+1}(k)\end{matrix}\right\}, \quad (69a)$$

$$\left.\begin{matrix} B''_{2n} \\ B'_{2n+1}\end{matrix}\right\} = 2(-)^n \sum_{m=0}^{\infty} D_{\mathrm{II}}(m,t)\left\{\begin{matrix} J_{2n}(k) \\ J_{2n+1}(k)\end{matrix}\right\}, \quad (69b)$$

where D_{I} and D_{II} denote the differential operators

$$\left.\begin{aligned} D_{\mathrm{I}}(m,t) &= (-)^m\left[b_{2m}\cos(\omega t+\epsilon_{2m})\left(\frac{\partial}{\partial k}\right)^{2m} - b_{2m+1}\sin(\omega t+\epsilon_{2m+1})\left(\frac{\partial}{\partial k}\right)^{2m+1}\right],\\ D_{\mathrm{II}}(m,t) &= (-)^m\left[b_{2m}\sin(\omega t+\epsilon_{2m})\left(\frac{\partial}{\partial k}\right)^{2m} + b_{2m+1}\cos(\omega t+\epsilon_{2m+1})\left(\frac{\partial}{\partial k}\right)^{2m+1}\right].\end{aligned}\right\} \quad (70)$$

Similarly, from (68) and (28) we find, for $n = 0, 1, 2, \ldots$,

$$\left.\begin{matrix} \Gamma'_{2n} \\ -\Gamma''_{2n+1}\end{matrix}\right\} = 2(-)^n \sum_{m=0}^{\infty} D_{\mathrm{II}}(m,t)\left\{\begin{matrix} kJ_{2n}(k) \\ kJ_{2n+1}(k)\end{matrix}\right\}, \quad (71a)$$

$$\left.\begin{matrix} -\Gamma''_{2n} \\ -\Gamma'_{2n+1}\end{matrix}\right\} = 2(-)^n \sum_{m=0}^{\infty} D_{\mathrm{I}}(m,t)\left\{\begin{matrix} kJ_{2n}(k) \\ kJ_{2n+1}(k)\end{matrix}\right\}, \quad (71b)$$

Upon substitution of the above relations in (31c), we obtain

$$A'_0 = 2\sum_{m=0}^{\infty}\{D_{\mathrm{II}}(m,t)\,\Omega(\sigma,k) + D_{\mathrm{I}}(m,t)\,Q(\sigma,k)\}, \quad (72a)$$

where

$$\Omega(\sigma,k) = (\sigma-k)\{F(\sigma)J_0(k) + G(\sigma)J_1(k)\}, \quad (72b)$$

$$Q(\sigma,k) = (\sigma-k)\{[1-F(\sigma)]J_1(k) + G(\sigma)J_0(k)\}. \quad (72c)$$

The other coefficients (namely $A'_1, A'_2, \ldots, A''_n, \ldots$) do not appear in $\langle T\rangle$ and $\langle P\rangle$; they will not be given here.

Finally, when the above expressions for B_0, B_1, Γ_0, Γ_1, A_0 are substituted in (49), we have

$$\frac{\langle T\rangle}{\pi\rho U^2} = 2\Big\langle \sum_{m=0}^{\infty}\sum_{r=0}^{\infty} [D_{II}(m,t)\,\Omega_* + D_I(m,t)\,Q][D_{II}(r,t)\,\Omega + D_I(r,t)\,Q_*]\Big\rangle + 2\sigma^2\Big\langle \sum_{m=0}^{\infty}\sum_{r=0}^{\infty} [D_I(m,t)\,J_0(k)][D_{II}(r,t)\,J_1(k)]\Big\rangle, \quad (73a)$$

where
$$\Omega_* = \Omega(\sigma,k) + kJ_0(k), \quad Q_* = Q(\sigma,k) + kJ_1(k). \quad (73b)$$

By making use of the results

$$\langle \sin(\omega t+\epsilon)\sin(\omega t+\delta)\rangle = \langle \cos(\omega t+\epsilon)\cos(\omega t+\delta)\rangle = \tfrac{1}{2}\cos(\epsilon-\delta),$$
$$\langle \sin(\omega t+\epsilon)\cos(\omega t+\delta)\rangle = \tfrac{1}{2}\sin(\epsilon-\delta),$$

we obtain, after some straightforward manipulation,

$$\begin{aligned}\frac{\langle T\rangle}{\pi\rho U^2} = {} & \Big(\sum_{n=0,2,4,\ldots}^{\infty}(-)^{\frac{1}{2}n}\sum_{r=0,2,\ldots}^{n} + \sum_{n=2,4,\ldots}^{\infty}(-)^{\frac{1}{2}n-1}\sum_{r=1,3,\ldots}^{n-1}\Big) b_r b_{n-r} \\ & \times\{[\Omega^{(r)}\Omega_*^{(n-r)} + Q^{(r)}Q_*^{(n-r)}]\cos(\epsilon_r-\epsilon_{n-r}) \\ & + [\Omega^{(r)}Q^{(n-r)} + \Omega_*^{(r)}Q_*^{(n-r)} + \sigma^2 J_1^{(r)}J_0^{(n-r)}]\sin(\epsilon_r-\epsilon_{n-r})\} \\ & + \sum_{n=1,3,\ldots}^{\infty}(-)^{\frac{1}{2}n-\frac{1}{2}}\sum_{r=0,2,\ldots}^{n-1} b_r b_{n-r}\{[\Omega^{(r)}\Omega_*^{(n-r)} + \Omega_*^{(r)}\Omega^{(n-r)} + Q^{(r)}Q_*^{(n-r)} \\ & + Q_*^{(r)}Q^{(n-r)}]\sin(\epsilon_r-\epsilon_{n-r}) + [Q^{(r)}\Omega^{(n-r)} + Q_*^{(r)}\Omega_*^{(n-r)} - \Omega^{(r)}Q^{(n-r)} \\ & - \Omega_*^{(r)}Q_*^{(n-r)} + \sigma^2(J_0^{(r)}J_1^{(n-r)} - J_1^{(r)}J_0^{(n-r)})]\cos(\epsilon_r-\epsilon_{n-r})\}, \end{aligned} \quad (74)$$

where the superscript numerals in the parentheses denote the order of differentiation with respect to k, e.g. $\Omega^{(n)} = \partial^n\Omega/\partial k^n$.

To calculate $\langle P\rangle$ it is convenient to use the relation $\langle P\rangle = \langle TU\rangle + \langle E_W\rangle$, since $\langle E_W\rangle$ can be readily derived from (54). From the definitions (21b) and (53a), we obtain by using (66) and (68) the following

$$\left.\begin{matrix}\lambda_0' \\ -\lambda_1''\end{matrix}\right\} = 2\sum_{m=0}^{\infty} D_{II}(m,0)\left\{\begin{matrix}(\sigma-k)J_0(k) \\ (\sigma-k)J_1(k)\end{matrix}\right\},$$
$$\left.\begin{matrix}\lambda_0'' \\ \lambda_1'\end{matrix}\right\} = -2\sum_{m=0}^{\infty} D_I(m,0)\left\{\begin{matrix}(\sigma-k)J_0(k) \\ (\sigma-k)J_1(k)\end{matrix}\right\}.$$

Substituting these expressions into (54) and rearranging the terms, we find that

$$\begin{aligned}\frac{\langle E_W\rangle}{\pi\rho U^3} = {} & [F-(F^2+G^2)]\Big\{\Big(\sum_{n=0,2,\ldots}^{\infty}(-)^{\frac{1}{2}n}\sum_{r=0,2,\ldots}^{n} + \sum_{n=2,4,\ldots}^{\infty}(-)^{\frac{1}{2}n-1}\sum_{r=1,3,\ldots}^{n-1}\Big) b_r b_{n-r} \\ & \times[(N_0^{(r)}N_0^{(n-r)} + N_1^{(r)}N_1^{(n-r)})\cos(\epsilon_r-\epsilon_{n-r}) - 2N_0^{(r)}N_1^{(n-r)}\sin(\epsilon_r-\epsilon_{n-r})] \\ & + 2\sum_{n=1,3,\ldots}^{\infty}(-)^{\frac{1}{2}n-\frac{1}{2}}\sum_{r=0,2,\ldots}^{n-1} b_r b_{n-r}[(N_0^{(r)}N_0^{(n-r)} + N_1^{(r)}N_1^{(n-r)})\sin(\epsilon_r-\epsilon_{n-r}) \\ & + (N_0^{(r)}N_1^{(n-r)} - N_1^{(r)}N_0^{(n-r)})\cos(\epsilon_r-\epsilon_{n-r})]\Big\}, \end{aligned} \quad (75a)$$

where
$$N_0(\sigma,k) = (\sigma-k)J_0(k), \quad N(\sigma,k) = (\sigma-k)J_1(k). \quad (75b)$$

With $\langle T\rangle$ and $\langle E_W\rangle$ determined as above, the average power required is then

$$\langle P\rangle = U\langle T\rangle + \langle E_W\rangle. \tag{76}$$

If the chord of the plate is c, then the above results hold valid if $\sigma = \omega c/2U$, $k = \pi c/\lambda$ (λ being the wavelength), $\langle T\rangle/\pi\rho U^2$ is replaced by $\langle T\rangle/\pi\rho U^2(\frac{1}{2}c)$, and $\langle E_W\rangle/\pi\rho U^3$ by $\langle E_W\rangle/\pi\rho U^3(\frac{1}{2}c)$.

If the series in (62a), which represents the amplitude function of the plate motion, has but a finite number of terms, then both series in (74) and (75) will terminate. In particular, we shall consider the following special example.

8. Waving plate with linearly varying amplitude

In order to exhibit the effects of the non-uniform amplitude of the progressing wave along the plate and the effect of the different phase angles, we consider the relatively simple case

$$\begin{aligned} h(x,t) &= b_0\cos(\omega t - kx) + b_1\cos(\omega t - kx + \epsilon) \\ &= Re\{[b_0 + b_1 x e^{j\epsilon}]e^{j(\omega t - kx)}\}, \quad \text{for} \quad -1 < x < 1. \end{aligned} \tag{77}$$

This is a special case of the general motion (62) with $b_2 = b_3 = \ldots = 0$, $\epsilon_0 = 0$, $\epsilon_1 = \epsilon$. From (74) it is readily verified that $\langle T\rangle$ now reduces to

$$\frac{\langle T\rangle}{\pi\rho U^2} = b_0^2 T_1(\sigma,k) + b_1^2 T_2(\sigma,k) + b_0 b_1[T_3(\sigma,k)\cos\epsilon + T_4(\sigma,k)\sin\epsilon], \tag{78}$$

where
$$T_1(\sigma,k) = \Omega(\sigma,k)\,\Omega_*(\sigma,k) + Q(\sigma,k)\,Q_*(\sigma,k),$$

$$T_2(\sigma,k) = \frac{\partial\Omega}{\partial k}\frac{\partial\Omega_*}{\partial k} + \frac{\partial Q}{\partial k}\frac{\partial Q_*}{\partial k},$$

$$T_3(\sigma,k) = Q\frac{\partial\Omega}{\partial k} + Q_*\frac{\partial\Omega_*}{\partial k} - \Omega\frac{\partial Q}{\partial k} - \Omega_*\frac{\partial Q_*}{\partial k} + \sigma^2\left[J_0^2 + J_1^2 - \frac{1}{k}J_0 J_1\right],$$

$$T_4(\sigma,k) = -\frac{\partial}{\partial k}T_1(\sigma,k).$$

The functions Ω, Q are given by (72) and Ω_*, Q_* by (73).

From (75) we derive, for the present case,

$$\frac{\langle E_W\rangle}{\pi\rho U^3} = b_0^2 W_1(\sigma,k) + b_1^2 W_2(\sigma,k) + b_0 b_1[W_3(\sigma,k)\cos\epsilon + W_4(\sigma,k)\sin\epsilon], \tag{79}$$

where
$$W_1(\sigma,k) = [F - (F^2+G^2)]\,[N_0^2 + N_1^2],$$

$$W_2(\sigma,k) = [F - (F^2+G^2)]\left[\left(\frac{\partial N_0}{\partial k}\right)^2 + \left(\frac{\partial N_1}{\partial k}\right)^2\right],$$

$$W_3(\sigma,k) = 2[F - (F^2+G^2)]\left[N_0\frac{\partial N_1}{\partial k} - N_1\frac{\partial N_0}{\partial k}\right],$$

$$W_4(\sigma,k) = -\frac{\partial}{\partial k}W_1(\sigma,k).$$

The functions N_0 and N_1 are given by (75b).

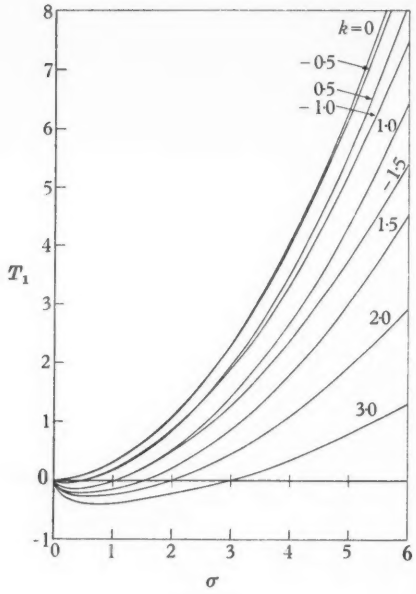

FIGURE 1

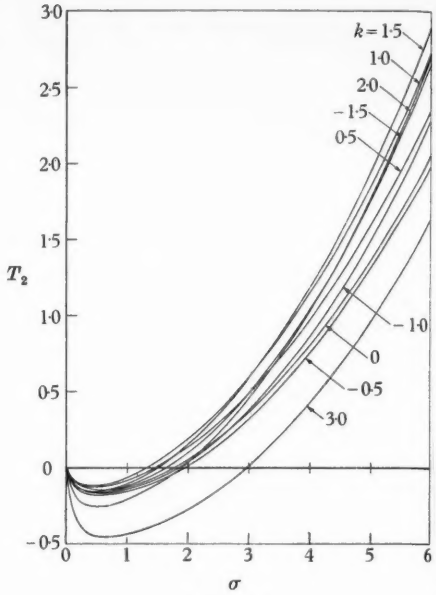

FIGURE 2

FIGURE 1. Variation of the thrust-coefficient function $T_1(\sigma, k)$ with the reduced frequency σ at several circular wave-numbers k (cf. statement below equation (76)).

FIGURE 2. Variation of the thrust-coefficient function $T_2(\sigma, k)$ with the reduced frequency σ at several values of k.

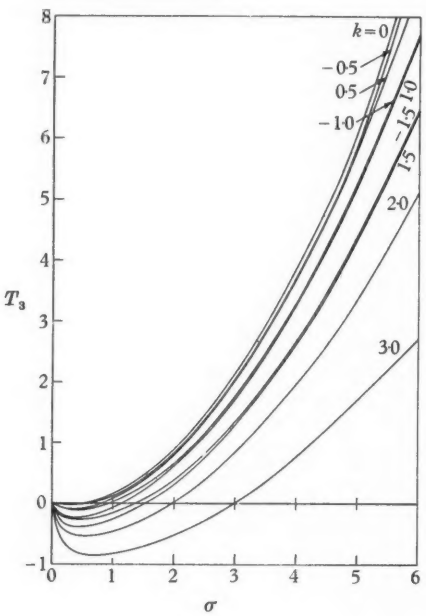

FIGURE 3

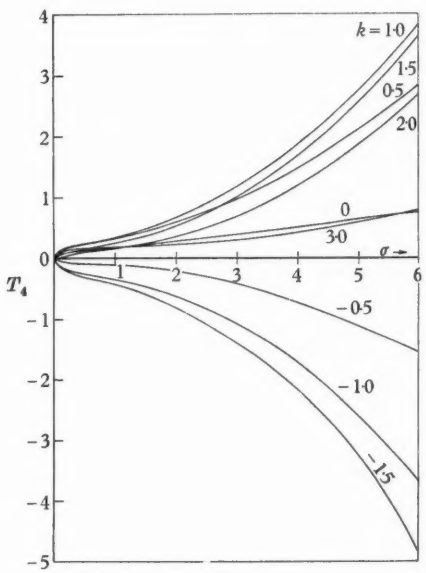

FIGURE 4

FIGURE 3. Variation of the thrust-coefficient function $T_3(\sigma, k)$ with the reduced frequency σ at several values of k.

FIGURE 4. Variation of the thrust-coefficient function $T_4(\sigma, k)$ with the reduced frequency σ at several values of k.

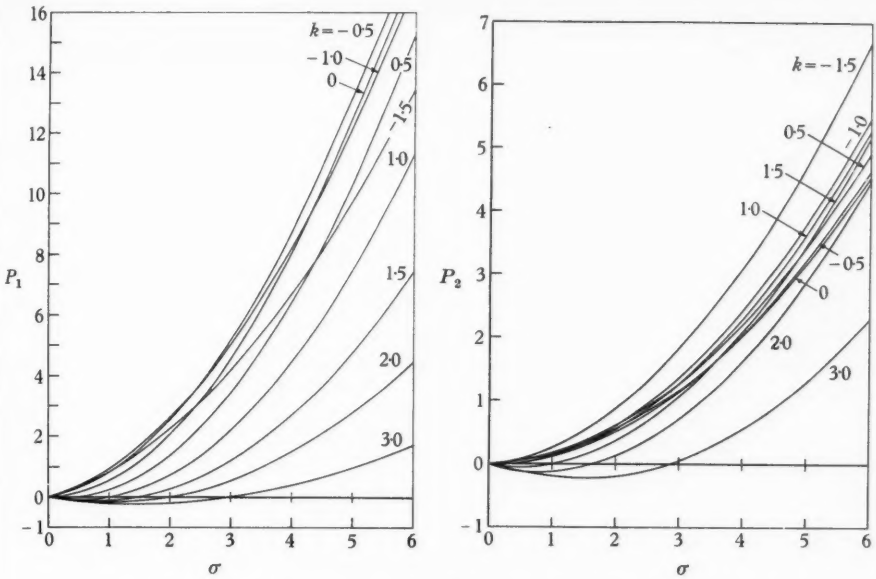

FIGURE 5. Variation of the power-coefficient functions $P_1(\sigma,k)$ and $P_2(\sigma,k)$ with the reduced frequency σ at several values of k.

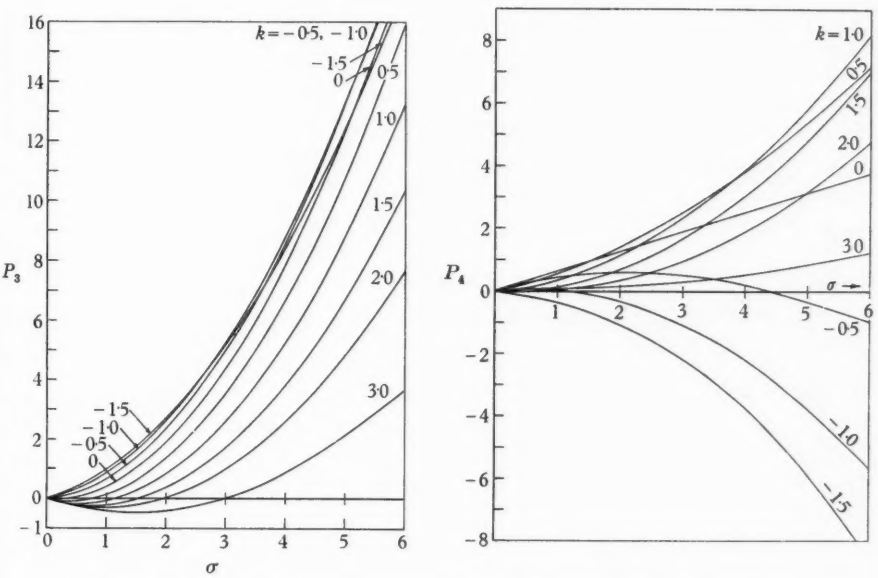

FIGURE 6. Variation of the power-coefficient functions $P_3(\sigma,k)$ and $P_4(\sigma,k)$ with the reduced frequency σ at several values of k.

The average power input, from (76), is therefore

$$\frac{\langle P\rangle}{\pi\rho U^3} = b_0^2 P_1(\sigma,k) + b_1^2 P_2(\sigma,k) + b_0 b_1 [P_3(\sigma,k)\cos\epsilon + P_4(\sigma,k)\sin\epsilon], \tag{80}$$

where $$P_i(\sigma,k) = T_i(\sigma,k) + W_i(\sigma,k) \quad (i = 1,2,3,4).$$

In figures 1–6 the above results for T_i and P_i are plotted versus the reduced frequency σ in the range $0 \leqslant \sigma \leqslant 6$ for the wave-numbers $k = -1{\cdot}5, -1, -0{\cdot}5, 0, 0{\cdot}5, 1, 1{\cdot}5, 2, 3$. The results show that T_i and P_i vanish at $\sigma = 0$, and, for large values of σ, the magnitudes of T_i and P_i behave like σ^2 and σ^3, respectively. For any given values of b_0 and b_1, the average thrust and the power required can be readily obtained by simple linear combination of these functions. Particularly simple are the cases (1) $b_0 \neq 0, b_1 = 0$, and (2) $b_0 = 0, b_1 \neq 0$; the solution for these cases, apart from a proportionality factor, are simply T_1, P_1 and T_2, P_2.

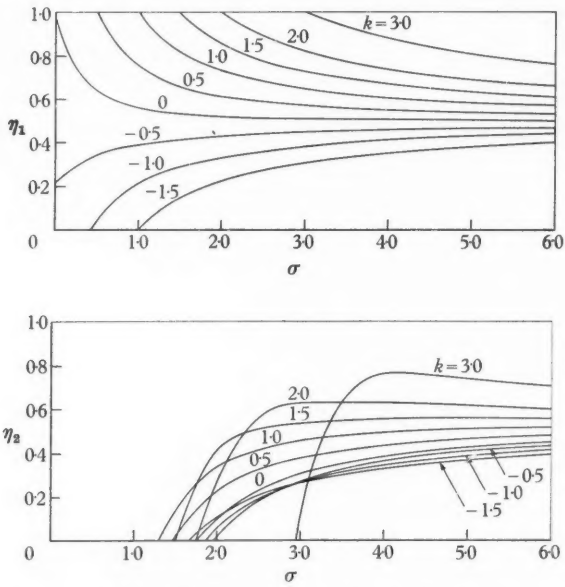

FIGURE 7. Swimming efficiency for two configurations, η_1 for a uniform wave amplitude, and η_2 for a linearly varying amplitude symmetrical about the plate centre.

The first case ($b_0 \neq 0$, $b_1 = 0$) represents a waving plate with a uniform wave amplitude. For a given positive k, implying that the wave travels toward the tail, both the thrust and the power required vanish at $\sigma = k$, when the wave velocity is equal to the free-stream velocity since the wave velocity is then

$$c = \omega/k = U\sigma/k = U.$$

This means that this wave form becomes frozen with respect to the fluid at infinity so that the plate merely travels along a sinusoidal path fixed in the space. As can be verified, this motion creates no circulation around the waving plate.

For positive k, the thrust $\langle T \rangle$ and the power required $\langle P \rangle$ are negative for $0 < \sigma < k$ and positive for $\sigma > k$. Negative values of $\langle P \rangle$ mean that energy is taken out of the fluid; this is possible only if $k > 0$. For a rigid plate in transverse oscillation ($k = 0$), $\langle P \rangle$ is non-negative, in agreement with the remark by Kármán that energy can be taken out the fluid only in the case of an oscillatory motion with at least two degrees of freedom. For a flexible plate with $k \neq 0$ the degrees of freedom are infinite in number. At every fixed σ, both T_1 and P_1 decrease with increasing positive k. In the range of negative k, corresponding to wave propagation toward the head, it is noted that T_1 and P_1 have the general trend of decreasing with decreasing k. Thus, T_1 and P_1 reach their maximum values near $k = 0$ for each given σ. Perhaps of more significance is the efficiency which becomes in this case $\eta_1 = T_1/P_1$. The values of η_1, plotted in figure 7, indicate that in the range of positive thrust ($T_1 > 0$) η_1 increases with increasing k (negative as well as positive) for fixed σ. This implies that the percentage rate of decrease in T_1 is slower than that in P_1 with respect to increasing k, for all k. Consequently, from the viewpoint of the efficiency, it is advantageous to have the waves propagating towards the rear. This result is interpreted here as affording a qualitative explanation of the observation that fishes in nature usually have the wave form of their body propagating from the head to the tail.

The functions T_2 and P_2 behave in much the same manner as T_1 and P_1, as may be seen from the figures. The function $\eta_2 = T_2/P_2$ is plotted in figure 7.

In the case of $U \to 0$, with $\omega = \sigma U$ fixed, the limiting solution becomes

$$\frac{\langle T \rangle}{\pi \rho \omega^2} = \frac{b_0^2}{4}(J_0^2 + J_1^2) + \frac{b_1^2}{4}\left[\left(J_0 - \frac{J_1}{k}\right)^2 + J_1^2\right] + \frac{b_0 b_1}{2}\left[\left(J_0^2 + J_1^2 - \frac{1}{k} J_0 J_1\right)\cos\epsilon + \frac{1}{k} J_1^2 \sin\epsilon\right],$$

$$\langle P \rangle \to 2\langle E_W \rangle \to 2U\langle T \rangle.$$

9. The basic mechanism of swimming

From the basic principle of action and reaction in mechanics, it is to be expected that, when the plate attains a forward momentum as it swims through a fluid, the fluid must be pushed in the backward direction with a net total momentum equal and opposite to that of the action. From the resulting flow picture it can be seen that the momentum of reaction is concentrated in the vortex wake and appears in the form of a jet of fluid expelled from the plate. This mechanism has been elucidated, for the simple case of a rigid plate in transverse oscillation, by Kármán & Burgers (1943, p. 308). It is not difficult to illustrate this mechanism for the present more general case by the following consideration.

Consider again the simple case $b_0 \neq 0$, $b_1 = b_2 = \ldots = 0$, as discussed previously. The plate motion is given by

$$h(x,t) = b_0 \cos(\omega t - kx) \quad \text{for} \quad -1 < x < 1,$$

so that the trailing edge moves according to

$$h(1,t) = b_0 \cos(\omega t - k).$$

The trailing edge will reach the highest position at $t = k/\omega$. At this instant the vortex sheet at the trailing edge, by (56) and (61), has strength

$$\gamma\left(1, \frac{k}{\omega}\right) = -\pi U Re\left[\frac{\lambda_0 + \lambda_1}{K_0(j\sigma) + K_1(j\sigma)} e^{j(k-\sigma)}\right].$$

Now for this case, by (66) and (68),

$$\beta_0 = 2b_0 J_0(k), \quad \beta_1 = -2b_0 jJ_1(k), \quad \gamma_0 = -2b_0 jkJ_0(k), \quad \gamma_1 = -2b_0 kJ_1(k).$$

Hence from (21*b*)

$$\lambda_0 + \lambda_1 = -[\gamma_0 + \gamma_1 + j\sigma(\beta_0 + \beta_1)] = -2b_0(\sigma - k)[J_1(k) + jJ_0(k)].$$

Furthermore,

$$K_0(j\sigma) + K_1(j\sigma) = -\tfrac{1}{2}\pi\{J_1(\sigma) + Y_0(\sigma) + j[J_0(\sigma) - Y_1(\sigma)]\},$$

where Y_n are the Bessel functions of the second kind. Hence

$$\gamma\left(1, \frac{k}{\omega}\right) = -4b_0 U \frac{(\sigma - k) H(\sigma, k)}{[J_1(\sigma) + Y_0(\sigma)]^2 + [J_0(\sigma) - Y_1(\sigma)]^2}, \tag{81}$$

where

$$\begin{aligned} H(\sigma, k) = {} & \{J_1(k)[J_1(\sigma) + Y_0(\sigma)] + J_0(k)[J_0(\sigma) - Y_1(\sigma)]\}\cos(\sigma - k) \\ & + \{J_0(k)[J_1(\sigma) + Y_0(\sigma)] - J_1(k)[J_0(\sigma) - Y_1(\sigma)]\}\sin(\sigma - k). \end{aligned}$$

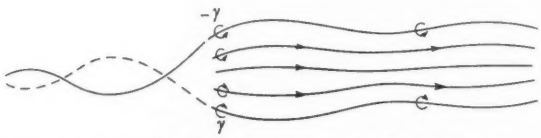

FIGURE 8. A qualitative sketch of the trailing vortex waves in the wake of a swimming plate.

By using the formula (Watson 1944, p. 77) $J_1(z)Y_0(z) - J_0(z)Y_1(z) = 2/\pi z$, it is readily seen that

$$H(k, k) = J_0^2(k) + J_1^2(k) + 2/\pi k,$$

which is positive definite for $0 < k < \infty$. Actually it can be shown that $H(\sigma, k) > 0$ for $0 < \sigma < \infty$, $0 < k < \infty$ (see Appendix). Therefore it follows that, so long as both σ and k are positive,

$$\gamma\left(1, \frac{k}{\omega}\right) \lesseqgtr 0 \quad \text{according as} \quad \sigma \gtreqless k.$$

Consider first the case $\sigma > k > 0$. When the trailing edge is at the highest position, the vorticity shed from the plate is negative, or in counterclockwise sense, as sketched in figure 8. On the other hand, when the trailing edge is at the lowest position, i.e. at the opposite phase in time, the vorticity shed from the plate is positive. This indicates that the more detailed structure of the wake will have the form of a series of parallel waves in which the vorticity varies across the wake from a negative strength at the top to a positive value at the bottom. If now the velocity field due to this vortex system is calculated, it is found that the fluid in

the vortex wake is expelled downstream of the plate, moving in the form of a jet in the positive x-direction. Consequently, by the principle of action and reaction, the plate experiences a positive thrust, as the result shows. For the same reason, the thrust is negative if $0 < \sigma < k$.

This work is sponsored by the Office of Naval Research of the U.S. Navy. The assistance rendered by Mr D. P. Wang, Mrs Zora Harrison and Mrs Luna Fung in the computations and by Mrs Rose Grant in preparing the manuscript is greatly appreciated.

Appendix

This note is to show that $H(\sigma, k) > 0$ for $0 < \sigma < \infty$, $0 < k < \infty$, where (see (81))

$$H(\sigma,k) = [J_1(k)A(\sigma)+J_0(k)B(\sigma)]\cos(\sigma-k)+[J_0(k)A(\sigma)-J_1(k)B(\sigma)]\sin(\sigma-k),$$

$$A(\sigma) = J_1(\sigma)+Y_0(\sigma), \quad B(\sigma) = J_0(\sigma)-Y_1(\sigma).$$

By using Schafheitlin's integral representations for the Bessel functions (Watson 1944, p. 169), for $Re\, z > 0$,

$$J_0(z) = \frac{2}{\pi}\int_0^{\frac{1}{2}\pi} \frac{\sin(z+\frac{1}{2}\theta)}{\cos^{\frac{1}{2}}\theta \sin\theta} e^{-2z\cot\theta}\, d\theta,$$

$$Y_0(z) = -\frac{2}{\pi}\int_0^{\frac{1}{2}\pi} \frac{\cos(z+\frac{1}{2}\theta)}{\cos^{\frac{1}{2}}\theta \sin\theta} e^{-2z\cot\theta}\, d\theta,$$

and the relation $J_1(z) = -J_0'(z)$, $Y_1(z) = -Y_0'(z)$, one readily obtains

$$A(\sigma) = J_1(\sigma)+Y_0(\sigma) = \frac{4}{\pi}\int_0^{\frac{1}{2}\pi} \frac{\sin(\sigma-\frac{1}{2}\theta)}{\cos^{\frac{1}{2}}\theta \sin^2\theta} e^{-2\sigma\cot\theta}\, d\theta,$$

$$B(\sigma) = J_0(\sigma)-Y_1(\sigma) = \frac{4}{\pi}\int_0^{\frac{1}{2}\pi} \frac{\cos(\sigma-\frac{1}{2}\theta)}{\cos^{\frac{1}{2}}\theta \sin^2\theta} e^{-2\sigma\cot\theta}\, d\theta.$$

Using these results, one finds, after some straightforward manipulation,

$$H(\sigma,k) = \frac{8}{\pi^2}\int_0^{\frac{1}{2}\pi}\int_0^{\frac{1}{2}\pi} \frac{[\cos\frac{1}{2}(\phi-\theta)-\cos\phi\,\cos\frac{1}{2}(4k+\phi-\theta)]}{(\cos\theta\cos\phi)^{\frac{1}{2}}\sin^2\theta\sin^2\phi} e^{-2(\sigma\cot\theta+k\cot\phi)}\, d\theta\, d\phi.$$

This shows that the sign of H depends only on the quantity in the square bracket in the numerator of the integrand, which is independent of σ, since the remaining part of the integrand is never negative. Therefore, the sign of $H(\sigma, k)$ is at least independent of σ. It follows that, for any given positive k, the function $H(\sigma, k)$ must have the same sign as the function

$$H_*(k) = J_0(k)\cos k + J_1(k)\sin k$$

which is the asymptotic representation of $\frac{1}{2}\pi\sigma H(\sigma, k)$ as $\sigma \to +0$.

Now the derivative of H_* is

$$H_*'(k) = -\frac{J_1(k)}{k}\sin k,$$

which vanishes at $k = m\pi$, $m = 0, 1, 2, \ldots$, and at $k = k_n$, the positive zeros of $J_1(k)$. The value of k_n is known to lie in $(n\pi + \pi/8, n\pi + \pi/4)$, $n = 1, 2, 3, \ldots$ (Watson 1944, p. 490). A study of the value of $H_*''(k)$ at these zeros of $H_*'(k)$ shows that the only minima of $H_*(k)$ are at $k = m\pi$, $m = 1, 2, 3, \ldots$. But

$$H_*(m\pi) = (-)^m J_0(m\pi) \quad (m = 1, 2, 3, \ldots),$$

which are all positive since it is known that $\operatorname{sgn}[J_0(m\pi)] = (-)^m$. Therefore $H_*(k) > 0$ for $0 < k < \infty$; the final result is then obvious.

REFERENCES

Erdélyi, A. 1953 (Ed.) *Higher Transcendental Functions* (*Bateman Manuscript Project*). New York: McGraw-Hill.

Erdélyi, A. & Kermack, W. O. 1945 Note on the equation $f(z)K_n'(z) - g(z)K_n(z) = 0$. *Proc. Camb. Phil. Soc.* **41**, 74–5.

Kármán, Th. van & Burgers, J. M. 1943 General aerodynamic theory—perfect fluids. Division E, vol. II, *Aerodynamic Theory* (Ed. W. F. Durand).

Küssner, H. G. & Schwarz, L. 1940 The oscillating wing with aerodynamically balanced elevator. *Luftfahrt-Forsch.* **17**, 337–54. (English translation: 1941, *NACA TM* 991.)

Lighthill, M. J. 1960*a* Mathematics and aeronautics. *J. Roy. Aero. Soc.* **64**, 373–94.

Lighthill, M. J. 1960*b* Note on the swimming of slender fish. *J. Fluid Mech.* **9**, 305–17.

Luke, Y. & Dengler, M. A. 1951 Tables of the Theordorsen circulation function for generalized motion. *J. Aero. Sci.* **18**, 478–83.

Nekrasov, A. I. 1948 Wing theory for unsteady flow. *Aero. Res. Coun.* no. 11792.

Robinson, A. & Laurmann, J. A. 1956 *Wing Theory*. Cambridge University Press.

Taylor, G. I. 1951 Analysis of the swimming of microscopic organisms. *Proc. Roy. Soc.* A, **209**, 447–61.

Taylor, G. I. 1952*a* The action of waving cylindrical tails in propelling miscroscopic organisms. *Proc. Roy. Soc.* A, **211**, 225–39.

Taylor, G. I. 1952*b* Analysis of the swimming of long and narrow animals. *Proc. Roy. Soc.* A, **214**, 158–83.

Watson, G. N. 1944 *A Treatise on the Theory of Bessel Functions*, 2nd ed. Cambridge University Press.

Experiments on the flow past a circular cylinder at very high Reynolds number

By ANATOL ROSHKO

Guggenheim Aeronautical Laboratory, California Institute of Technology, Pasadena, California

(Received 15 November 1960)

Measurements on a large circular cylinder in a pressurized wind tunnel at Reynolds numbers from 10^6 to 10^7 reveal a high Reynolds number transition in which the drag coefficient increases from its low supercritical value to a value 0·7 at $R = 3{\cdot}5 \times 10^6$ and then becomes constant. Also, for $R > 3{\cdot}5 \times 10^6$, definite vortex shedding occurs, with Strouhal number 0·27.

1. Introduction

Shortly after the closing and before the dismantling of the Southern California Co-operative Wind Tunnel (CWT), some time was made available to us for a high Reynolds number experiment on a circular cylinder. In this large pressurized wind tunnel (Millikan 1957) it was possible to reach a cylinder Reynolds number R of close to 10^7, compared to about 2×10^6, the highest value for which wind tunnel measurements were previously reported in the literature. There are, in addition, some measurements in natural wind, up to about $R = 4 \times 10^6$ (Dryden & Hill 1930; Pechstein 1940), about which we comment more fully later.

The many experimental measurements of drag coefficient C_d at subcritical Reynolds numbers are in fairly good agreement as to the values of $C_d(R)$, but in the supercritical range, i.e. after the transition to low values of C_d, there is little agreement, except that C_d lies between values of 0·2 and 0·4. It is not clear whether the relatively large discrepancies here are due to difficulties in measurement or whether the flow here is more sensitive to the conditions of the experiment. The measurements of Delany & Sorensen (1953) at Reynolds numbers up to 2×10^4 exhibit a multivaluedness which they attribute (private communication) to changes in the flow from a symmetrical to an unsymmetrical type, higher values of C_d occurring in the unsymmetrical flow. Other authors claim to observe no asymmetries.

On the question of vortex shedding at high Reynolds number there is little information. It is well known that vortex shedding occurs at Reynolds numbers below the critical value, with a dimensionless frequency (Strouhal number S) of about 0·2. At critical and supercritical Reynolds numbers there are, to our knowledge, only two sets of measurements. The early ones by Relf & Simmons (1924) indicate that in the transition range there is a predominant frequency in the wake, which they called 'aperiodic', compared to the 'accurately periodic' flow at $R < 10^5$. Their measurements show that the Strouhal number of these frequencies increases as the drag coefficient C_d decreases.

More recently, Delany & Sorensen (1953) obtained measurements at still higher Reynolds numbers (10^6 to 2×10^6) using a pressure pick-up in the wake close behind the cylinder. The shedding frequencies, which were determined from the predominant frequencies on an oscillograph record, show considerable scatter, as do those of Relf & Simmons; the values of S are between 0·35 and 0·45.

From these two sets of measurements, it would appear that S rises rapidly in the interval $R = 2 \times 10^5$ to 10^6, and that there may be a rapid decrease at about 2×10^6.

Our intention in the present experiments was to overlap the Reynolds number range of the existing measurements, while extending them to values of R as high as possible. The time available for preparing and performing the experiments was so short as to preclude a thorough investigation of all aspects of the flow, but it was hoped to obtain answers to a few obvious questions: Does the drag coefficient continue to change? Is there vortex shedding? Is there an asymptotic state, i.e. can we say anything about the ultimate form of the flow as $R \to \infty$, and at what values of R are we approaching it?

2. Experimental arrangement

The experiments were performed in the subsonic test section of the CWT, which had a height of 8·5 ft. and width of 11 ft. It could be pressurized to 4 atm; pressures of 1 and 2 atm were also used. To avoid compressibility effects, the flow speed was limited to a Mach number of about 0·25.

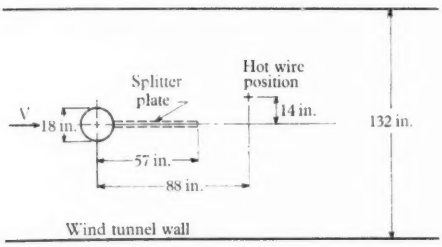

FIGURE 1. Arrangement of cylinder in the wind tunnel.

The cylinder was a seamless 'black steel' pipe which had been sandblasted to remove its protective paint and scale. This resulted in a surface roughness of about 200 μ-in. The cylinder had a diameter of 18 in. and was round to within $\frac{1}{16}$ in. (in diameter). It spanned the $8\frac{1}{2}$ ft. height of the test section. Pressure orifices were located every 10° (with additional ones at $\theta = 95°$ and 105°), over half the circumference at the middle section. These were connected to a pressure measuring system consisting of pressure transducers which read out to digital indicators and recorders. The sensitivity of this system was set to give full output at the highest dynamic pressure, consequently there was a deterioration of accuracy at lower values of the dynamic pressure.

A hot-wire anemometer was mounted at a fixed position, 7·3 diameters downstream of the cylinder axis and 0·7 diameters off the centreline, as shown in figure 1. The output of the hot wire, in a standard circuit, was fed into a spectral analyser,

which could scan the frequency spectrum and record it on a pen recorder. We were looking for possible vortex shedding peaks in the spectrum. Whenever one was indicated on the record, it was tuned by hand and its frequency accurately determined by comparing it to an oscillator signal whose frequency was measured by an electronic counter.

Provision was made to install a 'splitter plate' on the centreline behind the cylinder, as indicated in figure 1. It also spanned the $8\frac{1}{2}$ ft. height of the test section, extended 4 ft. along the centreline, and was 2 in. thick, being made up of two pieces of plywood bolted together.

3. Wall interference corrections

To obtain the highest possible Reynolds number, the cylinder diameter chosen was a little larger than might have been desirable from the point of view of the wall interference. With a diameter $d = 1{\cdot}5$ ft. and tunnel breadth $b = 11$ ft., the blockage ratio was $d/h = 0{\cdot}136$. To correct for the wall interference effects, we made use of the formulas of Allen & Vincenti (1944), which give, for the corrected values of velocity and drag coefficient V and C_d in terms of the measured values V' and C'_d,

$$\frac{V}{V'} = 1 + \tfrac{1}{4}C'_d\left(\frac{d}{h}\right) + 0{\cdot}82\left(\frac{d}{h}\right)^2, \tag{1}$$

$$\frac{C_d}{C'_d} = 1 - \tfrac{1}{2}C'_d\left(\frac{d}{h}\right) - 2{\cdot}5\left(\frac{d}{h}\right)^2. \tag{2}$$

These formulas were obtained, following the earlier work of Lock, Glauert and Goldstein, by using image doublets to represent the interference between wall and cylinder, and image sources to represent the interference between wall and wake; the two effects give the third and second terms, respectively, in the formulas. Such an analysis does not take into account possible interference effects on the separation mechanism and the structure of the wake close behind the body; changes in these could have an important effect on the drag. This would be especially important in regions where C_d is changing rapidly with R, but probably less important where C_d is nearly constant. The experimental evidence relating to wall interference on cylinders is not entirely satisfactory. We have used equations (1) and (2) as the best available, believing them to be fairly accurate at our highest Reynolds numbers, where C_d is nearly constant. The maximum corrections to V' and C'_d were about 4 and 10 %, respectively.

The uncorrected drag coefficient C'_d was obtained by integrating the measured pressure distribution $C'_p(\theta)$; it was then corrected with equation (2). When corrected values of pressure coefficient C_p were needed (e.g. figures 3 and 4), these were obtained from

$$(C_p - 1) = \left(\frac{V'}{V}\right)^2 (C'_p - 1). \tag{3}$$

Corrections for Reynolds number R and Strouhal number S are the same as for the velocity.

4. Results

(*a*) *Drag coefficient*

The corrected values C_d are plotted against R in figure 2. Also shown, for comparison, is the well-known curve of $C_d(R)$ at lower values of R. Different investigators do not agree exactly on this curve, but the differences are small, except in the supercritical region. We have chosen Wieselsberger's (1921) curve as representative and have also plotted the results of Delany & Sorensen (1953) in the supercritical range (all the dashed lines). The latter extend to a higher Reynolds number than any other wind tunnel experiments of which we are aware, and they illustrate the difficulty in obtaining consistency in the supercritical range. It had been hoped that our experiments would overlap the

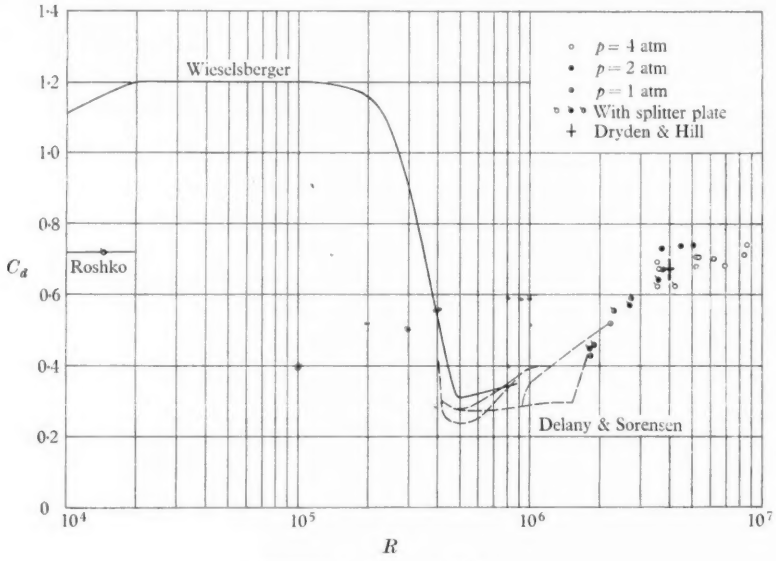

FIGURE 2. Drag coefficient.

existing measurements more than they do, but we were unable to obtain sufficient accuracy at our lowest Reynolds numbers, since the dynamic pressures were so low that the resolution of the pressure-measuring system became inadequate, and there was insufficient time to change it.

Our results match the trend of those at lower Reynolds numbers, as well as this can be determined from the multivalued behaviour, and it is apparent that C_d increases in the range $10^6 < R < 3{\cdot}5 \times 10^6$, from a value of about 0·3 to about 0·7, and then levels off at the latter value. It will be noted presently that the value $R = 3{\cdot}5 \times 10^6$ apparently marks the end of a transition range.

Also shown on figure 2 is the value of C_d obtained by Dryden & Hill (1930) in some experiments that are apparently not well known. These measurements were made on a smoke stack with a clear height of 120 ft., the values of C_d being obtained from pressure distributions at a section 41 ft. from the top, where the

diameter was 11·8 ft. The wind speeds were about 25–40 m.p.h., which corresponds to Reynolds numbers of $3–5 \times 10^6$. Their mean value of C_d for a group of observations is $0·67 \pm 0·04$, and it may be seen that this agrees quite well with our results. A point of interest is that Dryden & Hill inferred the wind speed from the measurements on the cylinder, making use of the fact that the maximum pressure is stagnation pressure, while the pressure at 31° on either side of that point must be nearly static pressure. For experiments in the natural wind, this technique is clearly better than one using a velocity measurement at some location removed from the cylinder.

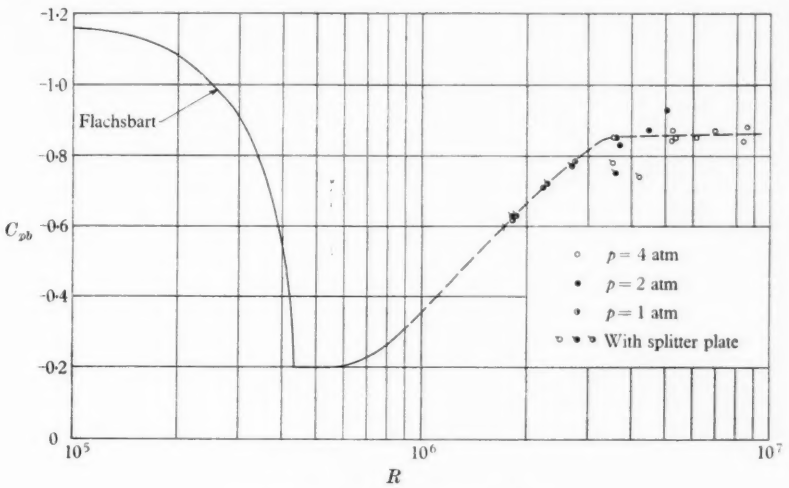

FIGURE 3. Base pressure coefficient.

In another set of experiments with a short stack ($l = 30$ ft., $d = 10$ ft.), Dryden & Hill obtained much lower values of C_d (approximately 0·4) at the same values of R. The lower value may be attributed to the small length–diameter ratio, as may the similar results of Pechstein (1940) on a cylinder of length 10 m and diameter 2 m in a natural wind.

(*b*) *Base pressure coefficient*

Changes in C_d are closely related to changes in C_{pb}, the pressure coefficient on the back of the cylinder. This was determined from the average pressure over 20 or 30° on either side of the rearmost point. The results (corrected values) are plotted in figure 3, together with a curve obtained by Flachsbart (1929) at lower Reynolds numbers. The curve determined by our points is faired into Flachsbart's curve. (We have not included other investigators' results on this plot; inclusion of these would show a scatter or multivaluedness at supercritical Reynolds numbers, like that on the $C_d(R)$ curve.)

(c) *Pressure distribution*

A pressure distribution at one of the highest Reynolds numbers ($8{\cdot}4 \times 10^6$) is shown in figure 4, in which the corrected pressure coefficient C_p is plotted against θ, the angle measured from the stagnation point. Shown for comparison are typical pressure distributions at lower Reynolds numbers, $R = 1{\cdot}1 \times 10^5$, which

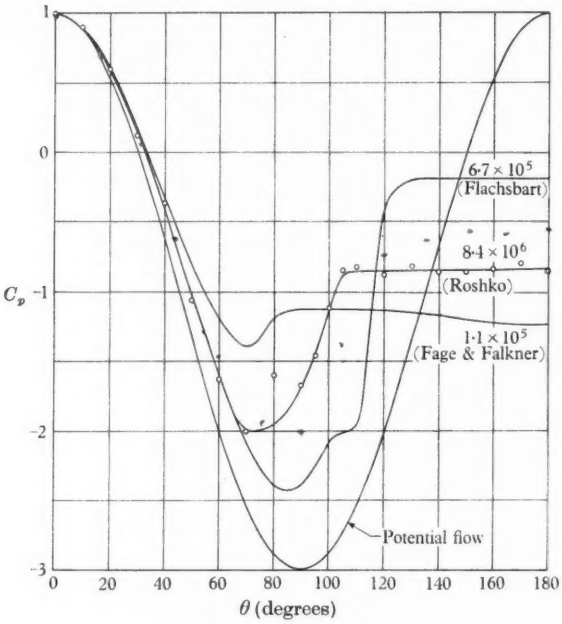

FIGURE 4. Pressure distributions.

is typical of subcritical Reynolds numbers, and $R = 6{\cdot}7 \times 10^5$, which is typical of Reynolds numbers just above the critical transition to low values of C_d. Our curve, which is nearly the same as the mean curve given by Dryden, differs from the other two. It shows a base pressure coefficient which is nearer to that of the subcritical distribution, but the distribution of pressure near $\theta = 90°$ indicates that the separation point is further back than in the subcritical flow, possibly at 90° or greater. (The point at $\theta = 80°$ is a bad point; it has no significance with respect to separation.)

The pressure distributions for all our experiments are similar to this; the main effects of Reynolds number and splitter plate are on the base pressure coefficient (cf. figure 3).

(d) *Shedding frequency*

The Strouhal number S of the vortex shedding frequency is plotted against R in figure 5, together with previous measurements in the transition range and at subcritical Reynolds numbers.

It should be pointed out that, with the technique used, the measurement of S is much more accurate than that of C_d, since the accuracy does not decrease with decreasing dynamic pressure. This improved accuracy is apparent from the small scatter in $S(R)$.

Of much significance also is the fact that at our measuring station, vortex shedding was not observed at $R < 3{\cdot}5 \times 10^6$, although observations were made at all Reynolds numbers down to $0{\cdot}9 \times 10^6$. The onset of shedding at $R = 3{\cdot}5 \times 10^6$ was quite definite. Below this value no peak frequency occurred; above this value there appeared a strong spectral peak, well above the turbulence level.

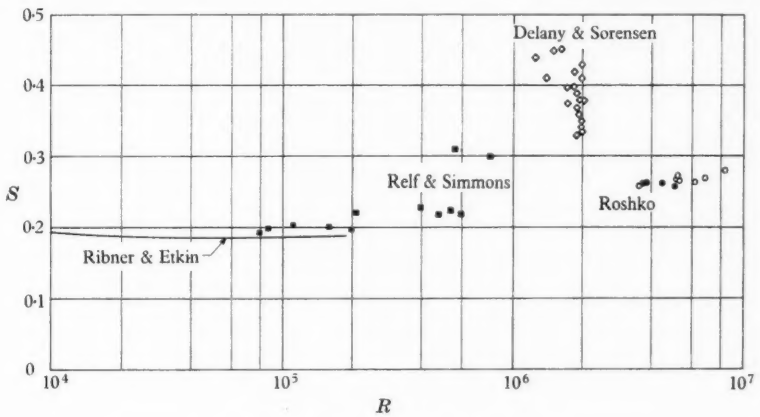

FIGURE 5. Strouhal number of vortex shedding frequency.

The (somewhat lower) harmonic (i.e. double the shedding frequency) also appeared, as is typical at subcritical Reynolds numbers for a hot wire not too far off the wake centreline. Although we were not able to make correlation measurements, say, at two wake positions, we have little doubt that what was observed was vortex shedding similar to that below $R = 10^5$.

This raises the question of why we did not observe the frequencies reported by Delany & Sorensen (1953) at values of R between 10^6 and 2×10^6. The latter measurements (as those of Relf & Simmons 1924) were made with a probe only 1 or 2 diameters behind the cylinder, whereas ours was 7·3 diameters downstream of the cylinder axis. It was not possible to move it closer during the course of our experiments. We shall return to this point later.

Relf & Simmons (1924) noted that an increase in shedding frequency is accompanied by a decrease in drag, and vice versa. This is illustrated in figure 6, in which C_d and $1/S$ are plotted over a wide range of values of R.

(*e*) *Effect of the splitter plate*

Experimental points for which the splitter plate was installed behind the cylinder are indicated on the figures by flagged symbols. The main effects of the splitter plate are as follows. (i) The shedding is suppressed; there is no indication of a peak in the spectrum. (ii) The plot of C_d (figure 2) indicates a small decrease

in C_d at values of R above $3{\cdot}5 \times 10^6$, but no effect at all at lower values. This is in contrast to the marked effect at subcritical Reynolds numbers observed in an earlier investigation (Roshko 1955). Evidence of a decrease is more obvious in figure 3, which clearly shows a decrease in $-C_{pb}$ at $R > 3{\cdot}5 \times 10^6$. (iii) There is no significant effect on the pressure distribution, other than that related to changes in the base pressure; the distributions are all similar to the example given in figure 4.

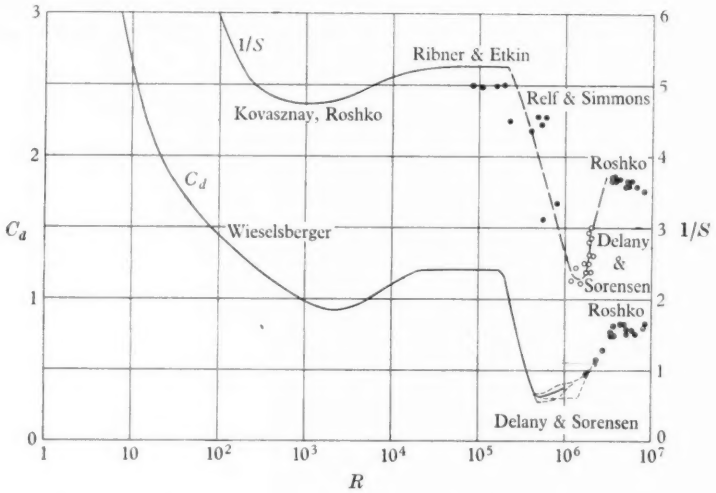

FIGURE 6. Drag coefficient and reciprocal of Strouhal number.

Unfortunately, it was not possible to go to Reynolds numbers as high as in the experiments without the splitter plate, because at the higher dynamic pressures severe flutter developed at the trailing edge of the splitter plate. The reason for this flutter is not clear; apparently it was not connected with vortex shedding off the cylinder, since this was suppressed by the plate. Possibly shedding off the trailing edge of the splitter plate itself had an effect.

5. Ideas about the flow

It was not possible in these experiments to make a detailed investigation of the wake structure, but from the results obtained we tentatively propose the following picture of the wake development.

(*a*) *Transitions and characteristic ranges*

The lower, or critical, transition at $2 \times 10^5 < R < 5 \times 10^5$, from high to low values of C_d, is followed by another (upper) transition, at $10^6 < R < 3{\cdot}5 \times 10^6$, to a new plateau on which the coefficients have the following mean values: $C_d = 0{\cdot}70$, $C_{pb} = -0{\cdot}86$, $S = 0{\cdot}267$. (Possibly the whole range from $R = 2 \times 10^5$ to $3{\cdot}5 \times 10^6$ could simply be called the transition range.) For convenience in referring to them, we call the range on either side of the lower transition 'subcritical'

($C_d = 1{\cdot}2$) and 'supercritical' ($C_d \doteqdot 0{\cdot}3$), respectively, according to established custom; let us call the plateau following the upper transition 'transcritical' ($C_d = 0{\cdot}7$).

As is well known, the (critical) Reynolds number at which the lower transition occurs can be lowered by introducing turbulence into the flow or roughness on the cylinder; we may expect a similar effect on the upper transition.

In the lower transition the wake width d_w decreases from values larger than the cylinder diameter d to values smaller than d, as the separation point moves from the front to the back of the cylinder. In the upper transition, the indication is that the wake 'opens' again, the separation point moving forward. However, it does not move to the front of the cylinder, and d_w remains less than d. This view is supported by the form of the pressure distribution (figure 4) and by the values of C_{pb} and S at transcritical Reynolds numbers; the reasons are outlined in the next section.

A rapid opening of the wake would also explain the fact that, for the narrow wakes, we did not observe shedding frequencies 7 diameters behind the cylinder whereas Delany & Sorenson did observe them close to the cylinder.

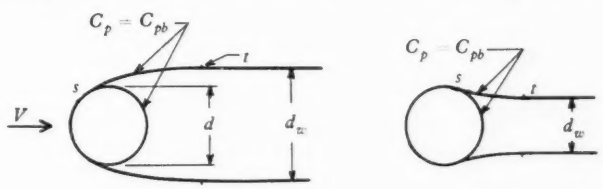

Type A ($d_w/d > 1$) Type B ($d_w/d < 1$)

FIGURE 7. Free-streamline model for relating base pressure coefficient to wake width.

(*b*) *Free-streamline model*

It has been found useful (Roshko 1954, 1955; Eppler 1954) to represent the mean flow in the vicinity of the cylinder by a free-streamline flow having the characteristics sketched in figure 7. In this model, the pressure on the wake boundary is constant ($C_p = C_{pb}$) from the separation point s to a point t at which the boundary becomes parallel to the free stream. Beyond t the wake width remains constant at the value d_w while the pressure recovers to the free stream value. In a wake of type A, which is characteristic of the subcritical region, separation is on the front of the cylinder, and $d_w/d > 1$; for type B, which is characteristic of supercritical and transcritical flow, separation is on the back of the cylinder and $d_w/d < 1$.

In some earlier work (Roshko 1954, 1955) we had postulated that the shedding frequency n must depend only on the wake parameters d_w and $V_w = V(1-C_{pw})^{\frac{1}{2}}$, and that in terms of these there must be a universal Strouhal number, defined by $S^* = nd_w/V_w$, which is independent of the body producing the wake. Thus, it is related to the conventional Strouhal number $S = nd/V$ by

$$\frac{S}{S^*} = \frac{d}{d_w}\frac{V_w}{V} = \frac{d}{d_w}(1-C_{pw})^{\frac{1}{2}}. \tag{4}$$

From experimental determinations of S and C_{pw} for circular cylinders, wedges and flat plates at subcritical Reynolds numbers, and from the theoretical relation between C_{pw} and d_w/d for flows of type A, we concluded that the universal Strouhal number has the value $S^* = 0{\cdot}16$.

Now if the nature of the vortex shedding at transcritical Reynolds numbers is basically the same as at subcritical values, then the universal Strouhal number should apply to this range also. We corroborate this as follows. It can be shown from a simple momentum consideration (Eppler 1954) that, for flows of the type shown in figure 7,

$$C_d = (-C_{ps})(d_w/d). \tag{5}$$

Applying this formula to our measurements in the transcritical range (type B), we obtain $d_w/d = 0{\cdot}70/(0{\cdot}86) = 0{\cdot}81$. This value in equation (5) then gives $S = (0{\cdot}16)(1{\cdot}86)^{\frac{1}{2}}/(0{\cdot}81) = 0{\cdot}27$, which checks very well with our mean experimental value 0·267.

These measurements seem to confirm, then, that at transcritical Reynolds numbers $d_w/d < 1$, but the vortex shedding is otherwise similar to that at subcritical values.

Attempts to make similar calculations in the supercritical régime are unsuccessful. Taking experimental values of C_d and C_{pb} from several sources, we find that calculated values of d_w/d vary from 0·3 to 1·2, the latter clearly in disagreement with observation, and calculated values of S vary from 0·15 to 0·7. We must conclude that either the experimental data in this region is inaccurate, due to an inherent capriciousness of the flow, or the free-streamline model is inapplicable here.

(c) *Effect of the splitter plate*

In experiments at subcritical Reynolds numbers (Roshko 1954) it was found that a splitter plate has a strong influence on the flow. Briefly, the flow changes from one with alternate shedding to a steady symmetrical flow in which the separation streamline reattaches on the splitter plate, forming two closed recirculation regions on either side of the plate. At Reynolds numbers of the order of 10^4, C_{pb} changes from about $-1{\cdot}0$ to $-0{\cdot}5$ and C_d from 1·2 to 0·7 (cf. figure 2).

The present experiments with a splitter plate at transcritical Reynolds numbers, while rather limited, due to the flutter problem mentioned earlier, also indicate a definite effect. The vortex shedding is stopped, C_{pb} is changed from $-0{\cdot}86$ to $-0{\cdot}76$, and C_d is changed from 0·70 to 0·63; the changes in the coefficients are not nearly so spectacular as at subcritical Reynolds numbers.

In the upper transition leading to the transcritical régime, the splitter plate appears to produce no effect whatsoever on C_d and C_{pb}. This raises the question as to whether, in the supercritical régime, there is true vortex shedding; interference with the alternating flow that must accompany vortex shedding should produce some effect.

In the experiments by Fung (1960) who measured the fluctuating forces on a cylinder at Reynolds numbers up to $1{\cdot}4 \times 10^6$, no definitely periodic force was observed, in contrast to the case at subcritical values (Ribner & Etkin 1958). Unfortunately we were not able to look for the frequencies reported by Relf & Simmons and Delany & Sorenson and to observe the effect of the splitter plate

on them, since we could not shift our hot-wire probe to a position near the cylinder.

(*d*) *Nature of the transitions*

The existence of the upper transition makes it somewhat difficult to interpret the flow in terms of the classical description of the critical Reynolds number, which is roughly as follows. 'At subcritical Reynolds numbers the separation is laminar, and occurs early on the front of the cylinder. With increasing Reynolds number, transition in the boundary layer moves ahead of the laminar separation point, the now turbulent boundary layer can withstand a greater pressure rise, and so separation moves to the rear of the cylinder, with a consequent decrease in the drag coefficient.' To include the new results in this picture we would now have to say that in the upper transition a turbulent separation moves forward, finally reaching a stationary point, still on the back of the cylinder, and C_d becomes constant.

It is probable that the actual events are somewhat more complicated. Bursnall & Loftin (1951) have pointed out that in the supercritical range there is evidence of a laminar separation 'bubble', that is, a localized region consisting of a laminar separation, transition, reattachment and turbulent separation. Such bubbles have been observed to play an important role in the stalling of thin airfoils. The occurrence of a bubble is indicated, for instance, by a 'flat' in a rising pressure distribution, such as that at about $\theta = 105°$ in Flachsbart's curve (figure 4). If the region of localized separation is small, the flat may not be so definite. It is possible that a separation bubble occurs throughout the supercritical range. On the other hand, it is certain that at sufficiently high Reynolds number there will be no bubble. We suggest that the disappearance of a separation bubble characterizes the transition from the supercritical to the transcritical régime. (We are indebted to Dr I. Tani for a discussion of this point.) This suggestion is tentative, subject to further experimental investigation, but we have no other explanation of the upper transition.

Thus we would propose the following classification: at subcritical Reynolds numbers the separation is laminar, in the supercritical range there is a laminar separation bubble followed by turbulent separation, and in the transcritical range the separation is purely turbulent.

6. Concluding remarks

It is unfortunate that the time available for our experiments was too short to permit an investigation of some of the points raised in the preceding paragraphs, particularly since facilities for obtaining such high Reynolds numbers are not generally available. But even in the more accessible range of supercritical Reynolds numbers, additional work is needed. The question of vortex shedding in this range needs more attention and a study of the development of the laminar separation bubble would be useful.

We are left with the question concerning the asymptotic nature of the flow for $R \to \infty$. What would be the further effect of increasing R beyond the values reached in our experiment? It seems unlikely that there will be any further transitions, since the point of boundary-layer transition can now only move

smoothly forward on the cylinder. This may affect the location of the separation point, but can hardly be expected to produce rapid changes. There is then the question of Reynolds number effects on the flow in the wake. To detach this problem from the problem of separation it would be very useful to have a set of experiments on a flat plate normal to the flow over as wide a range of Reynolds numbers as we now have for the circular cylinder. For a plate (or for other sharp-edged configurations, such as wedges) the separation point is fixed at the edge, and changes in C_d, C_{pb} and S must be dependent only on the effect of R on the wake mechanism. Such information should indicate the trend for $R \to \infty$.

We are indebted to the many people whose co-operation made this 'crash program' possible. The wind tunnel time was donated by the CWT owner companies, crews of the Guggenheim Aeronautical Laboratory and CWT assisted with the experiments, and the Fluid Mechanics group of the Jet Propulsion Laboratory provided instrumentation. David Russell and Dorothy Diamond assisted with the experiments and the computations, respectively.

REFERENCES

Allen, H. J. & Vincenti, W. G. 1944 Wall interference in a two-dimensional-flow wind tunnel, with consideration of the effect of compressibility. *Nat. Adv. Comm. Aero., Wash., Rep.* 782.

Bursnall, W. J. & Loftin, L. K. 1951 Experimental investigation of localized regions of laminar boundary layer separation. *Nat. Adv. Comm. Aero., Wash., Tech. Note* 2338.

Delany, N. K. & Sorensen, N. E. 1953 Low-speed drag of cylinders of various shapes. *Nat. Adv. Comm. Aero., Wash., Tech. Note* 3038.

Dryden, H. L. & Hill, G. C. 1930 Wind pressure on circular cylinders and chimneys. *Bur. Stand. J. Res., Wash.*, **5**, 653–93.

Eppler, R. 1954 Beiträge zu Theorie und Anwendung der unstetigen Strömungen. *J. Rational Tech. Anal.* **3**, 591–644.

Fage, A. & Falkner, V. M. 1931 The flow around a circular cylinder. *Aero. Res. Counc., Lond., Rep. and Mem.* no. 1369.

Flachsbart, O. 1929 From an article by H. Muttray 1932. *Handb. Experimentalphysik*, **4**, part 2 (Leipzig), 316.

Fung, Y. C. 1960 Fluctuating lift and drag acting on a cylinder in a flow at supercritical Reynolds numbers. *J. Aero Space Sci.* **27**, 801–14.

Kovasznay, L. S. G. 1949 Hot-wire investigation of the wake behind cylinders at low Reynolds numbers. *Proc. Roy. Soc.* A, **198**, 174–90.

Millikan, C. B. 1957 Advanced education and academic research in aeronautics. *J. R. Aero. Soc.* **61**, 793–808.

Pechstein, W. 1940 Der natürlichen Wind und seine Wirkung auf einen grösseren Kreiszylinder. *Dissertation, Tech. Hochschule Hannover*; reported by A. Pröll, 1942. *Z. Ver. dtsch. Ing.* **86**, 222–3.

Relf, E. F. & Simmons, L. F. G. 1924 The frequency of eddies generated by the motion of circular cylinders through a fluid. *Aero. Res. Counc., Lond., Rep. and Mem.* no. 917.

Ribner, H. S. & Etkin, B. 1958 Noise research in Canada. *Proc. 1st Int. Congr. Aero. Sci., Madrid* (publ. by Pergamon Press, London, 1959).

Roshko, A. 1954 On the drag and shedding frequency of bluff cylinders. *Nat. Adv. Comm. Aero., Wash., Tech. Note* 3169.

Roshko, A. 1955 On the wake and drag of bluff bodies. *J. Aero. Sci.* **22**, 124–32.

Wieselsberger, C. 1921 Neuere Feststellungen über die Gesetze des Flüssigkeits- und Luftwiderstands. *Phys. Z.* **22**, 321–8.

A dispersion relation for waves of finite amplitude in a two-stream plasma

By F. D. KAHN
Department of Astronomy, University of Manchester

(Received 28 October 1960)

A dispersion relation is derived for plane space-charge waves of finite amplitude in a plasma containing two oppositely charged streams of particles. The relation may be expressed simply in parametric form; it can also be quite well approximated, in two different ranges of amplitude, by expressions for the wavelength in terms of the maximum variation of the electrostatic potential.

1. Introduction

Much interest has been shown, during the past few years, in the properties of space-charge waves in a two-stream plasma. This is the simplest kind of plasma with a velocity dispersion, and yet it shows up some of the most common properties of plasmas in general. For example, linearized theory predicts that an oscillation in such a plasma can be exponentially amplified when its wavelength is below a certain critical value, determined by the densities and the relative velocity of the two streams, and the masses and the charges of the particles in them (see, for example, Kahn 1957). Buneman (1958) has proposed that this tendency to instability may prohibit too rapid a flow of electrons past the ions in a plasma, and may thus set a limit to the current density which can be attained. However, it has not apparently been possible yet to verify by experiment that the predicted instability exists, because the spread of velocities in each plasma stream cannot yet be made sufficiently small (Nexsen, Cummins, Coensgen & Sherman 1960).

An analytical expression, in parametric form, is derived in this paper for the dispersion relation of a two-stream plasma. The result is valid for finite amplitudes, but applies only to cases in which the two plasma streams are oppositely charged, and where neither set of particles is trapped by the wave. We shall consider only steady waves; however, the formulae here established can probably be used to study some classes of amplified space charge waves to an approximation higher than the linear one, and the author hopes to do this in another paper.

It is, of course, known that the problem of the construction of a plasma wave of finite and constant amplitude can be reduced to that of performing a quadrature (see, for example, Bernstein, Greene & Kruskal 1957). Thus let the wave pattern be at rest in the chosen co-ordinate system, let the mean densities of particles in the streams be $\overline{n}_r$, the particle masses m/μ_r, the particle charges $Z_r e$ and the particle energies χ_r ($r = 1, 2, 3, \ldots$). At a point where the electrostatic potential is V, the particle velocities will be

$$u_r = \sqrt{\{(2\mu_r/m)(\chi_r - Z_r eV)\}}. \tag{1}$$

We restrict our further discussion to the case in which none of the particles are trapped, so that u_r never vanishes or changes sign. If F_r is the particle flux in the rth stream, the particle density there will be

$$n_r = F_r/u_r, \tag{2}$$

and then Poisson's equation gives that

$$\frac{d^2V}{dx^2} = -4\pi e\Sigma\frac{Z_r F_r}{u_r}, \tag{3}$$

provided there is overall space charge neutrality, or

$$\Sigma\bar{n}_r Z_r = 0. \tag{4}$$

The right-hand side of (3) is a function of V only; the first integral of this equation can therefore be found immediately. A further quadrature gives x as a function of V, and, on inversion, V as a function of x. Thus an expression can be found for the wavelength of the plasma wave; the result will then be given in terms of the particle fluxes F_r and energies χ_r. From these results one can also find the values of $\bar{n}_r$ and of the mean velocities $\bar{u}_r$ of the different kinds of particle, and in principle the dispersion relation can then be expressed in terms of them, rather than in terms of F_r and χ_r, if desired.

But the process we have described involves much numerical work. In the next section we shall show how this may be avoided for the case of a two-stream plasma.*

2. A derivation of the dispersion relation

We begin the derivation with the help of the equations of motion and continuity and Poisson's equation for two oppositely charged streams of particles. Once again the frame of reference is chosen so that the wave pattern is stationary. We have:

the equations of motion

$$u_1\frac{du_1}{dx} = \frac{\mu_1 Z_1 e}{m}E, \tag{5}$$

$$u_2\frac{du_2}{dx} = \frac{\mu_2 Z_2 e}{m}E; \tag{6}$$

the equations of continuity

$$n_1 u_1 = \bar{n}_1\bar{u}_1, \tag{7}$$

$$n_2 u_2 = \bar{n}_2\bar{u}_2; \tag{8}$$

Poisson's equation

$$\frac{dE}{dx} = 4\pi e(n_1 Z_1 + n_2 Z_2), \tag{9}$$

and the condition of overall space-charge neutrality

$$\bar{n}_1 Z_1 + \bar{n}_2 Z_2 = 0. \tag{10}$$

* Langmuir (1929) has solved, by numerical integration, a problem of this kind for an ion-electron plasma.

The symbols u_r, μ_r, Z_r, n_r, x, $\overline{u}_r$ and $\overline{n}_r$ have the same meaning as they had in § 1, and further E = electric field intensity. The equations are made dimensionless by the substitutions

$$U_r = u_r/\overline{u}_r, \tag{11}$$

$$1 + S_r = n_r/\overline{n}_r, \tag{12}$$

$$k^2 = \frac{4\pi e^2}{m}\left(\frac{\overline{n}_1\mu_1 Z_1^2}{\overline{u}_1^2} + \frac{\overline{n}_2\mu_2 Z_2^2}{\overline{u}_2^2}\right), \tag{13}$$

$$X = kx, \tag{14}$$

$$\tan^2\epsilon = \frac{\overline{n}_1\mu_1 Z_1^2}{\overline{u}_1^2}\Big/\frac{\overline{n}_2\mu_2 Z_2^2}{\overline{u}_2^2}, \tag{15}$$

$$\mathscr{E} = \frac{k\sin\epsilon\cos\epsilon}{4\pi\overline{n}_1 Z_1 e}E; \tag{16}$$

in virtue of the condition of overall space charge neutrality (10), the relation (15) is equivalent to

$$\tan^2\epsilon = \frac{\mu_1|Z_1|}{\overline{u}_1^2}\Big/\frac{\mu_2|Z_2|}{\overline{u}_2^2}. \tag{17}$$

Finally, one can assume without loss of generality that Z_1 is positive and that $\tan^2\epsilon \geqslant 1$, so that

$$\tfrac{1}{4}\pi \leqslant \epsilon \leqslant \tfrac{1}{2}\pi. \tag{18}$$

Equations (5) to (10) are then equivalent to

$$U_1\frac{dU_1}{dX} = \mathscr{E}\tan\epsilon, \tag{19}$$

$$U_2\frac{dU_2}{dX} = -\mathscr{E}\cot\epsilon, \tag{20}$$

$$U_1(1+S_1) = 1, \tag{21}$$

$$U_2(1+S_2) = 1, \tag{22}$$

and

$$\frac{d\mathscr{E}}{dX} = \left(\frac{1}{U_1} - \frac{1}{U_2}\right)\sin\epsilon\cos\epsilon. \tag{23}$$

It follows from (19) and (20) that

$$U_1^2\cot\epsilon + U_2^2\tan\epsilon = \text{constant} = A^2, \quad \text{say.} \tag{24}$$

Hence U_1 and U_2 can be expressed in the form

$$U_1 = A\cos\phi\tan^{\frac{1}{2}}\epsilon \tag{25}$$

and

$$U_2 = A\sin\phi\cot^{\frac{1}{2}}\epsilon. \tag{26}$$

We have restricted the discussion to the case in which no particles are trapped, so that all the particles in a given stream move in the same direction at all times. The dimensionless variables $U_r \equiv u_r/\overline{u}_r$ are therefore always positive, and it follows from relations (25) and (26) that $0 \leqslant \phi \leqslant \frac{1}{2}\pi$, if A is positive. With the aid of (25) and (26), equations (19) and (20) both reduce to

$$-A^2\sin\phi\cos\phi\frac{d\phi}{dX} = \mathscr{E}. \tag{27}$$

With the substitution $$dX = \kappa \sin\phi \cos\phi \, d\tau \tag{28}$$

this equation becomes $$-\frac{A^2}{\kappa}\frac{d\phi}{d\tau} = \mathscr{E}. \tag{29}$$

With the aid of (25), (26) and (28), equation (23) becomes

$$\begin{aligned}\frac{d\mathscr{E}}{d\tau} &= \frac{\kappa}{A}\sin\epsilon\cos\epsilon(\sin\phi\cot^{\frac{1}{2}}\epsilon - \cos\phi\tan^{\frac{1}{2}}\epsilon)\\ &= \frac{\kappa}{A}(\sin\epsilon\cos\epsilon)^{\frac{1}{2}}\sin(\phi-\epsilon).\end{aligned} \tag{30}$$

From (29) and (30) it follows that

$$\frac{A^3}{\kappa^2(\sin\epsilon\cos\epsilon)^{\frac{1}{2}}}\frac{d^2\phi}{d\tau^2} + \sin(\phi-\epsilon) = 0. \tag{31}$$

Let $$\kappa = \frac{A^{\frac{3}{2}}}{(\sin\epsilon\cos\epsilon)^{\frac{1}{4}}}, \tag{32}$$

then $$\frac{d^2\phi}{d\tau^2} + \sin(\phi-\epsilon) = 0. \tag{33}$$

This equation has the first integral

$$\frac{d\phi}{d\tau} = [2\{\cos(\phi-\epsilon) - \cos\alpha\}]^{\frac{1}{2}}, \tag{34}$$

where α is an arbitrary angle. Values of ϕ therefore lie in the range $(\epsilon-\alpha, \epsilon+\alpha)$. Since $\cos\phi$ must not change sign, the range of permissible values of α is limited by $\alpha+\epsilon \leqslant \frac{1}{2}\pi$, or

$$\alpha \leqslant \tfrac{1}{2}\pi - \epsilon. \tag{35}$$

But our variables were chosen so that $\frac{1}{4}\pi \leqslant \epsilon \leqslant \frac{1}{2}\pi$, and so

$$\alpha \leqslant \tfrac{1}{4}\pi. \tag{36}$$

The condition that $\sin\phi$ shall not change sign is given by $\epsilon - \alpha \geqslant 0$, and this always holds, since ϵ exceeds and α is less than $\frac{1}{4}\pi$.

Now $d\phi/d\tau$ vanishes at $\phi = \epsilon-\alpha$ and $\phi = \epsilon+\alpha$. The expression on the right-hand side of (34) can be positive or negative; it follows that ϕ is periodic in τ, and therefore also in X. In dimensionless units the wavelength of the oscillation described by these equations becomes

$$\begin{aligned}\Lambda &= 2\int_{\phi=\epsilon-\alpha}^{\phi=\epsilon+\alpha} dX = 2\kappa\int_{\phi=\epsilon-\alpha}^{\phi=\epsilon+\alpha}\sin\phi\cos\phi\,d\tau\\ &= 2A^{\frac{3}{2}}(\sin\epsilon\cos\epsilon)^{-\frac{1}{4}}\int_{\epsilon-\alpha}^{\epsilon+\alpha}\frac{\sin\phi\cos\phi\,d\phi}{[2\{\cos(\phi-\epsilon)-\cos\alpha\}]^{\frac{1}{2}}}\\ &= 2^{\frac{1}{4}}A^{\frac{3}{2}}\sin^{-\frac{1}{4}}2\epsilon\int_{-\alpha}^{\alpha}\frac{\sin 2(\psi+\epsilon)\,d\psi}{\{2(\cos\psi-\cos\alpha)\}^{\frac{1}{2}}}\\ &= 2^{\frac{3}{4}}A^{\frac{3}{2}}\sin^{\frac{3}{4}}2\epsilon\int_{0}^{\alpha}\frac{\cos 2\psi\,d\psi}{(\cos\psi-\cos\alpha)^{\frac{1}{2}}}\\ &\equiv 2^{\frac{1}{4}}\pi A^{\frac{3}{2}}\sin^{\frac{3}{4}}2\epsilon\, I_2(\alpha).\end{aligned} \tag{37}$$

In (37), and from now on, we define

$$I_r(\alpha) = \frac{\sqrt{2}}{\pi}\int_0^{\alpha} \frac{\cos r\psi\, d\psi}{(\cos\psi - \cos\alpha)^{\frac{1}{2}}}. \tag{38}$$

A subsidiary condition to be satisfied is that the space average of S_1 shall vanish and therefore

$$\int_{\phi=\epsilon-\alpha}^{\phi=\epsilon+\alpha} \left(1 - \frac{1}{U_1}\right) dX = 0. \tag{39}$$

This is equivalent to

$$\begin{aligned}\Lambda \equiv 2\int_{\phi=\epsilon-\alpha}^{\phi=\epsilon+\alpha} dX &= 2\int_{\phi=\epsilon-\alpha}^{\phi=\epsilon+\alpha} \frac{dX}{U_1} \\ &= 2A^{\frac{3}{2}}(\sin\epsilon\cos\epsilon)^{-\frac{1}{4}} \int_{\epsilon-\alpha}^{\epsilon+\alpha} \frac{\sin\phi\cos\phi\, d\phi}{A\cos\phi\tan^{\frac{1}{2}}\epsilon[2\{\cos(\phi-\epsilon)-\cos\alpha\}]^{\frac{1}{2}}} \\ &= 2^{\frac{3}{2}}A^{\frac{1}{2}}(\sin\epsilon\cos\epsilon)^{\frac{1}{4}} \int_0^{\alpha} \frac{\cos\psi\, d\psi}{(\cos\psi-\cos\alpha)^{\frac{1}{2}}} \\ &= 2^{\frac{3}{2}}\pi A^{\frac{1}{2}}\sin^{\frac{1}{4}} 2\epsilon\, I_1(\alpha). \end{aligned} \tag{40}$$

Comparison of (37) and (40) now shows that the expression for A in terms of α is

$$A = 2^{\frac{1}{2}}\sin^{-\frac{1}{2}} 2\epsilon\, I_1(\alpha)/I_2(\alpha). \tag{41}$$

Equation (37) then gives

$$\Lambda = 2\pi I_1^{\frac{3}{2}}(\alpha)/I_{\frac{1}{2}}^{\frac{1}{2}}(\alpha). \tag{42}$$

The total variation of electrostatic potential in the wave is, in dimensionless units,

$$\Delta\mathscr{V} = \left|\int_{\phi=\epsilon-\alpha}^{\phi=\epsilon+\alpha} \mathscr{E}\, dX\right|, \tag{43}$$

and by equation (29)

$$\begin{aligned}\int_{\phi=\epsilon-\alpha}^{\phi=\epsilon+\alpha} \mathscr{E}\, dX &= -A^2\int_{\phi=\epsilon-\alpha}^{\phi=\epsilon+\alpha} d\phi\, \frac{dX}{\kappa\, d\tau} \\ &= -A^2\int_{\epsilon-\alpha}^{\epsilon+\alpha} \sin\phi\cos\phi\, d\phi, \end{aligned} \tag{44}$$

by virtue of relation (28). Hence

$$\begin{aligned}\Delta\mathscr{V} &= \tfrac{1}{4}A^2\{\cos 2(\epsilon-\alpha) - \cos 2(\epsilon+\alpha)\} \\ &= \tfrac{1}{2}A^2\sin 2\epsilon\sin 2\alpha = \frac{I_1^2(\alpha)}{I_{\frac{1}{2}}^2(\alpha)}\sin 2\alpha, \end{aligned} \tag{45}$$

with the aid of (41).

Equations (42) and (45) express, in terms of the parameter α, the relation between the wavelength Λ and the maximum variation $\Delta\mathscr{V}$ of the potential.

Another quantity of interest is the space average $\langle U_r\rangle_{\mathrm{sp}}$ of the particle velocities in the rth stream. This will be needed in later discussions of the stability of different kinds of plasma waves. For the particles in the first stream we have, in dimensionless units, that

$$\begin{aligned}\langle U_1\rangle_{\mathrm{sp}} &= \frac{2}{\Lambda}\int_{\phi=\epsilon-\alpha}^{\phi=\epsilon+\alpha} U_1\, dX \\ &= \frac{2}{\Lambda}\int_{\epsilon-\alpha}^{\epsilon+\alpha} \frac{A\cos\phi\tan^{\frac{1}{2}}\epsilon\,\kappa\sin\phi\cos\phi\, d\phi}{[2\{\cos(\phi-\epsilon)-\cos\alpha\}]^{\frac{1}{2}}} \\ &= \frac{2^{\frac{1}{2}}A^{\frac{5}{2}}\sin^{\frac{1}{4}}\epsilon}{\Lambda\cos^{\frac{3}{4}}\epsilon}\int_{\epsilon-\alpha}^{\epsilon+\alpha} \frac{\sin\phi\cos^2\phi\, d\phi}{\{\cos(\phi-\epsilon)-\cos\alpha\}^{\frac{1}{2}}}. \end{aligned} \tag{46}$$

With the usual substitution $\phi = \psi + \epsilon$, with formulae (41) and (42) for Λ and A, and after some reductions, one finds that (46) becomes

$$\langle U_1 \rangle_{\rm sp} = \frac{I_1(\alpha)}{4I_2^2(\alpha)\sin\epsilon\cos^2\epsilon}\{I_1(\alpha)\sin\epsilon + I_3(\alpha)\sin 3\epsilon\}$$

$$\equiv \frac{I_1(\alpha)}{I_2^2(\alpha)}[I_3(\alpha) + \tfrac{1}{4}\{I_1(\alpha) - I_3(\alpha)\}\sec^2\epsilon]; \tag{47}$$

similarly $$\langle U_2 \rangle_{\rm sp} = \frac{I_1(\alpha)}{I_2^2(\alpha)}[I_3(\alpha) + \tfrac{1}{4}\{I_1(\alpha) - I_3(\alpha)\}\operatorname{cosec}^2\epsilon]. \tag{48}$$

3. Discussion of formulae and some numerical results

We first consider the results predicted in the limit $\Delta\mathscr{V} \to 0$. This has two possible physical meanings, for it follows from formulae (14) and (16) that, in terms of the physical variables,

$$\Delta\mathscr{V} = \frac{k^2\sin\epsilon\cos\epsilon\,\Delta V}{4\pi\bar{n}_1 Z_1 e}. \tag{49}$$

Therefore the limit may imply that $\Delta V \to 0$, so that the variation of the physical potential is small, and the properties of the wave can be discussed by means of the linearized equations. Alternatively the limit may imply that $\cos\epsilon \to 0$, so that $\tan\epsilon \to \infty$, and by relation (17), that

$$\mu_2|Z_2|/\bar{u}_2^2 \to 0. \tag{50}$$

(The possibility that $\sin\epsilon$ tends to zero is excluded, because ϵ must exceed $\frac{1}{4}\pi$.) The physical meaning of (50) is that the particles in the second stream either have a large mass m/μ_2, or a small specific charge $Z_2 e$, or a high mean velocity $\bar{u}_2$ relative to the wave pattern. In any of these cases their motion is only slightly disturbed by the electrostatic field of the plasma wave; the second stream therefore essentially acts as a neutralizing background charge to an oscillation, possibly one of finite amplitude, which is taking place in the first stream.

It is readily shown that $\Delta\mathscr{V}$ and α tend to zero together, since, for small α,

$$I_r(\alpha) \doteqdot \frac{\sqrt{2}}{\pi}\int_0^\alpha \frac{d\psi}{\{\frac{1}{2}(\alpha^2 - \psi^2)\}^{\frac{1}{2}}} = 1, \tag{51}$$

for all values of r, and it follows from (45) that then

$$\Delta\mathscr{V} \doteqdot \sin 2\alpha \doteqdot 2\alpha. \tag{52}$$

Relations (42) and (51) show that, in this limit

$$\Lambda = 2\pi. \tag{53}$$

The wavelength of such oscillations, expressed in physical units, is

$$\lambda = \frac{2\pi}{k}, \tag{54}$$

with k given by (13). Our result therefore agrees with that of linearized theory in the case $\Delta V \to 0$. Our prediction, in the case $\mu_2|Z_2|/\bar{u}_2^2 \to 0$, is the same as in (54), with k now given by

$$k^2 = \frac{4\pi\bar{n}_1 e^2 \mu_1 Z_1^2}{m\bar{u}_1^2}. \tag{55}$$

Here the wavelength of the oscillation is independent of the amplitude, given the nature and density of the particles in the first stream, and their mean speed relative to the wave pattern. This prediction agrees with the results found by Polovin (1956) in his note on exact non-linear plasma oscillations of a single stream of particles—Polovin actually shows that, viewed from a frame of reference in which the plasma has no mean velocity, the frequency of the oscillation is independent of its amplitude. Now in dimensionless units this frequency is $2\pi/\Lambda$; our result is therefore equivalent to Polovin's.

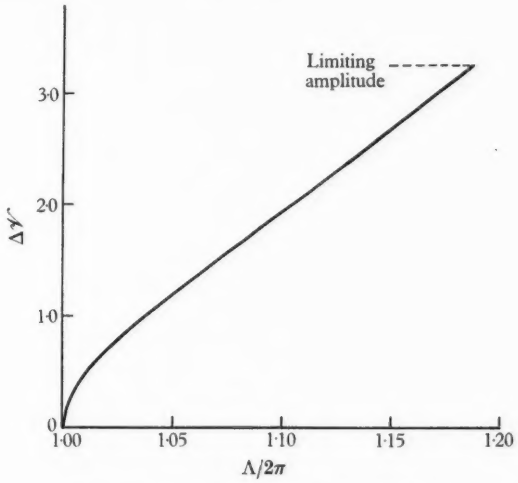

FIGURE 1. A plot of $\Delta\mathscr{V}$ against $\Lambda/2\pi$.

In a general case, with given values for μ_r, Z_r, $\bar{n}_r$ and $\bar{u}_r$, the wavelength is an increasing function of α, and therefore of the potential variation $\Delta\mathscr{V}$. The relation between $\Lambda/2\pi$ and $\Delta\mathscr{V}$ is readily found from equations (42) and (45); the functions $I_1(\alpha)$ and $I_2(\alpha)$ are expressible in terms of complete elliptic integrals of the first and second kind (see §290, Byrd & Friedman 1954). In the present case, with α restricted to the range $(0, \frac{1}{4}\pi)$, the I_r functions may also be expressed, to better than one per cent accuracy, in terms of elementary functions, and this is done in the appendix.

The table below gives some representative values of $\Lambda/2\pi$ in terms of $\Delta\mathscr{V}$, and figure 1 shows graphically how the two quantities are related. It will be seen that, for values of $\Delta\mathscr{V}$ larger than about 0·7, the dispersion relation is very well approximated by

$$\frac{\Lambda}{2\pi} = 1 + 0{\cdot}0654(\Delta\mathscr{V} - 0{\cdot}400). \tag{56}$$

For smaller values of $\Delta\mathscr{V}$, and therefore of α, one can see, from the formulae in the appendix, that

$$I_1(\alpha) \doteqdot 1 - 3\alpha^2/16 \quad \text{and} \quad I_2(\alpha) = 1 - 15\alpha^2/16, \tag{57}$$

so that

$$\frac{\Lambda}{2\pi} \doteqdot 1 + \frac{3\alpha^2}{16}. \tag{58}$$

In this range

$$\Delta\mathscr{V} \equiv \frac{I_1^2(\alpha)}{I_2^2(\alpha)} \sin 2\alpha \doteq \left(1+\frac{3\alpha^2}{2}\right)\left(2\alpha-\frac{4\alpha^3}{3}\right),$$

and so

$$\alpha \doteq \frac{\Delta\mathscr{V}}{2}\left\{1-\frac{5(\Delta\mathscr{V})^2}{24}\right\}. \tag{59}$$

It follows from (58) and (59) that the approximate dispersion relation for small $\Delta\mathscr{V}$, is

$$\frac{\Lambda}{2\pi} \doteq 1+\frac{3(\Delta\mathscr{V})^2}{64}\left\{1-\frac{5(\Delta\mathscr{V})^2}{12}\right\}. \tag{60}$$

A table of selected values of the dimensionless wavelength $\Lambda/2\pi$ in terms of the dimensionless potential variation $\Delta\mathscr{V}$. The maximum possible value of $\Delta\mathscr{V}$ in a double stream is 3·284 if there are to be no trapped particles.

$\Delta\mathscr{V}$	0·694	1·089	1·498	1·983	2·589	3·284
$\Lambda/2\pi$	1·020	1·043	1·073	1·104	1·144	1·188

Appendix: Elementary expressions for $I_r(\alpha)$

Formulae for $I_r(\alpha)$, correct to better than 1 % in the range $0 \leqslant \alpha \leqslant \frac{1}{4}\pi$, can be worked out as follows.

We have

$$I_r(\alpha) = \frac{\sqrt{2}}{\pi}\int_0^\alpha \frac{\cos r\psi\, d\psi}{(\cos\psi-\cos\alpha)^{\frac{1}{2}}}. \tag{61}$$

For integral values of r, $\cos r\psi$ can be expressed as a polynomial in terms of $\cos\psi$, say $\cos r\psi = F_r(\cos\psi)$. Let

$$\cos\psi = 1-2\sin^2\tfrac{1}{2}\alpha\sin^2\theta, \tag{62}$$

then $\theta = 0$ when $\psi = 0$, and $\theta = \frac{1}{2}\pi$ when $\psi = \alpha$. Further

$$\cos\psi-\cos\alpha = 2\sin^2\tfrac{1}{2}\alpha\cos^2\theta, \tag{63}$$

$$\sin\psi = 2\sin\tfrac{1}{2}\alpha\sin\theta(1-\sin^2\tfrac{1}{2}\alpha\sin^2\theta)^{\frac{1}{2}}, \tag{64}$$

and

$$d\psi = \frac{2\sin\tfrac{1}{2}\alpha\cos\theta\, d\theta}{(1-\sin^2\tfrac{1}{2}\alpha\sin^2\theta)^{\frac{1}{2}}}. \tag{65}$$

Thus

$$I_r(\alpha) = \frac{2}{\pi}\int_0^{\frac{1}{2}\pi} \frac{F_r(1-2\sin^2\tfrac{1}{2}\alpha\sin^2\theta)}{(1-\sin^2\tfrac{1}{2}\alpha\sin^2\theta)^{\frac{1}{2}}}\, d\theta. \tag{66}$$

In the present application $\alpha \leqslant \frac{1}{4}\pi$, and therefore

$$\sin^2\tfrac{1}{2}\alpha\sin^2\theta \leqslant \tfrac{1}{4}(2-\sqrt{2}) \doteq 0{\cdot}147,$$

for all possible θ. In writing

$$(1-\sin^2\tfrac{1}{2}\alpha\sin^2\theta)^{-\frac{1}{2}} \doteq 1+\tfrac{1}{2}\sin^2\tfrac{1}{2}\alpha\sin^2\theta \tag{67}$$

we thus make an error smaller than

$$\tfrac{3}{8}\sin^4\tfrac{1}{2}\alpha \leqslant 0{\cdot}0081. \tag{68}$$

Thus the integrand in (66) can be well approximated by a polynomial in $\sin^2\theta$; when this is done, the integration is straightforward.

After some reductions the following expressions are found for $I_0(\alpha)$, $I_1(\alpha)$, $I_2(\alpha)$ and $I_3(\alpha)$:

$$I_0(\alpha) \doteqdot (9-\cos\alpha)/8, \tag{69}$$

$$I_1(\alpha) \doteqdot (17+18\cos\alpha-3\cos^2\alpha)/32, \tag{70}$$

$$I_2(\alpha) \doteqdot (-11+21\cos\alpha+27\cos^2\alpha-5\cos^3\alpha)/32, \tag{71}$$

$$I_3(\alpha) \doteqdot (-39-116\cos\alpha+138\cos^2\alpha+180\cos^3\alpha-35\cos^4\alpha)/128. \tag{72}$$

REFERENCES

Bernstein, I. B., Greene, J. M. & Kruskal, M. D. 1957 *Phys. Rev.* **108**, 546.

Buneman, O. 1958 *Phys. Rev. Letters*, **1**, 8.

Byrd, P. F. & Friedman, M. D. 1954 *Handbook of Elliptic Integrals*. Berlin: Springer Verlag.

Kahn, F. D. 1957 *J. Fluid Mech.* **2**, 601.

Langmuir, I. 1929 *Phys. Rev.* **31**, 954.

Nexsen, W. R., Cummins, W. F., Coensgen, F. H. & Sherman, A. E. 1960 *Phys. Rev.* **119**, 1457.

Polovin, R. V. 1956 *J.E.T.P.* **31**, 354. (English translation in *Soviet Physics*, **4**, 290, 1957.)

Spectral flatness factor and 'intermittency' in turbulence and in non-linear noise

By D. A. KENNEDY AND S. CORRSIN
Mechanics Department, The Johns Hopkins University

(15 November 1960)

The flatness factor F of the signal transmitted through a band-pass filter has been measured for the turbulence in a free shear layer and for a squared Gaussian noise. They both show flatness factor increasing with centre frequency f_c. In the turbulence, band-passed signals look intermittent and have larger F than the full signal, but in the squared noise, band-passed signals all have smaller F than the full signal although they look more intermittent.

It is shown analytically that the derivative of a smoothed, squared Gaussian noise may have flatness factor either greater or less than the undifferentiated signal.

Batchelor & Townsend (1949) and Sandborn (1959) have shown experimentally that the fine structure of turbulence in grid flow, wakes and boundary layers tends to be intermittent (see also Batchelor 1949). The former experiments used essentially high-pass filters (the effect of successive differentiations). The latter used band-pass filters. A possible measure of intermittency in an intermittent variable b is the amount by which the flatness factor

$$F \equiv \overline{b^4}/(\overline{b^2})^2 \tag{1}$$

(also called kurtosis) exceeds the value 3·0 that is appropriate to a variable with Gaussian (or 'normal') probability density. Of course, this measure is useful only if the 'on' part of the intermittent variable is roughly Gaussian.

For the turbulence, qualitative explanation in terms of strong localization of vorticity into sheets and/or lines has been offered convincingly by Batchelor & Townsend. This vortex stretching is a result of the non-linear, convective acceleration term in the Navier–Stokes equations, so it seemed relevant to see whether other (simpler) non-linear random systems show similar spectral kurtosis properties. No analogy is implied between the squared Gaussian noise and turbulence.

Turbulent shear layer

A constant current hot-wire anemometer circuit was used. The hot-wire sensing element was mounted 12 in. downstream of the exit of an 18 in. square duct, on the extrapolation line of the wall (figure 1). The inside duct boundary layer was turbulent and about $\frac{1}{2}$ in. thick. The free-stream velocity was 25 ft./sec; the mean velocity at the wire was about half of that. No general intermittency at the wire was detectable on an oscilloscope. The flatness factor of the full turbulence signal (component along the flow) was 3·0.

Figure 2 is a block diagram of the measuring devices. The variable band-pass filter had a half-power point band width equal to half the centre frequency: $\Delta f/f_c \approx 0{\cdot}5$. Sandborn shows typical oscillograms of the full turbulence signal and a filtered turbulence signal which shows some intermittency.

The flatness factors measured for a range of f_c is included in figure 4. These results are in qualitative agreement with those of Sandborn; the band-passed signal has flatness factor above 3·0 for all f_c, and increases toward larger f_c.

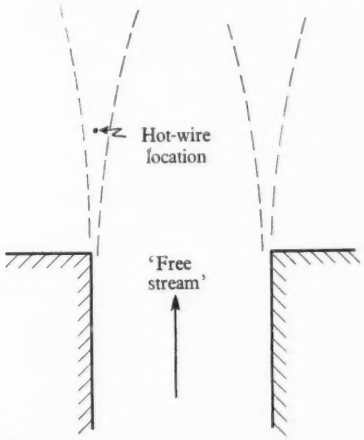

FIGURE 1. Experimental arrangement.

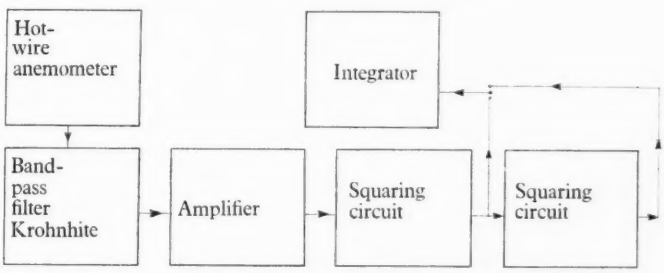

FIGURE 2. Block diagram of the measuring devices.

Gaussian noise

An electronic noise generator (H. H. Scott, type 811-A, ASA Band) was used as source of random signal with Gaussian probability density function. This was put in place of the hot-wire and its amplifier in the circuit of figure 2. As indicated in figure 4, this had a band-passed flatness factor close to 3·0. Neither of the corresponding oscillograms in figure 3, plate 1, looks particularly intermittent.

Squared Gaussian noise

As a typical simple non-linear process we chose an instantaneous squaring device. With Gaussian input, the output is a non-Gaussian random signal. The output of the noise generator was passed through an approximate squaring circuit and the

d.c. component was removed with a high-pass filter (figure 5), cutting off below 10 c/s.

The total signal does not look especially intermittent (figure 3), although its flatness factor is 9·1.* In contrast, the band-passed signals do have a more intermittent appearance (figure 3), but coupled with appreciably smaller flatness factors (figure 4).

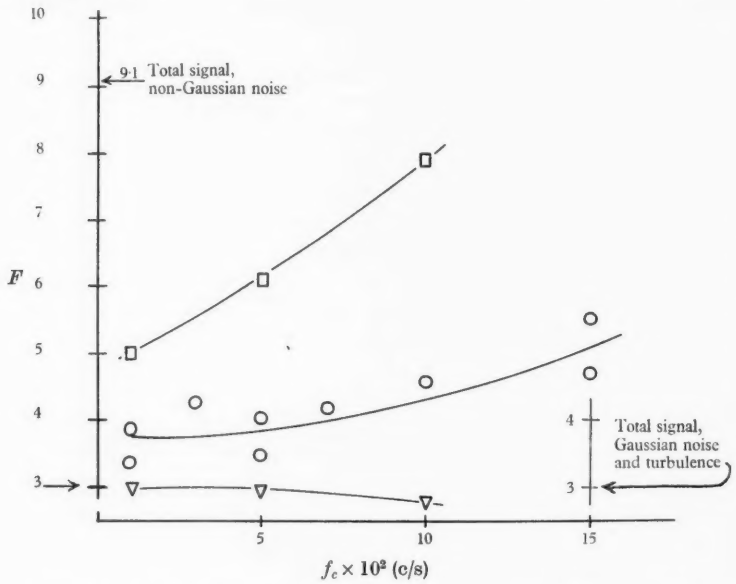

FIGURE 4. Flatness factors. ○, Free jet turbulence; □, non-Gaussian noise; ▽, Gaussian noise; $\Delta f/f_c = 0{\cdot}5$ for all cases.

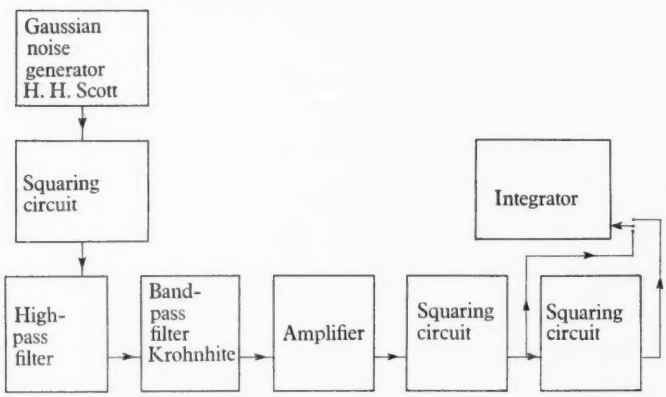

FIGURE 5. Block diagram showing use of high-pass filter.

* The theoretical value for a squared Gaussian with d.c. removed is 15. The value 9 corresponds theoretically to the power 1·7.

K

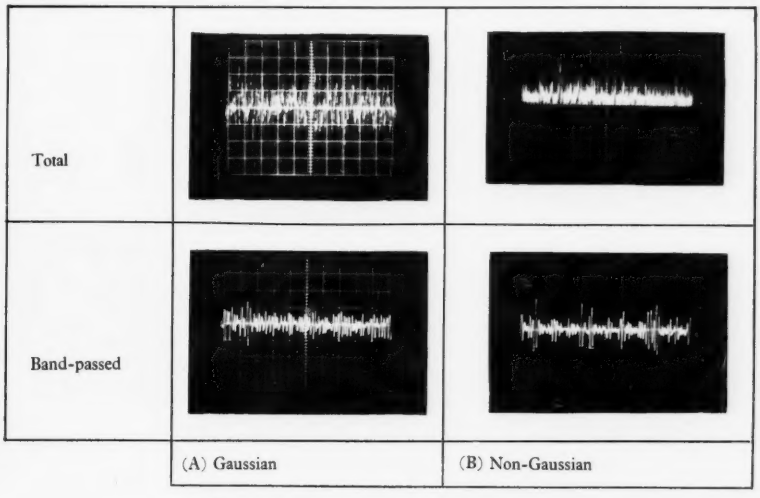

FIGURE 3. Oscillograms of 'noise'.

These results differ from the turbulence case in the two following ways.

(1) The band-passed signals here have smaller F than the total signal; for turbulence this is reversed.

(2) Here the signal with larger flatness factor (i.e. the total signal) is less intermittent in appearance; for turbulence this is reversed.

A point of similarity with the turbulence signal is that F increases with increasing f_c in both.

It seems desirable to pursue this sort of measurement through other classes of non-linear operations, especially non-linear differential equations with random forcing functions. It may turn out that the response will have flatness factor near 3 (as in some turbulent velocities) simply because it is in a sense a sum. This brings into play the effects that give us Central Limit Theorems in probability theory. In such a case we might then expect departure from Gaussian properties in the derivatives of the solution, hence in the higher frequencies. There seems to be as yet no corresponding qualitative argument to rationalize the fact that narrow-band signals in the lower frequency range (of turbulence) also have flatness factor larger than the full signal.

Finally, all such measurements should be made with a range of relative band widths extending to much smaller values than used so far.

A related exercise

Suppose $\theta(x)$ is a stationary 'Gaussian process' in the sense that the values chosen at n different points ($1 \leqslant n = \infty$) are jointly Gaussian. As we have seen, $[\theta^2(x) - \overline{\theta^2}]$ is a non-Gaussian random variable.

There is both experimental (Iribe 1949) and theoretical (Kac & Siegert 1947) evidence that the averaging ('smoothing') of a non-Gaussian variable tends to make it more nearly Gaussian. As indicated above, this is doubtless related to the conditions for Central Limit Theorems to be applicable.

Define the smoothed non-Gaussian variable

$$R_\xi(x) \equiv \frac{1}{\xi}\int_x^{x+\xi} [\theta^2(x_1) - \overline{\theta^2}]\, dx_1. \tag{2}$$

For $\xi \to 0$, it is obvious that

$$\lim_{\xi \to 0} [R_\xi(x)] = \theta^2(x) - \overline{\theta^2}. \tag{3}$$

For $\xi \to \infty$, we expect $R_\xi(x)$ to approach a Gaussian process (Kac & Siegert 1947).

Focusing attention on the flatness factor, $F_R \equiv \overline{R_\xi^4}/(\overline{R_\xi^2})^2$, we see that

$$\lim_{\xi \to 0} F_R = 15, \tag{4}$$

whereas we expect

$$\lim_{\xi \to \infty} F_R = 3. \tag{5}$$

The statistical properties of $R_\xi(x)$ are functionals of the properties of $\theta^2(x)$, so general results are difficult to obtain. However, one particular function of $R_\xi(x)$ is not only relevant here but also accessible:

$$R'_\xi(x) \equiv \frac{d}{dx} R_\xi(x) = \frac{1}{\xi}[\theta^2(x+\xi) - \theta^2(x)]. \tag{6}$$

With the condition that $\theta(x)$ is Gaussian, computation yields

$$F_{R'} \equiv \frac{\overline{R'^4_\xi}}{(\overline{R'^2_\xi})^2} = 9, \tag{7}$$

independent of ξ. This shows that for small enough ξ, the differentiated variable $R'_\xi(x)$ has smaller F than the undifferentiated one $R_\xi(x)$, whereas for large ξ it has larger F. The former situation corresponds to the measurements on squared Gaussian noise with no smoothing ($\xi = 0$). The latter result is qualitatively like that observed for turbulent velocity. We recall that differentiation is like a high-pass filter.

This work was supported by the National Science Foundation under Grant G-4542.

REFERENCES

BATCHELOR, G. K. 1949 The small-scale structure of turbulent motion. *Proc. Symp. U.S. Naval Ord. Lab.*

BATCHELOR, G. K. & TOWNSEND, A. A. 1949. The nature of turbulent motion at large wave-numbers. *Proc. Roy. Soc.* A, **199**, 238.

IRIBE, P. 1949 M.Sc. thesis, Johns Hopkins University.

KAC, M. & SIEGERT, A. J. F. 1947 On the theory of noise in radio receivers with square-law detectors. *J. Appl. Phys.* **24**, 383.

SANDBORN, V. A. 1959 Measurements of intermittency of turbulent motion in a boundary layer. *J. Fluid Mech.* **6**, 221.

Orifice flow at high Knudsen numbers

By RODDAM NARASIMHA

Guggenheim Aeronautical Laboratory, California Institute of Technology, Pasadena, California

(Received 28 November 1960)

Several interesting features of the flow field in free-molecule flow through an orifice are discussed. An estimate is then made of the deviation of the mass flow $\dot{m}$ through the orifice from its limiting free-molecule value $\dot{m}^0$ for small departures from the limit. Using an iteration method proposed by Willis, it is shown that this deviation is of the first order in ϵ, the inverse Knudsen number, defined as the ratio of the radius of the hole to the mean free path in the gas at upstream infinity. An estimate of the coefficient is obtained making some reasonable assumptions about the three-dimensional nature of the flow, and the value so derived, giving $\dot{m} = \dot{m}^0(1 + 0{\cdot}25\epsilon)$, shows fair agreement with the measurements of Liepmann. It appears that 'nearly' free-molecular conditions prevail up to $\epsilon \sim 1{\cdot}0$.

1. Introduction

The flow through an orifice has been investigated recently by Liepmann (1961) in considerable detail, especially with a view to understanding the difficult problem of the transition from gasdynamic to gaskinetic flow. As pointed out by him, the finite geometry, the relative independence from surface interaction effects and the already available knowledge (however partial!) of the flow in the limiting cases of zero and infinite Reynolds number make the circular orifice a highly worthwhile configuration for study. Liepmann's measurements were made through a range of Knudsen numbers which effectively covered the 'compressible' transition from continuum to free-molecule flow, with the pressure ratios across the orifice infinity for all practical purposes.

The purpose here is to investigate theoretically the flow under nearly free-molecular conditions. In terms of an inverse Knudsen number ϵ, defined as the ratio of the radius R of the orifice to the mean free path λ_1 in the gas far upstream, this means that we are interested in flows at small ϵ. The free-molecule or gaskinetic limit corresponds to $\epsilon \to 0$, and the mass flow rate $\dot{m}$ (per unit area) in this limit is well known from kinetic theory (Present 1958) to be

$$\dot{m}^0 = \tfrac{1}{4}\rho_1 \bar{c}_1, \tag{1.1}$$

where ρ_1 is the density and $\bar{c}_1$ the mean molecular speed at upstream infinity. In the following, attention will primarily be confined to the mass flow rate $\dot{m}$ at non-zero ϵ, as this is the quantity on which measurements are available, though all other flow quantities can also be calculated from the results.

Before proceeding further it seems worthwhile to discuss some features of the free-molecule flow itself, and this is done in § 2.

2. The free molecule limit

There is of course a definite flow field associated with even the free-molecule limit, and the field of any mean quantity, like density, pressure, etc., can be obtained by taking the appropriate moment of the molecular distribution function. Thus, if $f^0(\mathbf{v})$ denotes the distribution (the superscript 0 will always refer to free-molecule conditions), the corresponding density, 'gas' velocity, temperature and pressure, for instance, are given respectively by

$$\left.\begin{aligned} \rho^0 = mn^0 = m\int f^0(\mathbf{v})\,D\mathbf{v}, \\ \mathbf{u}^0 = \frac{1}{n^0}\int \mathbf{v} f^0(\mathbf{v})\,D\mathbf{v}, \\ T^0 = \frac{1}{2\mathscr{R}\beta^0} = \frac{1}{3\mathscr{R}n^0}\int c^2 f^0(\mathbf{v})\,D\mathbf{v}, \\ p_{ij}^0 = -m\int c_i c_j f^0(\mathbf{v})\,D\mathbf{v}, \end{aligned}\right\} \tag{2.1}$$

where m is the mass of a molecule, $\mathbf{v}$ its velocity and $\mathbf{c} = \mathbf{v} - \mathbf{u}$ the 'peculiar' velocity; $\mathscr{R}$ is the gas constant and $D\mathbf{v}$ is an element of volume in $\mathbf{v}$-space.

The function f^0 is obtained from the consideration that in the free-molecule limit there are no inter-molecular collisions. As the pressure ratio across the orifice p_1/p_2 tends to infinity, there will thus be no molecules travelling upstream across the orifice at all, and the distribution function at a point like $P(\mathbf{x})$ (see figure 1) will be Maxwellian everywhere in velocity space except in the 'vacant cone' C, which is the backward cone subtended by the orifice at P. The Maxwellian part corresponds of course to conditions at upstream infinity; thus (with subscript 1 denoting these conditions) we have

$$\begin{aligned} f^0(\mathbf{v}) &= 0 \quad \text{in} \quad C \\ &= n_1\left(\frac{\beta_1}{\pi}\right)^{\frac{3}{2}} e^{-\beta_1 v^2} \quad \text{everywhere else.} \end{aligned} \tag{2.2}$$

The function f^0 is similar downstream of the orifice too, except that now C is the major part of velocity space, and the backward cone is a 'full' Maxwellian. All across the orifice the cone becomes a half-space, and hence f^0 and all the mean quantities are constant.

The number density is relatively easy to calculate, being given (in non-dimensional form) by

$$N(\mathbf{x}) = \frac{n^0(\mathbf{x})}{n_1} = \int_0^\infty \left(\frac{\beta_1}{\pi}\right)^{\frac{3}{2}} e^{-\beta_1 v^2}(4\pi - \Omega)\,v^2 dv = \frac{1-\Omega(\mathbf{x})}{4\pi}, \tag{2.3}$$

where $\Omega(\mathbf{x})$, the solid angle subtended by the orifice at $\mathbf{x}$, is

$$\Omega = \int_0^{2\pi} z\,d\phi \int_0^R \frac{R'\,dR'}{(\eta^2 + z^2 - 2\eta\cos\phi R' + R'^2)^{\frac{3}{2}}}, \tag{2.4}$$

writing η for the cylindrical radius at $\mathbf{x}$.

The evaluation of this integral is fairly straightforward but somewhat tedious, and leads to the expression

$$\frac{\Omega}{4\pi} = \tfrac{1}{4}\{\Lambda_0(\alpha_1, \alpha_2) - \cos\alpha_1 \sin\alpha_2 F_0(\alpha_1)\}, \tag{2.5}$$

where Λ_0 is Heuman's lambda function and $\frac{1}{2}\pi F_0(\alpha_1)$ is the complete elliptic integral of the first kind, $K(\sin\alpha_1)$. Heuman (1941) has discussed the properties of

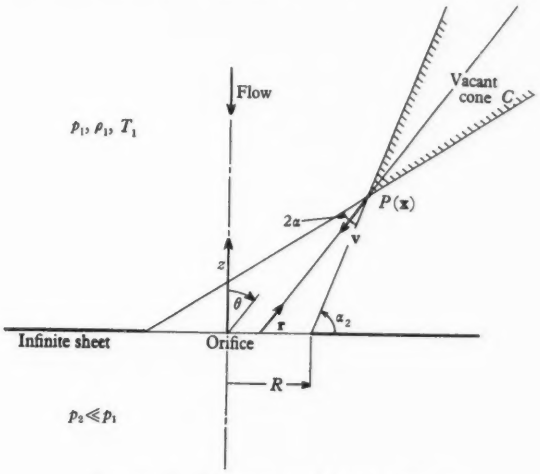

FIGURE 1. Diagram explaining notation.

the function Λ_0, and has also tabulated both Λ_0 and F_0. The arguments α_1, α_2 are given, in terms of polar co-ordinates (r, θ) from the centre of the orifice, by

$$\sin\alpha_1 = \left(\frac{4r\sin\theta}{r^2 + 2r\sin\theta + 1}\right)^{\frac{1}{2}}, \quad \tan\alpha_2 = \frac{r\cos\theta}{r\sin\theta - 1}.$$

(Distances have all been non-dimensionalized by dividing by R.) A relation corresponding to (2.5) has been derived by Sadowsky & Sternberg (1950) for the stream function of a source ring.

The density field calculated from (2.4) and (2.5) has been plotted in figure 2 for the region upstream of the orifice. The field downstream is obtained easily by making use of the symmetry

$$N(r, \pi - \theta) = 1 - N(r, \theta), \tag{2.6}$$

which follows from the nature of f^0 discussed before. In the plane of the orifice $\Omega = 2\pi$, so $N = \frac{1}{2}$. On the axis $\alpha_1 = 0$ and $\tan\alpha_2 = -r$, and (2.5) reduces to

$$\frac{\Omega}{4\pi} = \tfrac{1}{2}(1 - \sin\alpha_2);$$

hence

$$N = N(z) = \frac{\frac{1}{2}(z + \sqrt{(1+z^2)})}{\sqrt{(1+z^2)}} = \cos^2\tfrac{1}{2}\alpha, \tag{2.7}$$

if 2α is the included angle at the vertex of C.

The gas velocity can similarly be expressed as

$$\mathbf{U}(\mathbf{x}) = \sqrt{\beta_1}\,\mathbf{u}(\mathbf{x}) = -\frac{\sqrt{\beta_1}}{n^0(\mathbf{x})}\int_C n_1\left(\frac{\beta_1}{\pi}\right)^{\frac{3}{2}} e^{-\beta_1 v^2}\,\mathbf{v}\,D\mathbf{v}. \tag{2.8}$$

This integral unfortunately turns out to be too complicated to express analytically, and we must at present content ourselves with calculating it along $\theta = 0$ and 90^0. Along the axis we can show quite easily that

$$U(z) = -U_z(z) = \frac{1}{\sqrt{\pi}}\left(1 - \frac{z}{\sqrt{(1+z^2)}}\right) = \frac{2}{\sqrt{\pi}}\sin^2\tfrac{1}{2}\alpha; \tag{2.9}$$

across the orifice U is constant and equal to $-U_z(0) = 1/\sqrt{\pi}$ (or $u^0 = -u_z^0(0) = \frac{1}{2}\bar{c}_1$). However, it is not difficult to guess the qualititative behaviour of U for other

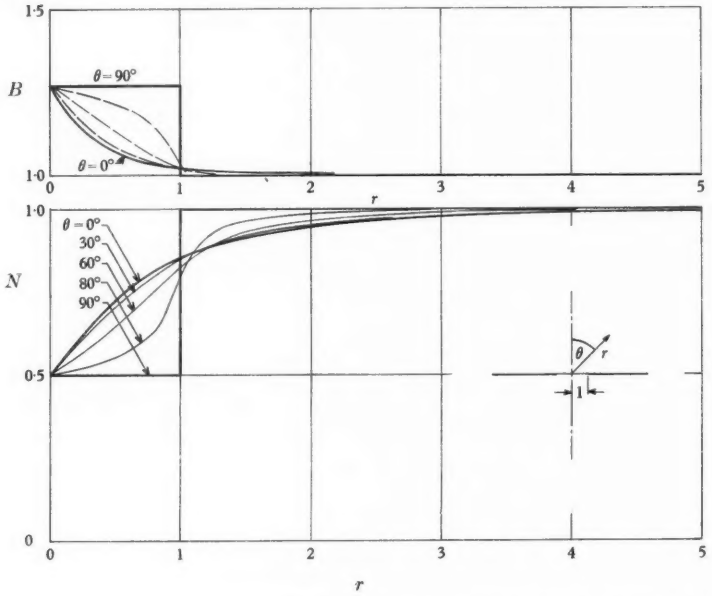

FIGURE 2. N is antisymmetric about $r = 0$, $N = \frac{1}{2}$. Full lines show exact results and dashed lines represent rough estimates.

values of θ, using N as a guide. It is interesting to note that we can immediately obtain the free-molecule mass flow from the mean field as

$$m^0 = \rho^0(-u_z^0) = (\tfrac{1}{2}\rho_1)(\tfrac{1}{2}\bar{c}_1) = \tfrac{1}{4}\rho_1\bar{c}_1.$$

A little thought shows that U, like N, is antisymmetric about the orifice and has the value

$$U(r, \pi - \theta) = 2\pi^{-\frac{1}{2}} - U(r, \theta). \tag{2.10}$$

Thus, far downstream the gas velocity is finite and tends to $\bar{c}_1$, but the density of course drops off to zero. It should be noticed that though the velocity field is antisymmetric about the plane $z = 0$ the stream line pattern will be perfectly symmetric as it depends only on the geometry of the cone C.

The temperature field is obtained from the relation $\mathscr{R}T^0(\mathbf{x}) = \frac{1}{3}\overline{c^2} = \frac{1}{3}(\overline{v^2} - u^2)$. But

$$\overline{v^2}(\mathbf{x}) = \frac{1}{n^0(\mathbf{x})}\int_0^\infty n_1\left(\frac{\beta_1}{\pi}\right)^{\frac{3}{2}} e^{-\beta_1 v^2} v^2(4\pi - \Omega)\, v^2 dv = (\overline{v^2})_1,$$

hence

$$\mathscr{R}T^0(\mathbf{x}) = \mathscr{R}T_1 - \tfrac{1}{3}u^2(\mathbf{x}),$$

or

$$\frac{T^0(\mathbf{x})}{T_1} = \frac{\beta_1}{\beta^0(\mathbf{x})} = \frac{1}{B} = 1 - \tfrac{2}{3}U^2(\mathbf{x}). \tag{2.11}$$

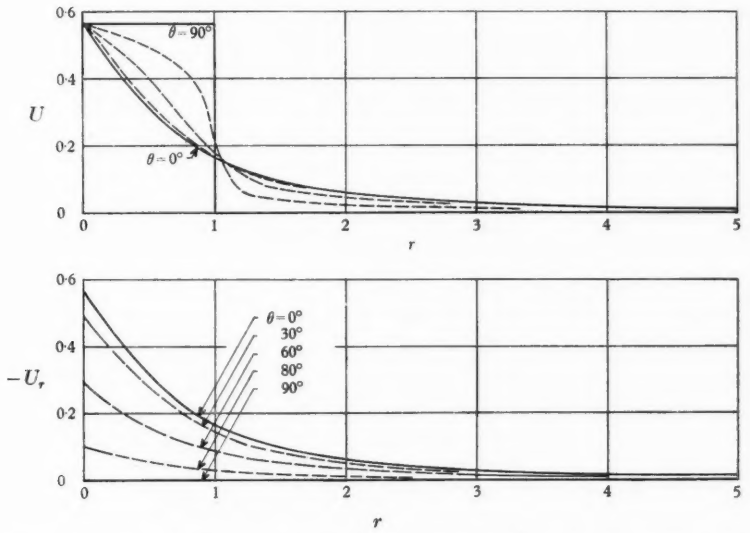

FIGURE 3. U is antisymmetric about $r = 0$, $U = \pi^{-\frac{1}{2}}$. Full lines show exact results and dashed lines represent rough estimates

Thus the temperature is very simply related to the velocity. It drops slightly from T_1 to $\{1 - 2/(3\pi)\}T_1 = 0{\cdot}7879T_1$ at the orifice and then sharply decreases to $T_2 = \{1 - 8/(3\pi)\}T_1 = 0{\cdot}1512T_1$ far downstream. Along the axis, we get from (2.9)

$$B = B(z) = \left[1 - \tfrac{2}{3}\pi^{-1}\frac{1}{(z^2+1)\{z+\sqrt{(z^2+1)}\}^2}\right]^{-1} = (1 - \tfrac{8}{3}\pi^{-1}\sin^4\tfrac{1}{2}\alpha)^{-1}. \tag{2.12}$$

From (2.1) the pressure tensor can be written as

$$p^0_{ij} = -\rho^0(\overline{v_i v_j} - u_i u_j).$$

The thermodynamic pressure $p = \frac{1}{3}p_{ii}$ can of course be obtained from the equation of state $p = \rho\mathscr{R}T$; some of the other components can also be easily evaluated but the results will not be quoted here.

The quantities N, B, U and U_r (the radial component of U which will turn out to be of interest later) are plotted in figures 2 and 3. As an illustration of the kind of flow pattern to be expected in free-molecule flow the streamlines have been worked out for a slit and are shown in figure 4. The calculations here are exactly

the same as for a circular orifice but have the advantage that they lead to closed expressions for all quantities; in particular

$$N = N(r, \theta) = 1 - \alpha/\pi,$$
$$U = U(r, \theta) = \sin\alpha/2\sqrt{\pi}(1 - \alpha/\sqrt{\pi}),$$

where $2\alpha = \tan^{-1}\{2r\cos\theta/(r^2 - 1)\}$ is again the included angle at P. The temperature is still given by (2.11). It can be easily shown that the vector **U** bisects the angle 2α at P, and this suggests an obvious geometric construction for drawing

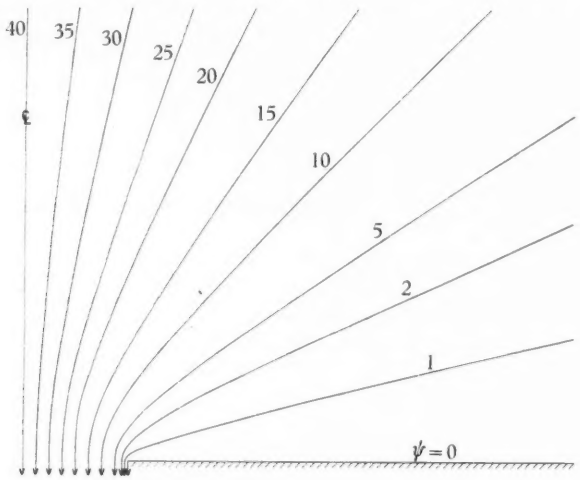

FIGURE 4. Streamlines in free-molecule flow through a slit. The pattern is symmetric about the plane of the slit and the centre-line.

the streamlines. As remarked earlier the streamlines are symmetric about the plane of the orifice. The effect of the wall in slowing down the flow is quite impressive.

One might make a few remarks here on the general validity of the above picture when the flow takes place from one *finite* reservoir into another. Conditions upstream are obviously not going to be affected too much if the linear size of the reservoir is sufficiently large compared to the orifice diameter and the mean free path. Downstream of the orifice, however, the presence of a wall tends to bring the gas temperature back to T_1, while we saw above that the temperature T_2 in the case of an infinite reservoir is much less than T_1. Thus heat transfer at the walls becomes important, and the mean field will presumably be rather different from the one discussed here. The point has been discussed by Liepmann (1961), and we will return to it briefly later.

3. The nearly free-molecule flow

For small departures from the free-molecule limit we can obtain the true distribution function f by perturbing f^0. This function f is governed by Boltzmann's equation, which for the steady flow of a monatomic gas (the only one we

consider here) in the absence of any external forces is (Chapman & Cowling 1952)

$$\mathbf{v}.\frac{\partial f(\mathbf{v},\mathbf{x})}{\partial \mathbf{x}} = \int f(\mathbf{v}')f(\mathbf{w}')gI\,d\Omega\,D\mathbf{w} - f(\mathbf{v})\int f(\mathbf{w})gI\,d\Omega\,D\mathbf{w}$$

$$= \mathscr{G}(f) - f\mathscr{L}(f). \tag{3.1}$$

Here g denotes the relative velocity between two molecules which have initial velocities $\mathbf{v}$, $\mathbf{w}$ and final velocities $\mathbf{v}'$, $\mathbf{w}'$, and I the differential cross-section for scattering into the solid angle $d\Omega$. For convenience we denote the integral operators by $\mathscr{G}$ and $\mathscr{L}$, the 'gain' and 'loss' operators on f.

To tackle the Boltzmann equation directly seems a rather hopeless task; we obtain here an approximate solution f^1 for small ϵ by an iteration procedure suggested by Willis (1958) in which we replace $\mathscr{G}(f)$ and $\mathscr{L}(f)$ by $\mathscr{G}(f^0)$ and $\mathscr{L}(f^0)$ and write

$$\mathbf{v}.\frac{\partial f^1(\mathbf{v},\mathbf{x})}{\partial \mathbf{x}} = \mathscr{G}(f^0) - f^1\mathscr{L}(f^0),$$

or, considering flow upstream of the orifice as shown in figure 1,

$$-v\frac{\partial f^1(\mathbf{v},\mathbf{x})}{dr} + f^1\mathscr{L}(f^0) = \mathscr{G}(f^0). \tag{3.2}$$

This is an ordinary differential equation with $\mathbf{v} = -v\hat{\mathbf{r}}$ as a parameter, for each value of which we require a solution of (3.2). (Note that r, at this stage, is not measured from the centre.) The solution of the equation, using the boundary condition that $f = f_1$ at $r = \infty$, is

$$f^1(\mathbf{v},\mathbf{x}) = f_1\exp\left\{-\int_\infty^r \frac{\mathscr{L}(f^0)}{-v}dr'\right\} + \int_\infty^r \frac{\mathscr{G}(f^0)}{-v}\exp\left\{-\int_{r'}^r \frac{\mathscr{L}(f^0)}{-v}dr''\right\}dr'. \tag{3.3}$$

As $\mathscr{L}(f)/v$ is like $1/\lambda$, the first term obviously vanishes for any finite r, leaving us with

$$f^1(\mathbf{v}, r=0) = \int_0^\infty \frac{\mathscr{G}(f^0)}{v}\exp\left\{-\int_0^{r'} \frac{\mathscr{L}(f^0)}{v}dr''\right\}dr'. \tag{3.4}$$

It is hoped, of course, that this first iterate gives a good approximation to the true perturbation. Incidentally (3.4) has an immediate and obvious physical interpretation, and could almost have been written down straightaway; for $\mathscr{G}(f^0)/v$ is the number of molecules which, after collision in unit distance, are travelling with velocity v, and the exponential multiplying it is the probability of such molecules reaching the orifice ($r = 0$).

The simplest molecular model we can use is the one due to Krook (Bhatnagar, Gross & Krook 1954, Krook 1959), namely,

$$\left.\begin{aligned}\mathscr{L}(f^0) &= An^0,\\ \mathscr{G}(f^0) &= A(n^0)^2(\beta^0/\pi)^{\frac{3}{2}}\exp\{-\beta^0(\mathbf{v}-\mathbf{u}^0)^2\},\end{aligned}\right\} \tag{3.5}$$

where n^0, $\mathbf{u}^0$ and β^0 are all given by (2.1). We choose A here to be a constant equal to $\bar{c}_1/n_1\lambda_1$ so that the number of collisions (per unit volume and unit time) when the distribution is completely Maxwellian, namely $\frac{1}{2}(n_1\bar{c}_1/\lambda_1)$, agrees with the

number given by Krook's model, which is $\frac{1}{2}A(n^0)^2$. Making these substitutions in (3.4) and introducing

$$\mathbf{v}\sqrt{\beta_1} = \mathbf{V}, \quad \epsilon/\sqrt{\pi} = \epsilon'$$

and other non-dimensional quantities already used in § 2, we get

$$f^1(\mathbf{V}, r=0) = f_1 2\epsilon' \int_0^\infty N^2 B^{\frac{3}{2}} \exp\{\mathbf{V}^2 - B(\mathbf{V}-\mathbf{U})^2\} \exp\left\{-\frac{\epsilon'}{V}\int_0^r 2N(r)\,dr'\right\}\frac{dr}{V}. \tag{3.6}$$

In principle this integral can now be evaluated for each velocity vector $\mathbf{V}$ at each point in the plane of the orifice, for all the quantities in the integrand refer to free-molecule flow and can be calculated as in § 2.

However the explicit and analytical calculation of the integral is rather difficult. But we can still get a good estimate of the result by making a few simple approximations. First we assume that the flow is uniform across the orifice: this is strictly true in free-molecule flow, and should be a good approximation in nearly free-molecule flow too. This means that we evaluate the integral at the centre of the orifice, and assume it is the same all across it.

We also notice, from figures 2 and 3 and from the discussion in § 1, that the values N, B and U—but not of U_r, which appears in $(\mathbf{V}-\mathbf{U})^2$ in (3.6)—at $r = 0$ and ∞ are independent of θ, though their variation in between is a function of θ. It is obvious, therefore, that the integral in (3·6) is similar for all rays, though its actual numerical value will vary somewhat. We shall in fact make use of this feature in what follows.

It is convenient for purposes of analysis to rewrite (3.6) as

$$f^1(\mathbf{V}, r=0) = f_1 2\epsilon' \int_0^\infty g_1(r)\, g_2(r, V)\, H(r, V; \epsilon')\frac{dr}{V}, \tag{3.7}$$

where

$$\left.\begin{aligned} g_1(r) &= N^2 B^{\frac{3}{2}} e^{-BU^2}, \\ g_2(r, V) &= \exp\{-2BU_r V + (1-B)\,V^2\} \\ &= \exp\{h_1(r)\,V + h_2(r)\,V^2\}, \\ H(r, V; \epsilon') &= \exp\left\{-\frac{\epsilon'}{V}\int_0^r 2N(r')\,dr'\right\} = \exp\left\{-\frac{\epsilon'}{V}h(r)\right\}. \end{aligned}\right\} \tag{3.8}$$

It is particularly instructive to work out the integral in (3.7) along the axis, $\theta = 0$, where N, B, U and $U_r\,(= -U)$ are all analytically known from (2.7), (2.9) and (2.12); also

$$h(z) = \int_0^z 2N(z)\,dz = z + \sqrt{(z^2+1)} - 1. \tag{3.9}$$

We have therefore

$$f^1(-V\hat{\mathbf{z}}, z=0) = f_1 2\epsilon' \int_0^\infty g_1(z)\, g_2(z, V)\, H(z, V, \epsilon')\frac{dz}{V}. \tag{3.10}$$

We want the lowest order term in ϵ' from this expression. Now it is shown in Appendix II that the integral for the mass flow (or, for that matter, any moment of f^1) can be split in a way which corresponds exactly to splitting the distribution function in (3.10) as follows:

$$f^1(-V\hat{\mathbf{z}}, z=0) = f_1 2\epsilon'\left[\int_0^\infty (g_1 g_2 - 1)\frac{dz}{V} + \int_0^\infty H\frac{dz}{V}\right]. \tag{3.11}$$

The error committed in this splitting is $o(\epsilon')$; the lowest order term in ϵ' turns out to be $O(\epsilon')$ and (3.11) reduces, correct to $O(\epsilon')$, to

$$f^1(-V\hat{\mathbf{z}}, z=0) = f_1\left\{1+\frac{2\epsilon'}{V}\left[\tfrac{1}{2}+\int_0^\infty (g_1 g_2 - 1)\,dz\right]\right\} \tag{3.11a}$$

using the integral evaluated in Appendix I. We expand g_2 as a series in V, obtaining

$$g_2 = 1 + Vh_1 + V^2(h_1^2/2! + h_2) + V^3(h_1^3/3! + h_1 h_2) + V^4(h_1^4/4! + h_1^2 h_2/2 + h_2^2/2) + \ldots.$$

Thus we can write $$f^1(-V\hat{\mathbf{z}}) = f_1\left\{1+\frac{2\epsilon'}{V}\,\phi_0(V)\right\}, \tag{3.12}$$

where

$$\phi_0(V) = \sum_{n=0}^{\infty} A_n V^n,$$

$$A_0 = \tfrac{1}{2} + \int_0^\infty (g_1 - 1)\,dz, \quad A_1 = \int_0^\infty g_1 h_1\,dz, \quad A_2 = \int_0^\infty (g_1 h_1^2/2! + g_1 h_2)\,dz, \ldots. \tag{3.13}$$

From arguments given previously we expect the distribution function to look similar on other rays, so we may assume

$$f^1(\mathbf{V}, r=0) = f_1\left\{1+\frac{2\epsilon'}{V}\,\phi(\mathbf{V})\right\}. \tag{3.14}$$

Looking at (3.6), (3.7) and (3.8) again, and surmising the variation of the integrand with θ from figures 2 and 3, we see (as remarked earlier) that N, B and U vary between the same limits at $r=0$ and $r=\infty$ for all θ, and so the effect on the integral of their being functions of θ must be small. (For instance $\int_0^\infty \{1-N(r)\}\,dr$ is exactly the same for $\theta = 0$ and $\theta = 90°$.) The predominant effect of the dependence on θ of the integral appears through U_r, which varies quite widely with θ. Near the origin we obviously have $U_r = U_z(z=r)\cos\theta$ as $|U_z| \simeq U$. For $r \gg 1$ it can be easily shown from (2.8) that

$$-U_r \simeq U \simeq \frac{2}{\sqrt{\pi}}\frac{\Omega}{4\pi};$$

but $\Omega \simeq \pi\cos\theta/r^2$, so again $U_r \simeq U_z(z=r)\cos\theta$. Thus, it is a very good approximation to take

$$U_r(r,\theta) \simeq U_z(z=r)\cos\theta. \tag{3.15}$$

Next we notice that h_2 accounts for a relatively small contribution to the final answer in comparison with h_1 (h_2 varies from about $-0{\cdot}27$ to zero as r goes from 0 to ∞, and appears only in V^2 and higher order terms); hence it appears that, approximately, the coefficients of V^n in (3.13) are multiplied by corresponding powers of $\cos\theta$ on other rays. We can therefore take

$$\phi(\mathbf{V}) \simeq \phi_0(V\cos\theta), \tag{3.16}$$

which also amounts to putting $g_2(r, V) = g_2(z, V\cos\theta)$. Using this in (3.14) we get the final result

$$f^1(\mathbf{V}, r=0) = f_1\left\{1+\frac{2\epsilon'}{V}\sum_{n=0}^{\infty} A_n V^n \cos^n\theta\right\}. \tag{3.17}$$

Results

The coefficients A_n have been calculated numerically for $n = 0$ to 5, and have the following values:

$$\left.\begin{aligned} A_0 &= -0{\cdot}3944, \quad A_1 = +0{\cdot}7549, \quad A_2 = +0{\cdot}1055, \\ A_3 &= +0{\cdot}0502, \quad A_4 = -0{\cdot}0045, \quad A_5 = -0{\cdot}0013. \end{aligned}\right\} \tag{3.18}$$

The mass flow through the orifice is easily obtained as

$$\dot{m} = m \int (-v_z) f(\mathbf{v})\, D\mathbf{v}. \tag{3.19}$$

Substituting from (3.17) we get

$$\begin{aligned} \dot{m} &= (m/\beta_1^2) \int_0^\infty \int_0^{\frac{1}{2}\pi} f_1 \{V \cos\theta + 2\epsilon' \cos\theta \, \Sigma A_n V^n \cos^n\theta\} \, 2\pi V^2 \sin\theta \, d\theta \, dV \\ &= \tfrac{1}{4}\rho_1 \bar{c}_1 \left[1 + 4\epsilon' \Sigma \frac{A_n}{n+2} \left(\frac{n+1}{2}\right)!\right]. \end{aligned} \tag{3.20}$$

Using the values of A_n given by (3.18) we get†

$$\dot{m} = \tfrac{1}{4}\rho_1 \bar{c}_1 (1 + 0{\cdot}25\epsilon). \tag{3.21}$$

The coefficient 0·25 obtained here is somewhat less than the value 0·26 given in a preliminary report (Narasimha 1960) where the calculations were based on an assumption slightly different from the one used here in (3.16), namely

$$\Phi(\mathbf{V}) \equiv \phi(\mathbf{V})/V = \Phi_0(V \cos\theta), \tag{3.22}$$

and h_2 was ignored. The approximation (3.16) is somewhat more consistent, but apparently the result obtained is not significantly different. No claim of great accuracy is made for the coefficient; nor indeed would it be justified, considering the approximate nature of the calculations.

Correction for backflow

The backflow through the orifice is nil under free molecule conditions, but one may in general expect some backflow when ϵ is finite, even though the pressure ratio p_1/p_2 is still infinite. Using exactly the same procedure as before, one can write down the distribution function for molecules travelling upstream as

$$f^1(V\hat{\mathbf{z}}, z = 0) = f_1 2\epsilon' \int_0^{-\infty} g_1(z)\, g_2(z, V)\, H(z, V; \epsilon') \frac{dz}{V}$$

where g_1, g_2 and H are still given by (3.8), but of course one now has to use the downstream field of N, B and U, obtained as shown in § 2. Both h_1 and h_2 are then negative, and $h(z) \to 1$ as $z \to -\infty$. By repeating the analysis made for the upstream integral one concludes that the highest order term in $f^1(V\hat{\mathbf{z}}, z = 0)$ is $O(\epsilon')$, and given by

$$f^1(V\hat{\mathbf{z}}, z = 0) = f_1 2\epsilon' \int_0^{-\infty} g_1(z)\, g_2(z, V) \frac{dz}{V}.$$

† I have to thank Dr Willis for pointing out a numerical mistake at this point in an earlier draft.

The approximation (3.16) for the radial component U_r is now rather crude, but conservative in the sense that it overestimates the backflow. The correction to the coefficient (3.21) can again be pressed as

$$a' = 4\Sigma \frac{A'_n}{n+2}\left(\frac{n+1}{2}\right)!$$

where

$$A'_0 = \int_0^{-\infty} g_1 dz, \quad A'_1 = \int_0^{-\infty} g_1 h_1 dz, \quad A'_2 = \int_0^{-\infty} \left(\frac{g_1 h_1^2}{2!} + g_1 h_2\right) dz, \ldots.$$

The coefficients alternate in sign, and using the Euler–Maclaurin technique one arrives at an upper bound of $-0{\cdot}03$ for a', i.e. the coefficient in (3.21) would be reduced at most to 0·22 by backflow.

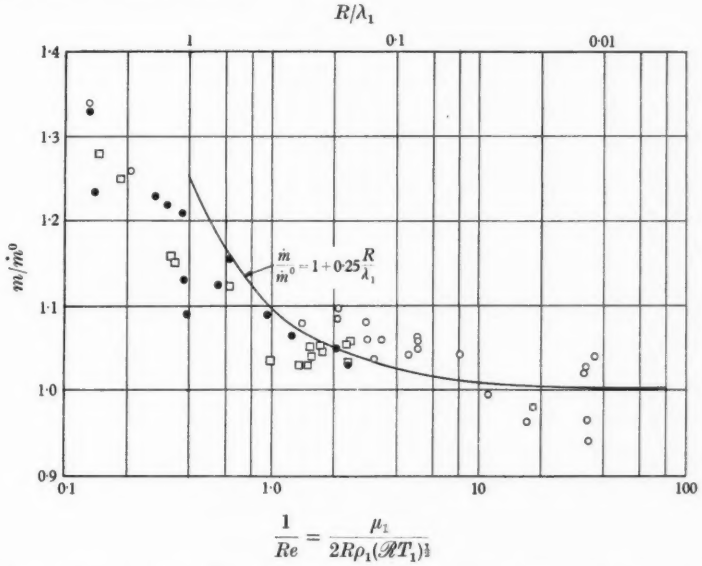

FIGURE 5. Comparison of theory with experimental data. Liepmann's measurements: ●, argon; ○, helium; □, nitrogen. —, values calculated with $\mu_1 = \frac{1}{2}\rho_1 \bar{c}_1 \lambda_1$.

Comparison with experiment

Figure 5 shows the experimental data of Liepmann, and also the result (3.21), which has been plotted assuming that the viscosity $\mu_1 = \frac{1}{2}\rho_1 \bar{c}_1 \lambda_1$. The backflow correction has not been included first because it is small and would not make much difference; secondly, because its exact value is rather uncertain in the case of flow into a finite reservoir, where the flow field is affected somewhat by the presence of walls as discussed in § 2.

Figure 5 shows reasonable agreement between theory and experiment (notice that a small backflow correction would make the agreement even better), and it seems safe to conclude that: (i) the prediction of the theory that the departure from free-molecule flow is linear in ϵ with a coefficient of the order of 0·25

is borne out by the experiments; and (ii) 'nearly' free-molecule conditions prevail up to $\epsilon \sim 1{\cdot}0$.

This work has been supported by the Office of Naval Research, contract no. N-onr 220-21 Task 21. I am grateful to Dr H. W. Liepmann and Dr J. D. Cole for discussing the problem with me and for their enthusiastic encouragement. I also want to thank Mrs Dorothy Diamond for making most of the computations.

Appendix I

We evaluate here an integral which we will need, namely:

$$\chi(a) = a\int_0^\infty \exp\{-a[z+\sqrt{(z^2+1)}]\}\,dz = \int_0^\infty \exp\{-[\zeta+\sqrt{(\zeta^2+a^2)}]\}\,d\zeta.$$

This transforms, using $\xi = \zeta+\sqrt{(a^2+\zeta^2)}$, $d\zeta/d\xi = (\xi^2+a^2)/2\xi^2$, to

$$\chi(a) = \int_a^\infty \frac{\xi^2+a^2}{2\xi^2}e^{-\xi}d\xi.$$

Integrating successively by parts, we can reduce this to

$$\chi(a) = \tfrac{1}{2}\{(1+a)\,e^{-a} - a^2\mathrm{Ei}(a)\},$$

where $\mathrm{Ei}(a)$ is the exponential integral, with the following expansion for small a (Bromwich, 1926):

$$\mathrm{Ei}(a) = -0{\cdot}5772\ldots - \ln a + a + \ldots.$$

Thus χ for small a is

$$\chi(a) = \tfrac{1}{2} + O(a^2\ln a) = \chi(0) + o(a). \tag{A-1}$$

Appendix II

From the discussion which led to (3.16) it was concluded that

$$g_2(r, V) \simeq g_2(z, V\cos\theta),$$

and that a good approximation to the distribution function is

$$f^1(\mathbf{V}, r=0) = f_1\,2\epsilon'\int_0^\infty g_1(z)\,g_2(z, V\cos\theta)\,H(z, V; \epsilon')\frac{dz}{V}. \tag{A-2}$$

Hence the mass flow, expressed as an integral, is (from 3.19)

$$\begin{aligned}\dot{m} &= 2\epsilon'\left(\frac{\rho_1}{\beta_1^2}\right)\left(\frac{\beta_1}{\pi}\right)^{\frac{3}{2}}\iiint e^{-V^2}g_1(z)\,g_2(z, V\cos\theta)\,H(z, V; \epsilon')\,2\pi V^2\cos\theta\sin\theta\,d\theta\,dz\,dV \\ &= 2\rho_1\bar{c}_1\epsilon'\int_0^\infty\int_0^\infty\int_0^{\frac{1}{2}\pi} V^2e^{-V^2}g_1(z)\,g_2(z, V\cos\theta)\,H(z, V; \epsilon')\cos\theta\sin\theta\,d\theta\,dz\,dV.\end{aligned} \tag{A-3}$$

Consider first the integrations with respect to z and V. Putting

$$g_1(z)\,g_2(z, V\cos\theta) = G(z, V\cos\theta),$$

we write

$$J(\epsilon') = \epsilon'\iint V^2e^{-V^2}(G-1)\,H\,dz\,dV + \epsilon'\iint V^2e^{-V^2}H\,dz\,dV = J_1(\epsilon') + J_2(\epsilon'), \tag{A-4}$$

the reason for the splitting being that $(G-1)$ is integrable in z. We want to extract from $J(\epsilon')$ the lowest order terms in ϵ'.

First writing $H = \exp\{-(\epsilon'/V)\,h(z)\}$, where $h(z) = z+\sqrt{(z^2+1)}-1$, >0 for all $z>0$,

$$J_1(\epsilon') = \epsilon'\int_{V=0}^{\delta(\epsilon')}\int_{z=0}^{\infty} V^2 e^{-V^2}(G-1)\exp\left\{-\left(\frac{\epsilon'}{V}\right)h(z)\right\}dz\,dV$$
$$+\epsilon'\int_{V=\delta}^{\infty}\int_{z=0}^{\infty} V^2 e^{-V^2}(G-1)\exp\left\{-\left(\frac{\epsilon'}{V}\right)h(z)\right\}dz\,dV.$$

Replacing $(G-1)$ by an upper bound and using (A-1), we see that the first term on the right is of order $\epsilon'(\delta^4/\epsilon')$. In the second term the coefficient in front of $h(z)$ is $\epsilon'/V \leqslant \epsilon'/\delta$. So if we can choose $\delta(\epsilon')$ such that $\delta^4/\epsilon' \to 0$ and $\epsilon'/\delta \to 0$ as $\epsilon' \to 0$, which is true whenever $\delta = \epsilon'^m$, $\frac{1}{4} < m < 1$, we can write

$$J_1(\epsilon') = \epsilon'\int_0^{\infty}\int_0^{\infty} V^2 e^{-V^2}(G-1)\,dz\,dV + o(\epsilon').$$

Similarly

$$J_2(\epsilon') = \epsilon'\left[\int_{V=0}^{\delta}\int_0^{\infty} V^2 e^{-V^2}\exp\left\{-\left(\frac{\epsilon'}{V}\right)h(z)\right\}dz\,dV\right.$$
$$\left.+\int_{\delta}^{\infty}\int_0^{\infty} V^2 e^{-V^2}e^{\epsilon'/V}\exp\left\{-\left(\frac{\epsilon'}{V}\right)[z+\sqrt{(z^2+1)}]\right\}dz\,dV\right]$$
$$= \epsilon' O\left(\frac{\delta^4}{\epsilon'}\right)+\epsilon'\int_{\delta}^{\infty} V^2 e^{-V^2}\left(1+\frac{\epsilon'}{V}+\ldots\right)$$
$$\times\int_0^{\infty}\exp\left\{-\left(\frac{\epsilon'}{V}\right)[z+\sqrt{(z^2+1)}]\right\}\left(\frac{dz}{V}\right)V\,dV.$$

Using the result (A-1) again

$$J_2(\epsilon') = O(\delta^4)+\int_{\delta}^{\infty} V^3 e^{-V^2}\left(1+\frac{\epsilon'}{V}+\ldots\right)\left\{\tfrac{1}{2}+O\left(\frac{\epsilon'^2}{V^2}\ln\frac{\epsilon'}{V}\right)\right\}dV.$$

It is clear that we can choose δ such that both δ^4 and ϵ'^2/δ^2 are $o(\epsilon')$ by taking $\delta = \epsilon'^m$, $\frac{1}{4} < m < \frac{1}{2}$. Thus

$$J_2(\epsilon') = \tfrac{1}{4}+\tfrac{1}{8}\sqrt{\pi}\epsilon'+o(\epsilon').$$

Putting these results in (A-3)

$$\dot{m} = 2\rho_1\bar{c}_1\left[\int_0^{\frac{1}{2}\pi}\left\{\tfrac{1}{4}+\tfrac{1}{8}\sqrt{\pi}\epsilon'+\epsilon'\int_0^{\infty}\int_0^{\infty} V^2 e^{-V^2}(G-1)\,dz\,dV\right\}\cos\theta\sin\theta\,d\theta\right]$$
$$= \tfrac{1}{4}\rho_1\bar{c}_1\left[1+\epsilon\left\{\tfrac{1}{2}+\tfrac{1}{8}\sqrt{\pi}\int_0^{\infty}\int_0^{\infty}\int_0^{\frac{1}{2}\pi} V^2 e^{-V^2}(G-1)\cos\theta\sin\theta\,d\theta\,dz\,dV\right\}\right], \quad \text{(A-5)}$$

which, after expanding $g_2 = \exp(h_1 V + h_2 V^2)$ as before, leads to exactly the same result as (3.20), thus justifying the splitting of the integral used in (3.11) and (3.11*a*).

A similar analysis will show that (3.11) and (3.11*a*) give correct results for all higher moments also.

REFERENCES

BHATNAGAR, P. L., GROSS, E. P. & KROOK, M. 1954 *Phys. Rev.* **94**, 511.

BROMWICH, T. J. I'A 1926 *Introduction to the Theory of Infinite Series.* London: Macmillan.

CHAPMAN, SYDNEY, & COWLING, T. G. 1952 *The Mathematical Theory of Non-Uniform Gases.* Cambridge University Press.

HEUMAN, C. 1941 *J. Math. Phys.* **20**, 127.

KROOK, M. 1959 *J. Fluid Mech.* **6**, 523.

LIEPMANN, H. W. 1960 *J. Fluid Mech.* **10**, 65.

NARASIMHA, R. 1960 *Phys. Fluids*, **3**, 476.

PRESENT, R. D. 1958 *Kinetic Theory of Gases.* New York: McGraw-Hill.

SADOWSKY, M. A. & STERNBERG, E. 1950 *Quart. Appl. Math.* **8**, 113.

WILLIS, D. R. 1958 *Princeton Univ. Rep.* no. 442.

Interaction between gravity waves and a shear flow

By B. A. HUGHES* AND R. W. STEWART
Institute of Oceanography and Department of Physics, University of British Columbia, Vancouver 8, B.C.

(Received 17 September 1960)

A series of experiments has been undertaken in which three major properties of a surface tension-gravity wave system have been examined. The results of these experiments have been compared with existing theories. The three properties are: (i) viscous decay in the absence of mean flow, the relevant theory being given in Lamb (1932, § 348); (ii) propagation velocities in the presence and absence of flow (Lamb 1932, § 267), and (iii) the change of wave energy on crossing a stable Couette shear flow. The measurements in the last case were compared with two theories, one obtained from the Navier–Stokes equations including terms up to second order in wave slope, the other, following previous authors, obtained on the assumption that any direct interaction of the waves with the shear flow is negligible. According to the theory obtained from the Navier–Stokes equations, the divergence of surface wave energy is equal to the rate of change of wave energy due to the interaction between the mean flow and the wave system plus the rate of change of wave energy due to viscous decay.

An optical system was used to measure the maximum wave slopes, the wave-numbers and the shear velocities.

Results indicate that an anomalous region of wave properties exists for wave-numbers near $2{\cdot}7\ \mathrm{cm}^{-1}$. For a set of data in which the wave-numbers were always less than $1{\cdot}8\ \mathrm{cm}^{-1}$, it was found that the viscous decay rate and the propagation laws agree with theory to within the experimental error, and the interaction measurements fit the theory with the non-linear term included rather than the traditional theories.

1. Introduction

The work discussed herein is an experimental investigation of three major properties of deep water surface waves in the régime where both surface tension and gravity are important. These properties are: viscous dissipation in the absence of any mean flow, propagation laws in the presence and absence of mean flow, and the non-linear interaction of waves with a horizontal mean shear. The first two of these are treated theoretically in Lamb (1932). The last has been investigated theoretically by Longuet-Higgins & Stewart (1961), and in a special case by Drent (1959).

The analysis given by Drent is for the case of plane, long crested waves and a rectilinear shear flow in the absence of surface tension and viscosity. The results

* Now at Pacific Naval Laboratory, H.M.C. Dockyard, Esquimalt, B.C.

indicate that there are two major causes of amplitude change as the waves traverse the flow: one is due to the refraction of the waves, causing a spreading or concentration of energy; the other is due to the radiation pressure, associated with the waves, interacting directly with the shear flow. For waves running directly into a converging flow, these two effects are about equal; for waves crossing a lateral shear at an angle, the former appears to be two to three times larger than the latter. Previous discussions have consistently neglected the direct interaction effects (for example, Johnson 1947), which are of the same nature as those treated recently by Longuet-Higgins & Stewart (1960, 1961).

This paper describes a laboratory experiment designed to measure the three properties listed above and a comparison of the results with the respective theoretical predictions. The wave-energy measurements in the presence of mean flow are compared with two theoretical models—one including the interaction effects, and the other omitting the interaction effects.

2. Experimental methods

Flow production

All experiments were carried out in a tank specially constructed to produce the required shear flow.

A stable, cylindrical Couette flow was created between the outer wall of a circular tank slightly greater than 2·5 m in diameter and an inner wall imposed by a raised centre portion 1·52 m in diameter (figure 1). A hollow annular ring, 2·44 m in diameter, floating freely, was concentric with and about 2·5 cm radially inside the outer wall of the circular tank (figure 1). A series of six drive jets situated in the outer wall of the tank were connected by rubber hoses to the water mains (figure 1). These jets were oriented so that water passing through them impinged on the wall of the annular ring at an angle of 45°, thereby making it rotate. In order to keep the annular ring rotating about the centre of the tank, three foam-padded castors, spring-mounted, were situated on the wall of the tank to bear gently on the outside of the rotating ring if it were not in the centre of the system (figure 1). It was found that if these castors were not used, the ring gradually shifted its axis of rotation until it hit the wall of the tank, creating a large disturbance on the surface of the water. It was necessary to construct a wooden form to fit snugly around the annular ring in order to hold it to a circular shape (figure 1). With the wooden form, the annular ring was circular to within 0·6 cm in its 2·44 m diameter.

Wave production

The device used to produce the waves consisted of a wooden truncated circular cone 1·9 cm deep with an upper diameter of 15·2 cm tapering to a lower diameter of 11·5 cm. It was firmly attached to the cone of a Jensen no. B 69 V elliptical loudspeaker. This assembly was situated on the top of the raised centre piece of the tank in such a way that excursions of the cone were perpendicular to the surface of the water. The cone extended about 1 cm under the surface.

The loudspeaker was driven by a low-frequency oscillator through a rotating switch (for pulse production) and a matching transformer. The voltage applied

to the wave-maker was continuously monitored by a single-beam oscilloscope. The performance of the oscillator was checked by a precision counter and its frequency found to be stable, over the time intervals of interest, to better than one part per thousand. The actual frequencies employed were measured either by use of a stop-watch or by comparison with the 60-cycle mains. (The mains frequency in the power grid to which we are connected, controlled at Boulder Dam, is noted for stability and accuracy.)

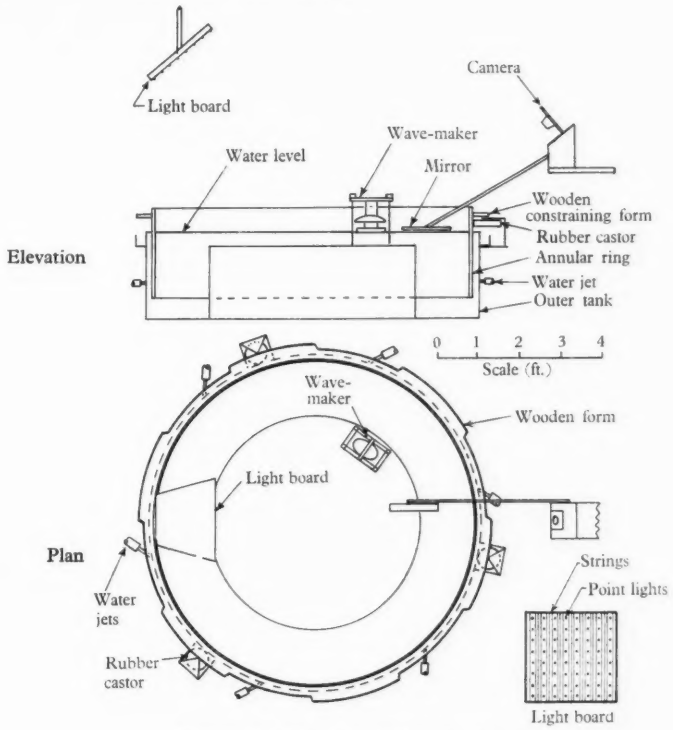

FIGURE 1. Experimental apparatus.

As in any experiment with waves, it was necessary to choose between an efficient wave absorber and the use of pulse techniques. No simple efficient absorber seemed compatible with the other requirements of the experiment, so a pulse system was adopted. Pulses of 10 sec duration at 1 min intervals were found to be reasonably satisfactory in eliminating disturbances due to reflected waves.

Two of the prime difficulties of wave production by this method arise from lobal pattern asymmetry and transient modulation. Asymmetry occurs because of the difficulty of properly orienting the wooden disk with respect to the water. It appears that the bottom of the disk should be accurately parallel to the surface of the water, and that the motion of the disk should be accurately perpendicular to it. Transient modulation occurs because a resonant system is driven by pulses of off-resonance frequency, and because an impulsive type of motion is imparted

to the surface of the water at the start of the pulse. Even though the voltage amplitude on the oscilloscope is constant to within 1 % there still is evidence of a transient modulation of 2–5 % in the waves themselves. A reduction of the effect of this modulation was obtained by averaging the results of amplitude measurements taken at a different stage of each of a large number of pulses.

Measurement of mean flow

Measurement of the horizontal shear-flow profiles was performed photographically during the experiment in the following way: ten circular pieces of white paper 0·6 cm in diameter were simultaneously dropped onto the surface of the water in a line approximately at right angles to the flow in the area under consideration. A photograph was taken of these with the camera shutter open for 0·98 sec (1 sec on camera settings). The lengths of the resulting streaks on the film are proportional to the speeds at the points where the pieces of paper were dropped. This was done ten times in order to achieve a smooth profile.

Visual observations of the vertical velocity profile were obtained by comparing the flow at a few cm depth and the flow right on the surface. A small plastic float about $\frac{1}{2}$ cm in diameter was attached to a relatively high drag body of about the same dimensions by a piece of thread a few cm long. The rate of movement of this unit when placed in the water was found to be not significantly different from the rate of movement of a plastic float by itself at the same radius. There is little reason to believe that an appreciable surface stress exists, so any depth-wise velocity gradient would be associated with secondary flow.

Such a secondary flow must of course exist. The stationary bottom of the tank must have associated with it an inward-flowing boundary layer. A compensating outward flow is thus required in the upper regions of the flow. If all the vertical movement occurs at the inner and outer walls of the tank, then in the main body of the annulus, solution of the vorticity equation yields for the tangential velocity V

$$V = B(r^n - r_0^{n+1} r^{-1}), \tag{1}$$

with B and n undetermined constants and r_0 the radius of the inner wall. The smooth curves shown in figures 2 and 3 were obtained by an empirical fit of equation (1) to the measured points. The velocity values used in the various calculations were taken from the theoretical curves (except in figure 3 for a distance less than 85 cm for which values were taken from the visually smoothed experimental data).

According to the above assumptions, the speed of the secondary flow is given by $(n-1)\,v/r$. With values of n obtained from the empirical fit this appears to be of the order of 10^{-4} cm/sec. The strength of the secondary flow was examined experimentally by observing the trajectories of the small plastic floats described above. These were somewhat irregular, but the trend was towards the outer wall, with a rate of radial progression estimated to be of the order of $\frac{1}{200}$ or less of the average tangential flow.

It should be noted that our results do not depend upon the accuracy of the assumptions leading to (1), since in practice the equation has been used merely as a framework for an empirical description of the mean velocity data.

Wave measurement

An optical system was used to measure the wave amplitudes, wave-number and wave direction. A board containing 64 light bulbs was fastened to the ceiling so that the light from these effective point sources reflected off the area of the shear

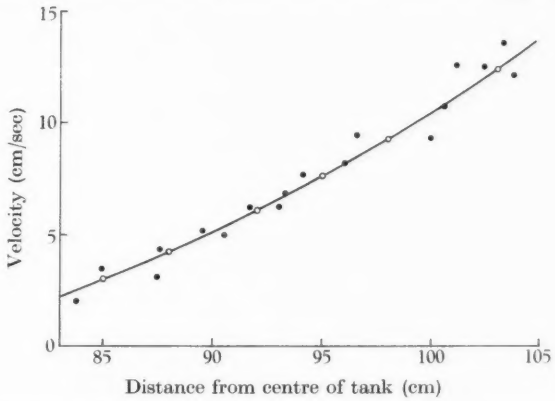

FIGURE 2. Velocity profile used for set I data. The 'theoretical' curve is obtained from equation (1) with empirically chosen constants. ○, Theoretical; ●, measured.

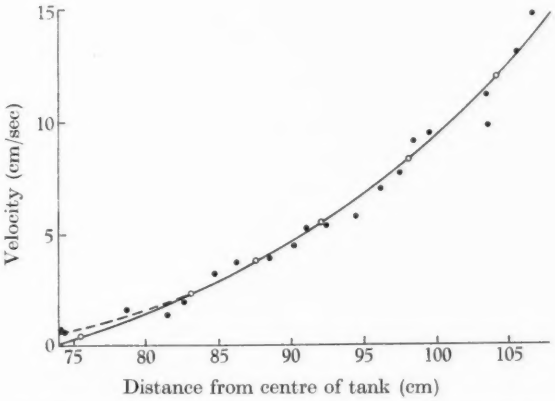

FIGURE 3. Velocity profile used for set II data. – – – –, Smoothed experimental data; —, theoretical curve.

flow to be studied into a properly oriented camera. The lights were in a square array each 7·6 cm apart. The board was approximately 3 m vertically above the surface of the water and approximately 3 m horizontally from the reflexion points on the surface of the water (figure 1). The camera used was a 35 mm Agfa Colorflex. It was positioned approximately 1 m vertically and horizontally from the reflexion points on the water surface, and angled so that the image of the 'light board' appeared in the centre of its field of view.

(i) *Amplitude*

As the waves cross the image of the board, the image of a light undergoes oscillatory excursions, the maximum of which is a direct measure of the maximum wave slope at the position on the surface of the water from which the undeviated light reflects. For each pulse the camera shutter was opened for somewhat longer than one wave period. The lengths of the streaks thus obtained on each frame are a measure of the maximum excursions of the images of the lights. A small alignment mirror, mounted just above the surface of the water and to one side of the image of the light board, was oriented to reflect one column of lights into the camera thus producing a constant reference line from frame to frame. (Examples of these photographs are given in figures 4*a* and 4*b*, plate 1.) The sensitivity of this technique is such that wave slopes of only 0·01 radians could be measured to within 1 %. The fact that the experimental waves had such small slopes justifies the use of first-order wave theory throughout.

(ii) *Wave-number*

The light board also has 23 straight white nylon strings mounted on it, each in a vertical plane (figure 1). These strings were photographed using an electronic flash unit. (Examples of these photographs are also shown in figures 4*c* and 4*d*, plate 2.)

As the waves cross the area in question, the images of the strings distort into sinusoids. Lines of constant phase were determined from photographs of this nature as follows: a photograph was first taken of the strings with no surface waves in the area, then photographs were taken when waves were present. When the first photograph was projected, the images of the straight strings were traced onto a piece of graph paper on the projection board and the images of the lights in the alignment mirror were traced out.* Then the photographs with waves were projected onto this same piece of graph paper. When the images of the lights in the alignment mirror correspond with the traced images, the traces of the straight strings form a baseline for each of the sinusoidal string images. The positions at which each sinusoidal image crossed its baseline were marked. Joining these marks along wave fronts then produced lines of constant phase.

(iii) *Projection system*

In order to facilitate measurement of the data on the films, a tilted board projection system was used with the focal length of the projector the same as the focal length of the camera. If the board onto which the film is projected is tilted with respect to the projector to the same angle as the surface of the water makes with the camera, the measurements obtained correspond directly to the plane of the surface of the water, to within a uniform scale factor.

* Because of the high contrast of the positive, the positions of the lights in the alignment mirror are not visible in figures 4*c* and 4*d*. They could be clearly seen, however, in the projected negatives.

3. Propagation in the absence of mean flow

Wave-number

Assuming irrotationality, incompressibility and infinitesimally small amplitudes, the phase velocity C for surface waves can be shown to be (Lamb, 1932, §267)

$$C = \left(\frac{g}{k} + \frac{kT}{\rho}\right)^{\frac{1}{2}}, \tag{2}$$

where T is the surface tension and k is the radian wave-number.

T was measured by observing the rise in a capillary tube of known bore, and found to be 67 ± 4 dynes/cm.

For a wave frequency of 8·00 c/s, the predicted wave-number is therefore

$$k_t = 2{\cdot}015 \pm 0{\cdot}02 \text{ cm}^{-1}.$$

Two experimental determinations at this frequency gave

$$k_e = 2{\cdot}028 \pm 0{\cdot}02 \text{ cm}^{-1}$$

and

$$2{\cdot}033 \pm 0{\cdot}02 \text{ cm}^{-1}.$$

It therefore appears that the theory is at least as reliable as the measurements (i.e. $\pm 1\,\%$) for small amplitude waves at this frequency.

Viscous dissipation

It is shown in Lamb (1932, §348) that if the motion in real waves is not significantly different from that in irrotational waves, then the expression for the amplitude a of plane waves as a function of time t is

$$a = a_0 e^{-2\nu k^2 t}, \tag{3}$$

where ν is the kinematic viscosity.

In terms of the parameters measured in our experiment, where we have cylindrically expanding waves, this becomes

$$\delta = \delta_0 (s_0/s)^{\frac{1}{2}} \exp\{-2\nu k^2 (s - s_0)/C_g\}, \tag{4}$$

where δ is the wave slope,

s is the distance from the centre of the wave-maker, and

C_g is the group velocity, which is taken as

$$C_g = \partial(kC)/\partial k, \tag{5}$$

where C is given by (2).

In practice the rate of dissipation of wave energy is changed severely by the presence of a surface film of oil or other immiscible surface material. Experience showed that the film must be continuous over dimensions comparable with a wavelength to be effective. Thus it was found that by slowly siphoning off surface water, and with it the surface film, the water could be kept adequately clean without requiring many special precautions to prevent contamination. The only essential was that the siphon draw off both air and water to ensure that the interfacial surface be carried away.

Viscosity was not measured. However, an examination of tabulated values shows that it is very insensitive to concentrations of solutes as dilute as are found in tap-water. The temperature of the surface water was measured and the viscosity taken from the *Handbook of Chemistry and Physics*, 41st ed., Chemical Rubber Publishing Co., Cleveland.

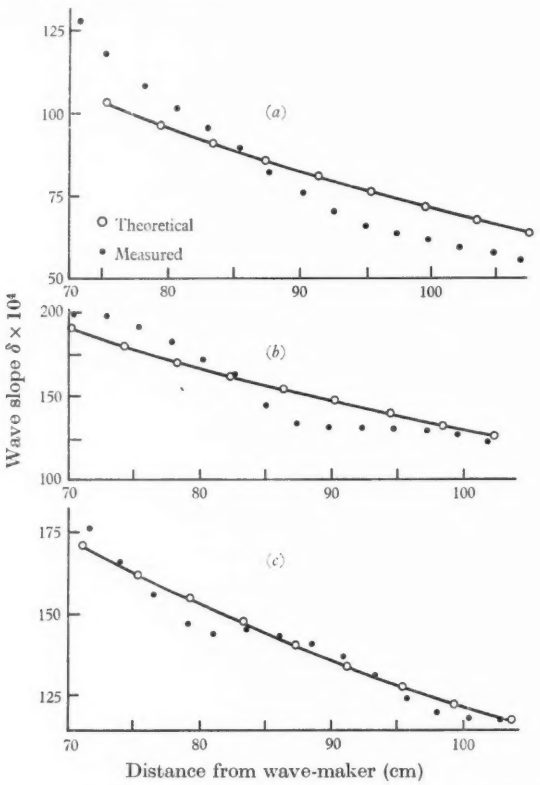

FIGURE 5. Viscous dissipation. ●, Experimental points; ○—○, theoretical line. (*a*) $f = 10{\cdot}00$ c/s, $k = 2{\cdot}69$ cm^{-1}; (*b*) $f = 8{\cdot}57$ c/s, $k = 2.21$ cm^{-1}; (*c*) $f = 8{\cdot}00$ c/s, $k = 2{\cdot}02$ cm.$^{-1}$

Figure 5 shows values of δ observed for frequencies of 8·00, 8·57 and 10·00 c/s, plotted as a function of s. The solid lines are obtained from equation (4). Since there is no preferred assignment to δ_0, the theoretical lines have been made to fit the experimental data near the centre of the range.

The 8·00 c/s data are seen to agree quite well with the theory except for the wavy characteristic of the measured points. This waviness is thought to be due to the presence of small amounts of reflected energy.

At 8·57 c/s the agreement is less satisfactory, but the observations cannot be said to conflict significantly with the theory.

The 10·0 c/s data were taken with the aim of measuring the viscous dissipation of a wave whose phase velocity is exactly the same as that of a wave twice its

frequency. Unfortunately, it appears that this condition has not been achieved. From the photographs used to measure the wave slopes it could be seen that an extra wave train was present, but in the distance covered by the measurements the phase of this extra wave with respect to the 10·0 c/s wave changed by 90°. It is thought that the apparently rapid decay over the left side of the graph in figure 5 is a combination of two factors. One is the fact that any wave of a frequency of 20·0 c/s which has appreciable amplitude that far from the wave-maker must have a continuous source of energy as it propagates. The only apparent source of energy is a non-linear wave-wave interaction with the 10·0 c/s wave. Between any crest of the fundamental and the preceding trough there is a region which is undergoing a continual rate of compression by the fluid particle velocities. If a part of an extra wave happens to coincide with this region for any length of time it will be increased in energy by the same sort of interaction as that between waves and a mean shear (Longuet-Higgins & Stewart 1960). The larger velocity gradients present in the 20·0 c/s wave result in a much faster decay of energy to viscosity; so presumably a balance is achieved between non-linear input and viscous decay. The 10·0 c/s wave thus experiences an increased rate of loss of energy through the intermediary of the 20·0 c/s wave. A phase photograph of a wave at 10·5 c/s is given in figure 4*d*, plate 2, clearly showing the complexity of the wave form when the frequency is near 10 c/s.

The other factor contributing to the anomalous measured decay rate of the 10·0 c/s waves is due to the change of phase that occurs between the two wave trains. The shape of the parts of the wave from which the light reflexions take place can be inferred from the character of the streak density obtained from an amplitude photograph. From such an examination it appears that the parts of the wave which give the maximum excursions of the reflected light change from having a slope more nearly like that of 20·0 c/s to that characteristic of a 10·0 c/s saw-tooth wave.

The peculiarities of waves in the neighbourhood of 10 c/s have been noted previously (Wilton 1915, Pierson & Fife 1960).

4. Wave-shear flow interaction

Drent's (1959) treatment was for a plane shear flow traversed by waves which would be straight-crested in any region where the shear was zero. Our case, while not different in principle, is more complex because we have a curved shear flow and a point source of waves.

Wave kinematics

The direction of phase propagation and the local wave-number are governed by two equations. The first is simply an expression of the fact that to an observer stationary relative to the wave-maker, the rate of change of phase is constant at all positions in the field. Thus

$$\omega_0 = kC - kV\sin\phi, \tag{6}$$

where ω_0 is the radian frequency at the wave-maker,

V is the local speed of the current,

and ϕ is the angle between the direction of the local wave front and the direction of the current velocity.

The second describes the refraction of the wave front. If η is a co-ordinate along a wave front and ξ a co-ordinate normal to it in the direction of propagation, then

$$(C - V\sin\phi)\frac{\partial\phi}{\partial\xi} = \frac{\partial C}{\partial\eta} - \frac{\partial}{\partial\eta}(V\sin\phi). \tag{7}$$

The rather complex relation (2) between C and k, together with the difficult semi-empirical form for V, (1), makes analytic treatment of these equations (6) and (7) formidable. However, in practice it was always found possible to work in a region where C, k and ϕ were all nearly independent of θ, the angular co-ordinate of a cylindrical co-ordinate system with centre at the centre of the tank. In this case an iterative successive approximation method permitted 'phase rays', defined everywhere by the direction of the vector sum of **C** and **V**, to be located without undue difficulty. The same calculation gives k and ϕ throughout the field.

Using the cylindrical co-ordinate system, equation (7) becomes

$$\cos\phi\frac{\partial\phi}{\partial r} - \sin\phi\frac{\partial\phi}{\partial\theta} + \frac{\sin\phi}{r} = -\sin\phi\frac{\partial\ln k}{\partial r} - \cos\phi\frac{\partial\ln k}{\partial r}. \tag{8}$$

Under the assumption that k and ϕ are independent of θ, this can be integrated to give

$$kr\sin\phi = k_0 L, \tag{9}$$

where k_0 is the wave-number at the wave-maker and L is the distance from the centre of the tank to the wave-maker. From equations (9) and (6), $\sin\phi$ is eliminated, leaving k as a function of r only,

$$kC - \omega_0 = k_0 VL/r. \tag{10}$$

Equation (6) can be used to estimate the accuracy of (10) using $\partial\phi/\partial\theta$ as evaluated in the absence of flow. This indicates that in the area investigated k is nowhere different from that given in (10) by more than 0·5 %.

Measurements of wave-number variation were obtained from two independent sets of data in the presence of flow: set I with an oscillator frequency of 8·23 c/s and a velocity profile as shown in figure 2, set II with an oscillator frequency of 6·00 c/s and a velocity profile as shown in figure 3.

For set I, a total of 40 wave-number pictures were taken of which 5 were chosen and measured. Judgement was based on the visual smoothness of the sinusoidal string images. Lack of smoothness results partially from velocity fluctuations and predominantly from the presence of any waves of a period different from the main component. Equations (6) and (8) indicate that waves of different period refract differently, thus the presence of spurious wave periods produces local variations along the lines of constant phase.

For set II, an attempt was made to take forty photographs but because of a faulty camera aperture mechanism only ten usable ones resulted. On the whole, these ten were much freer from discrepancies than those of set I so that no difficulty was encountered in choosing five frames.

Figures 6 and 7 contain typical lines of constant phase taken from data from two of each of the five frames of sets I and II, respectively.

The theoretical curves shown in figures 8 and 9 were plotted from equation (10) and were determined from set I information and set II information, respectively. The measured points were derived from the wavelengths obtained from the respective lines-of-constant-phase diagrams. The values used for the wavelengths

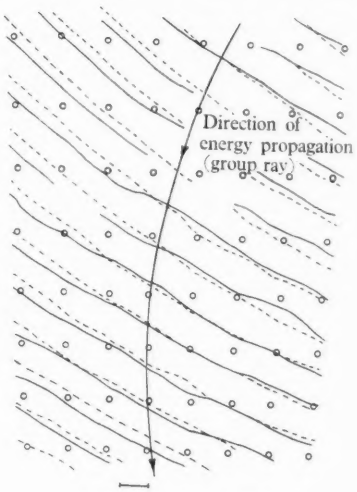

FIGURE 6. Lines of constant phase—set I (8·23 c/s). The circles are the average location of the images of lights used for amplitude measurement.

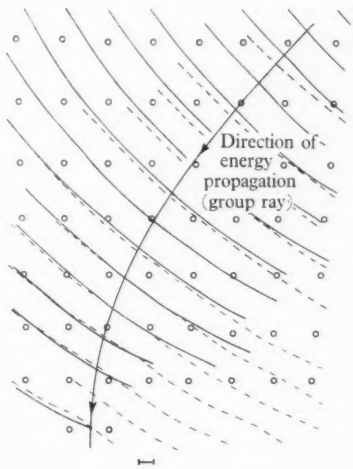

FIGURE 7. Lines of constant phase—set II (6·00 c/s).

are the averages, at each position, of the minimum distance from a point on a line of constant phase to the nearest lines of the same phase in both directions. In order to show the scatter yet not overcrowd the diagrams, only $\frac{1}{35}$ of all the points, chosen randomly, have been shown in each case. Smoothing of the measured points in figure 8 was done visually.

As can be seen from figures 8 and 9, set II data agree very well with equation (10) whereas set I differs significantly from it. The maximum discrepancy in figure 8 (approximately 5 %) occurs at $k = 2{\cdot}7\ \mathrm{cm}^{-1}$, and since the wave-number that propagates at the same phase velocity as a wave at twice the wave-number has a value of $2{\cdot}7\ \mathrm{cm}^{-1}$, calculated from equation (2), it is thought that the two phenomena are intimately linked, though exactly how is not yet understood. The most likely possibility is that the phase velocity in the vicinity of $k = 2{\cdot}7\ \mathrm{cm}^{-1}$ differs from that given by simple theory (equation 2) by approximately 5 %.

Interaction dynamics

(i) *Theory*

Longuet-Higgins and Stewart (1961) have shown that for steady currents and in the absence of wave dissipation

$$\nabla.[E(\mathbf{C}_g+\mathbf{U})]+\tfrac{1}{2}S_{ij}\left(\frac{\partial U_i}{\partial x_j}+\frac{\partial U_j}{\partial x_i}\right)=0, \tag{11}$$

where E is wave energy per unit surface area,

$\mathbf{C}_g$ is the local group velocity of the waves,

$\mathbf{U}$ is the horizontal current velocity, of which

U_i is a component,

S_{ij} is the (two-dimensional) radiation stress-tensor.

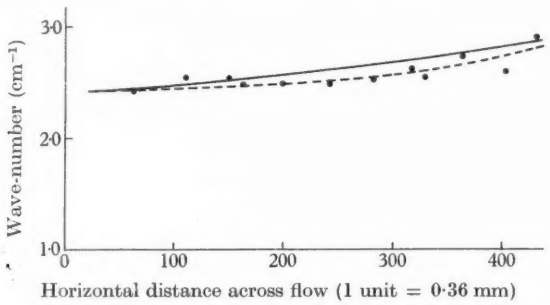

FIGURE 8. Measured and predicted wave-number data—set I (8·23 c/s). ●, Measured points; – – – –, smoothed experimental data; —, theoretical curve.

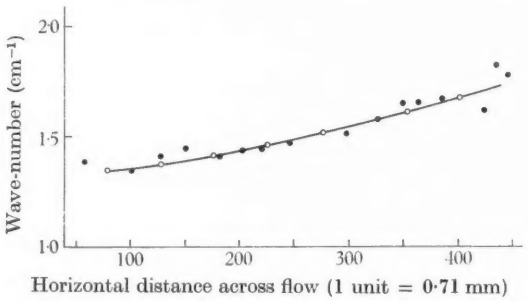

FIGURE 9. Measured and predicted wave-number data—set II (6·00 c/s). ●, Measured points; ○, theoretical curve.

In deep water the diagonal form of S_{ij} is

$$S_{ij} = \begin{pmatrix} \frac{1}{2}E & 0 \\ 0 & 0 \end{pmatrix}, \tag{12}$$

where the x_1 co-ordinate is here directed normal to the wave fronts.

Drent (1959) and Longuet-Higgins & Stewart (1961) analysed (11) for the particular case

$$\frac{\partial E}{\partial x_2} = \frac{\partial C}{\partial x_2} = \frac{\partial U_2}{\partial x_2} = U_1 = 0,$$

but previous authors (e.g. Johnson, 1947) have neglected the interaction term in S_{ij}.

In our case (11) becomes

$$\nabla . [E(\mathbf{C}_g + \mathbf{V})] = \tfrac{1}{4}E \sin 2\phi \left(\frac{\partial V}{\partial r} - \frac{V}{r} \right) - \text{viscous term}, \tag{13}$$

where $\mathbf{C}_g$ is in the direction of advance of the wave and normal to its front, and $\mathbf{V}$ is tangential to the mean streamline and in the direction of increasing θ.

The line obtained by integrating from the inner edge of the flow outwards with the direction of $\mathbf{C}_g + \mathbf{V}$, (a function of r and θ), tangent at every point to the path, shall be called a 'group ray'. A path line defined this way possesses the property that no wave energy crosses it. That is, given any two group rays, the rate that energy flows across any line joining these rays is the same as the rate that energy flows across any other line joining them in the absence of dissipating mechanisms and non-linear interactions. Therefore, by considering the configuration of the group rays on the water surface, the effect of the refraction and spreading of energy can be taken into account.

We shall assume that the effect of viscosity on the waves, being a purely local one, is not influenced by the shear flow and is given by (3) in the form

$$\left(\frac{dE}{ds}\right)_{\text{viscous}} = \frac{-4\nu k^2 E}{|\mathbf{C}_g + \mathbf{U}|}, \tag{14}$$

where s is the distance from the wave maker here measured along the local group ray.

Equation (13) can be put in a form suitable for numerical iteration by integrating it over the area contained between two differentially separated group rays and any two arbitrary points on the rays

$$E_2|\mathbf{C}_g + \mathbf{V}|_2 l_2 - E_1|\mathbf{C}_g + \mathbf{V}|_1 l_1 = \frac{1}{4}\int\int_1^2 E \sin 2\phi\left(\frac{dV}{dr} - \frac{V}{r}\right) dl\, ds - \text{viscous terms}, \tag{15}$$

or

$$\frac{\Delta(E|\mathbf{C}_g + \mathbf{V}|\, l)}{l\Delta s} = \tfrac{1}{4}\sin 2\phi\left(\frac{dV}{dr} - \frac{V}{r}\right) - \text{viscous terms}, \tag{16}$$

where l is the perpendicular distance separating the two group rays and Δs is an element of length along the group rays.

The theoretical curves used for comparison with the experimentally determined data have been obtained by a numerical integration of equation (16), including viscosity, along a previously determined group ray—the interaction curve including the term $\frac{1}{4}E \sin 2\phi(dV/dr - V/r)$, the non-interaction curve omitting it.

(ii) *Results*

For both sets of data, 100 amplitude photographs were taken and the 'best' twenty in each were measured. The criterion used to judge which frames were to be measured was based on overall smoothness of the streak lengths within the frame being judged. (See figures 4*a* and 4*b*, plate 1, for an example of a photograph rejected on this basis compared with one that was not.) The judgement was a purely visual one, i.e. it was performed before any of the streak lengths were actually measured. These anomalous streak variations are caused by the accumulative effect of fluctuations in the horizontal velocity that occur during the time required for the energy to propagate from the edge of the shear flow to the position of examination. The major effect of a local velocity fluctuation is a change of the rate of spreading from that point onwards along the group rays affected.

To determine the results of the interaction measurements a group ray was first plotted along which equation (16) was solved numerically with and without the interaction term. The group rays that were used were obtained simply from a graphical integration of the equation

$$-r\frac{d\theta}{dr} = \tan\phi - \frac{V}{C_g}\sec\phi, \tag{17}$$

where C_g is obtained from equation (5), assuming (2). The angle ϕ was in all cases determined from equation (10) using the measured values of k and V. The group rays so obtained are shown in figures 6 and 7, for set I and II, respectively. Eight wave slopes were then determined for each frame of amplitude photographs chosen to be measured—one for each row of lights. If the group ray happens to pass between two lights, the value of the slope at the ray was obtained by linear

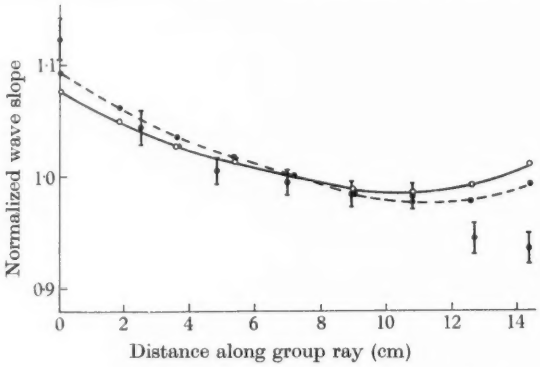

FIGURE 10. Wave slopes in presence of flow—set I (8·23 c/s). ○, Theoretical interaction; ●, theoretical non-interaction; ⧫, measured ± 1 S.E.

interpolation between the lights. Each frame was then normalized by setting the average wave slope along the group ray for each frame to unity. The normalized measured values for each point on the group ray were then averaged over all twenty frames. The standard errors of each point were then calculated from the normalized data. The final averages for set I are shown as the measured points in figure 10 with the vertical bars indicating one standard error on each side.

The theoretical curves plotted in figure 10 were calculated on the basis of zeroth-order kinematics—inclusion of first-order effects produced a negligible change. They incorporate the smoothed wave-number data of figure 8 in the conversion of energy to slope. They also were normalized to unity at the same position along the group ray at which the averaged wave slope occurred. It is evident that at large distances along the ray there is a loss of wave energy not accountable by the theory. This point will be returned to below.

The theoretical curves used for set II incorporated first-order iterated kinematics. The maximum deviation from zeroth-order theory encountered was 1·7 % in wave slope. Figure 11 presents the data obtained in set II plotted in the same manner as figure 10. Clearly the agreement between theory and experiment

is much better than in set I, and the inclusion of the interaction terms seems favoured. Figure 12 presents the same data as figure 11 in a somewhat different form. The points shown in the upper diagram of figure 12 are the difference between the measured points and the normalized theory omitting the inter-

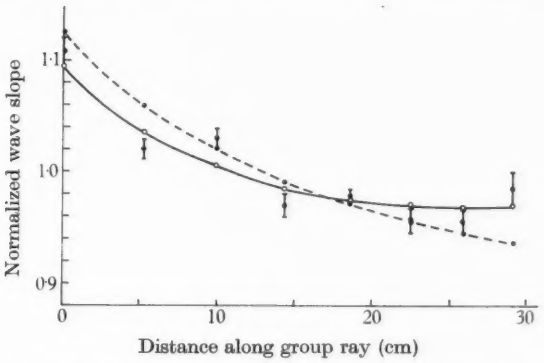

FIGURE 11. Wave slopes in presence of flow—set II (6·00 c/s). ○, Theoretical interaction; ●, theoretical non-interaction; ⧫, measured ± 1 S.E.

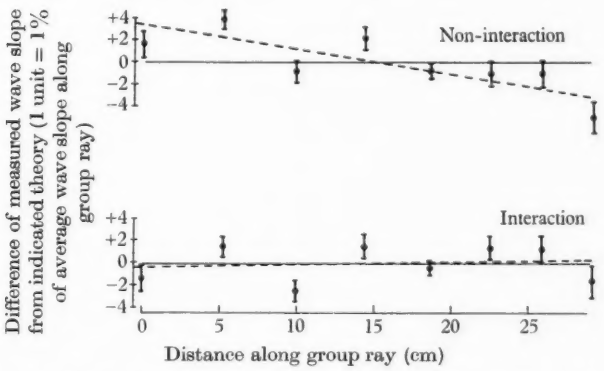

FIGURE 12. Normalized comparisons of theoretical curves with measured wave slopes—set II. – – – –, Least squares regression through measured points; ⧫, measured ± S.D. error.

action term. In the lower diagram of figure 12 the points plotted are this difference including the interaction term. In both cases, the vertical bars indicate one standard error on each side of the points, and the dashed straight line was obtained by least squares regression through the points. The interaction effect resulted in an added energy change of 12 % over the distance examined. As can be seen from the lower diagram of figure 12, the experimental data agrees very well with the theory (including the interaction term), but it appears likely that we have underestimated the standard error somewhat. It should be noted that the 12 % change in energy density produced by the interaction effect is to be compared with a 30 % change due to spreading.

5. Discussion

The optical methods used in this experiment were entirely satisfactory—it is estimated that an accuracy of 0·5 % was achieved in all the optical measurements.

The method used to create the shear flow, though extremely simple and adequate, possessed one major drawback—unsteadiness. Because of upwelling at the inner wall, a region of turbulence existed at the edge of the flow. This region produced most of the random variations of wave properties that were subsequently dealt with by statistical analysis.

Considerable time was spent trying to produce waves with very little transient modulation. Unfortunately, the problem was not entirely solved. The attempt to randomize the phase of the modulation from pulse to pulse appears to have succeeded for set I data but not completely for set II.

It appears that a further experimental investigation is warranted into viscous dissipation and propagation properties of waves near $k = 2{\cdot}7\ \mathrm{cm}^{-1}$ both in the presence and absence of mean flow.

The interaction measurements as presented in figure 10 are definitely anomalous. The difference in decay rate between the measured points and the theoretical curves is in the same sense and of approximately the same magnitude as the discrepancies noted in the viscous decay between 8·57 and 10·0 c/s. It is perhaps significant that a sudden decay of energy occurs very near the position along the group ray, 12 cm, at which $k = 2{\cdot}7\ \mathrm{cm}^{-1}$.

No anomalies were found in the information taken in set II and figures 11 and 12 clearly indicate that interaction theory is well favoured over non-interaction theory.

This work is a contribution of Defence Research Board of Canada. One of us (B. A. H.) was on study leave from the Pacific Naval Laboratory, Esquimalt, the other (R. W. S.) assigned by D. R. B. to special duty at the University of British Columbia. Equipment was purchased from a D.R.B. research grant.

We wish to thank the Department of Civil Engineering, University of British Columbia, for permission to conduct this experiment in the Hydraulics Laboratory.

REFERENCES

Drent, J. 1959 A study of waves in the open ocean and of waves on shear currents. Doctoral Thesis, University of British Columbia.

Johnson, J. W. 1947 *Trans. Amer. Geophys. Un.* **28**, 867.

Lamb, H. 1932 *Hydrodynamics.* 6th edition. Cambridge University Press.

Longuet-Higgins, M. & Stewart, R. W. 1960 *J. Fluid Mech.* **8**, 565.

Longuet-Higgins, M. & Stewart, R. W. 1961 *J. Fluid Mech.* (in the Press).

Pierson, W. J. & Fife, P. 1960 Some properties of long crested periodic waves with lengths near 2·44 centimeters. *Technical Report*, Dept. of Meteorology and Oceanography, Research Div., College of Engng, New York University.

Wilton, J. R. 1915 *Phil. Mag.* **29**, 688.

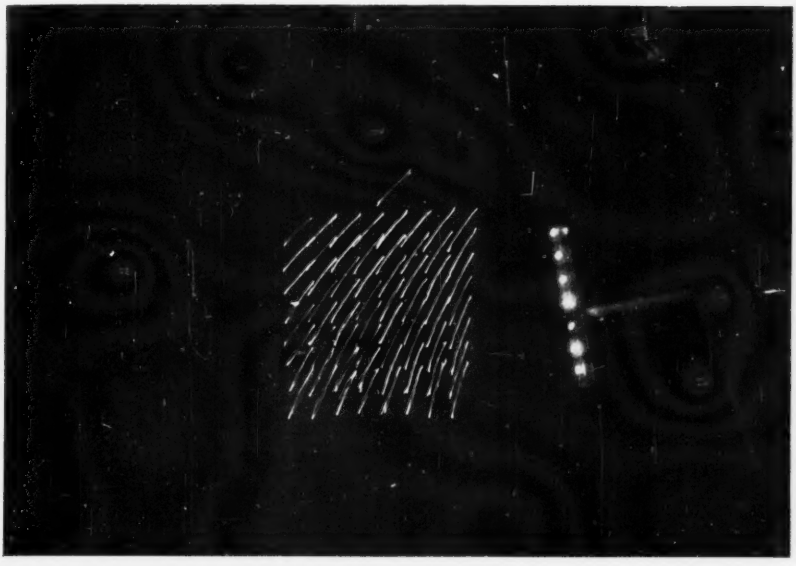

(*a*)

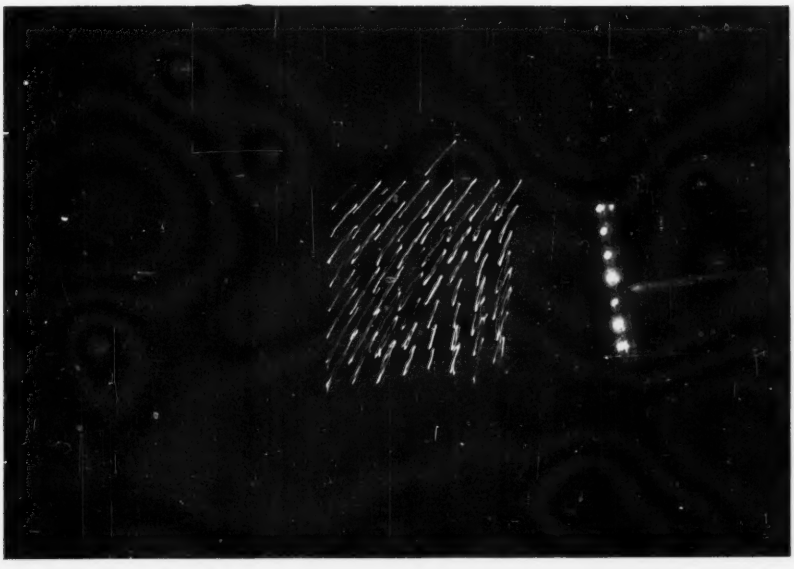

(*b*)

For legend see plate 2.

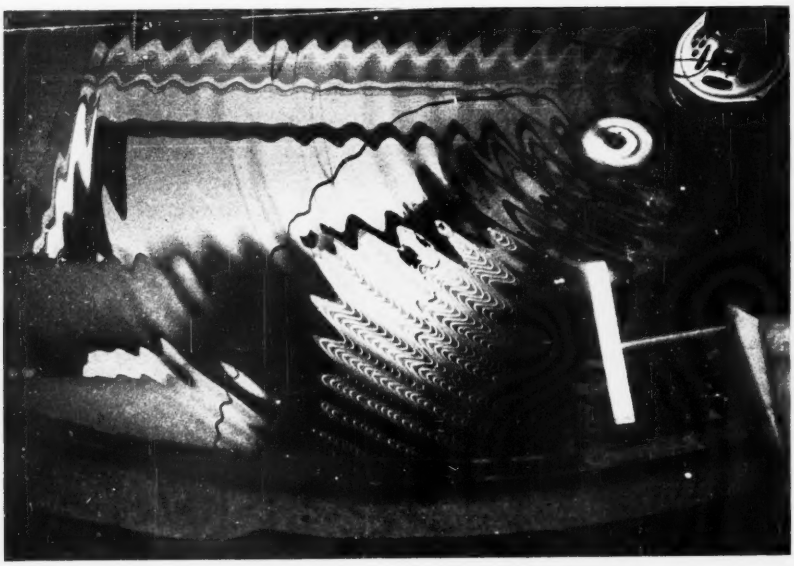

(*c*)

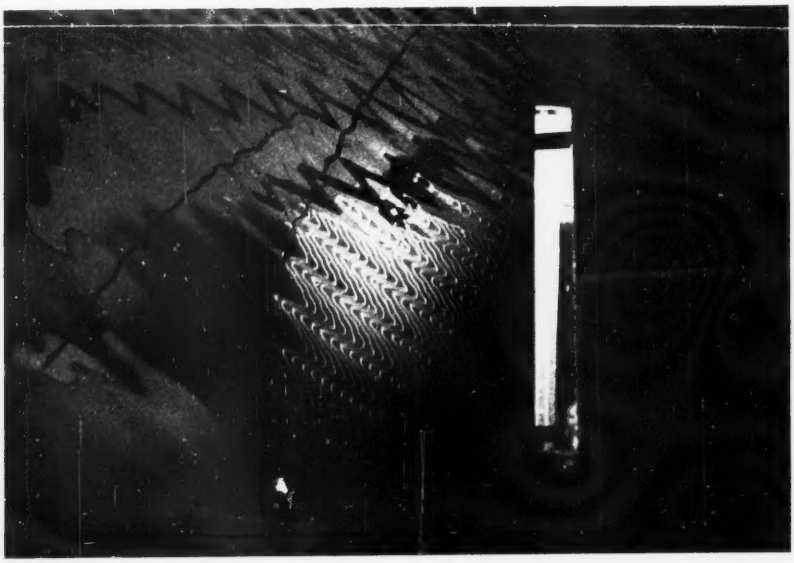

(*d*)

FIGURE 4. (Plates 1 and 2.) (*a*) Selected photograph for the determination of wave amplitudes in the presence of a shear flow (6·00 c/s). (*b*) Rejected wave amplitude photograph (6·00 c/s). (*c*) Wave-number photograph with shear flow (6·00 c/s). (*d*) Wave-number photograph without shear flow (10·5 c/s).

The development of three-dimensional disturbances in an unstable film of liquid flowing down an inclined plane

By T. BROOKE BENJAMIN

Department of Engineering, University of Cambridge

(Received 11 November 1960)

On the basis of results from a previous paper, expressions are found for the phase velocity and amplification rate of a wave travelling obliquely to the direction of flow. This wave comprises the general harmonic component of three-dimensional small disturbances, and accordingly a double Fourier integral is introduced to represent a bounded disturbance whose initial distribution over the free surface may be arbitrarily prescribed. Hence an asymptotic approximation is derived for a disturbance which is initially concentrated around a point on the free surface. Several distinctive properties of a localized unstable disturbance are noted: for instance, it lies mainly within an elliptical region whose area increases linearly with time as it moves downstream and which is modulated by long-crested waves. An experimental observation of a growing disturbance on an unstable film is recorded, and its main features are seen to be in agreement with the theory.

In so far as linearized perturbation theory remains applicable, the effects investigated are common to a wide class of parallel and nearly parallel laminar flows. In the final part of the paper the method used to analyse the instability of a film is generalized in order to reveal the connexion between this and other problems; this aim is achieved by demonstrating collective properties of the complete class of flows in question, but particular reference is made to the example of laminary boundary layers and Poiseuille flow between parallel planes.

1. Introduction

In an earlier paper concerning the stability of laminar flow down an inclined plane (Brooke Benjamin 1957; hereafter this paper will be referred to as I), expressions were obtained for the velocity and rate of growth of a small disturbance in the form of an infinitely long-crested sinusoidal wave travelling in the direction of flow. The main purpose of the present paper is to show how these results can be adapted to predict the properties of a wave directed obliquely to the flow and hence, by Fourier integration, can be used to analyse the development of an initially concentrated disturbance. While not adding to the essential solution of the stability problem as established in I, this analysis is useful in providing an interpretation of what actually happens when a film becomes unstable. A photograph is presented in §3 which shows a patch of waves on an unstable film, and the theory appears to account very well for the outstanding features of this disturbance.

The investigation in I used the same basic method that occupies most of the vast literature on the theory of hydrodynamic stability, its essentials being that a two-dimensional wave is assumed to disturb the two-dimensional primary flow and that when a stability criterion for such a disturbance is derived from the linearized equations of motion, it is tested over all values of the wavelength. Justification for considering only two-dimensional disturbances† is given by the theorem due to Squire (1933), which shows a three-dimensional wave disturbance to have the same properties as a two-dimensional one for a smaller flow velocity, i.e. for a smaller Reynolds number; therefore, if the flow is stable until the velocity exceeds a certain value, the neutral wave which marks the limit of stability at this critical value must be two-dimensional. Although Squire's theorem leaves no doubt as to the adequacy of two-dimensional theories in proving theoretical limits of stability, there remains the important yet sometimes neglected point that such theories are generally insufficient to account for the actual event of instability when these limits are exceeded. For unless special measures are taken to introduce disturbances which are approximately two-dimensional, the first manifestation of instability will be of an essentially three-dimensional character since initial disturbances will arrive at the unstable region of the flow more or less randomly in spatial distribution as well as in time.

Under slightly supercritical conditions in general, linearized theory indicates a range of amplified waves both two- and three-dimensional, yet with a varying rate of amplification which is greatest for a certain two-dimensional wave; and so, during the time the theory remains applicable, this wave will tend to become the predominant component in the Fourier analysis of a developing transient disturbance. This property accounts for the occasional successes of two-dimensional theories in predicting the 'most prominent' wave in observed cases of instability developing naturally (i.e. without artificial excitation); for instance, waves in keeping with the Tollmien–Schlichting theory were observed in the experiments of Schaubauer & Skramstad (see Schlichting 1955, ch. 16, §*e*) when the disturbances in a laminar boundary layer were allowed to arise spontaneously from background turbulence which had been reduced to the exceptionally low level of 0·03 %; and also in this respect the theory in I was found to check with experimental observations made by Binnie (1957). It is seldom the case, however, that initial disturbances are so small as to allow enormous amplifications following linearized theory, to the extent that the aforementioned selective process leaves the manifestation of instability with little trace of its original three-dimensional character. Linearized theory may nevertheless often account for a preliminary stage of amplification, during which the optimum long-crested wave may develop some degree of prominence yet other components still remain significant, particularly those three-dimensional ones neighbouring to the optimum.

These considerations rather suggest that the natural role of linearized perturbation theories in relation to many problems of hydrodynamic stability—particularly ones where non-linear effects are known to arise readily—is to de-

† More precisely, it is justification for considering only the components with $\beta = 0$ in a Fourier analysis of an arbitrary small disturbance in terms of wave-numbers α, β respective to the direction of flow and the transverse direction.

scribe the growth of localized essentially three-dimensional disturbances. As the basic element composing the preliminary stages of instability, one may usefully imagine an expanding region of perturbed flow which is initiated from a fairly tightly concentrated disturbance swept into the unstable part of the stream; as the region grows, the optimum long-crested wave will become progressively more prominent within it. To reiterate the main point of the present argument, we suggest there may often be a phase of significant duration described by linearized theory (even long enough to permit asymptotic approximations—as introduced in the following analysis) but in which the perturbed region does not expand so far as to cease to be an essentially three-dimensional entity—say by reaching all lateral boundaries of the flow. The over-all structure of the unstable flow, at least of its preliminary stages, may be conceived as an assembly of such elements; where they overlap, the optimum wave components need not coincide in phase, and it seems possible that phase randomness among the predominant spectral component often contributes largely to the disorder observed in hot-wire signals detecting the onset of boundary-layer instability.

The present problem may be proposed as a helpful illustration of this general aspect of stability theory, both because the properties of three-dimensional transient disturbances in a film can be found approximately without much difficulty, and also because the effects in question can readily be observed experimentally. In both these respects the problem is unusually straightforward; it is, for instance, much more so than the corresponding problem for an unstable boundary layer. Apparently no complete theory of the growth of small three dimensional disturbances in any flow of boundary-layer type has yet been given in the literature,† though there have been several investigations of the properties of individual three-dimensional waves (see particularly Watson 1960). Nor apparently have any directly relevant experimental observations been reported. Accordingly, one object of this paper is to emphasize the illustrative value of the film problem in this general connexion. The method of analysis applied in § 2 to the main problem will be generalized in § 4 in order to show how the properties exemplified by a film may prevail in other circumstances; and in particular it will be shown how, proceeding from the corresponding theory of two-dimensional disturbances, a calculation like that in § 2 can be completed for plane Poiseuille flow and for laminary boundary layers.

One feature to be demonstrated in § 4 is in fact absent from the main problem, which is thereby made specially simple. This is the dispersive effect arising from variations in the velocity of propagation of unstable waves. The velocity is constant in the approximate theory applied to the problem of an unstable film.

2. Analysis

The problem to be considered is indicated in figure 1. Liquid with density ρ, viscosity $\rho\nu$ and surface tension $\rho\Gamma$ flows in a uniform film of thickness h down a

† But Dr W. Criminale presented a paper on this subject at the AGARD conference on boundary-layer theory in London earlier this year (1960). He has made extensive calculations for a particular velocity profile, so dealing comprehensively with an example of the general problem covered briefly in § 4.

plane inclined at an angle θ to the horizontal. This primary flow is steady and laminar, so that the velocity profile is a parabolic arc with its vertex in the free surface. The velocity u_0 of the free surface will be taken as the unit of velocity for the purpose of defining dimensionless variables, and h will be taken as the unit of length. As shown in figure 1, Cartesian axes (x, y, z) are taken with x directed down the plane parallel to the flow and z directed transversely. Our main object is to find the properties of a small disturbance superposed on this flow and initially concentrated around a point in the (x, z)-plane; subsequently, if the flow is unstable, the disturbance will spread over a progressively wider area of the plane.

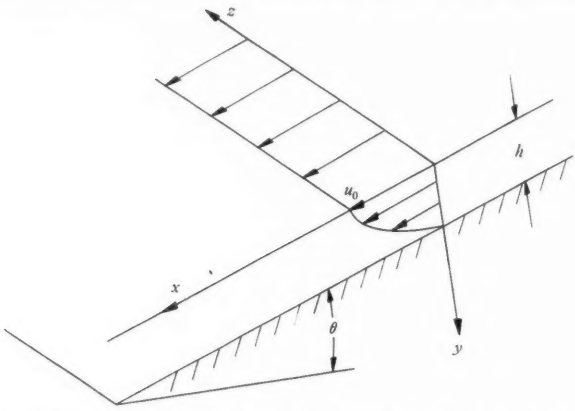

FIGURE 1. Diagram of the undisturbed flow, showing the velocity profile.

The analysis will be based on the following results which were obtained in I for the case of disturbances independent of z. The displacement of the free surface from its equilibrium plane was represented by the real part of

$$\eta = \delta e^{i\alpha(x-ct)}, \tag{1}$$

where δ is a constant representing the initial wave amplitude. There is no need here to express the corresponding velocity perturbations; it is sufficient to recall that they depend on x and time t in the same way as η, and that they are functions of y which vanish at the solid boundary. The waves observed in practice when the conditions of stability are slightly exceeded are extremely long compared with the film thickness; accordingly, an approximate theory was developed in I, §5, on the assumption that the dimensionless wave-number $\alpha\,(= 2\pi h/\text{wave-length})$ is small. On this basis, the real and imaginary parts of c were found to be

$$c_r = 2, \tag{2}$$

$$c_i = \tfrac{1}{3}R\{(\tfrac{8}{5} - G)\,\alpha - T\alpha^3\}, \tag{3}$$

where $R = u_0 h/\nu$ is the Reynolds number, and where $G = gh\cos\theta/u_0^2$ and $T = \Gamma/hu_0^2$ are numbers characterizing the effects of, respectively, gravity and surface tension on the disturbance. Note that c_r and c_i as given by (2) and (3) express the respective physical quantities as multiples of u_0. The parameters R

and G are not independent in this problem, since the primary flow itself constitutes a balance between viscous forces and the weight of the liquid (see I, § 2): their relationship is in fact

$$G = \frac{2\cot\theta}{R} = \frac{8R_c}{5R}, \tag{4}$$

in which R_c is the critical value of R defined in the next paragraph. (The notation of (3) differs somewhat from the original presentation in I; in particular, the Reynolds number in I was based on the mean velocity and so is equivalent to $\frac{2}{3}R$ here.)

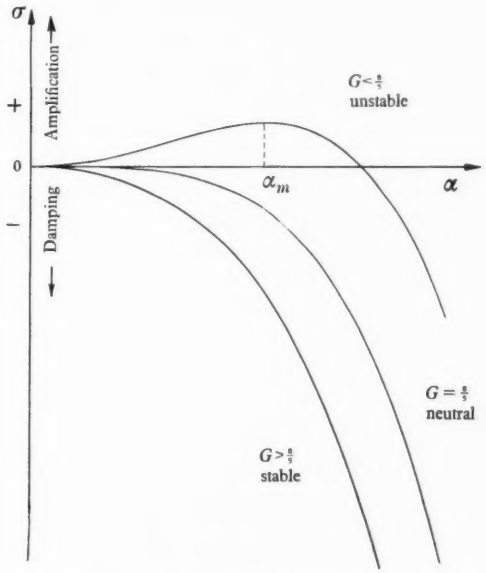

FIGURE 2. Typical graphs of amplification rate $\sigma = \alpha c_i$ as a function of wave-number α according to equation (3). Here σ is proportional to $k\alpha^2 - \alpha^4$, where k is a number which is positive, zero and negative, respectively, in the unstable, neutral and stable cases.

The sign of $\sigma = \alpha c_i$ is a criterion of stability since σt forms the real part of the exponent on the right-hand side of equation (1). Thus equation (3) shows that the flow is unstable when $G < \frac{8}{5}$ [i.e. $R > R_c$, where $R_c = \frac{5}{4}\cot\theta$], because then $\sigma > 0$ for a range of small values of α, that is, there are waves whose amplitude increases indefinitely with time. Some typical graphs of σ *vs* α are drawn in figure 2 in order to show clearly the meaning of this result. Under unstable conditions, σ has a positive maximum σ_m (i.e. there is a maximum rate of amplification) at a wave-number given by

$$\alpha_m^2 = \frac{\frac{8}{5} - G}{2T} = \frac{4(1 - [R_c/R])}{5T}; \tag{5}$$

and the fact that α_m is indefinitely small when the stability condition is just exceeded confirms the appropriateness of the small-α approximation. When the plane is vertical, we have $G = 0$ for every R and hence we see that the flow is

always unstable. However, it was shown in I that for a vertical film σ_m is extremely small for Reynolds numbers below a certain 'quasi-critical' range, but in this range it suddenly becomes large. This explains the sudden appearance of waves in experiments where the Reynolds number is gradually increased from small values. For water at normal temperatures the quasi-critical range is near $R = 6$, and the corresponding α_m is still quite small. Experiments made by Binnie (1957, 1959) have substantially confirmed the stability theory summarized here.

[It is noted incidentally that these results also apply to a film running down the under side of an inclinded plane. As $\frac{1}{2}\pi < \theta < \pi$ in this case, so that $G < 0$, equation (3) shows gravity to have a destabilizing effect, as would be expected on physical grounds. The film is always unstable for $\frac{1}{2}\pi \leqslant \theta \leqslant \pi$, and in the limit $\theta \to \pi$ which makes $u_0 \to 0$ the present results describe the Taylor instability of a stationary liquid layer (cf. I, p. 568).]

Let us next consider a three-dimensional disturbance for which the displacement of the free surface may be represented by

$$\eta = \delta \exp\{i(\alpha x + \beta z) - i\alpha c t\}. \tag{6}$$

Allowing complex values of δ and both positive and negative values of α and β, we see that this expression constitutes the most general Fourier component in the (x, z)-plane; that is, every possible simple-harmonic function of x and z is obtainable by linear superposition of the real parts of such expressions. At the same time we recognize that the disturbance represented is essentially a long-crested wave having a wave-number $\gamma = (\alpha^2 + \beta^2)^{\frac{1}{2}}$ and propagating at velocity $(\alpha/\gamma)\, c_r$ in a direction inclined at an angle $\tan^{-1}(\beta/\alpha)$ to the x-axis [i.e. c_r is the phase velocity in the x-direction, which is of course larger than the velocity in the direction of propagation].

Expressions for c_r and c_i in this case can at once be inferred from (2) and (3) by appeal to the well-known theorem due to Squire (1933), and further explained by Yih (1955), which states in effect that the properties of the disturbance depend on the primary flow only in respect of its component in the direction of propagation. Thus (2) is to be interpreted as an expression for the wave velocity in the oblique direction, with $(\alpha/\gamma)\, u_0$ instead of u_0 taken as the unit of velocity; and so, reverting to the original unit, we deduce immediately that the wave velocity in the x-direction is

$$c_r = 2 \tag{7}$$

in this case as before. A similar interpretation holds for (3) with $(\alpha/\gamma)\, u_0$ replacing u_0 in the definitions of R, G and T (e.g. $(\alpha/\gamma)\, R$ must be written in place of R if R is to retain its previous meaning); and hence we get

$$c_i = \frac{1}{3}\frac{\alpha}{\gamma} R\left\{\tfrac{8}{5}\gamma - G\frac{\gamma^3}{\alpha^2} - T\frac{\gamma^5}{\alpha^2}\right\}, \tag{8}$$

where R, G, and T mean the same as before. The logarithmic rate of growth is therefore

$$\sigma = \alpha c_i = \tfrac{1}{3} R\{\tfrac{8}{5}\alpha^2 - G(\alpha^2 + \beta^2) - T(\alpha^2 + \beta^2)^2\}. \tag{9}$$

Figure 3 shows a typical contour map of σ in the (α, β)-plane. The maxima of σ occur at points $\pm\alpha_m$ along the α-axis, this optimum value of α being, of

course, the value given by (5). The contour $\sigma = 0$ divides the plane into stable and unstable regions, since waves for which the point (α, β) lies outside this contour are damped ($\sigma < 0$) and waves for which (α, β) lies inside are amplified ($\sigma > 0$).

Introducing the moving axis $x' = x - c_r t$, whose origin travels downstream at the constant velocity $c_r = 2$, we now have that the most general harmonic component is

$$\delta \exp\{i(\alpha x' + \beta z) + \sigma(\alpha, \beta)\, t\},$$

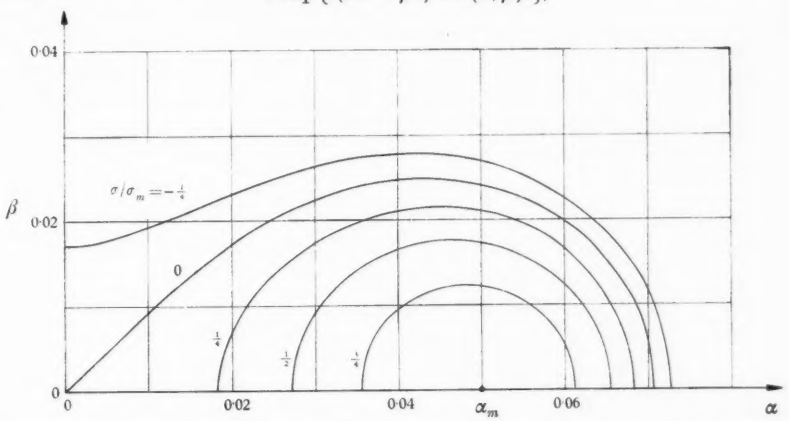

FIGURE 3. Contours of constant amplification rate σ in the first quadrant of the (α, β)-plane; the figure in the complete plane is symmetrical about both axes. In this example it is specified that $G = \frac{4}{9}$ and $T = 160$; hence $\sigma_m = R/3000$ and $\alpha_m = 0{\cdot}05$.

where δ is independent of x', z and t, and where α and β are any pair of positive or negative real numbers. Hence disturbances of arbitrarily prescribed form at $t = 0$ can be represented by double Fourier integrals of the type

$$\eta = \int_{-\infty}^{\infty}\int_{-\infty}^{\infty} \delta(\alpha, \beta) \exp\{i(\alpha x' + \beta z) + \sigma t\}\, d\alpha\, d\beta. \tag{10}$$

We are here restricted to initial disturbances $\eta(x', z, 0)$ for which there exists a Fourier transform $\delta(\alpha, \beta)$ in the real variables α and β (e.g. we cannot deal with functions, such as periodic ones, which do not vanish at infinite distances from the origin), but all cases relevant to the physical problem under consideration are clearly admissible.

Whatever the initial distribution $\delta(\alpha, \beta)$ of wave components, it is clear that, as t increases, those components for which σ lies very close to the maximum σ_m will eventually predominate over all others; and on this principle an asymptotic approximation to (10) may readily be obtained by Laplace's method (Erdélyi 1956, §2·4). The general result that η eventually depends only on $\delta(\alpha_m, 0)$ will be confirmed in §4, and for the present we shall fix attention on the following example. Taking $\delta(\alpha, \beta) = \text{const.}$ in (10), we have a disturbance which at $t = 0^+$ is highly concentrated in the vicinity of the point $x' = 0$, $z = 0$, and which at this and subsequent times is represented by

$$\eta = \int_0^{\infty}\int_0^{\infty} \cos \alpha x' \cos \beta z\, e^{\sigma t}\, d\alpha\, d\beta, \tag{11}$$

where for simplicity an amplitude factor of unity is taken. While the fact should be kept in mind that the asymptotic approximation to be derived is not dependent on the special choice of δ, this example serves particularly well to demonstrate esssentials. The initially uniform distribution of wave components is the most clearly conceivable starting-point for the process of selective amplification; and there is the important practical aspect that with such a distribution the asymptotic approximation becomes reliable sooner than with a non-uniform initial distribution having its greatest density away from the point of maximum amplification. Thus initially concentrated disturbances are the most likely to manifest the predicted asymptotic behaviour distinctly in practice, a conclusion that was borne out by the experiments described in §3.

Laplace's method takes the leading terms of the expansion of σ about σ_m, which are

$$\sigma = \sigma_m - a(\alpha - \alpha_m)^2 - b\beta^2, \tag{12}$$

with

$$a = \tfrac{2}{3}R(\tfrac{8}{5} - G), \quad b = \tfrac{8}{15}R. \tag{13}$$

The approximation to (11) is therefore

$$\eta \sim e^{\sigma_m t}\int_0^\infty \cos\alpha x' e^{-at(\alpha-\alpha_m)^2}d\alpha \int_0^\infty \cos\beta z e^{-bt\beta^2}d\beta. \tag{14}$$

In (14) the integral with respect to β is a standard result, and that with respect to α is reducible approximately to a similar integral by changing the lower limit to $-\infty$, the effect of this change being within the over-all error. The outcome is, apart from a numerical factor with no significance here,

$$\eta \sim \frac{1}{t}e^{\sigma_m t}\cos\alpha_m x' \exp\left\{-\frac{x'^2}{4at} - \frac{z^2}{4bt}\right\}. \tag{15}$$

The following features of this result are worth noting separately:

(1) The amplitude of the disturbance grows according to $t^{-1}e^{\sigma_m t}$, not exponentially as might be expected. [Note that for a two-dimensional localized disturbance the corresponding result would be $t^{-\frac{1}{2}}e^{\sigma_m t}$; in the present case each of the two integrals in (14) contributes a factor $t^{-\frac{1}{2}}$.]

(2) The disturbance remains centred at the origin of x'; thus the developing wave-pattern is transported downstream at the velocity $c_r = 2$.

(3) The disturbance is effectively confined within an elliptical region whose dimensions grow proportionally to $t^{\frac{1}{2}}$, i.e. its area increases linearly with time.

(4) The ratio of the axis of the ellipse in the flow direction to the transverse axis is

$$\epsilon = \left(\frac{a}{b}\right)^{\frac{1}{2}} = (2 - \tfrac{5}{4}G)^{\frac{1}{2}} = 2^{\frac{1}{2}}\left(1 - \frac{R_c}{R}\right)^{\frac{1}{2}}. \tag{16}$$

The ellipse is therefore very oblong in the transverse direction when the film is just unstable, i.e. when R slightly exceeds R_c. The outline of the disturbance becomes circular ($\epsilon = 1$) when $R = 2R_c$; and when R is more than twice its critical value, the disturbance becomes elongated in the flow direction. For a vertical film, $G = 0$ and so $\epsilon = \sqrt{2}$.

[Equation (16) also applies to a film on the under side of an inclined plane (i.e. $\frac{1}{2}\pi < \theta < \pi$, $G < 0$ and hence $\epsilon > \sqrt{2}$), provided the inclination is not too far from the vertical. When $\theta \to \pi$, (16) indicates that $\epsilon \to \infty$; but this result is

spurious, as readily appears on reconsideration of the expression (9) for σ. For, if the film lies beneath a nearly horizontal plane, so that $-G$ is large yet $G/T = gh^2 \cos\theta/\Gamma \to -gh^2/\Gamma$, then the optimum wave is determined primarily by the second and third terms on the right-hand side of (9). Hence σ is very nearly equal to σ_m for $\alpha^2+\beta^2 = gh^2/2\Gamma$, i.e. on a circle centred at the origin in the (α, β)-plane; and though, if the plane is not quite horizontal, absolute maxima σ_m still occur at $\alpha = \pm\alpha_m$, $\beta = 0$, they are not distinct enough for the present asymptotic approximation to be reliable.]

Finally, as regards physical applications of the foregoing analysis, the following points need mention:

(*a*) The expressions that were used for c_r and c_i are accurate only when α and β are small, yet the initial disturbance was represented as a synthesis of an indefinitely wide range of wave-numbers over which these expressions were taken to hold. This step is legitimate, however, as a convenient means to obtaining the asymptotic approximation, i.e. our description of the disturbance when it has grown large enough to be composed from the optimum part of the wave-number spectrum. (Our assumption that α is small in the optimum range relies, of course, on (5).) Components at large wave-numbers are known to be rapidly damped anyway (see I, §4), and so it is immaterial that they are assigned an incorrect though still rapid rate of damping.

(*b*) Regarding the accuracy of (15) as an asymptotic approximation, a statement as to a sufficient magnitude of t is still lacking. By developing the asymptotic expansion of which (15) is the first term, one can see that (15) would certainly be a close approximation whenever t is large enough to make $\sigma_m t/\alpha_m$ substantially greater than the major axis of the ellipse. When t is this large, (15) becomes accurately applicable whatever the form of the initial disturbance; but, at least for the case of a concentrated initial disturbance as represented by (11), it would appear that (15) still describes roughly the main features of the wave-pattern when t is much smaller than this. There seems little point in attempting to improve the present approximation on the basis of the simple formulae taken from I, because the limitations of these formulae in respect of the matter (*a*) above is probably just as important as the limitations of (15) as an approximation to (11) or, as it is more generally (cf. §4), an approximation to (10).

(*c*) A more serious consideration than either of the above is that before the asymptotic behaviour according to linearized theory is approximately established, a disturbance may grow to a size at which non-linear effects become important. The initial disturbance clearly must be quite small for the present results to be applicable at some subsequent stage, but it would be very difficult to predict the practical limitations in this regard, and the matter is best left to be settled by experiment.

3. An experimental observation

Figure 4 (plate 1) shows an example of the phenomenon in question, and this photograph happily bears out the approximate theory proposed above. It is thought desirable to include this isolated observation for its illustrative

value, even though a comprehensive experimental check on the predictions listed below equation (15) has not yet been made. The experiment that provided figure 4 was done in collaboration with Mr W. Troutman.

In the experimental arrangement a thin film was formed on an inclined sheet of plate glass by allowing water to flow through a gap under a rectangular bar spanning the sheet. The pool of water above the gap was supplied by seepage through layers of muslin, so that the pool was very little disturbed by the incoming flow; and by straining the glass sheet careful adjustments of the gap were made in order to produce a film that was approximately uniform over a fairly wide span. The velocity u_0 of the free surface was measured by timing the progress of dust particles in the surface, and then the film thickness h was calculated by means of the following formula given by rearrangement of (4):

$$h^2 = 2u_0\nu/g\sin\theta. \tag{17}$$

Hence the Reynolds number $R = u_0h/\nu$ was obtained. This estimate of R was found generally to agree closely with the estimate $R = 3Q/2\nu$ in which Q, the volume flow rate per unit span, was measured by collecting and weighing the flow.

The long-crested waves that can be seen near the bottom of figure 4 (plate 1) developed spontaneously, presumably as the outcome of small fluctuations in the stream which in turn were due to disturbances in the pool of water behind the gap or to vibrations picked up by the whole apparatus. The regularity of these waves can be attributed to the fact that any disturbance was rapidly transmitted over the surface of the pool and so communicated to the whole span of the film.

At a good distance above the place where the naturally excited waves first appeared, localized disturbances were introduced into the film either by touching the free surface momentarily with a fine wire or by delivering it a minute puff of air through a capillary tube; these methods were equally effective, though the first was more easily controlled. The disturbances were made at points about 2 cm downstream from the opening of the gap; it was unsuitable to make them any nearer than this to the beginning of the film since a disturbance was then liable to be spread unduly by being transmitted along the meniscus attached to the vertical face of the bar. A sequence of very short ripples was seen to radiate rapidly from the initial disturbance, but these ripples were damped out within a short distance. If, however, the film was unstable, a pattern of much longer waves was also seen to develop from the disturbance, increasing progressively in area and amplitude as it travelled downstream.

When the present photograph was taken, the slope θ was $13{\cdot}1^\circ$ and u_0 was found to be 6·35 cm/sec. The temperature of the water was $18{\cdot}6^\circ$ C, and hence it was estimated that $\nu = 0{\cdot}0104\,\mathrm{cm^2/sec}$ and $\Gamma = 73{\cdot}0\,\mathrm{cm^3/sec^2}$. With this u_0 and ν, (17) gives $h = 0{\cdot}0244$ cm, and it follows $R = 14{\cdot}9$. The critical Reynolds number for this slope is $R_c = \frac{5}{4}\cot\theta = 5{\cdot}4$, and thus it is confirmed that the film was unstable.

The disturbance shown in figure 4 was photographed when it had travelled about 25 cm downstream from its point of origin. This patch of waves is seen to have an approximately elliptical outline, and the wave crests are seen to be

approximately parallel at right angles to the flow direction. The patch is slightly oblong in the flow direction, and ϵ may be estimated to be about 1·1 With the data given in the last paragraph, the theoretical value of ϵ according to (16) is 1·13. From the photograph the optimum wavelength may be estimated as $\lambda_m = 2{\cdot}1$ cm, and the theoretical value found from (5) is $\lambda_m = 1{\cdot}85$ cm, corresponding to $\alpha_m = 0{\cdot}083$; this seems a reasonable agreement (cf. Binnie 1959). It was also confirmed, though only roughly, that the waves travelled at about twice the velocity of the free surface, and that after a disturbance had developed into a distinct pattern such as shown in figure 4, its area grew approximately linearly with time. The latter property was most readily checked by observing that the extremities of the transverse axis described a parabola as the axis moved downstream at constant speed.

The stage at which the theory ceased to apply, owing to the development of significant non-linear effects, was indicated by deformations of the wave-pattern in the following way. Along each transverse ridge formed by a wave crest, the central parts where the amplitude was largest began to travel considerably faster than the outlying parts, so that the ridge became progressively more convex in the downstream direction. However, it could sometimes be observed that even when the waves in the interior of a patch had grown so large as to be greatly distorted by the non-linear effects, the lateral outskirts of the patch continued to spread in the manner predicted by the linearized theory.

4. Generalization of the previous analysis with application to unstable laminar flows of boundary-layer type

An advantage of the problem previously considered is that it affords a simple illustration of properties common to a wide class of parallel or nearly parallel flows, which includes Poiseuille flow between parallel planes and laminar boundary layers. Accordingly, it will now be shown how the mathematical arguments used in §2 may be extended to other examples of hydrodynamic instability possessing the distinctive feature that a certain two-dimensional wave disturbance has a maximum rate of growth for given conditions of flow. The general method of approach will be explained with particular reference to the important cases just mentioned, for which the mechanism of instability depends only on fluid inertia and a constant viscosity; the previous example should suffice to indicate the procedure when there are other physical factors (e.g. gravity and surface tension acting on a free surface, or continuous variations of density or viscosity). The properties of a three-dimensional disturbance in plane Poiseuille flow or in a boundary layer will not, however, be evaluated explicitly as was done for the previous example; the aim here is merely to give a formal demonstration of their general character. In addition to properties already exemplified in §2, we have to consider the effects of variations of c_r with wave-number.

The solution to the stability problem for plane Poiseuille flow is now well established (Lin 1955, ch. 3), and this may be considered the archetype of the various available theoretical results which are adaptable to present treatment. The boundary layer formed by incompressible flow over a flat plate presents a closely related stability problem, having usually been treated as if the primary

flow were parallel (Lin 1955, ch. 5; Schlichting 1955, chs. 16 and 17). Various predictions based on this approximation have been confirmed experimentally; but we must note with caution that our use here of the approximate theory, neglecting boundary-layer growth and the change of Reynolds number in the direction of flow, stands in need of special justification. On this basis an analysis of the development of a discrete disturbance as it moves downstream remains secure only while the distance travelled, as well as the length of the disturbance, covers insignificant changes of boundary-layer thickness. Nevertheless, it seems reasonable to suppose that the usefulness of the theory could be considerably extended by taking the boundary-layer parameters to vary slowly in the results worked out on the assumption of fixed parameters.

In the existing analyses of these problems, the equations of motion are linearized in terms of velocity and stress perturbations in the general form

$$v = \hat{v}(y; \alpha, R)\, e^{i\alpha(x-ct)}, \tag{18}$$

where α is real. The 'wave amplitude distributions' $\hat{v}$ are functions only of the co-ordinate y perpendicular to the solid boundaries, i.e. they are indepenent of time t and the co-ordinate x in the flow direction; but they depend parametrically on α and Reynolds number R. For the velocity perturbation parallel to y, the respective function $\hat{v}$ is a solution of the well-known Orr–Sommerfeld equation, and for the velocity parallel to x the respective $\hat{v}$ is the first derivative of a solution (see Lin, ch. 1). There is no need, however, for us to recall the relationships among the velocity and stress components; and, to fix ideas regarding the physical meaning of the subsequent analysis, we can henceforth take $\hat{v}$ to refer specifically to the velocity parallel to y.

Consideration of two-dimensional wave disturbances in the form (18) is sufficient to solve the stability problem, since Squire's theorem proves that such a wave is the one maintained at the 'critical' Reynolds number—i.e. at the limit of stability. With the boundary conditions, the linearized dynamical equations and the continuity equation constitute a characteristic-value problem leading to a relationship of the type (see Lin, ch. 3)

$$F(\alpha, R, c) = 0. \tag{19}$$

Each pair of values α and R thus specifies a value of c, which is generally complex. (In other words, the Orr–Sommerfeld equation and the boundary conditions on its general solution comprise a system which provides *discrete* eigenvalues c and eigenfunctions $\hat{v}(y; \alpha, R)$.)

This relationship is extremely complicated, in contrast to the simple case discussed in § 2, and it cannot be solved so as to give c explicitly in terms of general values of α and R. The practical solution to the stability problem is instead usually presented as a 'curve of neutral stability' in the (α, R)-plane, which is worked out numerically by putting $c_i = 0$ and eliminating c_r between the real and imaginary parts of (19) [see Schlichting (1955, pp. 328, 329) for an example]. Further contours of c_i have been worked out for some problems (see figure 5). Though certain approximations can be made, justified by α being fairly small yet αR large, the calculations are still very laborious. Even so, and notwith-

standing the form of the numerical results, it is implicit in this procedure that c is a definite function of α and R. That is, we can write

$$c = c_r + ic_i = \mathbf{c}(\alpha, R), \tag{20}$$

using bold type to denote the prescribed function, and we know that this function may at least be estimated by interpolation on the available contour maps of c_r and c_i in the (α, R)-plane. [Incidentally, it is easily verified that $\mathbf{c}(-\alpha, R)$ is the complex conjugate of $\mathbf{c}(\alpha, R)$, which we denote by $\tilde{\mathbf{c}}(\alpha, R)$.]

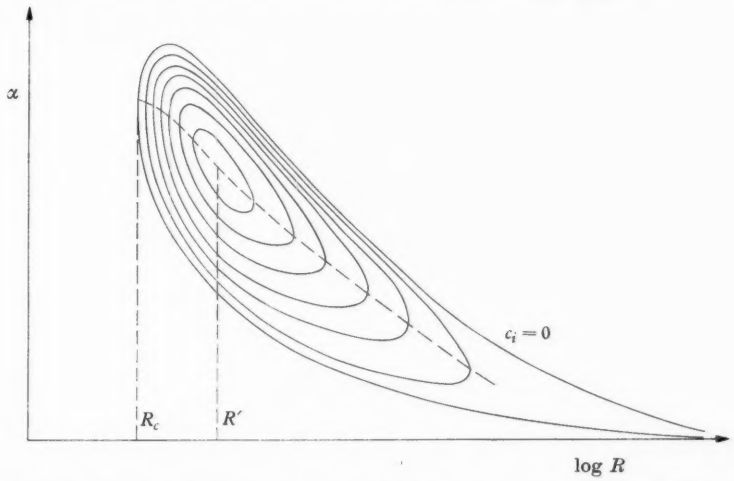

FIGURE 5. Contours of constant c_i (zero and positive values) in the (α, R)-plane, with R expressed on logarithmic scale. The dashed curve is the locus of the maxima of c_i for given values of R, and an absolute maximum occurs at $R = R'$; this curve necessarily lies below the locus of the maxima of σ.

As the key to the present application of stability theory, Squire's theorem may be restated as follows. For a perturbation in the form

$$v = \hat{v}(y) \exp\{i(\alpha x + \beta z) - i\alpha ct\}, \tag{21}$$

where z is the co-ordinate perpendicular to (x, y), the result corresponding to (20) is

$$c = \mathbf{c}(\gamma, R^*), \tag{22}$$

where $\gamma = (\alpha^2 + \beta^2)^{\frac{1}{2}}$ and $R^* = (\alpha/\gamma) R$ [this notation follows Watson (1960)], and where $\mathbf{c}$ is the *same* function of the two variables that occurs in the solution (20) to the two-dimensional problem. (Note that γ takes the same sign as α.) Furthermore, the amplitude factor in (21) satisfies a form of the Orr–Sommerfeld equation with parameters γ, R^* instead of α, R; thus $\hat{v} \equiv \hat{v}(y; \gamma, R^*)$ according to the definition used in (18).

Figure 5 shows a map of c_i in the (α, R)-plane, such as is obtained for plane Poiseuille flow on the basis of the two-dimensional theory. There is no need here to discuss the differences between this example and similar maps for boundary layers with negative, zero or positive pressure gradient; it seems enough to recog-

nize that, despite these differences which generally arise where R is much greater than the critical value R_c, there is in all cases a distinct range of R above R_c to which the conclusions explained in the next paragraph definitely apply (because, in effect, the different sets of curves all have the same character at the left-hand end of the unstable region). This range at least covers the phase of boundary-layer instability for which the linearized theory is most likely to be useful. Now, the present interest of diagrams like figure 5 is that, because of (22), the values of c_i for three-dimensional waves in the form (21) can also be found from them. Since $\gamma R^* = \alpha R$, these values are found simply by tracing a hyperbola $\alpha R = \text{const.}$ to the left from the respective point α on the ordinate for the given R. [For example, if we want c_i for $\alpha = 0{\cdot}2$ and $\beta = 0{\cdot}15$ at $R = 1000$, we have $\gamma = 0{\cdot}25$, $R^* = 800$, and so we find the value of c_i at the point $(0{\cdot}25, 800)$ on the (α, R)-diagram calculated for two-dimensional waves.]

For $\beta = 0$ a general property illustrated by figure 5 is that, at any given finite R greater than R_c, c_i is positive over a certain finite range of α and has a single maximum in this range. It follows that $\sigma = \alpha c_i$ has a positive maximum, say σ_m, and we write α_m for the respective value of α; thus α_m is determined as a function of R by satisfying the equation

$$\frac{\partial \sigma}{\partial \alpha} = \left[1 + \alpha \frac{\partial}{\partial \alpha}\right] \mathbf{c}_i(\alpha, R) = 0. \tag{23}$$

To admit the method of asymptotic approximation used in § 2, the present case must provide the property that, for a given supercritical value of R, σ_m is greater than any value of σ obtained with $\beta \neq 0$, i.e. the optimum two-dimensional wave is the most unstable for the given R. For confirmation on this point, which is actually a rather delicate one having no directly obvious proof, we may refer to the work of Watson (1960). He showed in general that $\sigma(\alpha, \beta, R)$ is greatest for $\alpha = \alpha_m$, $\beta = 0$ at least when R is given in the range above R_c terminated by the value at which c_i has its absolute maximum (e.g. R' in figure 5). For higher Reynolds numbers no definite result can be stated; but in the case of Poiseuille flow Watson assessed the available numerical evidence to imply that the most unstable wave is a two-dimensional one at all Reynolds numbers above the critical.†

† Being based on Squire's theorem these deductions depend crucially on the assumption that the flow is effectively unbounded in z, as also does the paramount deduction that the critical Reynolds number is determined by a two-dimensional wave. But it may be noted incidentally that the mathematical statement of Squire's theorem also holds for complex values of β, in which case the present conclusions are invalidated. In particular, for a disturbance with real exponential z-dependence, β is purely imaginary and we have $\gamma < \alpha$ for $|\beta| < \alpha$, which indicates by virtue of (22) that such a disturbance can be unstable at Reynolds numbers below the critical value for two-dimensional waves. Such disturbances are clearly possible in the presence of a lateral boundary to the flow; more precisely, there can be disturbances which become exponentially decreasing in z outside the extra 'boundary layer' formed in the primary flow. For this reason it may prove impossible to avoid some measure of 'premature' instability in experiments simulating plane Poiseuille flow; because whatever form of lateral boundaries are used, there can be disturbances between the parallel planes which are to some degree sensitive to the presence of these boundaries.

Proceeding from (21), the next step is to introduce a double Fourier integral to represent a localized disturbance. As an extension of the method that was used in § 2, we shall here take account of y-variations and so represent a three-dimensional disturbance *in toto*, rather than restricting as before to the distribution over a particular (x, z)-plane. We recognize in advance, however, that this extension scarcely adds to what is directly deducible by the original method which, if applied again, would still afford a complete description of events in any given (x, z)-plane consequent to arbitrary initial conditions in that plane. The following three-dimensional synthesis represents the y-dependence which is apparently concomitant with a (x, y)-distribution initially specified in a chosen plane, and so it does not add to the degree of arbitrariness available in setting an initial-value problem. We shall not attempt to establish whether or not the initial distribution in three dimensions might be represented with greater generality, i.e. to seek a uniqueness theorem supporting the present method of representation. But presumably the method is in fact adequate, particularly as disturbances of the type (22) with harmonic dependence on x and z are apparently the only ones possible in the present theoretical model which is unbounded in x and z, and also as the eigenfunctions $\hat{v}$ presumably may form a complete set. In any case it appears that at least every unstable element of any disturbance is represented here; and so in this context, where the aim is to derive properties due to the class of unstable waves, there would be little point in pursuing the mathematical issues relating to generalization of the initial-value problem.

We accordingly consider

$$v(x,y,z,t) = \int_{-\infty}^{\infty}\int_{-\infty}^{\infty} \delta(\alpha,\beta)\,\hat{v}(y;\gamma,R^*)\exp\{i(\alpha x+\beta z-\alpha c_r t)+\sigma t\}\,d\alpha\,d\beta, \quad (24)$$

where $\delta(\alpha, \beta)$ is an arbitrary function. If at $t = 0$ the perturbation v is prescribed over a certain plane $y = 0$, say, and if the Fourier transform of $v(x, 0, z, 0)$ is $g(\alpha, \beta)$, then we have that $\delta(\alpha, \beta) = g(\alpha, \beta)/\hat{v}(0; \gamma, R^*)$. Hence, when this expression for $\delta(\alpha, \beta)$ is substituted in the integral, v is determined by (24) for all $t \geqslant 0$.

In order to derive an asymptotic approximation to (24) for large t, the amplification rate σ has to be expanded as far as quadratic terms in $\alpha - \alpha_m$ and β. [For the time being we only consider the maximum at $(\alpha_m, 0)$, leaving the equal one at $(-\alpha_m, 0)$ to be treated later.] The corresponding expansion of the frequency $\omega = \alpha c_r$ is also needed. Considering further the case of Poiseuille flow or boundary layers, we shall now show how the required expansions may be deduced from $\omega + i\sigma = \alpha \mathbf{c}(\gamma, R^*)$, where the function $\mathbf{c} = \mathbf{c}_r + i\mathbf{c}_i$ is in principle known from the solution to the respective two-dimensional problem. Using suffix m to refer always to the optimum conditions $\beta = 0$, $\alpha = \gamma = \alpha_m$, $R^* = R$, we have $(\partial\sigma/\partial\alpha)_m = 0$ by definition (cf. (23)); and we get, using (23) to obtain the second equality,

$$\left(\frac{\partial^2\sigma}{\partial\alpha^2}\right)_m = 2\left(\frac{\partial \mathbf{c}_i}{\partial\gamma}\right)_m + \alpha_m\left(\frac{\partial^2 \mathbf{c}_i}{\partial\gamma^2}\right)_m$$

$$= -\frac{2}{\alpha_m}(\mathbf{c}_i)_m + \alpha_m\left(\frac{\partial^2 \mathbf{c}_i}{\partial\gamma^2}\right)_m = -2p, \quad \text{say}, \quad (25)$$

where p must be a positive constant since σ_m is a maximum. The first two equalities in (25) indicate how p can be evaluated from data such as are plotted in figure 5. It is next observed that

$$\frac{\partial\sigma}{\partial\beta} = \frac{\alpha\beta}{\gamma}\frac{\partial \mathbf{c}_i}{\partial\gamma} - \frac{\alpha^2\beta R}{\gamma^3}\frac{\partial \mathbf{c}_i}{\partial R^*}, \tag{26}$$

since
$$\frac{\partial\gamma}{\partial\beta} = \frac{\beta}{\gamma}, \quad \frac{\partial R^*}{\partial\beta} = \alpha R\frac{\partial}{\partial\beta}\left(\frac{1}{\gamma}\right) = -\frac{\alpha\beta R}{\gamma^3}.$$

Hence we get
$$\left(\frac{\partial\sigma}{\partial\beta}\right)_m = 0, \quad \left(\frac{\partial^2\sigma}{\partial\alpha\partial\beta}\right)_m = 0, \tag{27}$$

and
$$\left(\frac{\partial^2\sigma}{\partial\beta^2}\right)_m = \left(\frac{\partial \mathbf{c}_i}{\partial\gamma}\right)_m - \frac{R}{\alpha_m}\left(\frac{\partial \mathbf{c}_i}{\partial R^*}\right)_m$$
$$= -\frac{1}{\alpha_m}\left\{(\mathbf{c}_i)_m + R\left(\frac{\partial \mathbf{c}_i}{\partial R^*}\right)_m\right\} = -2q, \quad \text{say.} \tag{28}$$

Here q is positive as an implication of Watson's proof, referred to above, that σ is greatest for the optimum two-dimensional wave; and (28) shows how q also is deducible from data such as in figure 5. The required approximation to σ is therefore
$$\sigma = \sigma_m - p(\alpha-\alpha_m)^2 - q\beta^2. \tag{29}$$

Consider next the frequency $\omega = \alpha c_r$. In the same way that (26) leads to (27), we get
$$\left(\frac{\partial\omega}{\partial\beta}\right)_m = 0, \quad \left(\frac{\partial^2\omega}{\partial\alpha\partial\beta}\right)_m = 0,$$
and so we have
$$\omega = \omega_m + \left(\frac{\partial\omega}{\partial\alpha}\right)_m(\alpha-\alpha_m) + \frac{1}{2}\left(\frac{\partial^2\omega}{\partial\alpha^2}\right)_m(\alpha-\alpha_m)^2 + \frac{1}{2}\left(\frac{\partial^2\omega}{\partial\beta^2}\right)_m\beta^2 \tag{30}$$
to the second order in $\alpha-\alpha_m$ and β. Here $\omega_m = \alpha_m(\mathbf{c}_r)_m$, and the three derivatives can be found from the solution to the two-dimensional problem, just as was shown above for the derivatives of σ.

We now introduce
$$X = x - U_m t, \tag{31}$$
where
$$U_m = \left(\frac{\partial\omega}{\partial\alpha}\right)_m = (\mathbf{c}_r)_m + \alpha_m\left(\frac{\partial \mathbf{c}_r}{\partial\gamma}\right)_m$$
is the *group velocity* of the wave of maximum amplification, and we also write
$$\left.\begin{aligned} V = U_m - (c_r)_m = \alpha_m\left(\frac{\partial \mathbf{c}_r}{\partial\gamma}\right)_m, \quad \zeta = \alpha-\alpha_m, \\ 2\kappa = -\left(\frac{\partial^2\omega}{\partial\alpha^2}\right)_m, \quad 2\mu = -\left(\frac{\partial^2\omega}{\partial\beta^2}\right)_m. \end{aligned}\right\} \tag{32}$$

Hence, when the approximation (30) is substituted, the imaginary part of the exponent in (24) can be arranged in the form
$$\alpha_m(X+Vt) + \zeta X + \beta z + \kappa\zeta^2 t + \mu\beta^2 t. \tag{33}$$

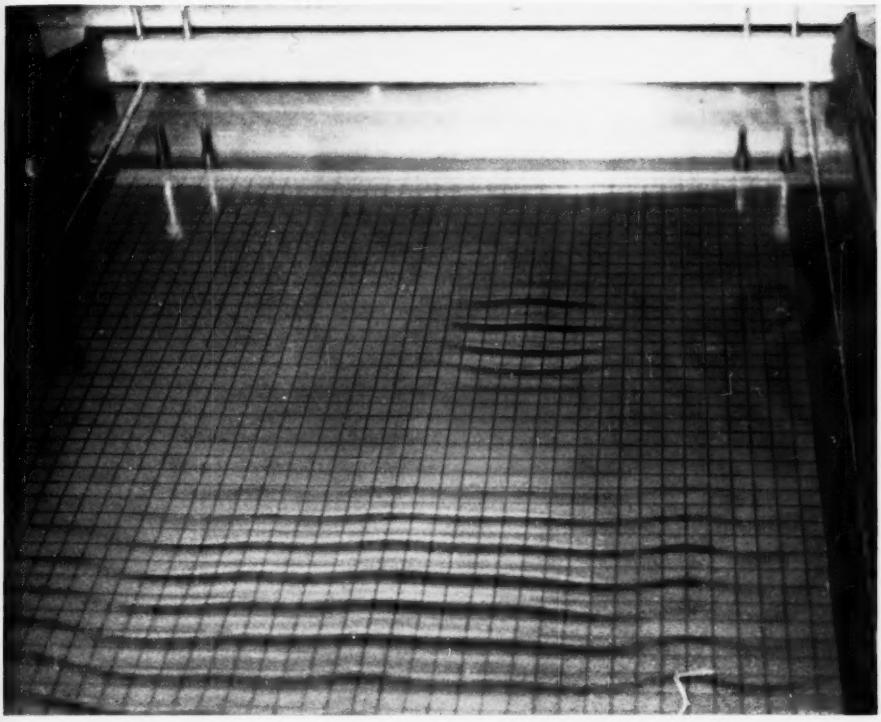

FIGURE 4. Photograph showing an elliptical patch of waves developing on an unstable film of water. The graticule which can be seen here consisted of $\frac{1}{2}$ in. squares and was attached to the under side of the sheet of glass down which the film was running.

(*Facing p.* 416)

In deriving an asymptotic approximation to (24) by Laplace's method, (29) and (33) are the expansions to second order required to account for the maximum of σ at $(\alpha_m, 0)$. The expansions appropriate to the other maximum at $(-\alpha_m, 0)$ are immediately deducible from (29) and (33) on recognition of the fact, noted below (20), that $\mathbf{c}(-\gamma, R^*) = \tilde{\mathbf{c}}(\gamma, R^*)$. In terms of the new variables $\zeta' = -(\alpha+\alpha_m)$, $\beta' = -\beta$, the form of the expansion of σ is seen to be unchanged from (29), while the form of the expansion of ω is seen to be the same as (33) except for an over-all change of sign. Thus, for the two maxima, the respective approximations to the exponential factor in (24) are complex conjugates. In keeping with Laplace's method, the areas of integration of the respective approximations may each be allowed to cover the whole plane; and the method also permits the factor $g(\alpha, \beta)\,\hat{v}(y; \gamma, R^*)/\hat{v}(0; \gamma, R^*)$ in the integrand to be evaluated at the maxima (where $\gamma = \pm\alpha_m, R^* = R$) and hence taken outside the integral signs. Use can also be made of the fact that $\hat{v}(y;\ -\alpha_m, R)$ is the conjugate of $\hat{v}(y; \alpha_m, R)$, which is easily verified from the Orr–Sommerfeld equation. The approximation to (24) is therefore expressible in the form

$$v \sim g(\alpha_m, 0)\, I + g(-\alpha_m, 0)\, \bar{I}, \tag{34}$$

where

$$I = \left[\frac{\hat{v}(y; \alpha_m, R)}{\hat{v}(0; \alpha_m, R)}\right] \exp\{\sigma_m t + i\alpha_m(X + Vt)\}$$
$$\times \int_{-\infty}^{\infty} \exp\{i\zeta X + (-p + i\kappa)\,\zeta^2 t\}\, d\zeta \int_{-\infty}^{\infty} \exp\{i\beta z + (-q + i\mu)\,\beta^2 t\}\, d\beta, \tag{35}$$

and $\bar{I}$ is the conjugate of I.

The exponential factor and the integrals in (35) provide the most interesting features of this result, and we may conveniently explain the other features and dismiss them here before performing the integrations. Two of the properties demonstrated might have been expected from the start. First, it is seen that whatever the initial distribution of wave components in the (α, β)-plane, the disturbance depends asymptotically only on the densities of the distribution at the points $(\pm\alpha_m, 0)$, i.e. on the measure of the optimum two-dimensional waves in a Fourier analysis of the initial disturbance. Secondly, the y-distribution of the developing disturbance is shown to become asymptotically the same as that of the optimum wave. Both these properties have been established by the simplest detail of Laplace's general method, namely that some factors in the integrand which are independent of the large parameter t can be evaluated at the maxima of the real exponent σt; the principle is, of course, that the (α, β)-variations of these factors are insignificant in comparison with variations of the real exponential. That the $\hat{v}$ factors can be so treated, whereas variations in the x- and z-dependent factors must be allowed for, derives from the nature of the function $\hat{v}$, or more specifically from the boundary conditions which it must satisfy. For whereas the ultimate range of an unstable disturbance has no prescribed limit in x or z, which accords with x and y entering the integrand in harmonic functions, the range of variation in y is essentially limited. Even for a boundary layer where v is required to vanish on only one plane, the condition that $\hat{v}$ remain bounded for $y \to \infty$ requires that $\hat{v} = e^{-\gamma y}$ outside the layer (see, for instance, Schlichting

1955, p. 320). Thus changes in y-structure cannot continue indefinitely, such as can on the other hand in the 'opening out' of a wave train; and it is easy to see physically that the y-structure 'fixes' when the wave components near the optimum become predominant [e.g. $v \sim e^{-\alpha_m y} \times$ (function of x, z, t) outside a boundary layer].

Evaluation of the integrals in (35) is straightforward. Leaving aside the features explained in the last paragraph, and also dropping a numerical factor which is immaterial here, we can state the general result as follows. On any plane inside the flow and parallel to the boundaries, the distribution of the disturbance is given asymptotically by some linear combination of the real and imaginary parts of

$$\frac{\exp\{\sigma_m t + i\alpha_m(X+Vt)\}}{t} \exp\left\{-\left(\frac{A+iB}{4t}\right)X^2 - \left(\frac{C+iD}{4t}\right)z^2\right\}, \tag{36}$$

where

$$A+iB = \frac{p+i\kappa}{p^2+\kappa^2}, \quad C+iD = \frac{q+i\mu}{q^2+\mu^2}. \tag{37}$$

The point needing emphasis here is that a result of this form is applicable to every problem of the general class in question. Special attention has been paid to Poiseuille flow and boundary layers because of their importance and also to give an example of how the coefficients in (36) may be evaluated; but it is implied that this set of coefficients is a definite attribute of every physical system which can be unstable in the general manner under consideration. (For a film of liquid flowing under gravity, we recall from §2 that $p = a$, $q = b$, $\kappa = 0$, $\mu = 0$; also $V = 0$ so that $X = x'$.)

The following is a list of the properties expressed by this result and stands as a generalization of the set of properties noted below (15) in §2:

(1) The over-all amplitude of the disturbance increases as $t^{-1}e^{\sigma_m t}$.

(2) The disturbance is centred at the origin of (X, z) since the factor $\exp\{-(AX^2+Cz^2)/4t\}$ describes a 'Gaussian' distribution of amplitude along any radius from the origin. The disturbance is therefore effectively confined within an expanding elliptical region outlined by

$$(AX^2+Cz^2)/4t = \text{const.}, \quad \text{say about 3.}$$

The axes of the ellipse both increase as $t^{\frac{1}{2}}$, and consequently its area increases linearly with t.

(There is apparently no general conclusion to be drawn as regards the relative magnitudes of A and C and hence the eccentricity of the ellipse. We recall from §2 that when a film is made marginally unstable, then $C/A = a/b \simeq 0$ and so the ellipse is greatly elongated in the z-direction; but this feature is peculiar to the problem and does not arise in general.)

(3) Since $x = U_m t$ at $X = 0$, the disturbance is carried downstream at the group velocity U_m associated with the two-dimensional wave of maximum amplification.

(4) The (X, z)-distribution of the disturbance is modulated by this wave travelling at velocity $-V$ relative to X; i.e. the wave travels downstream at its phase velocity $(\mathbf{c}_r)_m = U_m - V$, but is cancelled everywhere except in the elliptical patch which advances through the wave train at relative velocity V.

(5) Another effect of dispersion due to variable c_r is represented by the factor $\exp\{-i(BX^2+Dz^2)/4t\}$. The disturbance is thus modulated by undulations whose spacing rapidly decreases with distance from the centre; however, they will only appear as a prominent feature of the disturbance if B and D are considerably greater than A and C respectively. For these undulations the contours of constant phase are ellipses whose areas increase linearly with time, and the pattern formed by superposition of them upon the Gaussian distribution considered in (2) above is similar at all times.

Finally, the points labelled (*b*) and (*c*) at the end of §2 may be recognized to apply generally to the foregoing results. The matter (*c*) regarding limitations on the theory due to non-linear effects particularly deserves re-emphasis, since these limitations are liable to be more severe for other problems than for the one investigated in §2. For instance, disturbances in unstable boundary layers are known to develop dependence on non-linear interactions very readily unless under conditions where their initial magnitude is unusually small, and the extent to which the properties described here may be actually manifested remains in doubt in the absence of any direct evidence. Nevertheless, the reasons given in §1 seem definitely to suggest that present ideas may often be relevant to a certain incipient phase of instability, in plane Poiseuille flow and boundary layers as well as the incontestable example demonstrated in §§2 and 3, and these ideas may generally provide a rather more realistic account of events in this phase than the basic two-dimensional form of stability theory.

REFERENCES

Brooke Benjamin, T. 1957 *J. Fluid Mech.* **2**, 554; corrigendum, **3**, 657.

Binnie, A. M. 1957 *J. Fluid Mech.* **2**, 551.

Binnie, A. M. 1959 *J. Fluid Mech.* **5**, 561.

Crimnale, W. 1960 Paper read to the AGARD meeting on boundary layer research, London (April).

Erdélyi, A. 1956 *Asymptotic Expansions.* New York: Dover.

Lin, C. C. 1955 *The Theory of Hydrodynamic Stability.* Cambridge University Press.

Schlichting, H. 1955 *Boundary Layer Theory.* London: Pergamon.

Squire, H. B. 1933 *Proc. Roy. Soc.* A, **142**, 621.

Watson, J. 1960 *Proc. Roy. Soc.* A, **254**, 562.

Yih, C.-S. 1955 *Quart. Appl. Math.* **12**, 434.

Hydrodynamic stability and the inviscid limit

By K. M. CASE

Department of Physics, The University of Michigan, Ann Arbor, Michigan

(Received 16 December 1959 and in revised form 31 October 1960)

It is shown that for appropriately posed problems, the solutions of the linearized Navier–Stokes equations approach those of the linearized Euler equations as the viscosity tends to zero.

1. Introduction

The conventional approach to hydrodynamic stability problems considers the Navier–Stokes equations linearized around some basic stationary flow. Since the viscosity is usually quite small it seems reasonable, as a first approximation, to put it equal to zero at the outset. However, the relation of stability results so obtained to those using the full Navier–Stokes equations has been rather obscure. The difficulty arises for various mathematical reasons.

(1) It is commonly stated (to quote, for instance, Lin 1955, p. 126) '. . . that there are certain damped solutions in a viscous fluid which, in the limit of vanishing viscosity, do not reduce to solutions of the inviscid equation throughout the whole region of the flow.'

(2) The solutions of the Orr–Sommerfeld equation are quite complicated. In particular it is hard to find asymptotic solutions for small viscosity which are accurate throughout the entire physical region.

(3) The inviscid problem is frequently formulated so that the normal modes obtained are not mathematically complete. (It is readily shown that the Orr–Sommerfeld normal modes *are* complete.) This renders it difficult to see how the inviscid normal modes can be used to solve the appropriate initial-value problem.

Recently (Case 1960) it has been pointed out that there are solutions of the linearized Euler equations of stability theory which are, on occasion, overlooked. This suggests that, under certain conditions which it should be possible to state clearly, results of stability calculations starting from the Navier–Stokes equations should pass in the limit of vanishing kinematic viscosity, i.e. $\nu \to 0$, into the results calculated starting from the Euler equations.

There are several physical arguments which point in this direction. First, it may be noted that in quantum mechanics a rather parallel situation exists. In passing from the Navier–Stokes to the Euler equations the terms of highest order in the derivatives are dropped. Similarly, to pass over to the classical mechanics limit from the Schroedinger equation one must drop the terms of highest order in the derivatives. We do not doubt, though, that in classical mechanics we have a consistent and accurate description of a large, well-defined class of phenomena. A second argument is more important. The Euler equations are readily obtained

as a rough approximation from the equations of statistical mechanics. A better approximation gives the Navier–Stokes equations. These in turn are not exact. Indeed, it is possible to derive an improved approximation, which consists of a set of equations which reduce to the Navier–Stokes equations only on omitting certain terms. The essential point is that the omitted terms are those of highest order in the derivatives. Thus, if passing from the Navier–Stokes to the Euler equations completely changes the character of the theory, it would seem that passing from the higher-order equations to the Navier–Stokes equations would do the same. If so, hydrodynamics would be no description of nature at all.

We hope that the main point is clear. It is not that the Euler equations describe as wide a class of phenomena as do the Navier–Stokes equations. (Classical mechanics does not describe as much as does quantum mechanics.) Rather it will be shown that for *appropriately posed and restricted problems* the Euler equations lead to the same results as do the Navier–Stokes equations in the limit of zero viscosity.

Here an approach is followed which leads to the above mentioned 'omitted' solutions. The initial-value problem will be solved with the Laplace transform technique. The advantage is that we gain the additional freedom of an appropriate choice of the inversion contour in the complex plane. In particular it is possible always to stay in regions where it is simple to construct asymptotic (with respect to ν) solutions of the relevant differential equations. It will be shown that passing to the limit of zero viscosity in the solution of the initial-value problem corresponding to the Navier–Stokes equations yields almost exactly the solution of the initial-value problem which follows from the Euler equations. The limitations are that the initial perturbations are the same and are smooth in the sense of physically realizable perturbations. The method of proof also suggests a systematic expansion in terms of inverse powers of the square root of the Reynolds number. However, this possibility is not explored here.

2. Statement of the theorem

For simplicity attention is restricted to two-dimensional parallel flows of a homogeneous, incompressible fluid. The flow is between parallel plates at $y = 0$ and $y = y_1$. In the unperturbed state the flow is described by a component $u_0(y)$ in the x-direction (parallel to the plates) and a y-component $v_0 \equiv 0$. We linearize the Navier–Stokes equations around this basic flow and take a Fourier transform with respect to x and a Laplace transform with respect to time t. If

$$v_{pk}(y) = \frac{1}{\sqrt{(2\pi)}} \int_{-\infty}^{\infty} e^{-ikx} dx \int_0^{\infty} e^{-pt} v_1(x, y, t)\, dt, \tag{1}$$

where v_1 is the perturbed velocity component in the y-direction, then the resulting equations can be simplified to

$$\nu\left(\frac{d^2}{dy^2} - k^2\right) V_p - (p + iku_0) V_p + \nu\left(\frac{d^2}{dy^2} - k^2\right) \frac{iku_0''}{p + iku_0} v_{pk} = -V(y, 0), \tag{2}$$

with

$$V_p(y) = \left\{\frac{d^2}{dy^2} - k^2 - \frac{iku_0''}{p + iku_0}\right\} v_{pk}(y), \tag{3}$$

and
$$V(y,0) = \left(\frac{d^2}{dy^2} - k^2\right) v_k(y,0). \tag{4}$$

These equations are to be solved subject to the boundary conditions

$$v_{pk} = 0 = u_{pk} = \frac{i}{k}\frac{\partial v_{pk}}{\partial y} \tag{5}$$

at $y = 0, y_1$.

In the inviscid limit we start with the Euler equations. The same sequence of approximations and transformations again lead to equation (2)—but with $\nu = 0$. This equation is then to be solved with only the boundary conditions

$$v_{pk}^{inv} = 0 \quad \text{at} \quad y = 0, y_1. \tag{5'}$$

(Here and below the convention is adopted that functions labelled with a superscript *inv* describe solutions of the initial-value problem based on the Euler equations.)

Our essential point is the following theorem:

$$(a)\ \lim_{\nu\to 0} v_{pk}(y) = v_{pk}^{inv} \quad 0 \leqslant y \leqslant y_1, \tag{6}$$

$$(b)\ \lim_{\nu\to 0} u_{pk}(y) = \begin{cases} u_{pk}^{inv} & 0 < y < y_1, \\ 0 & y = 0, y_1. \end{cases} \tag{7}$$

In view of the introductory remarks this result is hardly surprising. The discontinuous behaviour of u_{pk} at the boundaries is also to be expected. In virtue of equation (5) we have $u_{pk} = 0$ at the boundaries for all ν. This should also be true in the limit. (The discontinuity is only the mathematical description of an infinitesimal boundary layer.)

3. Proof

First note that a formal solution of equation (3) subject to $v_{pk} = 0$ at $y = 0, y_1$ is readily constructed. Let $\phi_{1,2}$ be two solutions of the homogeneous equation

$$\left\{\frac{d^2}{dy^2} - k^2 - \frac{iku_0''}{p + iku_0}\right\}\phi = 0, \tag{8}$$

subject to the conditions
$$\phi_1(0) = \phi_2(y_1) = 0. \tag{9}$$

Then
$$v_{pk}(y) = \int_0^{y_1} G(y, y_0)\, V_p(y_0)\, dy_0, \tag{10}$$

where
$$G(y, y_0) = \frac{\phi_1(y_<)\,\phi_2(y_>)}{W(\phi_1, \phi_2)}. \tag{11}$$

(Here $y_<$ and $y_>$ denote the lesser and greater of y and y_0 respectively.)

Also
$$W(\phi_1, \phi_2) = \phi_1\phi_2' - \phi_2\phi_1' = \text{const.} \quad \text{(independent of } y\text{)}. \tag{12}$$

Explicitly,

$$v_{pk}(y) = \frac{1}{W(\phi_1, \phi_2)}\left\{\phi_2(y)\int_0^y \phi_1(y_0)\, V_p(y_0)\, dy_0 + \phi_1(y)\int_y^{y_1} \phi_2(y_0)\, V_p(y_0)\, dy_0\right\}, \tag{13}$$

and
$$u_{pk}(y) = \frac{i}{kW}\left\{\phi_2'(y)\int_0^y \phi_1(y_0)\, V_p(y_0)\, dy_0 + \phi_1'(y)\int_y^{y_1} \phi_2(y_0)\, V_p(y_0)\, dy_0\right\}. \tag{14}$$

For the inviscid case this provides a complete solution. Thus, with $\nu = 0$ it follows from equation (2) that

$$V_p^{inv}(y) = \frac{V(y,0)}{p + iku_0(y)}. \tag{15}$$

Insertion of this result in equations (13) and (14) yields the transforms of the perturbed flow velocities.

To prove the theorem, consider the solution V_p of equation (2) for very small, but finite, ν. Clearly, it is sufficient† to determine V_p from

$$\left\{\frac{d^2}{dy^2} - ikR\eta(y)\right\} V_p = -RV(y,0), \tag{16}$$

where
$$R = 1/\nu, \tag{17}$$

and
$$\eta(y) = u_0(y) - \frac{i}{k}p. \tag{18}$$

As usual in applying the Laplace transform method the transform variable p is chosen to have a positive real part. This has the result that $\eta(y)$ in (16) never vanishes.

To solve equation (16) we consider the homogeneous equation

$$\left\{\frac{d^2}{dy^2} - ikR\eta(y)\right\} \Lambda = 0. \tag{19}$$

The asymptotic forms of the solutions of this equation are readily obtained by the W.K.B. approximation. There are two solutions $\Lambda_{1,2}$ which *can be chosen* so that for large R (small ν)

$$\Lambda_{1,2}(y) \sim \frac{1}{2^{\frac{1}{2}}(kR)^{\frac{1}{4}}[i\eta(y)]^{\frac{1}{4}}} \exp\left\{\mp (kR)^{\frac{1}{2}} \int_0^y [i\eta(y')]^{\frac{1}{2}}\, dy'\right\}. \tag{20}$$

Since $\eta(y)$ does not vanish, these representations hold for $0 \leqslant y \leqslant y_1$. (There is no Stokes phenomenon.) In equation (20) the multiplicative constants have been chosen so that

$$W(\Lambda_1, \Lambda_2) = 1. \tag{21}$$

The following fact is important. Let

$$\arg \eta(y) = \psi(y). \tag{22}$$

Since $\mathrm{Re}(p) > 0$, we have
$$-\pi \leqslant \psi \leqslant 0. \tag{23}$$

We define the square root in equation (20) so that

$$[i\eta(y')]^{\frac{1}{2}} = |\eta(y')|^{\frac{1}{2}}\{\cos\theta + i\sin\theta\}, \tag{24}$$

where
$$\theta = \tfrac{1}{2}\psi + \tfrac{1}{4}\pi. \tag{25}$$

Then
$$-\tfrac{1}{4}\pi \leqslant \theta \leqslant \tfrac{1}{4}\pi. \tag{26}$$

Therefore,
$$\cos\theta(y') > 0 \tag{27}$$

for all y'. From this it follows that, for fixed k and large R, Λ_1 and Λ_2 are, respectively, rapidly decreasing and increasing functions of y.

† This assumes v_{pk} is finite and well behaved in the limit $\nu \to 0$. That this is indeed so is readily verified in the final result.

One solution of equation (16) is

$$V_p^{(0)}(y_0) = -R\int_0^{y_1} \mu(y_0, y_0')\, V(y_0', 0)\, dy_0' \tag{28}$$

with

$$\mu(y_0, y_0') = -\Lambda_1(y_>)\,\Lambda_2(y_<). \tag{29}$$

A general solution is obtained by adding a linear combination of independent solutions of the homogeneous equation [equation (19)]. Thus,

$$V_p(y_0) = V_p^{(0)}(y_0) + E_1\Lambda_1(y_0) + E_2\Lambda_2(y_0). \tag{30}$$

Here E_1 and E_2 are constants which can be determined from the requirements that $u_{pk} = 0$ at $y = 0, y_1$.

From equation (14) we find that these conditions are that

$$\int_0^{y_1} \phi_{1,2} V_p\, dy = 0. \tag{31}$$

Solving for $E_{1,2}$ gives

$$E_1 = \frac{CJ_2 - DI_2}{I_1J_2 - I_2J_1}, \tag{32}$$

$$E_2 = \frac{DI_1 - CJ_1}{I_1J_2 - I_2J_1}, \tag{33}$$

where

$$\begin{pmatrix} C \\ D \end{pmatrix} = -\int_0^{y_1} \begin{pmatrix} \phi_2 \\ \phi_1 \end{pmatrix} V_p^{(0)}\, dy, \tag{34}$$

$$I_{1,2} = \int_0^{y_1} \phi_2 \Lambda_{1,2}\, dy, \tag{35}$$

and

$$J_{1,2} = \int_0^{y_1} \phi_1 \Lambda_{1,2}\, dy. \tag{36}$$

In order to estimate $V_p^{(0)}$ and $E_{1,2}$ in the limit of large R it is useful to invoke the following lemmas.

Let $F(y)$ be a continuous function (independent of R) with bounded first derivative. Let $0 \leqslant \alpha < \beta \leqslant y_1$. Then

$$(1)\quad \int_\alpha^\beta \Lambda_1 F\, dy = \frac{1}{2^{\frac{1}{2}}(kR)^{\frac{3}{4}}}\left\{\exp\left[-(kR)^{\frac{1}{2}}\int_0^\alpha (i\eta)^{\frac{1}{2}}\, dy'\right]\left[\frac{F(\alpha)}{[i\eta(\alpha)]^{\frac{3}{4}}} + O(R^{-\frac{1}{2}})\right]\right\}, \tag{37}$$

$$(2)\quad \int_\alpha^\beta \Lambda_2 F\, dy = \frac{1}{2^{\frac{1}{2}}(kR)^{\frac{3}{4}}}\left\{\exp\left[(kR)^{\frac{1}{2}}\int_0^\beta (i\eta)^{\frac{1}{2}}\, dy'\right]\left[\frac{F(\beta)}{[i\eta(\beta)]^{\frac{3}{4}}} + O(R^{-\frac{1}{2}})\right]\right\}. \tag{38}$$

The proof of these lemmas is based on the rapidly decreasing and increasing properties of Λ_1 and Λ_2 noted above. It uses standard techniques of asymptotic estimation and hence is relegated to the Appendix.

Insertion of these results into (28) yields

$$\begin{aligned} V_p^{(0)}(y_0) &= \frac{V(y_0, 0)}{ik\eta(y_0)} + O(R^{-\frac{1}{2}}) \\ &= \frac{V(y_0, 0)}{p + iku_0(y_0)} + O(R^{-\frac{1}{2}}). \end{aligned} \tag{39}$$

Comparing with equation (15), we see that

$$\lim_{R\to\infty} V_p^{(0)}(y_0) = V_p^{inv}(y_0). \tag{40}$$

The evaluation of $E_{1,2}$ is similar. The results are

$$E_1\Lambda_1(y) \sim \frac{\left\{-\int_0^{y_1}\phi_2 V_p^{inv}\,dy\right\}}{\phi_2(0)}\left\{(kR)^{\frac{1}{2}}\frac{[i\eta(0)]^{\frac{3}{4}}}{[i\eta(y)]^{\frac{1}{4}}}\right\}\exp\left[-(kR)^{\frac{1}{2}}\int_0^y [i\eta]^{\frac{1}{2}}dy'\right], \tag{41}$$

and

$$E_2\Lambda_2(y) \sim \frac{\left\{-\int_0^{y_1}\phi_1 V_p^{inv}\,dy\right\}}{\phi_1(y_1)}\left\{(kR)^{\frac{1}{2}}\frac{[i\eta(y_1)]^{\frac{3}{4}}}{[i\eta(y)]^{\frac{1}{4}}}\right\}\exp\left[-(kR)^{\frac{1}{2}}\int_y^{y_1}[i\eta]^{\frac{1}{2}}dy'\right]. \tag{42}$$

Since the real part of $[i\eta(y')]^{\frac{1}{2}}$ is always positive, we see that

$$\lim_{R\to\infty} E_1\Lambda_1(y) = \begin{cases} 0 & y \neq 0, \\ \infty & y = 0, \end{cases} \tag{43}$$

and

$$\lim_{R\to\infty} E_2\Lambda_2(y) = \begin{cases} 0 & y \neq y_1, \\ \infty & y = y_1. \end{cases} \tag{44}$$

In order to see the nature of the singularity in these limit functions we consider the integral of their product with a smoothly varying function $F(y)$. As in the proof of the lemmas (Appendix A) one finds that

$$\lim_{R\to\infty}\int_0^{y_1} F(y)\,E_1\Lambda_1(y)\,dy = -\left(\frac{\int_0^{y_1}\phi_2 V_p^{inv}\,dy}{\phi_2(0)}\right)F(0), \tag{45}$$

and

$$\lim_{R\to\infty}\int_0^{y_1} F(y)\,E_2\Lambda_2(y)\,dy = -\left(\frac{\int_0^{y_1}\phi_1 V_p^{inv}\,dy}{\phi_1(y_1)}\right)F(y_1). \tag{46}$$

These results can be stated concisely in the form

$$\lim_{R\to\infty} E_1\Lambda_1(y) = -\left(\frac{\int_0^{y_1}\phi_2 V_p^{inv}\,dy}{\phi_2(0)}\right)2\delta(y) \tag{47}$$

and

$$\lim_{R\to\infty} E_2\Lambda_2(y) = -\left(\frac{\int_0^{y_1}\phi_1 V_p^{inv}\,dy}{\phi_1(y_1)}\right)2\delta(y_1-y). \tag{48}$$

(Here the delta function is interpreted so that

$$\int_0^{y_1}\delta(y)\,dy = \tfrac{1}{2}.) \tag{49}$$

Thus, we have found that

$$\lim_{R\to\infty} V_p(y_0) = V_p^{inv} - \left(\frac{\int_0^{y_1}\phi_2 V_p^{inv}\,dy}{\phi_2(0)}\right)2\delta(y_0) - \left(\frac{\int_0^{y_1}\phi_1 V_p^{inv}\,dy}{\phi_1(y_1)}\right)2\delta(y_1-y_0). \tag{50}$$

If this form is inserted into equations (13) and (14), the theorem follows. [The difference in behaviour between v_{pk} and u_{pk} at the boundary points occurs because $\phi_1(0) = 0 = \phi_2(y_1)$ which is not true of $\phi_1'(0)$ and $\phi_2'(y_1)$.]

4. Conclusion

In the previous section an identity between the Laplace transform of the inviscid solution and the limit for small viscosity of the transform of the viscous solution was demonstrated. We would like to conclude from this that the solutions of the initial-value problem coincide in the limit. To do this we must show that the limiting process and the Laplace inversion integration can be interchanged. It is readily seen that the only difficulty that could occur is that the region of integration over p is infinite. However, for large p we may neglect the terms involving $u_0(y)$ in the basic equations (i.e. for large p we can regard the unperturbed flow as quiescent). Thus, to conclude that the solutions of the initial-value problems are identical it is sufficient to show this for the problem with $u_0(y) \equiv 0$. This is done in Appendix B. (The results there also show the form of the functions for finite viscosity which pass over into the singular functions described above.)

The conclusion is then the following. Consider a given initial perturbation. The flow at a fixed time later is, except for the singular behaviour of the tangential velocity at the boundaries, exactly the same whether computed with the Euler equations or with the Navier–Stokes equations and passage to the limit of zero viscosity.

The restriction to a fixed (finite) value of the time is important. We cannot justify interchange of the limits $\nu \to 0$ and $t \to \infty$. Thus, in the example in Appendix B, it is seen that

$$\lim_{t\to\infty} u_1, v_1 = 0 \quad \text{(all finite } \nu\text{)}, \tag{51}$$

but

$$\lim_{t\to\infty} u_1^{inv}, v^{inv} \neq 0. \tag{52}$$

This work was supported in part by the Office of Naval Research, U.S. Navy Department.

REFERENCES

Case, K. M. 1960 *Phys. Fluids*, **3**, 143.

Lin, C. C. 1955 *The Theory of Hydrodynamic Stability*. Cambridge University Press.

Appendix A: proof of the lemmas

Since the proofs are quite similar we restrict ourselves to sketching a proof for the first lemma.

It is desired to show that if $F(y)$ is a slowly varying function then, for large R,

$$K \equiv \int_\alpha^\beta \Lambda_1(y)\, F(y)\, dy$$

$$= \frac{1}{2^{\frac{1}{2}}(kR)^{\frac{1}{4}}} \left\{ \exp\left[-(kR)^{\frac{1}{2}} \int_0^\alpha (i\eta)^{\frac{1}{2}}\, dy \right] \left[\frac{F(\alpha)}{[i\eta(\alpha)]^{\frac{1}{4}}} + O(R^{-\frac{1}{2}}) \right] \right\}. \tag{A 1}$$

For large R we use the asymptotic representation, equation (20), for Λ_1. Then

$$K \sim \frac{1}{2^{\frac{1}{2}}(kR)^{\frac{1}{4}}} \int_\alpha^\beta \frac{F(y)}{[i\eta(y)]^{\frac{1}{4}}} \exp\left[-(kR)^{\frac{1}{2}} \int_0^y (i\eta)^{\frac{1}{2}}\, dy'\right] dy. \tag{A 2}$$

Insert the identity

$$\exp\left[-(kR)^{\frac{1}{2}} \int_0^y (i\eta)^{\frac{1}{2}}\, dy'\right] = -\frac{1}{(kR)^{\frac{1}{2}}} \frac{1}{[i\eta(y)]^{\frac{1}{2}}} \frac{d}{dy} \exp\left[-(kR)^{\frac{1}{2}} \int_0^y (i\eta)\, dy'\right], \tag{A 3}$$

and integrate by parts. Since the exponential factor vanishes rapidly with increasing y it is clear that the main contribution is that due to the part evaluated at the lower limit. If $F(y)$ is subject to the appropriate restrictions, we see by repeating the process in the remaining integral that the corrections are of the indicated order of magnitude. In this way the result, equation (A 1), is found for K.

Appendix B

It is necessary, as indicated in § 4, to show the identity of the solutions of the initial-value problem for the special case $u_0(y) = 0$. To keep the algebra simple we consider $y_1 = \infty$ and

$$V(y, 0) = \delta(y - y_0'). \tag{B 1}$$

Thus, for finite viscosity, we are to solve the equations

$$V_p = \left\{\frac{d^2}{dy^2} - k^2\right\} v_{pk}, \tag{B 2}$$

and

$$\nu\left(\frac{d^2}{dy^2} - k^2\right) V_p - pV_p = -\delta(y - y_0'), \tag{B 3}$$

subject to the boundary conditions

$$v_{pk} = 0 = u_{pk} = \frac{i}{k} \frac{\partial v_{pk}}{\partial y} \quad \text{at} \quad y = 0, \infty. \tag{B 4}$$

For the inviscid problem equations (B 2) and (B 3) with $\nu = 0$ are to be solved using only the condition

$$v_{pk}^{inv} = 0 \quad \text{at} \quad y = 0, \infty. \tag{B 5}$$

The solution of equation (B 2) which satisfies equation (B 5) is, in either case,

$$v_{pk}(y) = \int_0^\infty G(y, y_0)\, V(y_0)\, dy_0, \tag{B 6}$$

where (assuming $k > 0$)

$$G(y, y_0) = -\frac{1}{k} e^{-ky_>} \sinh ky_<. \tag{B 7}$$

In the inviscid case we find from equation (B 3) that

$$V_p^{inv} = \frac{\delta(y - y_0')}{p}. \tag{B 8}$$

Therefore

$$v_{pk}^{inv}(y) = G(y, y_0')/p. \tag{B 9}$$

Since the inverse Laplace transform of $1/p$ is 1 for all $t > 0$ we see that

$$v_1^{inv}(y, t) = G(y, y_0') \quad \text{for} \quad t > 0. \tag{B 10}$$

For finite ν the general solution of equation (B 3) subject to the condition of vanishing at infinity is

$$V_p(y_0) = V_p^{(0)}(y_0) + E_1 \Lambda_1(y_0), \tag{B 11}$$

where

$$V_p^{(0)}(y_0) = -R\mu(y_0, y_0'), \tag{B 12}$$

$$\mu(y_0, y_0') = -\Lambda_1(y_>)\,\Lambda_2(y_<), \tag{B 13}$$

and

$$\Lambda_{1,2} = \frac{e^{\mp \gamma y}}{(2\gamma)^{\frac{1}{2}}}, \tag{B 14}$$

with

$$\gamma = R^{\frac{1}{3}}(p + k^2/R)^{\frac{1}{3}}. \tag{B 15}$$

The constant E_1 is determined by the requirement

$$\frac{\partial v_{pk}}{\partial y} = 0 \quad \text{at } y = 0.$$

This gives

$$E_1 \Lambda_1(y_0) = \left\{ -\frac{\int_0^\infty V_p^{(0)} e^{-ky}\,dy}{\int_0^\infty \Lambda_1 e^{-ky}\,dy} \right\} \Lambda_1(y_0)$$

$$= -\frac{R}{\gamma}\, e^{-ky_0} e^{-\gamma y_0} + \frac{R}{2\gamma} e^{-\gamma(y_0 + y_0')} - R e^{-\gamma y_0} \frac{[e^{-ky} - e^{-\gamma y_0'}]}{\gamma - k}. \tag{B 16}$$

The inverse Laplace transformation then gives

$$v_1(y, t) = \int_0^\infty G(y, y_0) \{V^{(0)}(y_0, t) + (E_1 \Lambda_1)(y_0, t)\}\, dy_0, \tag{B 17}$$

with

$$V^{(0)}(y_0, t) = \frac{1}{2\pi i} \int_C V_p^{(0)}(y_0)\, e^{pt}\, dp, \tag{B 18}$$

$$(E_1 \Lambda_1)(y_0, t) = \frac{1}{2\pi i} \int_C E_1 \Lambda_1 e^{pt}\, dp. \tag{B 19}$$

Here C is a contour parallel to the imaginary axis and to the right of all singularities of the integrand. After some straightforward manipulation these become

$$V^{(0)}(y_0, t) = \Delta(y_0 - y_0', t), \tag{B 20}$$

$$(E_1 \Lambda_1)(y_0, t) = -2e^{-ky_0'} \Delta(y_0, t) + \Delta(y_0 + y_0', t) + \Gamma(y_0, t), \tag{B 21}$$

where

$$\Delta(y, t) = \frac{e^{-k^2 t/R}}{2\pi} \int_{-\infty}^{\infty} \{\exp[isy - s^2 t/R]\}\, ds, \tag{B 22}$$

and

$$\Gamma(y, t) = \frac{ik}{\pi} \int_{-\infty}^{\infty} \frac{e^{isy}[e^{-ky_0'} - e^{isy_0'}]\, e^{-s^2 t/R}\, ds}{s - ik}. \tag{B 23}$$

Passing to the limit in the integral expression for Δ clearly gives

$$\lim_{R \to \infty} \Delta(y, t) = \delta(y). \tag{B 24}$$

We can, of course, evaluate $\Delta(y, t)$ for all finite ν also. This gives

$$\Delta(y, t) = e^{-k^2 t/R} \frac{\{e^{-y^2 R/4t}\}}{(4\pi t/R)}. \tag{B 25}$$

Except for the first factor this is just the familiar heat pole solution. It vanishes as $R \to \infty$ for all fixed $y \neq 0$ and is such that the integral over all y is $e^{-k^2 t/R}$. (This serves again to justify equation (B 24).) Inserting the expression for $V^{(0)}$ in terms of Δ into equation (B 17) shows that for small, but finite viscosity, the first term is just the inviscid result averaged with respect to y_0' over a distance which is of order $(4t/R)^{\frac{1}{2}}$.

Since the function Γ is non-singular when $R \to \infty$, it suffices to pass to the limit under the integration sign. Thus

$$\lim_{R\to\infty} \Gamma(y_0, t) = \frac{ik}{\pi} \int_{-\infty}^{\infty} e^{isy_0} \frac{\{e^{-ky_0'} - e^{isy_0'}\}}{s - ik}\, ds. \tag{B 26}$$

Closing the contour with a large circle in the upper half plane yields then

$$\lim_{R\to\infty} \Gamma(y, t) = 0. \tag{B 27}$$

Combining these results shows that

$$\lim_{R\to\infty} \{V^{(0)}(y_0, t) + (E_1 \Lambda_1)(y_0, t)\} = \delta(y_0 - y_0') - 2e^{-ky_0'} \delta(y_0). \tag{B 28}$$

Using this result in (B 17) then gives

$$\lim_{R\to\infty} v_1(y, t) = v_1^{inv}(y, t) \qquad 0 \leqslant y < \infty, \tag{B 29}$$

$$\lim_{R\to\infty} u_1(y, t) = \frac{i}{k} \frac{\partial v_1}{\partial y}(y, t) = \begin{cases} u_1(y, t) & 0 < y < \infty, \\ 0 & y = 0. \end{cases} \tag{B 30}$$

Some mathematical problems in the theory of the stability of parallel flows

By C. C. LIN

Department of Mathematics, Massachusetts Institute of Technology

(Received 17 February 1960 and in revised form 6 January 1961)

By applying the method of initial values to the theory of stability of shear flows, Case has recently found certain results which are in apparent conflict with those obtained by the theory of normal modes. It is shown how these differences may be reconciled. Some new features in the theory of normal modes are also brought out. The relative merits of the two theories are compared.

1. Introduction

The usual theory of hydrodynamical stability is based on a study of the normal modes. There has been frequent controversy over this theory, because the behaviour of these normal modes are indeed very complicated at very large Reynolds numbers. For example, this writer (Lin 1955) has shown, from purely mathematical analysis, that '. . . there are certain damped solutions in a viscous fluid which, in the limit of vanishing viscosity, do not reduce to solutions of the inviscid equation throughout the whole region of the flow.' To those familiar with the theory of turbulence, such a behaviour is not at all surprising. Indeed, it is welcome as a concrete example of one of the fundamental characteristics of turbulent flow—i.e. that the flow field has an *intermittent spotty structure*. However, it is clear that the mathematical analysis leading to such a conclusion must be very complicated. In trying to clarify this situation as much as possible (and for other reasons), several attempts have been made to develop the theory of uniformly valid asymptotic solutions (see Langer 1940). Indeed, the old conclusions are found to be justified.

Recently, Case (1960, 1961) investigated the stability of parallel flows with respect to infinitesimal disturbances by considering the initial value problem. It is, of course, to be expected that there should be complete equivalence (cf. § 2) between this approach and the theory based on normal modes. Yet Case found that there were apparent inconsistencies, especially in connexion with the above-mentioned problem of the asymptotic limit as the Reynolds number becomes infinite. These apparent discrepancies disappear upon closer inspection. However, since they concern the fundamentals of the theories of stability and turbulence, and the problem is of general interest in the theory of singular perturbations of boundary-value problems of partial differential equations, it seems worth while to discuss the relationship between the two approaches in some detail so as to gain a deeper understanding of the issues. This is the purpose of the present note. The relative merits of the two approaches will be discussed in the concluding section of this paper.

It might be noted in passing, since the issue has been raised by Case (1961), that there is as yet no experimental evidence to suggest that the Navier–Stokes equations are inadequate to describe the phenomena of turbulent motion under ordinary conditions. For rarefied gases, the molecular structure should be considered once the Kolmogoroff scale of turbulence becomes comparable with the scales of molecular phenomena, e.g. the mean free path.

2. Some fundamental issues

We shall first formulate some of the fundamental questions that may be raised about the normal-mode theory of hydrodynamic stability, as a result of the conclusions reached by Case from the initial value theory. We consider the stability of a parallel flow†, for example, the pressure flow in a channel between parallel plates placed at $y = \pm 1$. The flow is in the x-direction with a velocity distribution $U(y) = 1-y^2$ (or some other parabolic function). The equation for small disturbances is

$$\frac{\partial \zeta'}{\partial t} + U\frac{\partial \zeta'}{\partial x} + v'\frac{d^2U}{\partial y^2} = \nu \Delta \zeta', \tag{2.1}$$

where ζ' is the disturbance vorticity, related to the disturbance stream function $\psi'(x, y, t)$ by

$$\zeta' = \frac{\partial^2 \psi'}{\partial x^2} + \frac{\partial^2 \psi'}{\partial y^2} = \Delta \psi', \tag{2.2}$$

and the velocity components are given by

$$u' = \frac{\partial \psi'}{\partial y}, \quad v' = -\frac{\partial \psi'}{\partial x}. \tag{2.3}$$

The constant ν is the kinematic viscosity coefficient, or the inverse of the Reynolds number R in the present dimensionless formulation. The boundary conditions are

$$u' = v' = 0 \quad \text{at} \quad y = \pm 1. \tag{2.4}$$

The solution of (2.1) can be treated either in terms of the theory of normal modes or by the initial value approach. In the first approach, we superpose particular solutions of the form

$$\psi'(x, y, t) = \mathrm{Re}\{\phi(y)\, e^{i\alpha(x-ct)}\}, \tag{2.5}$$

where $\phi(y)$ satisfies the familiar Orr–Sommerfeld equation

$$\phi^{\mathrm{iv}} - 2\alpha^2\phi'' + \alpha^4\phi = i(\alpha/\nu)\,[(U-c)\,(\phi'' - \alpha^2\phi) - U''\phi], \tag{2.6}$$

which is to be solved with the boundary conditions

$$\phi(\pm 1) = \phi'(\pm 1) = 0. \tag{2.7}$$

In the initial value approach used by Case, we consider the Laplace transform of $\psi'(x, y, t)$ with respect to t and its Fourier transform with respect to x (α real, $\mathrm{Re}(p) > 0$):

$$\overline{\psi}'(y;\alpha, p) = \iint \psi'(x, y, t)\, e^{-i\alpha x} dx\, e^{-pt} dt. \tag{2.8}$$

† Since Case did not formulate his theory in terms of the stream function, we develop below such a formulation in some detail to facilitate comparison with the normal-mode theory.

After solving for $\overline{\psi}'(y;\alpha,p)$ in terms of the initial conditions and the boundary conditions, we calculate $\psi'(x,y,t)$ by the inverse transform

$$\psi'(x,y,t) = \iint \overline{\psi}'(y,\alpha,p)\, e^{-i\alpha x} d\alpha\, e^{pt} dp, \tag{2.9}$$

where the integration with respect to p is taken along the line $\mathrm{Re}(p) = p_0 > 0$ in the direction of increasing $\mathrm{Im}(p)$. The normal mode representation is obtained by evaluating the p-integral at the singularities of $\overline{\psi}'$ in the p-plane by the theory of residues.

Apparent differences arise when one considers the *inviscid problem*, which is obtained by *formally* putting $\nu = 0$ in the above formulation and dropping the boundary condition $u' = 0$ in (2.4). For this case, Case has shown, by the consideration of the initial value problem, that normal modes associated with certain *continuous* spectra† of eigenvalues must be included. The eigenfunctions found are continuous functions with discontinuous first derivatives.

Case has further shown that for a set of initial conditions *independent of the Reynolds' number*, the solution of the viscous problem, in the limit $\nu \to 0$, approaches the solution of the inviscid problem except for a boundary-layer correction near the walls.

It might be tempting to suggest, as was done at one time, that the above conclusions combined would contradict the existence of the type of solutions described by this writer, as quoted in § 1. However, since the type of solutions considered, being of the type $\mathrm{Re}\{\phi(y,\nu)\, e^{i\alpha(x-ct)}\}$, is *dependent* on ν at *all* times, it is clear that they fall outside the scope of Case's theorem, because of his restriction on the initial conditions. There is therefore no contradiction. (In this connexion, it should be emphasized that the existence of the type of solution under discussion was established on *mathematical* grounds and *supplemented* by *physical* arguments—not the reverse.)

However, other questions may be raised about the theory of normal modes. For example, since the inviscid problem has normal modes associated with a continuous spectrum, and the solution of the viscous problem in general approaches the inviscid solutions as $\nu \to 0$, one may naturally pose the following question:

(1) are there continuous spectra of eigenvalues for the Orr–Sommerfeld equation?

We shall show in § 4 that the answer is negative. This answer leads to the next question:

(2) what is the viscous solution that corresponds to an inviscid normal mode, especially the one associated with the continuous spectrum?

We may also pose this question in terms of an initial value problem. Suppose we start with a set of *initial conditions* corresponding to an inviscid normal mode $\psi'_0(x,y,t) = \mathrm{Re}\{\phi_0(y)\, e^{i\alpha(x-ct)}\}$, i.e. suppose we require

$$\psi'(x,y,0) = \phi_{0r}(y)\cos\alpha x - \phi_{0i}(y)\sin\alpha x,$$

† The importance of studying the continuous spectra was pointed out earlier by Friedrichs (1941), but he did not give any detailed analysis.

and we consider the solution of (2.1) both in the inviscid case and in the viscous case. In the inviscid case, we naturally get the solution $\psi'_0(x, y, t)$ back. In the viscous case, the solution should also be close to $\psi'_0(x, y, t)$, according to Case. If there exists a normal mode

$$\psi'_N(x, y, t) = \mathrm{Re}\{\phi_N(y, \nu)\, e^{i\alpha(x-ct)}\}$$

that approaches the normal mode $\psi'_0(x, y, t)$, the natural answer to the initial value problem is then $\psi'(x, y, t) = \psi'_N(x, y, t) +$ small correction terms. But suppose such a normal mode does not exist,† what is the nature of the solution? The logical conjecture is also at hand; namely, the solutions should be represented as an infinite sum of normal modes (as any solution can be so represented), the sum being *not* dominated by a single mode. But is this logical answer also *plausible*?

In the following section, we shall show that this answer is indeed plausible by considering some simple examples where the solutions are explicitly known. These examples will also show the various ways in which the eigenfunctions of the viscous problem can behave in the limit of vanishing viscosity. In particular, we shall see that the limiting eigenfunctions may still form a discrete set while the inviscid problem has a continuous set of eigenfunctions. It is also possible for the inviscid problem to have eigenfunctions, while the limit of every viscous eigenfunction does not exist.

3. Examples of singular perturbation

In this section we shall examine the limiting behaviour of the solution of certain well-known parabolic equations as the 'diffusion coefficient' approaches zero. These properties are essentially well known; here they are presented in such a manner as to bring out the points of greatest interest to the issues at hand.

Example I. Consider the diffusion equation (which is applicable to the unsteady parallel flow between two parallel plates)

$$\frac{\partial u}{\partial t} = \nu \frac{\partial^2 u}{\partial y^2} \tag{3.1}$$

with the boundary conditions $u(0) = u(1) = 0$. The 'inviscid' problem is simply

$$\frac{\partial u_0}{\partial t} = 0 \tag{3.2}$$

with no boundary conditions required. The normal modes (solutions obtained by the method of separation of variables) in the viscous case are

$$u_n(y, t, \nu) = \sin n\pi y\, e^{-n^2\pi^2\nu t}, \tag{3.3}$$

where n must take on the *discrete* set of values $1, 2, 3, \ldots$. For the inviscid equation (3.2), any continuous function $f(y)$ is a normal mode.

† This occurs not only in the case of continuous spectra of eigenvalues but also in the case when the inviscid problem has an unstable mode. The complex conjugate operation yields a damped inviscid solution

$$\tilde{\psi}'(x, y, t) = \mathrm{Re}\,\{\phi_0^*(y)\, e^{i(x-c^*t)}\}$$

which has no counterpart among the normal modes of this viscous problem.

In the limit $\nu \to 0$, the normal modes (3.3) become

$$u_n(y, t, 0) = \sin n\pi y \quad (n = 1, 2, 3, \ldots). \tag{3·4}$$

This is but one *discrete* set of normal modes of the *continuous* set $f(y)$ of the normal modes of (3.2). *Thus, the existence of a continuous set of eigenvalues and eigenfunctions in the inviscid case does not necessarily imply the existence of a corresponding set in the viscous case, even in the inviscid limit.*

Consider now the initial value problem, with

$$u(y, 0) = F(y). \tag{3.5}$$

Clearly, the inviscid solution is simply

$$u_0(y, t) = F(y). \tag{3.6}$$

The viscous solution is in general given by the series

$$u(y, t) = \sum_{n=1}^{\infty} A_n \sin n\pi y e^{-n^2\pi^2\nu t}, \tag{3.7}$$

where A_n is given by

$$A_n = \frac{2}{\pi}\int_0^{\pi} F(y) \sin n\pi y \, dy. \tag{3.8}$$

Clearly, as $\nu \to 0$, the viscous solution (3.7) approaches the inviscid solution (3.6) for all finite t. This is the gist of the theorem proved by Case for the hydrodynamical problem. On the other hand, if the initial condition (3.5) should contain ν, e.g. if the condition were $u(y, 0) = \sin(y/\nu)$, such a correspondence would not exist.

We note in passing that the limiting processes $\nu \to 0$ and $t \to \infty$ are not interchangeable for the solution (3.7), exactly as Case (1961) noted in his treatment of the hydrodynamical problem.

The solution (3.7) shows clearly that *all* the normal modes are in general excited in an initial value problem in the viscous case, even though the solution in the inviscid case is just a *single* mode. [The initial condition $u(y, 0) = \delta(y - y_c)$ yields the set of coefficients $A_n = \sin n\pi y_c$, which remain finite even as $n \to \infty$. In this case, a clear description of the solution for small t is the spread of a singularity, and not conveniently given by the method of normal modes. Our understanding can also be improved by examining the limiting process $\nu \to 0$ in the Laplace integral representation of the solution (see Appendix).]

Exceptional cases occur when the initial conditions correspond to the *inviscid limit* of a single viscous normal mode, $\sin n\pi y$ (or a finite sum of such terms). In this case, only that particular mode is excited. This example thus gives plausibility to the answers given at the end of the last section.

We note that the *inviscid limit* of the viscous normal modes *happens* to form a complete set of *inviscid* normal modes. In the next example, we shall see that *all* the viscous normal modes do not even have inviscid limits.

Example II. Consider now the equation

$$\frac{\partial u}{\partial t} + k\frac{\partial u}{\partial y} = \nu\frac{\partial^2 u}{\partial y^2}. \tag{3.9}$$

The normal modes are

$$u_n(y) = w_n(y)\, e^{p_n t}, \tag{3.10}$$

with

$$w_n = e^{(k/2\nu)y} \sin n\pi y,$$

$$p_n = -\frac{k^2}{4\nu} - \nu n^2\pi^2. \tag{3.11}$$

The inviscid problem has the normal modes

$$u = e^{\alpha y} e^{-k\alpha t}. \tag{3.12}$$

For the initial condition $e^{\alpha y}$, the viscous problem has a solution of the form

$$u(y, t, \nu) = \sum_1^\infty A_n(\nu)\, w_n(y, \nu)\, e^{p_n(\nu)t},$$

where the dependence of A_n, w_n and p_n on ν is specifically noted. It is obviously a complicated problem if one tries to calculate the limit of $u(y, t, \nu)$ as $\nu \to 0$ from the above series, since each *individual eigenfunction* $w_n(y, \nu)$ *does not have a limit as* $\nu \to 0$.

4. Continuous and discrete characteristic values

The examples examined in the last section serve to illustrate the type of behaviour that may occur in the asymptotic limit of the solution of a partial differential equation of the second order. Since the hydrodynamical problem involves an equation of the fourth order, it is not surprising that the behaviour of the solution could be even more complicated. (See § 5 for the description of some important normal modes.) With this general background, let us return to the characteristic value problem (2.6), (2.7), and consider the question of a continuous spectrum of characteristic values.

Since the equation (2.6) is regular in the independent variable y as well as in the parameters R, α, c, there exists a fundamental system of four solutions which are analytic in y and the parameters R, α, c. Indeed they are entire functions. Furthermore since the boundary conditions (2.7) are to be satisfied for finite values of y, the secular equation for the determination of eigenvalues

$$F(R, \alpha, c) = 0 \tag{4.1}$$

is an entire function of the three parameters R, α, c, regarded as complex variables. If now there were a continuous set of eigenvalues for c, with R, α given, the equation (4.1) must reduce to an identity, by the theory of analytic continuation. Thus, the eigenvalues of the problem defined by (2.6) and (2.7) must all be *discrete*.

The above is merely an elementary proof, for our special case, of a general theorem for regular operators. The conclusion is thus obvious once it is pointed out.

Continuous spectra are expected for the inviscid equation,

$$(U - c)(\phi_0'' - \alpha^2\phi_0) - U''\phi_0 = 0, \tag{4.2}$$

(at least for the case $U'' = 2 \neq 0$), with the boundary conditions

$$\phi_0(\pm 1) = 0, \tag{4.3}$$

because the operator is now singular. Let us try to see this fact more directly in terms of the solutions of equation (4.2). This equation is well known to have solutions of the forms

$$\phi_1(y) = (y - y_c)[1 + \ldots] \tag{4.4}$$

and

$$\phi_2(y) = 1 + \ldots + \frac{U_c''}{U_c'}\phi_1(y)\log(y - y_c), \tag{4.5}$$

where $1 + \ldots$ denotes a regular power series in $(y - y_c)$, and $U(y_c) = c$. In the case of real eigenvalues c, the *real* and *imaginary* parts of $\phi_2(y)$ are separately solutions of (4.2). The real part is the *continuous* function

$$\phi_{2r}(y) = 1 + \ldots + \frac{U_c''}{U_c'}\phi_1(y)\log|y - y_c|, \tag{4.6}$$

and the imaginary part is another *continuous* function

$$\left.\begin{aligned} \phi_{2i}(y) &= 0, & y \geqslant y_c; \\ \phi_{2i}(y) &= -\pi\frac{U_c''}{U_c'}\phi_1(y) & y \leqslant y_c. \end{aligned}\right\} \tag{4.7}$$

We have thus *three* linearly independent solutions (4.4), (4.6) and (4.7) by permitting the solutions to have discontinuous or singular derivatives. With three linearly independent solutions for (4.2) and two boundary conditions (4.3), it is obvious that the characteristic values have a continuous spectrum.

However, if one regards the inviscid solution as the limit of the viscous solution as $\nu \to 0$, only the linear combination $\phi_{2r}(y) + i\phi_{2i}(y)$ is a solution, not $\phi_{2r}(y)$ and $\phi_{2i}(y)$ separately. Continuous spectra are therefore not obtained. The point is that the inviscid limit *does* exist in a properly defined region,† and remains an *analytic* function of the complex variable y. (This region, however, does not necessarily include the complete physical region.) Thus, the solution for $y > y_c$, when continued to the range $y < y_c$ must represent the same analytic function. The functions $\phi_r(y)$ and $\phi_i(y)$ do not satisfy this requirement.

5. Concluding remarks

Let us now summarize our conclusions and compare the relative merits of the methods of normal modes and initial values.

(i) Mathematically speaking, it should first be borne in mind that the Laplace integral representation of the solution can be decomposed into an infinite series of normal modes by the method of residues, and that the two approaches are essentially equivalent (see (vi) below).

(ii) Secondly, a great deal of apparent contradictions can be avoided if the following facts are kept in mind. A normal mode in the inviscid theory may not be the limit of a normal mode in the viscous theory. Conversely, a normal mode in the viscous theory may not have an inviscid limit. These conclusions are based on mathematical investigations of the solutions of the Orr–Sommerfeld equation. They are illustrated by simple examples in §3. The calculations in the Appendix

† This region is defined by two of the three lines $\mathrm{Re}\int_{y_c}^{y}\sqrt{\{i(U-c)\}}\,dy = 0$, chosen in such a manner as to include the two end points of our boundary-value problem. See Lin (1955, figure 8·1, p. 130).

illustrate fully the lack of direct correspondence between the inviscid eigenfunctions and the inviscid limit of the viscous ones.

(iii) If we are dealing with disturbances where the viscous effects are restricted to a boundary-layer region of the order of $(\alpha R)^{-\frac{1}{2}}$ near the solid surface, the initial value approach leads to the familiar boundary-layer theory; i.e. the solution is composed of an inviscid solution plus a boundary-layer correction. In this method of description, the normal modes belonging to the continuous spectrum (or spectra), which occur in the inviscid case, must be used. This description is simpler than in terms of the normal modes in the viscous theory (which are discrete). The type of simplification is similar to that occurring with the examples of § 3.

(iv) However, there are important types of disturbances not of the type described above, In particular, the unstable disturbances responsible for the initiation of turbulence in the channel or the boundary layer are of a different type. These disturbances extend over a layer of the order of $(\alpha R)^{-\frac{1}{3}}$, which is thicker than the layer in the previous case. For these disturbances, the viscous forces have a well-known destabilizing influence typical of the instability of shear flows.

(v) There are also exponentially damped normal modes which have the intermittent spotty structure characteristic of turbulence. There are also normal modes which have no inviscid limit anywhere in the physical region. When, to attempt a description of the transition process, the non-linear theory is considered these normal modes are expected to play an important role.

(vi) The initial value theory has not yet been developed to study the two types of disturbances just mentioned. It would be interesting to carry out these investigations to see whether different features can be revealed by the Laplace integral representation. In particular, it should be possible to bring out the destabilizing influence of the viscous forces mentioned in (iv). It would appear, from the fact that there are only a finite number of unstable modes, that the two methods would yield essentially the same results with regard to the unstable behaviour of the flow. On the other hand, it is likely that one would find only stable disturbances for the flow through a channel, if the viscous forces are restricted to boundary-layer regions which have a thickness of the order of $(\alpha R)^{-\frac{1}{2}}$ (cf. Lin & Rabenstein 1960).

This work was done while the author was at the Institute for Advanced Study, Princeton, N.J. The author is grateful to Professor J. R. Oppenheimer for the hospitality extended to him during his stay. He wishes also to thank Professors F. J. Dyson and C. N. Yang for their interest and discussions. The partial support of the office of Naval Research is acknowledged.

Appendix A

To get a closer comparison with Case's investigation (1961) of the hydrodynamical problem, let us explicitly use the method of the Laplace transformation (for the equation (3.1)). The solution is then given by

$$u(y,t) = \frac{1}{2\pi i}\int_C \bar{u}(y,p)\, e^{pt} dp, \tag{A 1}$$

where $\overline{u}(y, p)$ satisfies the differential equation

$$\frac{d^2\overline{u}}{dy^2} - q^2\overline{u} = \frac{1}{k}u(y, 0), \quad q^2 = \frac{p}{\nu}, \tag{A 2}$$

and the contour C is the line $\mathrm{Re}(p) = p_0 > 0$, taken in the direction of increasing $\mathrm{Im}(p)$. For the purposes in hand, we need only consider the simple case $u(y, 0) = \text{const}$. We then have

$$\overline{u} = \frac{1}{p \sinh q}\{\sinh qy + \sinh q(1-y) - \sinh q\}. \tag{A 3}$$

We make two observations.

(i) If we deform the contour C so as to evaluate the integral (A 1) in terms of the residues at the poles of (A 3), $p = -\nu n^2\pi^2 (n = 1, 2, \ldots)$, we recover the series solution (3.7) in terms of the eigenfunctions. Notice that $\overline{u}$ does not have a singularity at $p = 0$.

(ii) In the limit $\nu \to 0$, the singularities of (A 3) become dense along the whole negative part of the real axis in the p-plane, but the limiting function is

$$\lim_{\nu \to 0} \overline{u} = -\frac{1}{p} \quad \text{for} \quad 0 < y < 1. \tag{A 4}$$

This limiting form (A 4) agrees with the inviscid transform

$$\overline{u}_0 = -\frac{1}{p}, \tag{A 5}$$

but its singularity lies at $p = 0$, and does not coincide with any one of the singularities of (A 3) for $\nu > 0$.

REFERENCES

Case, K. M. 1960 Stability of inviscid plane Couette flow. *Phys. Fluids*, **3**, 143.

Case, K. M. 1961 Hydrodynamic stability and the inviscid limit. *J. Fluid Mech* **10**, 420.

Friedrichs, K. O. 1941 *Fluid Dynamics* (Brown University Lecture Notes), p. 209.

Langer, R. E. 1940 *Bull. Amer. Math. Soc.* **46**, 257.

Lin, C. C. 1955 *The Theory of Hydrodynamic Stability*. Cambridge University Press.

Lin, C. C. & Rabenstein, A. L. 1960 Asymptotic solutions of a class of differential equations of the fourth order. *Trans. Amer. Math. Soc.* **94**, 24.

Magnetohydrodynamic flow constructions with fundamental solutions

By MEREDITH C. GOURDINE
Plasmadyne Corporation, Santa Ana, California

(Received 26 July 1960 and in revised form 27 December 1960)

In this paper steady flows of an incompressible, viscous, electrically conducting fluid are constructed from fundamental solutions of magnetohydrodynamics in which the applied magnetic field is parallel to the velocity at infinity. The flat plate and the sphere are considered as examples, and approximate solutions are presented for the limiting cases of large and small Reynolds and magnetic Reynolds numbers. The effects of currents in the body are also considered, and it is found that unless the magnetic Prandtl number is larger than unity, currents in the body have negligible effect on the flow.

1. Introduction

A certain class of magnetohydrodynamic (MHD) problems involving the flow of an incompressible electrically conducting fluid over a solid body, in the presence of an applied magnetic field parallel to the main flow, can be described approximately by a set of linear equations (Gourdine 1960). Simple MHD flows over solids can then be constructed by superposing fundamental solutions of these equations to satisfy appropriate boundary conditions. Examples of this technique are presented in this paper

Chester (1957) treats MHD flow over a sphere as a perturbation of the Stokes flow, while Ludford (1959) treats the same problem as a perturbation of the Oseen flow. Lary (1960) studies this class of problems assuming the fluid has zero viscosity and finds that when the Alfvén number α is larger than unity the body produces a forward wake due to the propagation of Alfvén disturbances upstream. Hasimoto (1959) finds a similar phenomenon is his study of the problem with a fluid of infinite electrical conductivity. Other investigators have also considered problems in this class: Gotoh (1960), Yosinobu (1960), Blerkom (1960), Greenspan & Carrier (1959), and Greenspan (1960). In this paper, the fundamental solution or singular body approach is employed. This is not a new technique (Blerkom 1960), but it has the advantage of providing physical insight into the problem, and it also allows easy generalization of the problem to include the effects of currents in the body.

2. Mathematical description of the problem

The following set of dimensionless linearized equations describes the induced velocity field $\mathbf{u}$ and the induced magnetic field $\mathbf{h}$ (Gourdine 1960):

$$\frac{\partial \mathbf{u}}{\partial x} - \frac{1}{Re}\nabla^2\mathbf{u} - \alpha^2\frac{\partial \mathbf{h}}{\partial x} = -\nabla\bar{p} + \mathbf{f}, \tag{1a}$$

$$\frac{\partial \mathbf{h}}{\partial x} - \frac{1}{Rm}\nabla^2\mathbf{h} - \frac{\partial \mathbf{u}}{\partial x} = \mathbf{g}, \tag{1b}$$

$$\nabla.\mathbf{u} = \nabla.\mathbf{h} = 0, \tag{1c}$$

where $\mathbf{f} = \delta(r)\,\mathbf{a}$ represents a singular velocity disturbance in the flow and $\mathbf{g} = \delta(r)\,\mathbf{b}$ represents a singular magnetic disturbance in the flow; here $\delta(r)$ is the Dirac delta function, r being measured radially from the origin, and $\mathbf{a}$ and $\mathbf{b}$ are unit vectors. The other symbols are defined as follows: Re is the Reynolds number, Rm is the magnetic Reynolds number, α is the Alfvén number, and $\bar{p}$ is the *net* pressure—the sum of hydrostatic and magnetic pressure.

The solutions of equations (1) are the fundamental solutions for this class of MHD problems, and it has been shown (Gourdine 1960) that they can be written in the following form

$$u_{ij}(x,y,z) = u^u_{ij} + u^h_{ij} = \sum_{n=0}^{2} (U^u_n + U^h_n)\,\Gamma_{ij}(\lambda_n x, y, z), \tag{2a}$$

$$h_{ij}(x,y,z) = h^u_{ij} + h^h_{ij} = \sum_{n=0}^{2} K_n(U^u_n + U^h_n)\,\Gamma_{ij}(\lambda_n x, y, z). \tag{2b}$$

The *net* pressure is proportional to the x-component of the zeroth mode of the velocity ($n = 0$):

$$\bar{p}_j(x,y,z) = \bar{p}^u_j + \bar{p}^h_j = -(1-\alpha^2)\,(U^u_0 + U^h_0)\,\Gamma_{xj}(\lambda_0 x, y, z). \tag{3}$$

The fundamental solutions u_{ij}, h_{ij} and $\bar{p}_j$, are the velocity and magnetic field disturbances in the i-direction and the net pressure, respectively, due to singular disturbances that are in the j-direction at the origin. The fundamental solutions consist of contributions from the velocity singularity (superscript u) and the magnetic singularity (superscript h).

The function $\Gamma_{ij}(\lambda_n x, y, z)$ represents the fundamental solution of the Oseen-type equations

$$\frac{\partial \mathbf{u}}{\partial x} - \frac{1}{\lambda_n}\nabla^2\mathbf{u} = \delta(r)\,\mathbf{j}, \tag{4a}$$

$$\nabla.\mathbf{u} = 0. \tag{4b}$$

Here λ_n has the following three values

$$\lambda_0 = 0, \tag{5a}$$

$$\lambda_1 = \tfrac{1}{2}Re[(1+Pm) + \{(1+Pm)^2 - 4Pm(1-\alpha^2)\}^{\frac{1}{2}}], \tag{5b}$$

$$\lambda_2 = \tfrac{1}{2}Re[(1+Pm) - \{(1+Pm)^2 - 4Pm(1-\alpha^2)\}^{\frac{1}{2}}], \tag{5c}$$

where $Pm \equiv \sigma\mu\nu$ is the so-called magnetic Prandtl number. These are plotted in figures 1 and 2.

The magnetic mode parameters K_n have the three values

$$K_0 = 1, \tag{6a}$$

$$K_1 = \tfrac{1}{2}\alpha^{-2}[(1-Pm)-\{(1-Pm)^2+4\alpha^2 Pm\}^{\frac{1}{2}}], \tag{6b}$$

$$K_2 = \tfrac{1}{2}\alpha^{-2}[(1-Pm)+\{(1-Pm)+4\alpha^2 Pm\}^{\frac{1}{2}}]. \tag{6c}$$

These are plotted in figures 3 and 4.

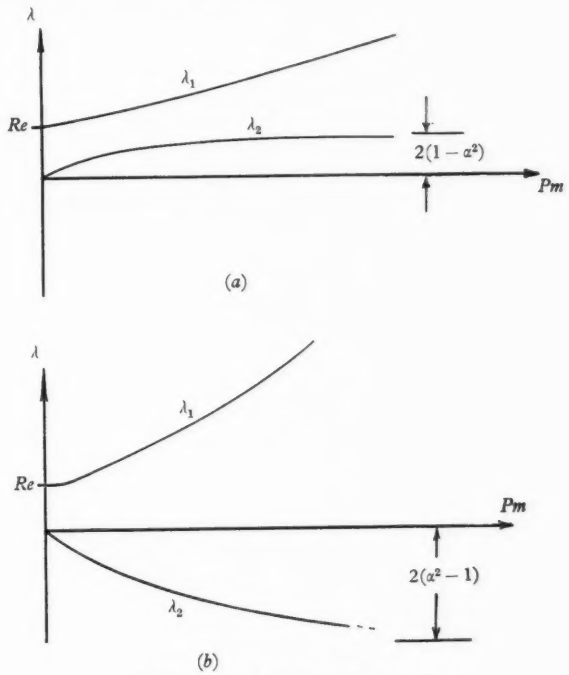

FIGURE 1. (*a*) $\alpha < 1$; (*b*) $\alpha > 1$.

The mode strengths in equations (2*a*) and (2*b*) consist of two parts; U_n^u is due to a velocity singularity and U_n^h is due to a magnetic singularity. A study of the equations (1) near the singularities at the origin yields the following expressions for the velocity singularity mode strengths,

$$U_0^u = 1, \tag{7a}$$

$$U_1^u = K_2/(K_2-K_1), \tag{7b}$$

$$U_2^u = -K_1/(K_2-K_1), \tag{7c}$$

and corresponding expressions for the magnetic singularity mode strengths,

$$U_0^h = 1, \tag{8a}$$

$$U_1^h = -Pm/(K_2-K_1), \tag{8b}$$

$$U_2^h = Pm/(K_2-K_1). \tag{8c}$$

These relations ensure that the fields are divergence free even at the origin.

MHD flow over a finite body may be described in terms of the fundamental solutions by the integral

$$u_i(x,y,z) = \iiint_{-\infty}^{\infty} u_{ij}^u(x,y,z;\xi,\eta,\zeta)\, S_j^u(\xi,\eta,\zeta)\, d\xi\, d\eta\, d\zeta + \iiint_{-\infty}^{\infty} u_{ij}^h(x,y,z,\xi,\eta,\zeta)\, S_j^h(\xi,\eta,\zeta)\, d\xi\, d\eta\, d\zeta, \tag{9}$$

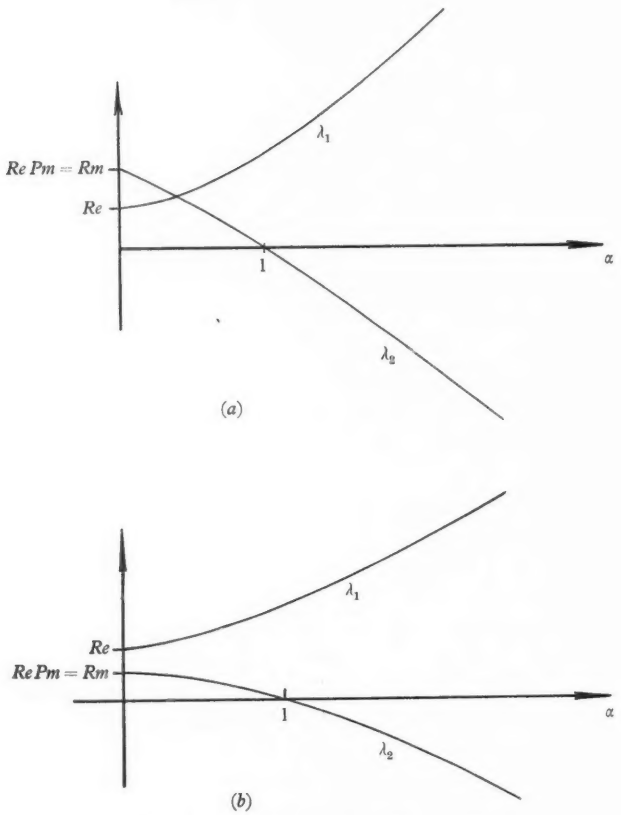

FIGURE 2. (*a*) $Pm > 1$; (*b*) $Pm < 1$.

where S_j^u and S_j^h are the strengths per unit volume of the distributed velocity and magnetic singularities respectively. A similar integral can be written for the magnetic field which, of course, also involves S_j^u and S_j^h. These two distribution functions can be determined, in principle at least, by satisfying two boundary conditions on the body. One boundary condition is that the total velocity must vanish at the body; therefore that $u_x = -1$, $u_y = 0$, $u_z = 0$ at the body. The other boundary condition is either on the magnetic field or the current density at the body. In the most general problem, the body carries an internal electric generator which establishes currents within itself.

The remainder of this paper concerns itself with the problem of solving for S_j^u and S_j^h. Only special cases are attempted because a general solution is probably impossible.

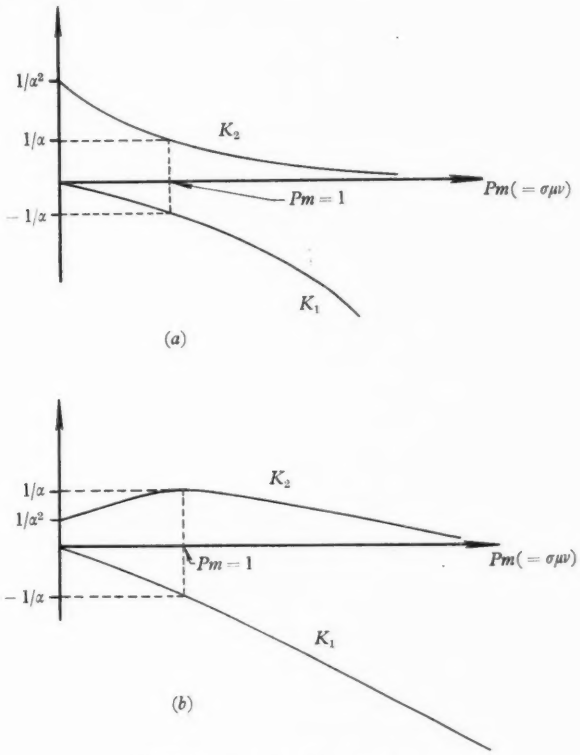

FIGURE 3. (*a*) $\alpha < 1$; (*b*) $\alpha > 1$.

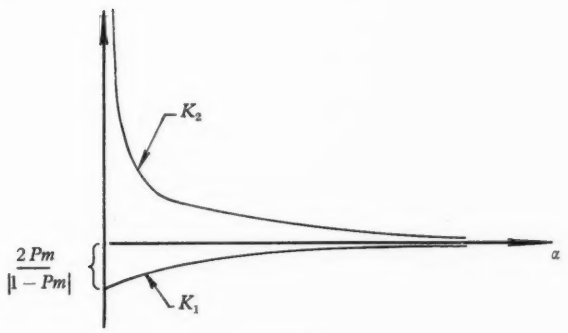

FIGURE 4

3. MHD drag of a finite flat plate

Following the usual procedure for constructing flows by superposition, let $S_x^u = f(\xi)$ be the strength of the velocity singularity in the range $\xi < x < \xi + d\xi$, and let $S_x^h = Mf(\xi)$ be the strength of the magnetic singularity in the same range. This is a special case in which the distribution of magnetic singularities is assumed to be proportional to the distribution of velocity singularities in order to demonstrate in a simple way the effects of currents in the body. The fundamental solution for this case can be written immediately in terms of Oseen's solution, that is

$$u_{ij} = U_1 \Gamma_{ij}(\lambda_1 x, y) + U_2 \Gamma_{ij}(\lambda_2 x, y), \tag{10}$$

where the mode strengths are given by

$$U_1 = U_1^u + MU_1^h, \tag{11a}$$

$$U_2 = U_2^u + MU_2^h. \tag{11b}$$

Oseen's solution for a singular flat plate with unit drag is

$$\Gamma_{i1} = U\left[\frac{1}{\lambda}\nabla(\chi - \phi) - \chi \mathbf{i}\right], \tag{12}$$

where $U = Re/\lambda\pi$ and $\lambda = Re$. The function $\phi(r) = \ln r$ is the potential of a two-dimensional source; it is the longitudinal part of the solution, and is chosen such that the flow is divergence-free near the origin. The Oseen function in two dimensions is $\chi = e^{\frac{1}{2}\lambda x} K_0(\frac{1}{2}\lambda r)$, where K_0 is the modified Bessel function of the second kind. At large distances from the origin, χ has the asymptotic behaviour $\chi \sim e^{-\frac{1}{2}\lambda(r-x)}/(\frac{1}{2}\lambda r)^{\frac{1}{2}}$. Near the origin $\chi \simeq \ln r$. Therefore χ behaves like a potential source near the origin; but for large positive x, it is essentially zero outside a parabolic region bounded by $y = c(x/\lambda)^{\frac{1}{2}}$. The strength of χ inside the parabola vanishes slowly, like $(1/x)^{\frac{1}{2}}$. However, for negative x, χ vanishes exponentially. Thus Oseen's solution contains a parabolic wake extending dowstream from the body.

According to equations (4) there are two wakes in this problem. If $\lambda_2 > 0$, there is a second wake downstream, and if $\lambda_2 < 0$, there is a second wake upstream. Equations (5) show that $\lambda_2 < 0$ if $\alpha > 1$, and $\lambda_2 > 0$ if $\alpha < 1$.

The distribution function $f(\xi)$ is such that the x-component of velocity on the plate vanishes; that is,

$$u_x(x, 0) = -1 = \int_{-1}^{1} \{U_1 \Gamma_{11}[\lambda_1(x-\xi), 0] + U_2 \Gamma_{11}[\lambda_2(x-\xi), 0]\} f(\xi)\, d\xi. \tag{13}$$

On the plate, the argument $\lambda(x-\xi) \leqslant \lambda < 1$, therefore

$$\Gamma_{11}[\lambda(x-\xi), 0] \simeq (Re/2\pi)(1 - \ln \tfrac{1}{4}\gamma_0 \lambda\, |x-\xi|), \tag{14}$$

where $\gamma_0 = e^{\gamma}$ and $\gamma = 0{\cdot}577$ (Euler's constant). Substitution of this into equation (13) yields

$$-1 = \int_{-1}^{1} \{U_1(C_1 - \ln|x-\xi|) + U_2(C_2 - \ln|x-\xi|)\} f(\xi)\, d\xi, \tag{15}$$

where

$$C_1 = 1 - \ln(\tfrac{1}{4}\gamma_0 \lambda_1), \tag{16a}$$

$$C_2 = 1 - \ln(\tfrac{1}{4}\gamma_0 \lambda_2). \tag{16b}$$

The solution of equation (15) is

$$f(\xi) = \frac{2/Re}{\{U_1(C_1 + \ln 2) + U_2(C_2 + \ln 2)\}} \frac{1}{(1-\xi^2)^{\frac{1}{2}}}. \tag{17}$$

The drag coefficient per unit length is therefore

$$C_D \equiv \int_{-1}^{1} f(\xi)\, d\xi = \frac{2\pi}{Re} \frac{1}{\{U_1(C_1 + \ln 2) + U_2(C_2 + \ln 2)\}}. \tag{18}$$

In the limit of zero magnetic interaction C_D approaches the classical hydrodynamic value

$$C_{D_0} = \frac{2\pi}{Re} \frac{1}{\{1 - \ln(\gamma_0 Re/8)\}}, \tag{19}$$

where $Re = U_\infty a/\nu$.

Now consider the effect of the magnetic singularities on the mode strengths U_1 and U_2:

$$U_1 = \frac{K_2 - MPm}{K_2 - K_1}, \tag{20a}$$

$$U_2 = \frac{-K_1 + MPm}{K_2 - K_1}. \tag{20b}$$

The effect of a positive M is to decrease U_1 and increase U_2, and vice-versa for a negative M. In fact if $MPm = K_2$ the first mode is cancelled out entirely, and if $MPm = K_1$, the second mode is cancelled out. In the former case, with only the second mode remaining,

$$C_D \simeq \frac{2\pi}{Re} \frac{1}{C_2 + \ln 2} = \frac{2\pi}{Re} \frac{1}{1 - \ln(\gamma_0 Rm/8)}, \tag{21}$$

and in the latter case, with only the first mode remaining,

$$C_D \simeq \frac{2\pi}{Re} \frac{1}{C_1 + \ln 2} = \frac{2\pi}{Re} \frac{1}{1 - \ln \gamma_0 Re/8} = C_{D_0}. \tag{22}$$

Notice that the effect of currents in the body is proportional to the magnetic Prandtl number Pm, which is usually a very small number.

It is also possible to solve equation (13) for $f(\xi)$ when λ_1 and λ_2 are large, because in the limit $\lambda \to \infty$,

$$\Gamma_{11}[\lambda x, 0] \sim -\frac{Re}{2\pi} \left(\frac{\pi}{\lambda |x|}\right)^{\frac{1}{2}}. \quad (x \neq 0). \tag{23}$$

Furthermore, for $\alpha > 1$ (strong magnetic interaction), the first mode only produces disturbances downstream of the singularity, while the second mode only produces disturbances upstream of the singularity; therefore the integral equation for $f(\xi)$ becomes

$$-1 = -\frac{Re}{2\pi} \int_0^x U_1 \left(\frac{\pi}{\lambda_1 (x-\xi)}\right)^{\frac{1}{2}} f(\xi)\, d\xi - \frac{Re}{2\pi} \int_x^1 U_2 \left(\frac{\pi}{\lambda_2 (\xi - x)}\right)^{\frac{1}{2}} f(\xi)\, d\xi. \tag{24}$$

For $\alpha < 1$ (weak magnetic interaction), the first mode and the second mode only create disturbances downstream of the singularity; therefore,

$$-1 = -\frac{Re}{2\pi} [U_1 (\pi/\lambda_1)^{\frac{1}{2}} + U_2 (\pi/\lambda_2)^{\frac{1}{2}}] \int_0^x \frac{f(\xi)\, d\xi}{(x-\xi)^{\frac{1}{2}}} \quad (\alpha < 1). \tag{25}$$

This is Abel's integral equation, and has the solution

$$f(\xi) = \frac{1}{\sqrt{\xi}} \frac{2}{Re} \frac{1}{U_1 (\pi/\lambda_1)^{\frac{1}{2}} + U_2 (\pi/\lambda_2)^{\frac{1}{2}}}, \quad (\alpha < 1). \tag{26}$$

The drag coefficient is

$$C_D \equiv \int_0^1 f(\xi)\,d\xi = \frac{4}{Re\sqrt{\pi}}\frac{1}{U_1\lambda_1^{-\frac{1}{2}} + U_2\lambda_2^{-\frac{1}{2}}}. \tag{27}$$

Notice that as α or Pm tends to zero C_D approaches the classical value for high Reynolds number flow

$$C_{D_0} \sim 4/(\pi Re)^{\frac{1}{2}}. \tag{28}$$

For $\alpha > 1$, finding $f(\xi)$ from equation (24) is somewhat more difficult; however, Greenspan (1960) provides the solution. In the special cases in which either U_1 or U_2 vanishes, equation (24) is again easy to solve. If U_2 vanishes we again have Abel's integral equation, and the solution

$$f(\xi) = \frac{1}{\sqrt{\xi}}\frac{2}{Re}\frac{1}{U_1(\pi/\lambda_1)^{\frac{1}{2}}}. \tag{29}$$

If U_1 vanishes we have an equation which can be converted into Abel's equation by the substitution $\xi = 1-\eta$, and the resulting solution is

$$f(\xi) = \frac{1}{(1-\xi)^{\frac{1}{2}}}\frac{2}{Re}\frac{1}{U_2(\pi/\lambda_1)^{\frac{1}{2}}}. \tag{30}$$

Thus, when the second mode vanishes ($U_2 = 0$), the leading edge is singular and there is a trailing wake, but when the first mode vanishes ($U_1 = 0$) the trailing edge is singular and there is a leading wake.

For a flat plate without internal currents, U_2 vanishes if the electrical conductivity is zero, and U_1 vanishes if the electrical conductivity is infinite. It is also possible to make U_2 or U_1 vanish by properly distributing the currents in the flat plate as suggested by equations (20*a*) and (20*b*). Thus, by making $MPm = K_2$ we can make U_1 vanish, and by making $MPm = K_1$, we can make U_2 vanish. The current density generated in the plate, and the vorticity, must be at right angles to the flow and in opposite directions on the top and bottom sides.

The results presented in this section are in agreement with the results of Greenspan (1960). Greenspan uses an entirely different mathematical technique to arrive at equation (24), and does not concern himself with currents generated in the flat plate.

4. MHD drag of a sphere

In ordinary hydrodynamics, low Reynolds number flow over a sphere is constructed approximately by superposing a uniform flow, the flow of a singular needle, and the flow of a potential dipole; therefore it is reasonable to expect that low MHD Reynolds number flow over a sphere can be approximated by replacing the singular needle by a singular MHD needle as follows:

$$\begin{aligned}\mathbf{U} = \mathbf{i} &+ U_1^u\left\{-\frac{1}{\lambda_1}\nabla\left[\frac{e^{-\frac{1}{2}\lambda_1(r-x)}-1}{r}\right] + \frac{e^{-\frac{1}{2}\lambda_1(r-x)}}{r}\mathbf{i}\right\} \\ &+ U_2^u\left\{-\frac{1}{\lambda_2}\nabla\left[\frac{e^{-\frac{1}{2}\lambda_2(r-x)}-1}{r}\right] + \frac{e^{-\frac{1}{2}\lambda_2(r-x)}}{r}\mathbf{i}\right\} \\ &+ U_0^u\left\{\nabla\left[\frac{\partial}{\partial x}\left(\frac{1}{r}\right)\right]\right\},\end{aligned} \tag{31}$$

where the ratio of mode strengths for the singular MHD needle is

$$U_2^u/U_1^u = -K_1/K_2. \tag{32}$$

The mode strengths U_1^u and U_0^u are then determined by expanding the exponentials in equation (31) while satisfying the boundary condition on the sphere which demands that $U = 0$; they are

$$U_1^u \simeq -\frac{3}{2}\frac{K_1}{K_2-K_1}\frac{1}{1-\frac{3}{8}(K_2\lambda_2-K_1\lambda_1)/(K_2-K_1)}, \tag{33a}$$

$$U_0^u \simeq \frac{1}{4}\frac{1}{1-\frac{3}{8}(K_2\lambda_2-K_1\lambda_1)/(K_2-K_1)}, \tag{33b}$$

where, from equations (5) and (6)

$$(K_2\lambda_2-K_1\lambda_1)/(K_2-K_1) = Re. \tag{33c}$$

The drag of the sphere is due to a singular MHD needle of strength

$$\tfrac{3}{2}(4\pi/Re)\,(1+\tfrac{3}{8}Re),$$

therefore the drag is

$$D = 6\pi\rho\nu U_\infty a(1+\tfrac{3}{8}Re). \tag{34}$$

This is precisely the same drag as is obtained without magnetic interaction. It appears that for $\alpha < 1$, up to terms of order λ, the magnetic interaction has no effect on drag.

It is easy to obtain the solution for $\alpha > 1$ simply by changing the sign of x in equation (31) to account for the upstream wake when $\lambda_2 < 0$. The result is

$$U_1^u \simeq -\frac{3}{2}\frac{K_1}{K_2-K_1}\frac{1}{1-\frac{3}{8}(-K_2\lambda_2-K_1\lambda_1)/(K_2-K_1)}, \tag{35a}$$

$$U_0^u \simeq \frac{1}{4}\frac{1}{1-\frac{3}{8}(-K_2\lambda_2-K_1\lambda_1)/(K_2-K_1)}, \tag{35b}$$

where

$$K \equiv \frac{K_2\lambda_2+K_1\lambda_1}{K_2-K_1} = \frac{2Ha^2+Re^2-ReRm}{\{(Re-Rm)^2+4Ha^2\}^{\frac{1}{2}}}, \tag{35c}$$

and the drag is

$$D = 6\pi\rho\nu U_\infty a(1+\tfrac{3}{8}K) \tag{36}$$

provided that Ha, Re, Rm are all less than unity. In the limit Re, $Rm \to 0$ with $a \to \infty$, such that $Ha^2 \equiv ReRma^2$ is finite but less than unity, Chester's (1957) result is obtained:

$$D = 6\pi\rho\nu U_\infty a(1+\tfrac{3}{8}Ha). \tag{37}$$

These results also agree with those of Ludford (1959).

5. Conclusions

The fundamental solution approach to this class of MHD flow problems is a convenient method of constructing solutions. With a knowledge of the properties of the MHD singularities involved it is a simple matter to deduce the physical properties of the solutions. Some of these solutions may eventually prove useful in the design of probes to measure certain physical properties of a flowing conductor.

The author wishes to express his gratitude for the continued interest and numerous suggestions afforded by Prof. Julian Cole, California Institute of Technology.

REFERENCES

BLERKOM, H. VAN 1960 Magnetohydrodynamic flow of a viscous fluid past a sphere. *J. Fluid Mech.* **8**, 3.

CHESTER, W. 1957 The effect of a magnetic field on Stokes flow in a conducting fluid. *J. Fluid Mech.* **3**, 304.

GOTOH, K. 1960 Magnetohydrodynamic flow past a sphere. *J. Phys. Soc. Japan*, **15**, 189–6.

GOURDINE, M. C. 1960 Generalization of Oseen's solutions to magnetohydrodynamics. *American Rocket Society Symposium.* Baltimore, Md.

GREENSPAN, H. P. 1960 Flat plate drag in magnetohydrodynamic flow. *Phys. Fluids*, **3**, 581–7.

GREENSPAN, H. P. & CARRIER, G. F. 1959 The magnetohydrodynamic flow past a flat plate. *J. Fluid Mech.* **6**, 77–96.

HASIMOTO, H. 1959 Viscous flow of a perfectly conducting fluid with a frozen magnetic field. *Phys. Fluids*, **2**, 337–8.

LARY, E. C. 1960 A theory of thin airfoils and slender bodies in fluids of arbitrary electrical conductivity. Thesis, Cornell University.

LUDFORD, G. S. S. 1959 The effect of an aligned magnetic field on Oseen flow of a conducting fluid. *Interim Tech. Rep. no.* 43, *Dept. of Math., Univ. of Maryland.*

YOSINOBU, H. 1960 A linearized theory of magnetohydrodynamic flow past a fixed body in a parallel magnetic field. *J. Phys. Soc. Japan*, **15**, 175–88.

A new approach to the measurement of turbulent fluxes in the lower atmosphere

By R. J. TAYLOR

C.S.I.R.O. Division of Meteorological Physics, Aspendale, Victoria, Australia

(Received 28 November 1960)

A method is described for the measurement of turbulent shearing stress and vertical heat flux by way of 'structure functions'—the mean square velocity and temperature differences between two points a known distance apart. The method is particularly suitable for shipboard use because it does not require the measurement of velocity components relative to a fixed frame of reference. An analysis of the available observations, although they are not ideally suited to the purpose, is encouraging and points the way to further development of the method.

1. Introduction

It has several times been noted (e.g. by McCready 1953; Taylor 1955) that, when autocorrelations in horizontal wind velocity components at two points are measured in the lower atmosphere, they show the particular dependence on the distance between the two points which is characteristic of the inertial subrange of eddy sizes, up to unexpectedly large distances—often as much as several times the height of observation. A rather convincing explanation of this phenomenon has been put forward by Gifford (1959), but, whatever the cause, there is no doubt that this simple property does, in fact, hold good over an extensive range of distances.

Within this range, it is possible to derive expressions relating the vertical turbulent fluxes of heat and momentum with the mean square differences in temperature and velocity between two points—the so-called 'structure functions'. As pointed out by Deacon (1959), these could form the basis of a method for measuring the fluxes which would have obvious applications at sea since the only functions of velocity required would be differences. These, though affected to some extent by the ship's motion, could be measured more accurately than velocity components relative to a fixed frame of reference.

The theoretical basis of the method is set out below, and the available observations are used to test it. Although the observations are not entirely suited to the purpose, a preliminary assessment is possible.

2. Theoretical basis of the method

If we write

$$D_u(r) = \overline{[u(x)-u(x+r)]^2}, \tag{1}$$

where u is the velocity component in the downwind (x) direction and r is an increment of distance in the same direction, then, in the inertial subrange,

$$D_u(r) \propto \epsilon^{\frac{2}{3}} r^{\frac{2}{3}}, \tag{2}$$

where ϵ is the rate of dissipation of kinetic energy per unit of mass. Obukhov & Yaglom (1951) derived a value for the constant in (2) and wrote

$$D_u(r) = 1{\cdot}6\epsilon^{\frac{2}{3}}r^{\frac{2}{3}}. \tag{3}$$

Their derivation rests on a value of $-0{\cdot}4$ for the skewness in distribution of $[u(x)-u(x+r)]$. Some measurements by Stewart (1951) suggest that a rather smaller absolute value may be more appropriate and this would involve a larger constant in (3). For the present, equation (3) will be accepted as it stands, in the knowledge that some adjustment of this constant may later prove to be necessary.

Equation (3) links ϵ with a measurable function of wind velocities. As is well-known, ϵ can also be expressed by the equation

$$\epsilon = \frac{\tau}{\rho}\frac{\partial \overline{u}}{\partial z} + \frac{gH}{c_p \rho \overline{T}} \tag{4}$$

(neglecting divergence of vertical diffusion of turbulent kinetic energy) where τ is the shearing stress, H is the vertical turbulent heat flux and the other symbols are standard notation. It is thus clearly possible, by way of equations (3) and (4) to estimate τ from measurements of D_u and the other quantities involved.

The distribution of temperature fluctuations in a turbulent flow has not received as much attention as the dynamically more interesting problem of the velocity fluctuations. The earliest relevant work appears to be that of Obukhov (1949) who discussed temperature structure functions of the form

$$D_T(\mathbf{r}) = \overline{[T(\mathbf{x}) - T(\mathbf{x}+\mathbf{r})]^2} \tag{5}$$

where $T(\mathbf{x})$ and $T(\mathbf{x}+\mathbf{r})$ are the temperatures at points having co-ordinates x_i and x_i+r_i respectively ($i = 1, 2, 3$).

Obukhov introduces a dissipation function for temperature fluctuations

$$\chi = \kappa(\partial T/\partial x_i)^2, \tag{6}$$

where κ is the thermal diffusivity of the fluid. (The summation convention for subscripts applies in equation (6).) He assumes that there exists a range of eddy sizes for which D_T is a function of r, χ and ϵ only, and dimensional analysis then leads to the result that, for this range of sizes,

$$D_T(r) \propto \chi\epsilon^{-\frac{1}{3}}r^{\frac{2}{3}}. \tag{7}$$

Similarly, Corrsin (1951) obtained a spectrum of temperature fluctuation proportional to the minus five-thirds power of the wave-number, a result which is exactly equivalent to Obukhov's. In sharp contrast, however, is a paper by Inoue (1952) who, using a very different theoretical basis, reached the conclusion that $D_T(r)$ is proportional to $r^{\frac{4}{3}}$.

A relationship between χ and H was found by Tatarskii (1956) by assuming a logarithmic form of temperature profile and taking a simplified form of the equation of conservation of internal energy. It is possible, however, to show that his relationship is valid even when the profile is not logarithmic and when certain terms, neglected by him, are taken into account.

The equation of motion of a fluid of variable density (see Jeffreys 1952) is

$$\rho\frac{\partial u_i}{\partial t}+\rho u_j\frac{\partial u_i}{\partial x_j}+\frac{\partial p}{\partial x_i}+\rho\frac{\partial\phi}{\partial x_i}-\frac{\partial\sigma_{ij}}{\partial x_j}=0, \tag{8}$$

in which the summation convention applies. Here the u_i are the velocity components, ϕ is the geopotential and σ_{ij} is a viscous stress given in full by

$$\sigma_{ij}=\rho\nu\left(\frac{\partial u_i}{\partial x_j}+\frac{\partial u_j}{\partial x_i}-\frac{2}{3}\frac{\partial u_k}{\partial x_k}\delta_{ij}\right),$$

where ν is the kinematic viscosity and $\delta_{ij}=1$ or 0 according as $i=j$ or not. By multiplying equation (8) throughout by u_i, we obtain the equation for conservation of kinetic and potential energies:

$$\rho\frac{\partial}{\partial t}(\tfrac{1}{2}u_i^2)+\rho u_j\frac{\partial}{\partial x_j}(\tfrac{1}{2}u_i^2)+u_i\frac{\partial p}{\partial x_i}+\rho u_i\frac{\partial\phi}{\partial x_i}-u_i\frac{\partial\sigma_{ij}}{\partial x_j}=0. \tag{9}$$

If radiative transfer is neglected, the equation for the conservation of energy (see de Groot, 1951) is

$$\frac{\partial}{\partial t}\rho[c_vT+\tfrac{1}{2}u_i^2+\phi]+\frac{\partial}{\partial x_j}\rho u_j[c_vT+\tfrac{1}{2}u_i^2+\phi]-\lambda\frac{\partial^2T}{\partial x_j^2}+\frac{\partial pu_j}{\partial x_j}-\frac{\partial\sigma_{ij}u_j}{\partial x_i}=0, \tag{10}$$

where λ is the thermal conductivity.

The equation for the conservation of internal energy is now derived from equations (9) and (10) by subtraction, using the equation of continuity, and is

$$\rho\frac{\partial}{\partial t}c_vT+\rho u_j\frac{\partial}{\partial x_j}c_vT+p\frac{\partial u_j}{\partial x_j}=\sigma_{ij}\frac{\partial u_i}{\partial x_j}+\lambda\frac{\partial^2T}{\partial x_j^2}, \tag{11}$$

which reduces to

$$c_p\rho\frac{T}{\theta}\left(\frac{\partial\theta}{\partial t}+u_j\frac{\partial\theta}{\partial x_j}\right)=\sigma_{ij}\frac{\partial u_i}{\partial x_j}+\lambda\frac{\partial^2T}{\partial x_j^2}, \tag{12}$$

where θ is the potential temperature.

If this equation is now multiplied through by a temperature fluctuation T' and averaged and, further, the assumptions of steadiness in time and horizontal uniformity are made, it reduces to

$$H\frac{\partial\overline{\theta}}{\partial z}+\tfrac{1}{2}c_p\frac{\partial}{\partial x_j}\overline{\{(\rho u_j)'\,T'^2\}}=\overline{\rho\epsilon T'}+\lambda\frac{\partial^2}{\partial x_j^2}(\tfrac{1}{2}\overline{T'^2})-\rho c_p\chi, \tag{13}$$

since fluctuations in T and θ are nearly equal. The order of magnitude of terms in this equation will be estimated later.

3. The observations

The only available data suitable for testing the proposed method are those of Swinbank (1955). He gives, *inter alia*, values of momentum flux (which is equivalent to the shearing stress) and heat flux, determined from the covariance of the vertical velocity component with the horizontal-downwind component and with the temperature respectively. Records of velocity and temperature fluctuations at one point as a function of time were made as part of this investigation and it is possible to estimate structure functions from them as follows.

Following G. I. Taylor (1938) it will be assumed that the autocorrelations behave as if the whole turbulent velocity and temperature fields were being swept along unchanged at the mean wind speed. The validity of this assumption in the lower atmosphere seems well established (see Gifford 1956; Taylor 1957). Thus structure functions for a distance r, where r is aligned along the mean wind direction, are to be taken as equal to mean square differences for a time interval σ where $r = \bar{u}\sigma$. This artifice is introduced solely in order to make use of existing data and is valid only if the point at which observations are made is fixed or in uniform motion. Aboard a ship, where the motion of the point of measurement would itself have autocorrelation, differences between two points would have to be measured directly.

Those records made by Swinbank at heights of 23 m and 29 m for which all the necessary subsidiary data were available have been used in this analysis. Observations at these heights only were used because previous work had suggested that at lower levels much of the interesting part of the eddy structure was of too short a period to be properly taken into account by the recording galvanometers used (natural period nominally 2·3 sec).

The stresses tabulated by Swinbank are available to test the present method. Unfortunately, the decision to use autocorrelations at 23 m and 29 m only involved the use of stresses measured at the same height for comparison purposes, and it has been shown by Deacon (1955) that the 5 min recording period used was not long enough for all the eddies contributing to the momentum flux at those heights to be fully accommodated. His comparison of the stress measurements there with those at 1·5 to 2 m led him to conclude that both sets of measurements are low by similar amounts, the former through the exclusion of low-frequency contributions, the latter through high-frequency cut-off. The latter effect has since been shown to amount to 20–30 % so, in what follows, Swinbank's stresses have been corrected by an increase of 30 % and are used as reference values denoted by τ.

No such correction to allow for apparent loss of flux due to the shortness of the observation period has been made to Swinbank's values of heat flux because the effect does not seem to be as severe here (Deacon 1955). The tabulated heat fluxes have been taken without change and are denoted by H.

It is clear from the above that these observations are far from ideal for testing the proposed structure-function method of estimating fluxes. Nevertheless, their application to this purpose is an obvious first step in verifying the method and will help in deciding whether a more refined programme of observations is justified.

4. First estimate of shearing stress

A total of 31 records with all necessary subsidiary observations was available and autocorrelations in u were calculated from them for time lags, σ, of about 1, 2, 5 and 9 sec for which experience had shown that equation (2) was fairly well obeyed at these heights. As a further test of this equation, the values of D_u so obtained were plotted logarithmically against σ so as to determine the index p in the proportionality

$$D_u \propto \sigma^p.$$

These values of p are shown in table 1 and the mean $0{\cdot}63 \pm 0{\cdot}03$ is in satisfactory agreement with the expected value.

Seven values of stress had previously been calculated (Taylor 1955) by the methods of §2 and had shown reasonable agreement on average with those measured by Swinbank. In this calculation, however, the second term on the right of equation (4) was ignored since the observations concerned were mainly in the near-neutral condition. This comparison has now been extended by calculating stresses from the 31 new sets of structure functions.

Date*	Run no.*	p	ϵ erg (g^{-1} sec^{-1})	$\partial\overline{u}/\partial z$ (sec^{-1})	T_1 (dyne cm^{-2})	τ (dyne cm^{-2})	T_1/τ
8. xi. 51	2	0·75	76·4	0·0291	3·00	1·83	1·64
9. i. 52	3	0·49	27·8	0·0134	−3·28	2·66	−1·23
16. i. 52	6	0·45	60·3	0·0386	1·20	3·22	0·37
21. i. 52	4	0·49	88·4	0·0156	3·22	2·35	1·37
4. ii. 52	2	0·75	39·6	0·0122	3·17	2·58	1·22
4. ii. 52	4	0·75	40·0	0·00513	−2·29	1·90	−1·21
4. ii. 52	6	0·75	132	0·00566	18·0	4·29	4·20
13. ii. 52	9	0·87	4·92	0·0751	0·11	0·56	0·20
13. ii. 52	11	0·81	2·35	0·0496	0·06	0·26	0·23
25. ii. 52	6	0·40	34·9	0·0532	0·09	2·06	0·05
25. ii. 52	11	0·73	45·5	0·0502	1·00	1·53	0·66
25. ii. 52	13	0·81	17·7	0·0390	0·34	2·26	0·15
25. ii. 52	15	0·51	53·1	0·0383	1·61	1·38	1·17
25. ii. 52	17	0·47	26·4	0·0485	0·76	1·34	0·57
25. ii. 52	19	0·60	12·6	0·0540	0·33	0·66	0·50
26. ii. 52	37	0·40	20·0	0·0239	0·73	0·44	1·66
26. ii. 52	39	0·73	21·4	0·0117	−0·35	2·72	−0·13
26. ii. 52	46	0·60	38·9	0·0239	1·16	1·90	0·62
26. ii. 52	48	0·78	79·7	0·0274	2·40	3·39	0·71
26. ii. 52	50	0·53	68·5	0·0241	2·16	2·46	0·88
3. iii. 52	4	0·65	101	0·0304	1·47	1·23	1·19
3. iii. 52	6	0·62	57·5	0·0153	−3·53	8·01	−0·44
3. iii. 52	10	0·47	53·5	0·00996	3·20	5·43	0·59
3. iii. 52	16	0·65	11·7	0·0414	0·43	0·35	1·23
4. iii. 52	48	0·55	33·1	0·0209	1·10	0·57	1·93
19. iii. 52	8	0·84	79·3	0·0575	2·03	4·70	0·43
19. iii. 52	10	0·70	80·9	0·0268	3·55	2·75	1·29
19. iii. 52	12	0·90	90·3	0·0328	2·90	4·71	0·62
19. iii. 52	16	0·67	37·2	0·0410	0·95	2·00	0·48
9. vii. 52	1	0·38	6·08	0·120	0·08	0·32	0·25
9. vii. 52	3	0·47	4·03	0·104	0·06	0·21	0·29
	Mean	0·63	—	—	—	—	0·69
Standard error of mean		0·03	—	—	—	—	0·18

* As shown by Swinbank (1955).

TABLE 1. Results of velocity autocorrelation analysis.

Values of ϵ (as shown in table 1) were calculated according to equation (3) by plotting $D_u(\sigma)$ against $\sigma^{\frac{2}{3}}$ and fitting a straight line through the origin by eye. To calculate the stress then by equation (4) it is also necessary to know the heat

flux and the velocity gradient at the height of observation. The values H tabulated by Swinbank were accepted for the former and the latter was calculated by fitting to the wind-speed observations at all available heights (which lay within the range 0·5–32 m) an interpolation formula of the form $\partial u/\partial z = az^{-\beta}$ where a and β are disposable constants. The values of shearing stress so calculated are denoted by T_1 and are shown in table 1.

The ratio T_1/τ was also calculated for each run (see table 1) and its mean is $0{\cdot}69 \pm 0{\cdot}18$. The expected value of unity is barely within the range of twice the standard deviation from that observed and it might appear that some adjustment of the constant in equation (3) is needed. This possibility is hardly surprising when it is recalled that the constant rests ultimately on a laboratory measurement of the skewness in distribution of $[u(x) - u(x+r)]$ which is itself open to doubt and that a very great change in scale is involved in its application here.

5. The heat flux

Little experimental evidence has been brought to bear on the question of whether $D_T(r)$ is proportional to $r^{\frac{2}{3}}$ or $r^{\frac{1}{3}}$. Inoue (1952) quotes some observations by Crain & Gerhardt (1951) and claims that they support his own proposed $r^{\frac{1}{3}}$ relationship. On the other hand, Shiotani (1955) and Tatarskii (1956), on the basis of observations which they adduce, both support the proposals of Obukhov and Corrsin. In view of this disagreement, it seemed desirable to examine the available observations on the point.

Autocorrelations at time lags, σ, were therefore calculated from temperature records of Swinbank's (1953) investigation. There were available 28 records suitable for this purpose which were also accompanied by the subsidiary data needed for heat flux estimation (see below). It was assumed that the limits of inertial subrange behaviour would be similar to those for velocity fluctuations and approximately the same values of σ were used. Logarithmic plotting of D_T against σ then gave the index p as shown in table 2. The mean p of $0{\cdot}64 \pm 0{\cdot}03$ unequivocally supports the 'two-thirds' law for the structure function, as expressed in equation (7). The constant of proportionality in this equation is, of course, not yet determined and a purely empirical value will later be derived.

To obtain some idea of the relative magnitudes of the terms in equation (13), four of the available records were analysed in detail. They were made in lapse conditions with an average Richardson number (at 1·5 m) of $-0{\cdot}051$. On the average over these four runs, it was found that:

$$H\frac{\partial\overline{\theta}}{\partial z} = -14{\cdot}4\,\text{erg °C cm}^{-3}\,\text{sec}^{-1},$$

$$\tfrac{1}{2}c_p\overline{\rho w' T'^2} = +0{\cdot}30\,\text{erg °C cm}^{-2}\,\text{sec}^{-1},$$

$$\overline{\rho\epsilon(T'^2)^{\frac{1}{2}}} = +0{\cdot}02\,\text{erg °C cm}^{-3}\,\text{sec}^{-1},$$

$$\lambda\frac{\partial^2}{\partial z^2}(\tfrac{1}{2}\overline{T'^2}) \approx 10^{-5}\,\text{erg °C cm}^{-3}\,\text{sec}^{-1};$$

(w is the vertical velocity component).

As far as this evidence takes us, therefore, we are clearly justified in writing approximately

$$\chi = -\frac{H}{c_p \rho}\frac{\partial \overline{\theta}}{\partial z}. \tag{14}$$

This is equivalent to the equation finally arrived at by Tatarskii (1956).

Date	Run no.	p	χ 10^{-4}(°C)^2 sec^{-1}	$\partial\theta/\partial z$ 10^{-6} °C cm^{-1}	H_1 (mW cm^{-2})	H (mW cm^{-2})	H_1/H
16. i. 52	6	0·65	7·36	−159	5·58	8·0	0·70
21. i. 52	2	0·51	25·6	−200	15·3	21·0	0·73
21. i. 52	4	0·45	25·2	−156	19·4	17·1	1·13
4. ii. 52	2	0·34	5·31	−136	4·70	2·7	1·74
4. ii. 52	4	0·58	11·1	−142	9·40	18·3	0·51
4. ii. 52	6	0·78	41·0	−192	25·6	17·4	1·47
13. ii. 52	9	0·65	0·233	98·5	−0·28	− 0·8	0·35
25. ii. 52	6	0·93	3·44	−125	3·31	11·3	0·29
25. ii. 52	11	0·47	0·415	−61·8	0·80	1·3	0·62
25. ii. 52	13	0·49	0·710	−17·4	4·90	2·4	2·04
25. ii. 52	15	0·73	0·221	−11·4	2·33	0·6	3·89
25. ii. 52	17	0·47	0·971	44·1	−2·64	−1·6	1·65
25. ii. 52	19	0·62	1·27	44·7	−3·41	−0·8	4·26
26. ii. 52	37	0·78	1·23	−138	1·07	2·0	0·54
26. ii. 52	39	0·97	1·89	−130	1·75	9·1	0·19
26. ii. 52	46	0·58	5·35	−145	4·42	5·8	0·76
26. ii. 52	48	0·75	13·1	−145	10·8	9·1	1·19
26. ii. 52	50	0·58	10·6	−150	8·49	9·2	0·92
3. iii. 52	4	0·78	24·0	−169	17·0	23·4	0·73
3. iii. 52	6	0·78	24·3	−217	13·4	37·7	0·36
3. iii. 52	10	0·78	1·89	−206	1·10	9·9	0·11
3. iii. 52	16	0·87	0·916	116	−0·95	−1·1	0·86
4. iii. 52	48	0·67	1·32	−42·9	3·69	5·1	0·72
19. iii. 52	10	0·58	0·864	−296	0·35	0·6	0·58
19. iii. 52	12	0·36	1·66	−114	1·75	4·0	0·44
19. iii. 52	16	0·90	1·26	−111	1·36	1·7	0·80
9. vii. 52	1	0·27	1·87	440	−0·51	−0·7	0·73
9. vii. 52	3	0·47	2·29	300	−0·92	−0·3	3·06
	Mean	0·64	—	—	—	—	1·12
Standard error of mean		0·03	—	—	—	—	0·20

TABLE 2. Results of temperature autocorrelation analysis.

Values of χ as shown in table 2 were calculated from the temperature autocorrelations by means of equation (7), tentatively taking the constant of proportionality as unity and using ϵ as given in table 1. Heat fluxes, H_1, were then obtained from equation (14). The potential temperature gradients required were derived from the original observations of temperature at heights within the range 0·5–30 m by fitting an interpolation formula of the form $\partial\theta/\partial z = az^{-\beta}$.

These values of H_1 are shown in table 2 and are compared with Swinbank's values, H, by calculating H_1/H. The mean value of H_1/H was $1{\cdot}12 \pm 0{\cdot}20$ and it thus appears that 1·12 is the best available estimate for the constant in equation (7). New heat fluxes, H_2, were calculated on this basis and it is obvious that the mean H_2/H must be $1{\cdot}00 \pm 0{\cdot}18$.

6. The second estimate of stress

The stress estimation in §4 involved a heat flux derived from the covariance between the temperature and the vertical velocity component. It is obviously desirable particularly for shipboard use to eliminate this type of measurement altogether and to use heat fluxes derived as in §5. If we write

$$a = D_u(r)\, r^{-\frac{2}{3}}, \quad b = D_T(r)\, r^{-\frac{2}{3}},$$

then, using the proposed value of 1·12 for the constant in (7), it follows that

$$\epsilon = 0{\cdot}5a^{\frac{3}{2}}, \quad H = -0{\cdot}893\frac{c_p \rho b \epsilon^{\frac{1}{3}}}{\partial\bar{\theta}/\partial z},$$

and hence, by the use of (4), we derive a new estimate, T_2, for the shearing stress. This has been done for those 27 observations for which both temperature and velocity information was available, and it was found that the mean value of T_2/τ was $0{\cdot}99 \pm 0{\cdot}15$. The individual values of T_2/τ are given in table 3.

Date	Run no.	T_2/τ	Date	Run no.	T_2/τ	Date	Run no.	T_2/τ
16. i. 52	6	0·44	25. ii. 52	15	1·07	3. iii. 52	6	0·25
21. i. 52	4	1·34	25. ii. 52	17	0·60	3. iii. 52	10	1·12
4. ii. 52	2	1·06	25. ii. 52	19	0·70	3. iii. 52	16	1·15
4. ii. 52	4	2·05	26. ii. 52	37	1·98	4. iii. 52	48	2·45
4. ii. 52	6	3·40	26. ii. 52	39	0·63	19. iii. 52	10	1·29
13. ii. 52	9	0·16	26. ii. 52	46	0·73	19. iii. 52	12	0·67
25. ii. 52	6	0·29	26. ii. 52	48	0·68	19. iii. 52	16	0·49
25. ii. 52	11	0·67	26. ii. 52	50	0·96	9. vii. 52	1	0·22
25. ii. 52	13	0·08	3. iii. 52	4	1·86	9. vii. 52	3	0·35

TABLE 3. Values of T_2/τ.

During a 5 min observation period it is not likely that all the assumptions made in deriving the expression for T_2 will hold good. Those of horizontal uniformity and steadiness in time, in particular, may break down over short periods. However, the coefficient of correlation between T_2 and τ is 0·49 which is significant at the 1 % level, while the coefficient of regression of T_2 on τ is $1{\cdot}00 \pm 0{\cdot}36$. Figure 1 shows the T_2 and τ values with the calculated regression line.

In the practical use of the structure-function method it is quite reasonable that a number of 5 min runs—or of runs over a longer period of observation—should be taken in order to average out the effects referred to above. The values of T_2 and τ were therefore subdivided into groups according to the magnitude of τ, and mean T_2 and τ were calculated for each group as shown in table 4. The coefficient of correlation between the two groups of means is 0·99.

A further subdivision of the T_2 results according to Richardson number at 1·5 m ($Ri_{1{\cdot}5}$) was made and is shown in table 5.

Application of the method of combining probabilities due to Fisher (1948, p. 99) indicates that the probability of the set of deviations of T_2/τ from unity

being due to chance is 0·03 and it appears, therefore, that the trend of T_2/τ with stability shown in table 5 is significant.

This trend may, in part, be explained in terms of instrumental response characteristics. T_2 and τ were obtained ultimately from the same galvanometer records but, as stability increases, the turbulent energy moves further and further into smaller eddy sizes. Since the eddies contributing to the structure function measurement are smaller than the strongly anisotropic ones entering into the

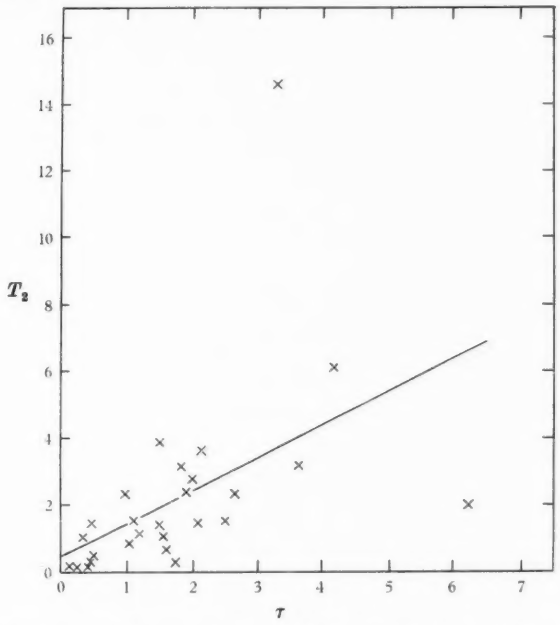

FIGURE 1. Comparison of stresses measured by two methods (individual 5 min runs).

Group	No. of observations	Mean τ	Mean T_2
A	5	0·29	0·30 ± 0·15
B	6	0·86	1·24 ± 0·26
C	5	1·56	1·41 ± 0·65
D	6	2·06	2·49 ± 0·34
E	5	3·98	5·63 ± 2·36

TABLE 4. Means of T_2 and τ, according to magnitude of τ.

Group	No. of observations	Mean $Ri_{1.5}$	Mean T_2/τ
F	6	+0·029	0·53 ± 0·15
G	5	−0·007	0·59 ± 0·15
H	6	−0·015	0·84 ± 0·24
J	5	−0·031	1·38 ± 0·29
K	5	−0·087	1·72 ± 0·52

TABLE 5. Values of T_2/τ, according to stability.

covariances, it might well be expected that the failure of the galvanometers to respond fully to the fine detail of the turbulence would affect T_2 more strongly than τ and the more so as stability increases. However, it would also be expected that this effect would cause T_2 to be less than τ in all conditions of stability so that all the features of table 5 cannot be explained in this way. This fact, together with the rather large difference between the means of T_1/τ and T_2/τ, make it unlikely that the values of the constants used in equations (3) and (7) can yet be regarded as firm for use in the lower atmosphere.

7. Conclusion

The results of the previous sections are encouraging and suggest that it may be possible to estimate stress or heat flux from a group of some thirty 5 min measurements of structure function with a standard error of 15–20 %. More observations, specially designed for the purpose, need to be made, however, to get more secure values for the two constants of proportionality and to elucidate stability effects, particularly in so far as they concern the instrumental response characteristics required.

It is worthy of note that equation (12) is essentially a conservation equation and that a similar equation could be constructed for water-vapour concentration. A structure-function method, involving mean-square humidity differences, could thus probably be developed for the assessment of the vertical turbulent flux of water-vapour, that is, the rate of evaporation from the underlying surface.

I have had the benefit of much discussion with Dr U. Radok and Mr E. K. Webb. Mr E. L. Deacon provided information on the probable errors in the reference stresses and the differential-analyser calculations of the autocorrelations were carried out under the direction of Mr N. E. Bacon.

The material included in this paper has formed part of a thesis submitted to the University of Melbourne.

REFERENCES

Corrsin, S. 1951 *J. Appl. Phys.* **22**, 469.
Crain, C. M. & Gerhardt, J. R. 1951 *J. Met.* **8**, 363.
Deacon, E. L. 1955 *C.S.I.R.O. Div. Met. Phys. Tech. Pap.* no. 4.
Deacon, E. L. 1959 *Advanc. Geophys.* **6**, 211.
Fisher, R. A. 1948 *Statistical Methods for Research Workers*, 10th ed. Edinburgh: Oliver and Boyd.
Gifford, F. 1956 *J. Met.* **13**, 289.
Gifford, F. 1959 *J. Met.* **16**, 344.
de Groot, S. R. 1951 *Thermodynamics of Irreversible Processes.* Amsterdam: North-Holland Publishing Co.
Inoue, E. 1952 *J. Met. Soc. Jap.* **30**, 289.
Jeffreys, H. 1952 *Cartesian Tensors.* Cambridge University Press.
MacCready, P. B. 1953 *J. Met.* **10**, 434.
Obukhov, A. M. 1949 *Izv. Akad. Nauk. SSSR* (*Ser. geog. i. geof.*), **13**, 58.
Obukhov, A. M. & Yaglom, A. M. 1951 *Prik. Mat. i Mekh.* **15**, 3.
Shiotani, M. 1955 *J. Met. Soc. Jap.* **33**, 17.
Stewart, R. W. 1951 *Proc. Camb. Phil. Soc.* **47**, 146.
Swinbank, W. C. 1955 *C.S.I.R.O. Div. Met. Tech. Pap.* no. 2.
Tatarskii, V. I. 1956 *Izv. Akad. Nauk. SSSR* (*Ser. geof.*), no. 6, 689.
Taylor, G. I. 1938 *Proc. Roy. Soc.* A, **164**, 476.
Taylor, R. J. 1955 *Aust. J. Phys.* **8**, 535.
Taylor, R. J. 1957 *J. Met.* **14**, 378.

The effect of a magnetic field on the flow of a conducting fluid past a body of revolution

By W. CHESTER

Department of Mathematics, University of Bristol

(Received 6 December 1960)

The problem described by the title is investigated when both the magnetic field and the streaming motion of the fluid at infinity are uniform and parallel to the axis of symmetry of the body. The flow pattern depends on three parameters, the Reynolds number R, the magnetic Reynolds number R_m and the Hartmann number M. In this paper it is assumed that $M \gg 1$, $M \gg R$, $M \gg R_m$ (no other restrictions on the parameters are imposed, so that R and R_m need not be small). The flow pattern then consists of an undisturbed uniform stream outside a cylinder circumscribing the body with generators parallel to the stream. Inside this cylinder the fluid is at rest. The leading term in the expression for the drag on the body is obtained.

1. Introduction

In an earlier paper (Chester 1957) the author considered the effect of a magnetic field on the flow of a conducting fluid past a sphere. It was shown that the magnetic field, assumed to be parallel to the uniform stream at infinity, produces a body force which opposes the natural tendency of the fluid to flow round the body and thereby increase the drag. An expression for the drag was obtained as an expansion in increasing powers of the Hartmann number.

The object of the present investigation is to consider the same problem, but for large values of the Hartman number. Because of the insensitivity of the flow to the detailed shape of the body, it is possible to generalize the argument to deal with an arbitrary body of revolution.

2. Formulation of the problem

The fluid is assumed to be incompressible, viscous and conducting. It flows steadily past a body of revolution whose axis defines the x-axis of a system of Cartesian co-ordinates with origin inside the body. Both the flow direction and the magnetic field are parallel to the x-axis at infinity.

The equations to be solved are then, with the usual notation for electromagnetic quantities (measured in M.K.S. units),

$$\nabla' \wedge \mathbf{H} = \mathbf{j} = \sigma(\mathbf{E} + \mu \mathbf{V}' \wedge \mathbf{H}), \quad \nabla' . \mathbf{H} = 0, \quad \nabla' \wedge \mathbf{E} = 0, \tag{1}$$

$$\nabla' . \mathbf{V}' = 0, \tag{2}$$

$$\rho(\mathbf{V}' . \nabla') \mathbf{V}' = -\nabla' p' + \rho \nu \nabla'^2 \mathbf{V}' + \mu \mathbf{j} \wedge \mathbf{H}, \tag{3}$$

where $\mathbf{V}'$, p', ρ, ν denote respectively the velocity, pressure, density and kinematic viscosity. The prime has been used here so that the same symbols without the prime can later be used to denote non-dimensional quantities.

We note first that, because of the symmetry of the problem, the vector $\mathbf{V}' \wedge \mathbf{H}$ has zero divergence and hence, by equations (1),

$$\nabla' . \mathbf{E} = 0, \quad \nabla' \wedge \mathbf{E} = 0. \tag{4}$$

The electric field is thus identically zero, since this is a solution of (4) which violates no boundary conditions at the body or at infinity.

Now let U be the speed of the uniform stream at infinity, and let the body lie within a sphere of radius a and centre at the origin. The space co-ordinates may then be made non-dimensional with the factor a^{-1}, and the pressure and velocity by the relations

$$p = \frac{a}{\rho\nu U}(p' - p'_\infty), \quad \mathbf{V} = \mathbf{V}'/U, \tag{5}$$

where p'_∞ is the pressure at infinity.

It follows, from the first of equations (1), that

$$R_m \mathbf{V} \wedge \mathbf{H} = \nabla \wedge \mathbf{H}, \tag{6}$$

where
$$R_m = Ua\mu\sigma = \text{magnetic Reynolds number}. \tag{7}$$

If the left-hand side of (6) were neglected, $\mathbf{H}$ would also satisfy equations (4). If, in addition, the permeabilities of the fluid and the body were equal, the magnetic field would be uniform and parallel to the x-axis. We thus write

$$\mathbf{H} = \pm H(\mathbf{i} + R_m \mathbf{A}), \tag{8}$$

where the first term is taken to be dominant. The validity of this assumption will be discussed later. For the moment we take $\mathbf{H} = \pm H\mathbf{i}$ approximately, and equation (3) then reduces to

$$R(\mathbf{V} . \nabla)\mathbf{V} = -\nabla p + \nabla^2 \mathbf{V} + M^2(\mathbf{V} \wedge \mathbf{i}) \wedge \mathbf{i}, \tag{9}$$

where
$$R = Ua/\nu = \text{Reynolds number}, \tag{10}$$

$$M = \mu H a(\sigma/\rho\nu)^{\frac{1}{2}} = \text{Hartmann number}. \tag{11}$$

Note that the Hartmann number, like the Reynolds number and magnetic Reynolds number, is essentially non-negative.

Equation (9) is further simplified by neglecting the term on the left-hand side. The techniques of this paper are not sufficiently refined to discuss the precise condition for which the neglect of the convective terms is valid. However, in the paper immediately following, a much more careful analysis of the whole flow field is made for the special case of a circular disk. There it is shown that the approximation is justified provided that $M \gg R$. (This is also the condition required when $M \ll 1$.) While this is not completely general it is also not so restrictive as might at first appear, for it is also found that the flow field is insensitive to the detailed shape of the body when M is large. The uniform stream is undisturbed outside an elongated cylinder circumscribing the body; inside the cylinder the fluid is substantially at rest. The thickness of the shear layer at the

surface of this cylinder is $O(M^{-\frac{1}{2}})$ near the body and gradually thickens towards far distant points, where the contour of the cylinder becomes less well defined and the flow merges into the pattern of a uniform stream at infinity.

3. General solution of the equations

With the indicated simplifications, (2) and (9) now give

$$\nabla . \mathbf{V} = 0, \tag{12}$$

$$-\nabla p + \nabla^2 \mathbf{V} + M^2 (\mathbf{V} \wedge \mathbf{i}) \wedge \mathbf{i} = 0. \tag{13}$$

These have the particular solution (Chester 1957)

$$\mathbf{V} = \mathbf{i} + e^{Mx} \nabla \phi_1 + e^{-Mx} \nabla \phi_2, \tag{14}$$

$$p = M e^{Mx} \frac{\partial \phi_1}{\partial x} - M e^{-Mx} \frac{\partial \phi_2}{\partial x}, \tag{15}$$

where

$$\nabla^2 \phi_1 + M \frac{\partial \phi_1}{\partial x} = 0, \tag{16}$$

$$\nabla^2 \phi_2 - M \frac{\partial \phi_2}{\partial x} = 0. \tag{17}$$

Equations (14) and (15) contain the most general solutions for p, and u, the x-component of $(\mathbf{V} - \mathbf{i})$. For it is easily deducible from (13) and (14) that

$$\nabla^2 (p + Mu) - M \frac{\partial}{\partial x} (p + Mu) = 0, \tag{18}$$

$$\nabla^2 (p - Mu) + M \frac{\partial}{\partial x} (p - Mu) = 0, \tag{19}$$

so that $(p + Mu)$ and $(p - Mu)$ can be identified with $M e^{Mx} \phi_{1x}$ and $-M e^{-Mx} \phi_{2x}$ respectively. Thus the most general solution may contain extra terms which contribute to the velocity components perpendicular to the x-axis. Since such terms must satisfy the continuity equation, they may be expressed in the form $\nabla \chi \wedge \mathbf{i}$. Since also the conditions of symmetry require that there be no component of vorticity in the x-direction, χ must be a solution of the two-dimensional Laplace's equation. This solution is to be regular at all points in a plane perpendicular to the x-axis and so can be at most a constant, which has no significance in the velocity field. Equations (14) and (15) therefore represent the complete solution.

It also follows, from (1), (6) and (8) that the equations satisfied by $\mathbf{A}$ outside the body are approximately

$$\nabla \wedge \mathbf{A} = \mathbf{V} \wedge \mathbf{i}, \quad \nabla . \mathbf{A} = 0, \tag{20}$$

with the solution

$$\mathbf{A} = -M^{-1} e^{Mx} \nabla \phi_1 + M^{-1} e^{-Mx} \nabla \phi_2 + \nabla \phi', \tag{21}$$

where

$$\nabla^2 \phi' = 0.$$

Inside the body, where $\nabla \wedge \mathbf{A} = 0$, $\nabla . \mathbf{A} = 0$, $\mathbf{A}$ is a harmonic function. This function, together with ϕ', is determined by the continuity of $\mathbf{A}$ on the surface of the body. Now the first two terms in (21) are at most $O(M^{-1})$ for, as will be shown, each term in (14) for the velocity is at most $O(1)$. It follows that $\mathbf{A}$ itself

is at most $O(M^{-1})$ and hence that the approximation implied by taking the magnetic field to be $H\mathbf{i}$ is valid provided that $M \gg R_m$.

The assumptions made also imply that the Alfven wave speed $(\mu^{\frac{1}{2}}H/\rho^{\frac{1}{2}})$ is large compared with U, for their ratio is M^2/RR_m. The effect on disturbances associated with this speed may be compared to the effect on compressive disturbances of the assumption of small Mach number.

4. Solution for large Hartmann number

To obtain the solution for $M \gg 1$, it is sufficient to note that p and each of the components of $(\mathbf{V}-\mathbf{i})$ can be written as the sum of two terms satisfying respectively the equations

$$\nabla^2\psi_1 - M\frac{\partial\psi_1}{\partial x} = 0, \tag{22}$$

$$\nabla^2\psi_2 + M\frac{\partial\psi_2}{\partial x} = 0. \tag{23}$$

The asymptotic behaviour of solutions of the first equation has already been discussed in the literature (Oseen 1927; Stewartson 1956) with reference to Oseen's equation for viscous flow past solid bodies, and the second equation is also amenable to similar treatment. We follow here the interpretation given by Stewartson (1956) of Oseen's original argument.

Let

$$\psi_1 = A_1(y', z'), \quad \frac{\partial\psi_1}{\partial\alpha} = MB_1(y', z'), \tag{24}$$

$$\psi_2 = A_2(y', z'), \quad \frac{\partial\psi_2}{\partial\alpha} = MB_2(y', z'), \tag{25}$$

at the point (x', y', z') of the body, where $\partial/\partial\alpha$ represents differentiation along the outward normal. (It will appear later that the normal derivatives can be $O(M)$ on the body.) Then, by a simple extension of Kirchhoff's solution of the wave equation, we can write

$$4\pi\psi_1(x,y,z) = \iint\left\{M(B_1 - lA_1)\frac{e^{\frac{1}{2}M(x-x'-R)}}{R} - A_1\frac{\partial}{\partial\alpha}\left(\frac{e^{\frac{1}{2}M(x-x'-R)}}{R}\right)\right\}dS, \tag{26}$$

$$4\pi\psi_2(x,y,z) = \iint\left\{M(B_2 + lA_2)\frac{e^{-\frac{1}{2}M(x-x'+R)}}{R} - A_2\frac{\partial}{\partial\alpha}\left(\frac{e^{-\frac{1}{2}M(x-x'+R)}}{R}\right)\right\}dS, \tag{27}$$

where (x', y', z') is a point on the body where the outward drawn normal has direction cosines (l, m, n), and

$$R^2 = (x-x')^2 + (y-y')^2 + (z-z')^2.$$

Consider first the asymptotic behaviour of

$$\iint M(B_1 - lA_1)\frac{e^{\frac{1}{2}M(x-x'-R)}}{R}dS \tag{28}$$

for large M. The integrand is exponentially small unless $(y-y')^2 + (z-z')^2$ is small. This implies that the integral itself is exponentially small unless a line through (x, y, z) parallel to the x-axis cuts the body. If it does cut the body at a point

(ξ, y, z) then the sensible contribution to (28) comes from the integral over that part of the body in the neighbourhood of this point, together with similar contributions from the other points of intersection. The contribution from one point of intersection may then be written

$$M\{B_1(y,z) - lA_1(y,z)\} \iint \frac{e^{\frac{1}{2}M(x-x'-R)}}{R}\, dS, \tag{29}$$

where l is also a function of y and z, and the integration can be taken over the infinite plane $lx' + my' + nz' = l\xi + my + nz$.

With the transformation

$$\begin{aligned} x' - \xi &= -(1-l^2)^{\frac{1}{2}} r\sin\theta + (1-l^2)(x-\xi), \\ y' - y &= \frac{nr\cos\theta}{(1-l^2)^{\frac{1}{2}}} + \frac{mlr\sin\theta}{(1-l^2)^{\frac{1}{2}}} - lm(x-\xi), \\ z' - z &= \frac{-mr\cos\theta}{(1-l^2)^{\frac{1}{2}}} + \frac{nlr\sin\theta}{(1-l^2)^{\frac{1}{2}}} - nl(x-\xi), \end{aligned}$$

the integral (29) becomes

$$\begin{aligned} M(B_1 - lA_1) &\int_0^\infty \frac{r\,dr}{\{r^2 + l^2(x-\xi)^2\}^{\frac{1}{2}}} \int_0^{2\pi} \exp\tfrac{1}{2}M[l^2(x-\xi) + (1-l^2)^{\frac{1}{2}} r\sin\theta \\ &\qquad - \{r^2 + l^2(x-\xi)^2\}^{\frac{1}{2}}]\, d\theta \\ &= 2\pi M(B_1 - lA_1) \int_0^\infty \frac{r\,dr}{\{r^2 + l^2(x-\xi)^2\}^{\frac{1}{2}}} I_0\{\tfrac{1}{2}Mr(1-l^2)^{\frac{1}{2}}\} \\ &\qquad \times \exp\tfrac{1}{2}M[l^2(x-\xi) - \{r^2 + l^2(x-\xi)^2\}^{\frac{1}{2}}] \\ &= \frac{4\pi(B_1 - lA_1)}{|l|} \exp[\tfrac{1}{2}Ml^2\{(x-\xi) - |x-\xi|\}] \\ &= \begin{cases} 4\pi(B_1 - lA_1)/|l| & \text{for} \quad x > \xi, \\ \dfrac{4\pi(B_1 - lA_1)}{|l|} \exp[Ml^2(x-\xi)] & \text{for} \quad x < \xi. \end{cases} \end{aligned} \tag{30}$$

Similarly, the contribution to

$$\iint A_1 \frac{\partial}{\partial\alpha} \frac{(e^{\frac{1}{2}M(x-x'-R)})}{R}\, dS$$

is sensibly

$$\begin{aligned} -A_1 &\left(l\frac{\partial}{\partial x} + m\frac{\partial}{\partial y} + n\frac{\partial}{\partial z}\right) \iint \frac{e^{\frac{1}{2}M(x-x'-R)}}{R}\, dS \\ &= \begin{cases} 0 & \text{for} \quad x > \xi, \\ -4\pi A_1 \operatorname{sgn} l\, e^{Ml^2(x-\xi)} & \text{for} \quad x < \xi. \end{cases} \end{aligned} \tag{31}$$

Similar contributions come from the other points of intersection. The final result is that ψ_1 tends exponentially to zero outside a cylinder circumscribing the body with its axis along the x-axis. Inside this cylinder on the downstream side of the body ($x > 0$) the asymptotic form of ψ_1 is independent of x so that

$$\psi_1 = \psi_1(y,z),$$

and on the upstream side ($x < 0$)

$$\psi_1 = \beta(y, z)\, e^{Ml^2(x-\xi)},$$

where ξ is the value of x at the point on the body nearest the point (x, y, z), for which $y = y'$, $z = z'$.

The argument for ψ_2 is similar and only the final results are quoted. Inside the circumscribing cylinder $\psi_2 = \psi_2(y, z)$ on the upstream side, and on the downstream side

$$\psi_2 = \beta'(y, z)\, e^{-Ml^2(x-\xi)}.$$

It is now a simple matter to write down the asymptotic forms of the velocity components and the pressure. If we consider only the perturbed field, all the components are asymptotically zero outside the circumscribing cylinder. Inside this cylinder on the downstream side of the body

$$M^{-1}p = u_0 - u_1 e^{-Ml^2(x-\xi)},$$

$$\mathbf{V} = \mathbf{i} + \mathbf{V}_0 + \mathbf{V}_1 e^{-Ml^2(x-\xi)},$$

where u_0, u_1 are the x-components respectively of $\mathbf{V}_0$, $\mathbf{V}_1$, these vectors being functions of y and z only. (Because of the symmetry of the flow they are in fact functions of $y^2 + z^2$ only.) Since $\mathbf{V}$ satisfies the continuity equation (12), the same must also be true of $\mathbf{V}_0$ and $\mathbf{V}_1 \exp\{-Ml^2(x-\xi)\}$ separately. If $\mathbf{V}_0$ is to be regular on the axis it cannot satisfy both the continuity equation and the requirements imposed by symmetry unless $\mathbf{V}_0 \wedge \mathbf{i}$ is zero. Also on the body the boundary condition $\mathbf{V} \wedge \mathbf{i} = 0$ must be satisfied and this now implies $\mathbf{V}_1 \wedge \mathbf{i} = 0$. The continuity condition then requires that $\mathbf{V}_1$ itself be zero. Finally the remaining boundary condition at the body (on the x-component of the velocity) is satisfied if $u_0 = -1$.

Similar arguments apply on the upstream side of the body, the only difference being that the contribution from the terms corresponding to ψ_1 and ψ_2 are interchanged. Since the boundary conditions are unchanged, the velocity fields on the upstream and downstream sides of the body are identical. But, because of the interchange of the roles of ψ_1 and ψ_2, the pressures on the two sides of the body are equal in magnitude but of opposite sign.

The following description of the flow field now emerges.* Outside the circumscribing cylinder the uniform flow field parallel to the axis of the body continues unchecked. Inside the cylinder the fluid is stagnant, the non-dimensional pressure p is equal to M on the upstream side and $-M$ on the downstream side. The drag is clearly given by

$$\frac{D}{\rho\nu a U} = \frac{2MA}{a^2}$$

or

$$D = 2\mu H U (\sigma\rho\nu)^{\frac{1}{2}} A,$$

where A is the cross-sectional area of the circumscribing cylinder. (Note that $D/\rho\nu a U$ and A/a^2 are the non-dimensional representations respectively of the drag and cross-sectional area corresponding to the pressure $p = ap'/\rho\nu U$.)

* The result is qualitatively similar to that of Stewartson (1960) for a similar problem in which the fluid was perfectly conducting and inviscid.

The discontinuity in velocity at the surface of the cylinder arises from the fact that the arguments used to obtain the asymptotic behaviour of ψ_1 and ψ_2 break down wherever l (the x-component of the unit normal to the body) is zero. This discontinuity is discussed in greater detail in the following paper where it is shown that it is an approximation to a region of rapid transition which, however, becomes more diffuse as $x \to \pm\infty$. It will also be shown that this thickening of the shear layer at far distant points explains a further anomaly of the present analysis, namely that the boundary condition on the velocity at infinity is not satisfied inside the circumscribing cylinder. It is in fact more accurate to picture the cylinder as being of length $O(M)$ and the uniform stream being dominant everywhere at distances large compared with $O(M)$.

One further point requires comment. The above argument is sufficient to deal with the upstream and downstream sides of the body. However, it may happen that a line parallel to the x-axis cuts the body in more than two points so that a pocket of fluid appears in the vicinity of the body. If one such pocket is described by $\xi_1 < x < \xi_2$, then the asymptotic form of the velocity vector there will be

$$\mathbf{V} = \mathbf{i} + \mathbf{V}_0 + \mathbf{V}_1 e^{-Ml^2(x-\xi_1)} + \mathbf{V}_2 e^{Ml^2(x-\xi_2)}.$$

Moreover $\mathbf{V}_0$ will contain contributions from integrals over planes for which $x > \xi$ and $x < \xi$. These contributions to u_0 must now be known separately before an expression for the pressure can be deduced. The present theory does not predict this, and the pressure is indeterminate unless some further condition is invoked such as continuity at the boundary of the pocket. But as far as the drag is concerned, it is sufficient that the pressure be independent of x, and this is so since it is easily shown that $\mathbf{V}_0 \wedge \mathbf{i} = \mathbf{V}_1 = \mathbf{V}_2 = 0$.

REFERENCES

Chester, W. 1957 *J. Fluid Mech.* **3**, 304.

Oseen, C. W. 1927 *Neuere Methoden und Ergebnisse in der Hydrodynamik.* Leipzig: Akademische Verlagsgesellschaft M.B.H.

Stewartson, K. 1956 *Phil. Mag.* **1**, 345.

Stewartson, K. 1960 *J. Fluid Mech.* **8**, 82.

The effect of a magnetic field on the flow of a conducting fluid past a circular disk

By W. CHESTER AND D. W. MOORE
Department of Mathematics, University of Bristol

(Received 6 December 1960)

In the previous paper (Chester 1961) it was shown that, for large values of the Hartmann number, the asymptotic solution for the flow past a body of revolution has a discontinuity on the surface of a cylinder which circumscribes the body. The flow in the region of this discontinuity is now investigated in more detail when the body is a circular disk broadside-on to the flow. It will be shown that there is actually a region of transition whose thickness is $O(|x|^{\frac{1}{2}}/M^{\frac{1}{2}})$, where x is the axial distance from the disk and M is the Hartmann number. This region is thin near the disk, but gradually thickens until it merges into the over-all flow field for $x = O(M)$.

The leading terms in the expression for the drag are given by

$$\frac{D}{D_s} = \frac{M\pi}{8}\left(1+\frac{2}{M}\right),$$

where D_s is the Stokes drag.

1. Introduction

We consider here a special case of the problem investigated in the preceding paper (Chester 1961, henceforth this paper is denoted by C). The same approximations are assumed to be valid, and the body is taken to be a circular disk of radius a, with its axis parallel to the uniform streaming motion at infinity. It will be shown that the mathematical problem for this particular case can be discussed in greater detail than the more general arguments of the previous investigation allowed. In particular the properties of the shear layer, which for $M \gg 1$ must exist at the periphery of the circumscribing cylinder, can now be discussed, and this is the main purpose of this paper. Since it has been shown that the flow field for large values of the Hartmann number is insensitive to the detailed shape of the body, it may reasonably be assumed that the results also describe the situation for a more general class of bodies.

2. The basic equations

The non-dimensional velocity and pressure are given by equations (C14)–(C17), namely

$$\mathbf{V} = \mathbf{i} + e^{Mx}\nabla\phi_1 + e^{-Mx}\nabla\phi_2, \tag{1}$$

$$p = M e^{Mx}\frac{\partial\phi_1}{\partial x} - M e^{-Mx}\frac{\partial\phi_2}{\partial x}, \tag{2}$$

where
$$\nabla^2\phi_1 + M\frac{\partial\phi_1}{\partial x} = 0, \tag{3}$$

$$\nabla^2\phi_2 - M\frac{\partial\phi_2}{\partial x} = 0, \tag{4}$$

and the length parameter used in the definition of M is now the radius of the disk. Because of symmetry the radial component of $\mathbf{V}$ must be zero on $x = 0$, and this implies that $\phi_1 + \phi_2 = 0$ on $x = 0$. Thus $(\phi_1 + e^{-Mx}\phi_2)$ satisfies the equation

$$\left(\nabla^2 + M\frac{\partial}{\partial x}\right)(\phi_1 + e^{-Mx}\phi_2) = 0, \tag{5}$$

and is zero on $x = 0$. It is therefore identically zero, and so we write

$$\phi_1 e^{mx} = -\phi_2 e^{-mx} = \phi \tag{6}$$

say, where $2m = M$ and
$$(\nabla^2 - m^2)\,\phi = 0, \tag{7}$$

$$\mathbf{V} = \{1 - 2m\phi\cosh mx\}\,\mathbf{i} + 2\sinh mx\nabla\phi, \tag{8}$$

$$\frac{p}{2m} = 2\frac{\partial\phi}{\partial x}\cosh mx - 2m\phi\sinh mx. \tag{9}$$

The remaining boundary conditions to be applied are that

$$\mathbf{V} = 0 \quad \text{for} \quad x = 0 \quad \{\eta = (y^2+z^2)^{\frac{1}{2}} < 1\}.$$

Also, it is consistent with the equations and boundary conditions to look for a solution such that ϕ is symmetrical, and hence p is anti-symmetrical, about $x = 0$. Since p is also continuous for $\eta > 1$, we must have

$$p = 0 \quad \text{for} \quad x = 0 \quad (\eta > 1).$$

In terms of ϕ, these boundary conditions imply that

$$\left.\begin{aligned} \phi &= \frac{1}{M} \quad \text{for} \quad x = 0 \quad (\eta < 1), \\ \frac{\partial\phi}{\partial x} &= 0 \quad \text{for} \quad x = 0 \quad (\eta > 1). \end{aligned}\right\} \tag{10}$$

3. Approximate solution for large Hartmann number

Any solution of (7), which is continuous together with its derivatives inside a closed surface S, may be written

$$\phi(P) = -\frac{1}{4\pi}\iint_S \left(G\frac{\partial\phi}{\partial n} - \phi\frac{\partial G}{\partial n}\right) dS, \tag{11}$$

where n is the inward-drawn normal to S, P is a point within S, and G is another function satisfying the same conditions as ϕ save that, near P, $G \sim \rho^{-1}$ where ρ is the distance from P. If, in addition $\partial G/\partial n = 0$ on S, then G is called the Green's function for this particular problem and

$$\phi(P) = -\frac{1}{4\pi}\iint_S G\frac{\partial\phi}{\partial n}\,dS. \tag{12}$$

When S is the plane $x = 0$, together with a large hemisphere in the positive half-plane on which the integral tends to zero as the radius tends to infinity, then

$$G = \frac{\exp\left[-m\{(x-x_0)^2+(y-y_0)^2+(z-z_0)^2\}^{\frac{1}{2}}\right]}{\{(x-x_0)^2+(y-y_0)^2+(z-z_0)^2\}^{\frac{1}{2}}} + \frac{\exp\left[-m\{(x+x_0)^2+(y-y_0)^2+(z-z_0)^2\}^{\frac{1}{2}}\right]}{\{(x+x_0)^2+(y-y_0)^2+(z-z_0)^2\}^{\frac{1}{2}}}, \quad (13)$$

where P is the point (x_0, y_0, z_0).

Thus, if

$$\frac{\partial\phi}{\partial x} = \chi(y,z) \quad \text{on} \quad x = 0,$$

we have, omitting the suffix,

$$\phi(x,y,z) = -\frac{1}{2\pi}\iint \chi(y',z')\frac{\exp\left[-m\{x^2+(y-y')^2+(z-z')^2\}^{\frac{1}{2}}\right]}{\{x^2+(y-y')^2+(z-z')^2\}^{\frac{1}{2}}}\,dy'\,dz'. \quad (14)$$

Consider now the argument used in C. We note first that, by (10), $\chi = 0$ except on the surface of the disk. Hence, for large m, $e^{mx}\,\phi$ is exponentially small unless a line through (x, y, z) parallel to the x-axis meets the surface of the disk. If it does, then the sensible contribution to the integral comes from the neighbourhood of the point $(0, y, z)$. Thus we write, approximately

$$\phi(x,y,z) = -\frac{\chi(y,z)}{2\pi}\iint \frac{\exp\left[-m\{x^2+(y-y')^2+(z-z')^2\}^{\frac{1}{2}}\right]}{\{x^2+(y-y')^2+(z-z')^2\}^{\frac{1}{2}}}\,dy'\,dz' \quad (15)$$

for points inside the cylinder circumscribing the disk. The argument then proceeds by integrating over the whole plane $-\infty < y' < \infty$, $-\infty < z' < \infty$. This gives

$$\phi(x,y,z) = -\frac{1}{m}e^{-mx}\chi(y,z), \quad (16)$$

and since, by (10),

$$\phi = \frac{1}{2m} \quad \text{for} \quad x = 0 \quad [(y^2+z^2) < 1],$$

we have, finally, $\chi = -\frac{1}{2}$ and so

$$\phi = \frac{1}{2m}e^{-mx} \quad \text{for} \quad x > 0.$$

In particular, by (9), $p = -2m$, which agrees with the result in C.

The argument fails for points near the surface of the circumscribing cylinder. It makes χ discontinuous at the edge of the disk, and the variation of χ in this region will affect the integral in (14) significantly if (y^2+z^2) is close to unity. However, when m is large, any point for which this is true must lie within a distance $O(m^{-1})$ from the surface $y^2+z^2 = 1$, otherwise the exponential factor in the integrand of (14) will be small enough to make the error in χ unimportant. (This is true only for $x \ll M$. Further comment on this point will appear later.) On such a length scale, the radius of curvature of the edge of the disk is large, and the previous argument can be refined by replacing the disk by a *semi*-infinite plane. The edge of this plane is to be tangential to the disk at the point of its

edge nearest the point (x, y, z) at which ϕ is being evaluated. It is sufficient to consider only points $(x, y, 0)$; the value of ϕ at other points is then deducible from symmetry. The disk is then replaced by the semi-infinite plane $x = 0, y < 1$.

To return to the original equations, the problem now presents itself in the following form. A two-dimensional solution of $(\nabla^2 - m^2)\phi = 0$ is required under the boundary conditions

$$\left.\begin{aligned} \phi &= \frac{1}{M} \quad \text{for} \quad x = 0 \quad (-\infty < y < 1), \\ \frac{\partial \phi}{\partial x} &= 0 \quad \text{for} \quad x = 0 \quad (1 < y < \infty). \end{aligned}\right\} \tag{17}$$

We also require that $\phi \to 0$ at infinity, except for $x = 0$, $y \to -\infty$. This last qualification is necessary because of the artificial boundary condition now imposed on the plane $x = 0$. This will not incur any serious error since we are interested in the solution only in the vicinity of $y = 1$.

Problems similar to this have been familiar in diffraction theory for some time (Gunn 1947; Chester 1950), and it is not difficult to derive the appropriate solution in the present case.

We first substitute $x = r\cos\theta$, $(y-1) = r\sin\theta$, so that the two sides of the semi-infinite plane become $\theta = -\frac{1}{2}\pi$, $\theta = \frac{3}{2}\pi$. Then the equation

$$\frac{\partial^2 \phi}{\partial x^2} + \frac{\partial^2 \phi}{\partial y^2} = m^2 \phi$$

has solutions of the form

$$e^{\pm mx} \int^{(2r)^{\frac{1}{2}} \sin \frac{1}{2}(\theta - \theta_0)} e^{-m\lambda^2} d\lambda. \tag{18}$$

These solutions are most easily obtained by transforming to parabolic coordinates (Lamb 1932; Gunn 1947). If the various possible solutions are combined, it is found that the appropriate function satisfying all the boundary conditions is

$$\phi = \frac{1}{2}\left(\frac{1}{m\pi}\right)^{\frac{1}{2}} \left\{ e^{-mx} \int_{(2r)^{\frac{1}{2}} \sin \frac{1}{2}\theta}^{\infty} e^{-m\lambda^2} d\lambda + e^{mx} \int_{(2r)^{\frac{1}{2}} \cos \frac{1}{2}\theta}^{\infty} e^{-m\lambda^2} d\lambda \right\} \quad (-\tfrac{1}{2}\pi < \theta < \tfrac{3}{2}\pi). \tag{19}$$

This is the unique solution of the problem as presented. It is continuous in the whole plane, but $\partial\phi/\partial x$ is discontinuous across $x = 0$, $y < 1$. On the plane $x = 0$, ϕ is essentially zero for $y > 1$ and $1/2m$ for $y < 1$ with an error which is exponentially small except near $y = 1$. There $\phi = 1/2m$ and is continuous in its neighbourhood. Also $\partial\phi/\partial x = 0$ for $x = 0$, $y > 1$, and for $y < 1$, $\theta = -\frac{1}{2}\pi$,

$$\frac{p}{2M} = \frac{\partial \phi}{\partial x} = -\frac{1}{2} + \frac{1}{\pi^{\frac{1}{2}}} \int_{m^{\frac{1}{2}}(1-y)^{\frac{1}{2}}}^{\infty} e^{-\lambda^2} d\lambda - \frac{e^{-m}(1-y)}{2\{m\pi(1-y)\}^{\frac{1}{2}}}. \tag{20}$$

Thus $\partial\phi/\partial x = -\frac{1}{2}$ with an error which is exponentially small except near $y = 1$ where $\partial\phi/\partial x$ has an integrable singularity. It is also discontinuous across $x = 0$, $y < 1$, taking equal and opposite values at corresponding points on the two sides.

Away from the disk, say for $x > 1$, equations (8) and (9) show that the velocity and pressure are given asymptotically by

$$\left.\begin{aligned} \mathbf{V}-\mathbf{i} &\sim e^{2mx}\nabla(e^{-mx}\phi), \\ p/2m &\sim e^{2mx}\frac{\partial}{\partial x}(e^{-mx}\phi). \end{aligned}\right\} \tag{21}$$

Now, from (19)

$$e^{2mx}\frac{\partial}{\partial x}(e^{-mx}\phi) \sim -\left(\frac{1}{\pi}\right)^{\frac{1}{2}}\int_{(2mr)^{\frac{1}{2}}\sin\frac{1}{2}\theta}^{\infty} e^{-\lambda^2}\,d\lambda, \tag{22}$$

$$e^{mx}\frac{\partial\phi}{\partial y} = -\frac{1}{2}\left(\frac{1}{2m\pi r}\right)^{\frac{1}{2}}(\cos\tfrac{1}{2}\theta+\sin\tfrac{1}{2}\theta)\,e^{-2mr\sin^2\frac{1}{2}\theta}, \tag{23}$$

which shows that there is a region of sharp transition in the neighbourhood of $\theta = 0$, across which p/M and the x-component of $(\mathbf{V}-\mathbf{i})$ change rapidly from -1 ($\theta < 0$) to 0 ($\theta > 0$). The y-component of $\mathbf{V}$ is exponentially small everywhere save in the region of transition. This region contains the points for which $mr\sin^2\frac{1}{2}\theta$ is not large, and so is roughly parabolic in profile with thickness $O(|x|^{\frac{1}{2}}/M^{\frac{1}{2}})$ (by symmetry there is a similar region on the negative side of the plane $x = 0$). Thus it is thin where $|x| = O(M)$ but gradually thickens until it is smeared out completely for $|x| = O(M)$.

When the solution is applied to the circular disk, the co-ordinate r is to be interpreted as the distance from the field point considered to the nearest point on the edge of the disk, the angle θ is the inclination of this line to the x-axis. Some comment is also necessary on the validity of the solution when applied to the disk problem. It is correct only in the shear layer, and only where that layer is thin, so that the effects of curvature are of secondary importance in determining the nature of the flow. It is not really correct to regard it as extending beyond this region, although for $x \ll M$, it does agree with what the results of C would lead one to expect.

The situation resembles that in boundary-layer theory. The equations of that theory are assumed valid in a thin region of the flow, and outside this region it is assumed that there is a known main stream flow. The latter is used as a boundary condition for the edge of the boundary layer, and it is a common procedure to apply this boundary condition at infinity. In the present problem the 'main stream flow' can be thought of as that given by the more elementary theory of C, both inside and outside the circumscribing cylinder. This provides the boundary conditions at infinity for the problem of the semi-infinite plane.

The breakdown of the solution for large values of x also has its analogue in boundary-layer theory and can be explained by the fact that the radial scale of length in the transition layer eventually becomes comparable with the length scale in the other directions. Alternatively by reference to (14) it will be seen that as $r = (x^2+y^2+z^2)^{\frac{1}{2}}$ increases, the sensible contribution to the integral depends more and more on the over-all value of χ, rather than its value in some small neighbourhood of the disk. In fact, for $r \gg M$ it is readily seen from (14) that

$$\phi \sim -\frac{e^{-mr}}{2\pi r}\iint \chi(y',z')\,dy'\,dz' \sim \frac{e^{-mr}}{4r},$$

where the integration is now taken over the plane of the disk. If this value of ϕ is substituted in (8), it follows that the perturbation velocity components tend to zero exponentially at infinity in every direction except the x-direction, where

$$|\mathbf{V}-\mathbf{i}| = O\left\{\frac{m\,e^{-m(r-x)}}{r}\right\}.$$

Finally we may add that a uniformly valid solution for ϕ could be obtained from (14), since the value of $\chi(y', z')$ on the disk is now known. The results will not be given since all the essential information has already been obtained from the 'boundary-layer' theory. The qualitative picture is essentially that given above. There is a thin shear layer in the neighbourhood of the circumscribing cylinder, which gradually thickens as $|x|$ increases until eventually it fuses into the main stream flow for $|x| = O(M)$.

The drag for large values of M is easily obtained by integrating the pressure (given by (20), with y now interpreted as the radial co-ordinate) over the surface of the disk. Note that the pressure over the interior of the disk contributes a term of more significant order to the integrated pressure than the contribution from the edge effect. Now the pressure over the interior is in error by an exponentially small amount. Near the edge the error is more significant, but of less significance than the terms already displayed in (20). This means that (20) should yield the first two leading terms in the drag. When evaluated, they give

$$\frac{D}{\rho v a U} = 2M\pi(1+2/M). \tag{24}$$

4. The validity of the basic equations

In C the equation of motion is derived in the form (C 9)

$$R(\mathbf{V}.\nabla)\,\mathbf{V} = -\nabla p + \nabla^2\mathbf{V} + M^2(\mathbf{V}\wedge\mathbf{i})\wedge\mathbf{i}, \tag{25}$$

and the whole of the analysis is based on the assumption that the term on the left-hand side of this equation may be neglected. When $M \ll 1$, this is valid provided $R \ll M$. For the term $M^2(\mathbf{V}\wedge\mathbf{i})\wedge\mathbf{i}$ modifies the Stokes solution by a factor $\{1+O(M)\}$ (Chester, 1957) whereas the term $R(\mathbf{V}.\nabla)\,\mathbf{V}$ modifies the solution by a factor $\{1+O(R)\}$.

We consider here the validity of the assumption for $M \gg 1$, and the significant region is then the shear layer. From (19) one can deduce that in this layer,

$$\begin{aligned}
&\text{the axial component of velocity} &&= O(1),\\
&\text{the radial component of velocity} &&= O(M^{-\frac{1}{2}}),\\
&\text{the pressure} &&= O(M),\\
&\partial/\partial x &&= O(1),\\
&\partial/\partial\eta &&= O(M^{\frac{1}{2}}).
\end{aligned}$$

It then follows that the four terms in (25) have respectively the following orders of magnitude for the axial component of that equation,

$$R,\quad M,\quad M,\quad 0$$

and, for the radial component,

$$RM^{-\frac{1}{2}}, \quad M^{\frac{1}{2}}, \quad M, \quad M^{\frac{3}{2}}.$$

Thus the same condition, namely $R \ll M$, is also required for $M \gg 1$. It is worth noting that, for $M \gg R$ and $M \gg 1$, equation (25) simplifies to

$$\frac{\partial p}{\partial x} = \frac{\partial^2 V_x}{\partial \eta^2}, \quad \frac{\partial p}{\partial \eta} = -M^2 V_\eta,$$

where $\mathbf{V} = (1 + V_x, V_\eta)$. One may verify that the approximate solutions do, in fact, satisfy these equations. Note also that the second of these equations explains the mechanism by which the large pressure gradient across the shear layer is maintained by balancing the Lorentz force.

REFERENCES

Chester, W. 1950 *Phil. Trans.* A, **242**, 527.

Chester, W. 1957 *J. Fluid Mech.* **3**, 304.

Chester, W. 1961 *J. Fluid Mech.* **3**, 459.

Gunn, J. C. 1947 *Phil. Trans.* A, **240**, 327.

Lamb, H. 1932 *Hydrodynamics*, 6th ed. Cambridge University Press.

The action of Vlasov waves on the velocity distribution in a plasma

By J. W. DUNGEY

Atomic Weapons Research Establishment, Aldermaston

(Received 19 December 1960)

A one-dimensional model with no magnetic field is considered. It is supposed that the plasma starts in thermal equilibrium and then a current is forced to grow. Instability leads to the growth of waves, which are shown to stir the distribution in phase space, but only over a limited range of velocity. It is concluded that in order to restore stability the energy in the wave must become comparable to the energy of drift.

1. Introduction

Vlasov waves grow when a plasma is electrostatically unstable. This kind of instability may be expected in a great variety of devices designed for confining a plasma and in particular has been suggested as the cause of 'pump out' in Stellarators (Bernstein, Friedman, Kulsrud & Rosenbluth 1960). The existing theory tells us little more than the stability condition in the simplest case, in which the problem is one-dimensional, the plasma is uniform in space and all magnetic effects are ignored. From here it is possible to proceed in various directions by removing different simplifying assumptions, and obviously one should not remove more than one at a time. The aim of this investigation is to remove the assumption of linearization. Linearized theory gives the stability condition, but it is important to know how strong the waves grow and this is an essentially non-linear problem.

The problem is posed as follows. Suppose that a plasma is initially in thermal equilibrium and a gradually increasing current is driven through it by an electric field. If U_D is the difference between the mean velocities of the electrons and ions and v_{te} is the thermal velocity of electrons, Vlasov instability sets in when U_D reaches about $0{\cdot}93v_{te}$. It is evident that the instability takes energy from the electric field, but suppose that the external circuit is such that the current still increases (this is usual in practice). How strong do the Vlasov waves grow and what is their effect on the overall behaviour of the plasma?

If the velocity distribution were always Maxwellian, one could say that the Vlasov waves heat the plasma and the rise in temperature tends to restore stability. The time scale of the Vlasov waves is related to the plasma frequency, which in practice is very large. Typically the plasma period may be 10^{-12} sec, while the time scale T for the growth of the current is seldom less than 10^{-6} sec. Consequently, even if the growth time of the waves were hundreds of plasma periods it would still be short compared with T. This suggests that the waves will

adjust their amplitude in the following way. The heating due to the waves should raise the temperature at such a rate that the plasma is always near the critical condition: drift velocity $\approx 0{\cdot}93 \times$ thermal velocity. Then the temperature must rise with a time scale $\sim T$, which suggests that the wave amplitude is not large. If so, the linear theory may be valid, in which case the heating should be obtained from the second-order terms.

In the linear theory the distribution function f, for say the electrons, is written $f^{(0)}+f^{(1)}$, where $f^{(1)}$ is the first-order perturbation. The linearized collision-free Boltzmann equation then gives

$$i(\omega+kv)f^{(1)} = \frac{e}{m}E\,\partial f^{(0)}/\partial v, \tag{1}$$

where ω the angular wave frequency is complex, k the wave number is real and E the electric field is a first-order quantity proportional to $\exp[i(\omega t+kx)]$ (there is no applied field in the linear theory). The heating must depend on the component of the electron current density in phase with the electric field and this is proportional to the imaginary part of

$$\int \frac{v\,\partial f^{(0)}/\partial v\,dv}{\omega+kv} = -\frac{\omega}{k}\int \frac{\partial f^{(0)}/\partial v\,dv}{\omega+kv}.$$

Now it has been suggested that the imaginary part of ω (the growth rate) is small and in this case the imaginary part of the integral comes almost entirely from a small range of velocity near the wave velocity. This is familiar. The growth, or, in the case of Landau damping, decay, is almost entirely due to 'trapped' particles with velocities near the wave velocity. The width of the velocity range involved is of order $k^{-1}\mathscr{I}(\omega)$. Now, because few particles are involved, we can have no confidence in the assumption that the velocity distribution remains Maxwellian, and a deeper investigation is required.

2. The general stability condition

The stability condition for any velocity distribution (uniform in space) has been obtained by several authors and is given in an elegant form by Penrose (1960).

Penrose's analysis also enables us to obtain the velocity and an estimate of the wavelength of the fastest growing wave and his results will now be summarized. They involve the function $F(u)$ defined by

$$F(u) = \sum_j 4\pi e_j^2 f_j(u)/m_j,$$

where $f_j(u)$ is the one-dimensional distribution function for the jth type of particle. The dispersion equation is then

$$k^2 = Z(\omega/k),$$

where

$$Z(\zeta) = \int_{-\infty}^{\infty} (u-\zeta)^{-1}(dF/du)\,du \tag{2}$$

in the upper half-plane and is continued analytically across the real axis.

Penrose represents this by drawing the curve of real ζ on the Z-plane and obtains a necessary and sufficient condition for instability, which is that $F(u)$ should have a minimum at some value ζ of u such that

$$\int_{-\infty}^{\infty} (u-\xi)^{-2}[F(u)-F(\xi)]\,du > 0. \tag{3}$$

In the present problem it is easy to see that $F(u)$ already has a minimum when U_D exceeds a small fraction of v_{te} and hence that the onset of instability at $U_D = 0{\cdot}93v_{te}$ is due to the integral in (3) changing from negative to positive.

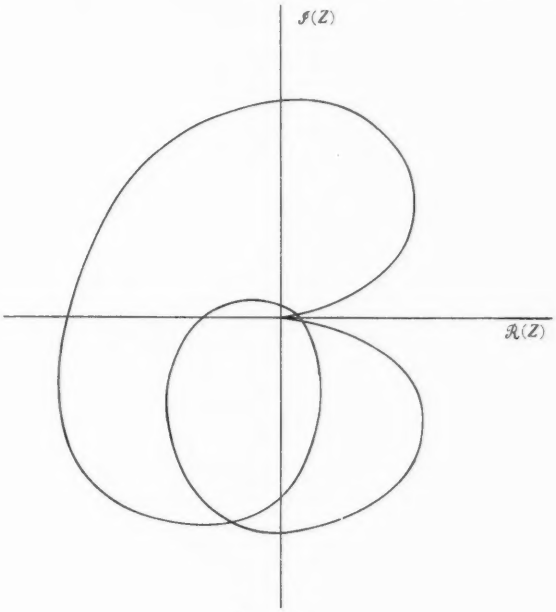

FIGURE 1

When U_D just exceeds the critical value, the curve of real ζ on the Z-plane looks like figure 1, and the minimum $\zeta = \xi$ is the point where the curve intersects the positive real axis. The growing waves are represented by points between here and the origin and, so long as the growth rate is small, satisfy the approximate dispersion relation

$$k^2 - k_0^2 \approx (\zeta - \xi)\,(dZ/d\zeta)_{\zeta=\xi}, \tag{4}$$

where k_0^2 is the value of Z at $\zeta = \xi$. The velocity of the waves is close to ξ and the growth rate is related to the wavelength by

$$\mathcal{I}(\omega) \approx k(k^2 - k_0^2)\,\mathcal{I}[(dZ/d\zeta)_{\xi=\xi}^{-1}].$$

The fastest growing wavelength is given by $k_1 = k_0/\sqrt{3}$, and hence

$$k_1^3 \approx -\tfrac{1}{2}\mathcal{I}(\omega)\{\mathcal{I}[(dZ/d\zeta)_{\xi=\xi}^{-1}]\}^{-1}. \tag{5}$$

To obtain an order of magnitude for k_1, $\{\mathscr{I}[(dZ/d\zeta)_{\zeta=\xi}^{-1}]\}^{-1}$ may be approximated by $\mathscr{I}[(dZ/d\zeta)_{\zeta=\xi}]$, assuming that $\mathscr{R}(dZ/d\zeta)_{\zeta=\xi}$ is smaller. When ζ is on the upper side of the real axis, we see from (2) that

$$\mathscr{I}(Z) = \pi(dF/du)_{u=\zeta}, \tag{6}$$

and then

$$\mathscr{I}(dZ/d\zeta) = \pi(d^2F/du^2)_{u=\zeta}.$$

For a Maxwellian distribution

$$d^2f/dv^2 = \pi^{-\frac{1}{2}}n(m/2kT)^{\frac{3}{2}}(mv^2/kT - 1)\exp(-mv^2/2kT).$$

Now at the minimum, mv^2 is the same for protons and electrons and near the critical condition is about $1{\cdot}7kT$. Consequently, the ion contribution dominates in $(d^2F/du^2)_{u=\xi}$ and we find

$$k_1^3 \sim 0{\cdot}3\mathscr{I}(\omega)\,ne^2(\pi^3 m_i/2k^3T^3)^{\frac{1}{2}} \sim 5.10^{-7}\mathscr{I}(\omega)\,nT^{-\frac{3}{2}}\,\mathrm{cm}^{-3}$$

for deuterium.

With $\mathscr{I}(\omega) \sim 10^6\,\mathrm{sec}^{-1}$, $n \sim 10^{16}\,\mathrm{cm}^{-3}$ and $T \sim 10^7\,^\circ\mathrm{K}$ this gives a wavelength $2\pi/k_1$ of about 1 mm.

3. Stirring in phase space

We now consider the effect of the wave on the velocity distribution. This may not be very sensitive to the growth rate and, since we are interested in the case where the growth rate is small, it seems sensible to consider the case in which there is no growth or decay, that is the frequency is real. Such waves

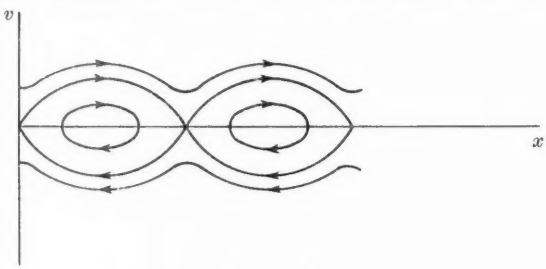

FIGURE 2

have been studied by Bernstein, Greene & Kruskal (1957), who showed that solutions representing waves of finite amplitude and having a considerable degree of arbitrariness exist. Their method is to use a frame moving with the wave and demonstrate the existence of steady solutions. We also use this frame, but study the effect of the electric field belonging to the wave on the distribution function, supposing that the latter is not chosen to give a steady state. In the chosen frame we neglect the variation of the electric field with time and it is then possible to draw the trajectories of particles in phase space. This is done in figure 2 for an electric field $E\cos kx$, which is chosen for simplicity. It is seen that there is a row of 'eddies' with their centres on the zero velocity of this frame. Outside the eddies the trajectories are wavy lines whose amplitude decreases with the mean value of v like v^{-1}, because the frequency seen by a particle with mean velocity v is k/v.

The period of rotation in the centre of an eddy is given by the period of simple harmonic motion in a field $-Ekx$. Hence the angular velocity in the centre of an eddy is

$$S = (eEk/m)^{\frac{1}{2}}. \tag{7}$$

The electrostatic potential is $-k^{-1}E\sin kx$ and the half-width of the eddies in velocity is

$$a = 2(eE/mk)^{\frac{1}{2}} = 2k^{-1}S. \tag{8}$$

This may be compared with the range of velocities of trapped particles found above from the linear theory; when the growth rate is small we may expect a to be the larger.

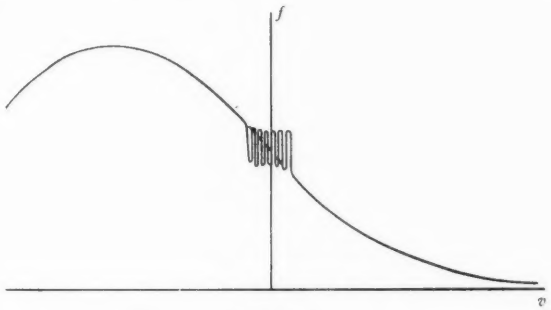

FIGURE 3

Now the collision-free Boltzmann equation is equivalent to Liouville's theorem which states that if one follows the trajectory of a particle in position, velocity and time the distribution function remains constant. Thus in a steady state the contours of constant f must be the trajectories of figure 2. In a non-steady state the motion depicted in figure 2 will 'stir' the distribution and this will be much more effective in the region of the eddies than elsewhere. The effect on the distribution may be seen by supposing that there is a contour of constant f passing through the centres of all the eddies. As the eddies rotate this will be wound into spirals, one in each eddy. Each rotation of an eddy adds a turn to the spiral and hence the spiral becomes tighter. The effect on the distribution function at a position corresponding to the centre of an eddy (that is a potential trough) is shown in figure 3. The dotted line represents the unperturbed distribution function, and the full line shows the rapid variations caused by the stirring; each turn of the eddy increases the numbers of maxima and minima in this curve by two. It then follows that the scale of variation of f with velocity in the eddies becomes smaller and hence that $|\partial^2 f/\partial v^2|$ becomes larger. This shows that collisions must be taken into account and the Fokker–Planck equation is appropriate. The full Fokker–Planck expression (Rosenbluth, MacDonald & Judd 1957) is complicated, but for a preliminary study we need only note that it has the form

$$\frac{\partial}{\partial v}\left[G(v)\frac{\partial f}{\partial v} + H(v)f\right],$$

where G and H depend on integrals over v involving f, but these are unlikely to be greatly altered by the sort of disturbance shown in figure 3. Thus the Fokker–

Planck term may be described as representing diffusion of particles in velocity, the stable distribution function towards which they tend to diffuse being the Maxwellian distribution determined by the number of particles and their total momentum and energy. Like a diffusion term it removes small-scale variations more quickly than large-scale variations. As $|\partial^2 f/\partial v^2|$ is increased by the stirring the Fokker–Planck term must eventually become important. When it smooths out the oscillations in figure 3, the full curve of figure 4 results. This then gives a qualitative idea of the effect of the wave on the distribution function: the distribu-

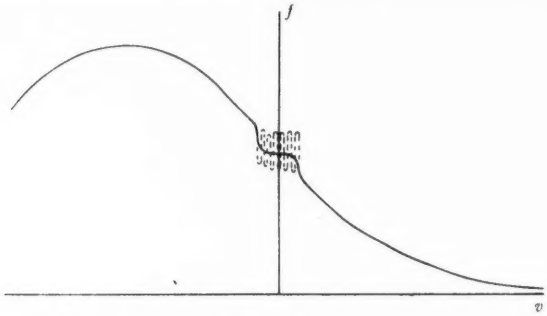

FIGURE 4

tion function develops a ledge centred on the wave velocity. Clearly particles have been transported across the wave velocity from the side of high f to that of low f. When the wave velocity is at the minimum of F, this reduces the current density as expected. The stirring mechanism is similar to a Fermi mechanism in that it tends to produce a flat distribution in the velocity range in which it operates. The effect on the velocity distribution tends to make it more stable, but it has been assumed that the current is forced to increase by the external circuit.

4. The mechanism of stabilization

The Penrose criterion is strictly applicable only when the distribution functions are uniform in space. It may be used to discuss the development of the waves, however, by formulating the problem as 'if the waves stabilize themselves and die away and the spatial variation of the distribution is smeared out, does a new wave grow?' On this basis the Penrose criterion will be applied to distributions in which ledges have developed as a result of the waves' action.

The difference between the effect of the waves on the electron and proton distributions can be seen by noting that S and a are both proportional to $m^{-\frac{1}{2}}$. For a wave at the velocity of the original minimum the two distributions can be scaled, all velocities being smaller for the ions in the ratio $(m_e/m_i)^{\frac{1}{2}}$ and times being longer for the ions in the ratio $(m_i/m_e)^{\frac{1}{2}}$. The collision time also behaves in this way and hence the Fokker–Planck term also scales. Because the ledge developed in the electron distribution is wider than that of the ions, the minimum in the new distribution is at the inner edge of the electron ledge, that is at a velocity nearer the mean electron velocity than the original minimum. The electric field driving the current also moves the electron distribution in this

direction, and only moves the ion distribution by a fraction m_e/m_i as much. Consequently, one expects the minimum to move away from the mean ion velocity, and one may expect from Penrose's criterion that the velocity of the wave U_w will follow that of the minimum. As U_w changes, the eddies in figure 2 sweep across the distribution and churn particles down the slope. If U_w could sweep far enough across the electron distribution, it would be possible by means of a succession of weak waves to stabilize the plasma for a given current density; this has been verified by computations. It is unreasonable that the minimum can move very far from the mean ion velocity, however. On the ledge formed by the action of the wave $\partial f_e/\partial v$ is small, but not very small; even though f_e is very nearly constant in the centre of an eddy, there must be an appreciable variation between the eddies which contributes to the space average. In the tail of the Maxwell distribution for ions, however, $\partial f_i/\partial v$ decreases very rapidly and so the minimum cannot be far out in their tail; more precisely the difference between the velocity at the minimum and the mean velocity of the ions cannot be many times v_{ti} unless the ion tail itself were spread by the wave sufficiently, but it has already been seen that the effect of the wave on the ions is much less than its effect on the electrons.

The argument based on figure 1 that U_w must be near the velocity of minimum F breaks down when F is nearly constant over a range of velocities including the minimum, which is the case after the formation of a ledge. Then from (6), $\mathscr{I}(Z)$ for real ζ is small over the whole range of velocity in which F is nearly constant. It is then possible for the fastest growing wave to have its velocity anywhere in this range and, if U_w were near the end of the range nearest the electrons, stabilization by weak waves would be possible. In order for this to happen $\mathscr{R}(Z)$ for U_w must be less than $\mathscr{R}(Z)$ for ξ but still positive. With a Maxwellian distribution distorted by a small ledge, however, one finds that $\mathscr{R}(Z)$ increases as ξ moves towards the electrons, and consequently U_w can still not be far from the ion velocity. When the current density grows to several times its original critical value, it is necessary to redistribute the velocities of a large proportion of the electrons in order to restore stability. This requires the trapping of a large fraction of the electrons and hence the potential difference in the wave must be comparable to the energy of relative motion $\sim \frac{1}{2}m_e U_D^2$; the energy of the wave is also of this order. With the numerical values given previously the rate of stirring S is then $\sim 5.10^{10}\,\mathrm{sec}^{-1}$ for electrons and $\sim 10^9\,\mathrm{sec}^{-1}$ for deuterons. Thus the stirring process, which has been assumed to form ledges in the distributions, has plenty of time to occur.

I am indebted to Dr F. D. Kahn for several enjoyable and very helpful discussions.

REFERENCES

Bernstein, I. B., Frieman, E. A., Kulsrud, R. M. & Rosenbluth, M. N. 1960 *Phys. Fluids*, **3**, 136.

Bernstein, I. B., Greene, J. M. & Kruskal, M. D. 1957 *Phys. Rev.* **108**, 546.

Penrose, O. 1960 *Phys. Fluids*, **3**, 258.

Rosenbluth, M. N., MacDonald, W. M. & Judd, D. L. 1957 *Phys. Rev.* **107**, 1.

REVIEWS

Similitude Physique: Examples d'Applications à la Mécanique des Fluides. By André Martinot-Lagarde. Paris: Gauthier-Villars, 1960. 70 pp. 14.00 N.F. or $3.00.

This little book deals with the notions of similarity and dimensional analysis. The first chapter gives a clear definition of the basic concepts of similarity conditions and similarity results in mechanics and physics, and states the fundamental theorem of Bridgman on the 'product of powers'. A very complete proof, which includes the case of discontinuous functions, may be found in an appendix. Chapters II and III are devoted to dimensional analysis; it starts with Vaschy's Theorem (or π theorem) which gives the key to the method. But, as everybody knows, some care is required, especially for physical constants which are not dimensionless, and for the arbitrary choice of the group of fundamental dimensions. The apparent paradoxes arising from these difficulties are explained with some interesting examples chosen from fluid mechanics. The author also shows in great detail how to apply this method in practice.

In Chapter IV, the author deals with the 'direct method'; in such a method all the equations and boundary conditions of the problem have to be written down and the task is to investigate how the relations may remain invariant by some change of scale. This method is explained with a few good examples which provide opportunities for some useful remarks. In particular, it is clearly shown that in many cases this last method may lead to the required result in an easier way than the apparently simpler method of dimensional analysis.

The danger with a monograph on this topic is that it may be either too long and too theoretical, or too short and too vague. In the reviewer's opinion, Professor Martinot-Lagarde has succeeded in writing a very convenient and useful book which is rigorous without using too many abstract concepts, and at the same time never loses contact with the physics.

P. Germain

JOURNAL OF FLUID MECHANICS

Volume 10, Part 3 May 1961

CONTENTS

Swimming of a waving plate
by T. YAO-TSU WU *page* 321
Experiments on the flow past a circular cylinder at very high Reynolds number
by ANATOL ROSHKO 345
A dispersion relation for waves of finite amplitude in a two-stream plasma
by F. D. KAHN 357
Spectral flatness factor and 'intermittency' in turbulence and in non-linear noise
by D. A. KENNEDY and S. CORRSIN 366
Orifice flow at high Knudsen numbers
by RODDAM NARASIMHA 371
Interaction between gravity waves and a shear flow
by B. A. HUGHES and R. W. STEWART 385
The development of three-dimensional disturbances in an unstable film of liquid flowing down an inclined plane
by T. BROOKE BENJAMIN 401
Hydrodynamic stability and the inviscid limit
by K. M. CASE 420
Some mathematical problems in the theory of the stability of parallel flows
by C. C. LIN 430
Magnetohydrodynamic flow constructions with fundamental solutions
by MEREDITH C. GOURDINE 439
A new approach to the measurement of turbulent fluxes in the lower atmosphere
by R. J. TAYLOR 449
The effect of a magnetic field on the flow of a conducting fluid past a body of revolution
by W. CHESTER 459
The effect of a magnetic field on the flow of a conducting fluid past a circular disk
by W. CHESTER and D. W. MOORE 466
The action of Vlasov waves on the velocity distribution in a plasma
by J. W. DUNGEY 473
REVIEWS
Similitude Physique: Examples d'Applications à la Mécanique des Fluides 480

Printed in Great Britain at the University Press, Cambridge
(Brooke Crutchley, University Printer)